14
5113

Applied Optics

September
1962

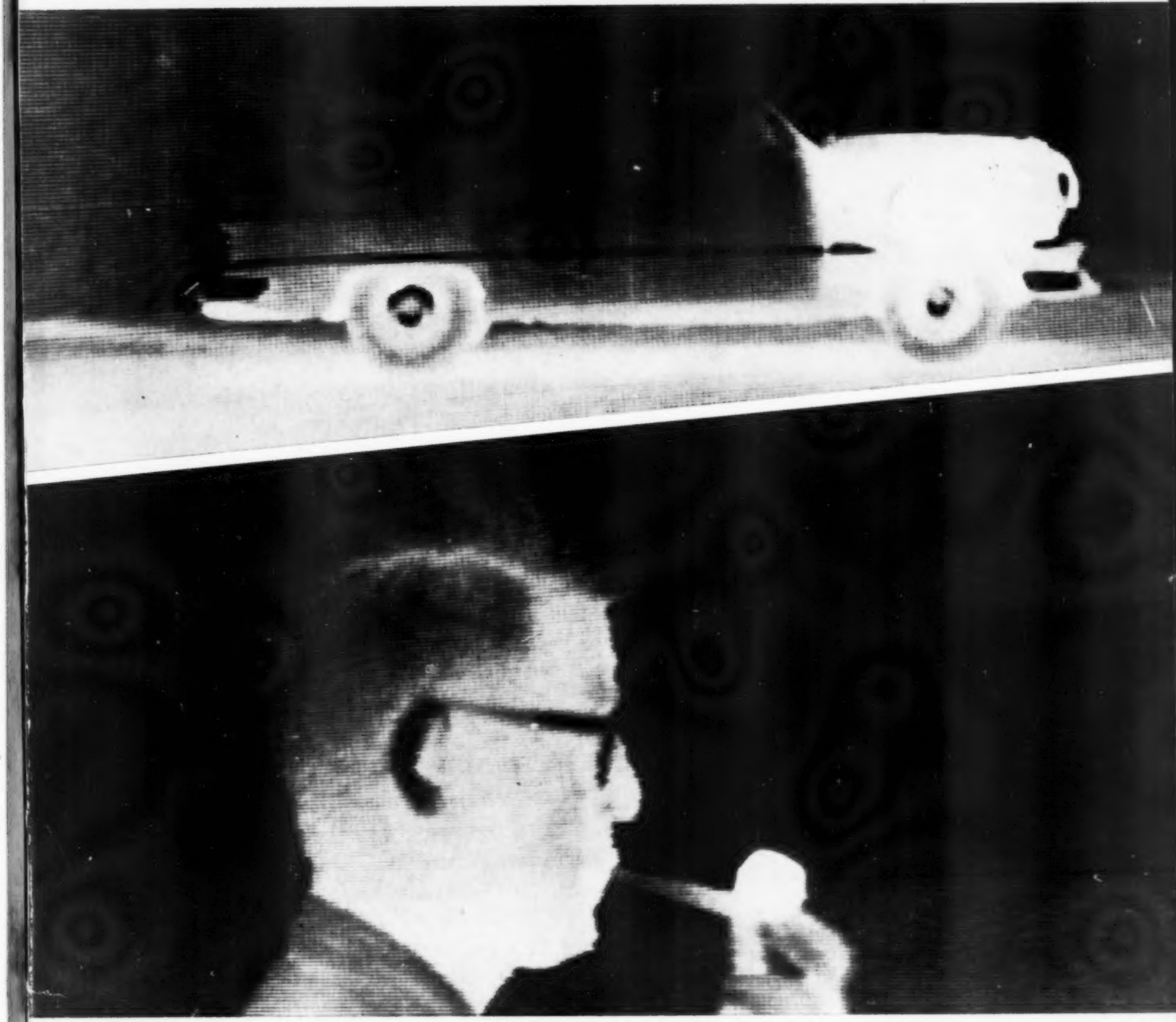

INFRARED

ENGINEERS

ELECTRO-OPTICAL SYSTEMS

explore your Future in

SATELLITE AND SPACE VEHICLE DEVELOPMENT

at RCA's new Space Center in Princeton, N. J.

Here is an opportunity to let your imagination soar with the team that created Tiros. Now at this rapidly growing division of RCA, a number of challenging opportunities are available for electronic engineers.

To qualify Supervisory Engineers must have 5 to 10 years experience . . . Engineers, 3 to 5 years experience in the following fields:

TELEVISION CAMERA DESIGN and EVALUATION
SOLID STATE CIRCUIT DESIGN EXPERIENCE
KNOWLEDGE OF ELECTRO-OPTICAL SYSTEMS and
OPTICAL SYSTEMS

Work to be performed must conform to stringent operational and environmental specifications.

FOR A CONFIDENTIAL INTERVIEW call collect:

MR. D. D. BRODHEAD
609-448-3400 or write:

MR. D. D. BRODHEAD, DEPT. NY-12
ASTRO-ELECTRONICS DIVISION
PRINCETON, NEW JERSEY

An Equal Opportunity Employer

RCA

The Most Trusted Name in Electronics
RADIO CORPORATION OF AMERICA

Applied Optics

VOLUME 1
NUMBER 5
September
1962

A bimonthly publication of the
Optical Society of America

John N. Howard, Editor

Patricia R. Wakeling, Managing Editor

COVER: The thermographs were made with the Barnes Engineering Company's infrared camera [see J. Opt. Soc. Am. **49**, 184 (1959)]. This optical-mechanical scanning system, utilizing thermistor infrared detectors, gives a quantitative record of the infrared radiation emitted by the scene scanned. A gray scale is included to calibrate tones in the picture in terms of blackbody temperature differentials. For the thermograph of the man smoking a pipe, the smallest discernible gray step is equivalent to 0.3°C, while white in the picture represents 7.5°C or more. The thermograph of the automobile shows the emission from the hot motor and exhaust pipe and reflections from the pavement. The gray steps range from a minimum of 0.7°C to a maximum of 17°C.

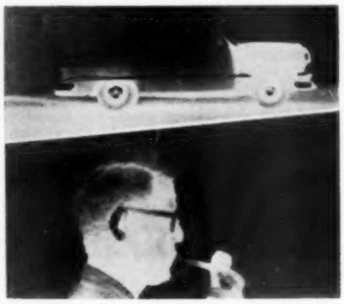

Published bimonthly by the Optical Society of America, Inc., in cooperation with the American Institute of Physics, at 20th and Northampton Streets, Easton, Pa. Editorial offices: 1155 16th St. N.W., Washington 6, D.C. Supported in part by a grant from the National Science Foundation. Advertising Office: 55 West 16th Street, New York 11, N.Y. A. P. Oppenheim—Chelsea 2-1311. Subscription rates: $6.00 to OSA members, $8.00 other AIP Societies' members; nonmembers and libraries: $10.00 per year. Single copies $2.00. Second class postage paid at Easton, Pa.
©Copyright 1962 by the Optical Society of America.

547 **Recent Developments in Infrared Technology—**Stanley S. Ballard and William L. Wolfe
559 **University Research in Infrared Physics—**John S. Garing and John N. Howard
567 **Infrared Photodetectors: A Review of Operational Detectors—**R. F. Potter and W. L. Eisenman
575 **Quelques Resultats Nouveaux dans la Mesure des Indices de Refraction (Liquides et Solides) dans l'Infrarouge—**Josette Vincent-Geisse et Jean Lecomte
587 **Total Absorptance of Carbon Monoxide and Methane in the Infrared—**Darrell E. Burch and Dudley Williams
595 **Emittance Measurements on Infrared Windows Exhibiting Wavelength Dependent Diffuse Transmittance—**S. E. Hatch
603 **Durable Narrow Absorption Band Infrared Filters Utilizing Powdered Mineral Materials on Polyethylene Substrates—**Hugh R. Carlon
607 **Immersed Radiation Detectors—**R. Clark Jones
615 **Wedge-Immersed Thermistor Bolometer—**Marc G. Dreyfus
621 **Performance of the Beckman IR-7 Infrared Spectrophotometer 2. Frequency Reproducibility and Accuracy (200–800 cm^{-1})—**Peter J. Krueger
627 **The Detectivity of Infrared Photodetectors—**S. Nudelman
637 **A Study of the Angular Response of Lead Sulfide Photoconductors—**Gustave J. Schaefer
643 **Interference Filters and Fabry-Perot Interferometers for the Far Infrared—**K. F. Renk and L. Genzel
649 **An Analytical Infrared Radiation Model of the Earth—**R. A. McGee
655 **New Backscattering Computation and Tables for Dielectric and Metal Spheres—**Simpson B. Adler and Robert S. Johnson
661 **Measurements of Second Harmonic Generation of the Ruby Laser Line in Piezoelectric Crystals—**Albert Savage and Robert C. Miller
665 **Relationship between the Near Field Characteristics of a Ruby Laser and Its Optical Quality—**Michael Hercher

DEPARTMENTS

670 **Letters to the Editor**
  Mean Atmospheric Moisture Profiles to 31 km for Middle Latitudes—Murray Gutnick
  Spatial Distribution of Light Across the End of a Ruby Laser—David Weisman
  Mode Selection and Enhancement with a Ruby Laser—John A. Baker and C. W. Peters
  An Image Reducer—Immersed Detector System for the Infrared—Robert G. Greenler
  Spectra Associated with High-Speed Projectiles in Rarefied Air Obtained with a Large-Aperture Slit Spectrograph—I. D. Liu
558 **Meetings Calendar**
565 **Patents**
585 **Optical Activities in the Universities**
601 **Of Optics and Opticists**
605 **From the Editor**
619 **Books**
641 **Meeting Reports**

New Light Pumps for EXPANDING PARAMETERS IN OPTICAL LASER RESEARCH

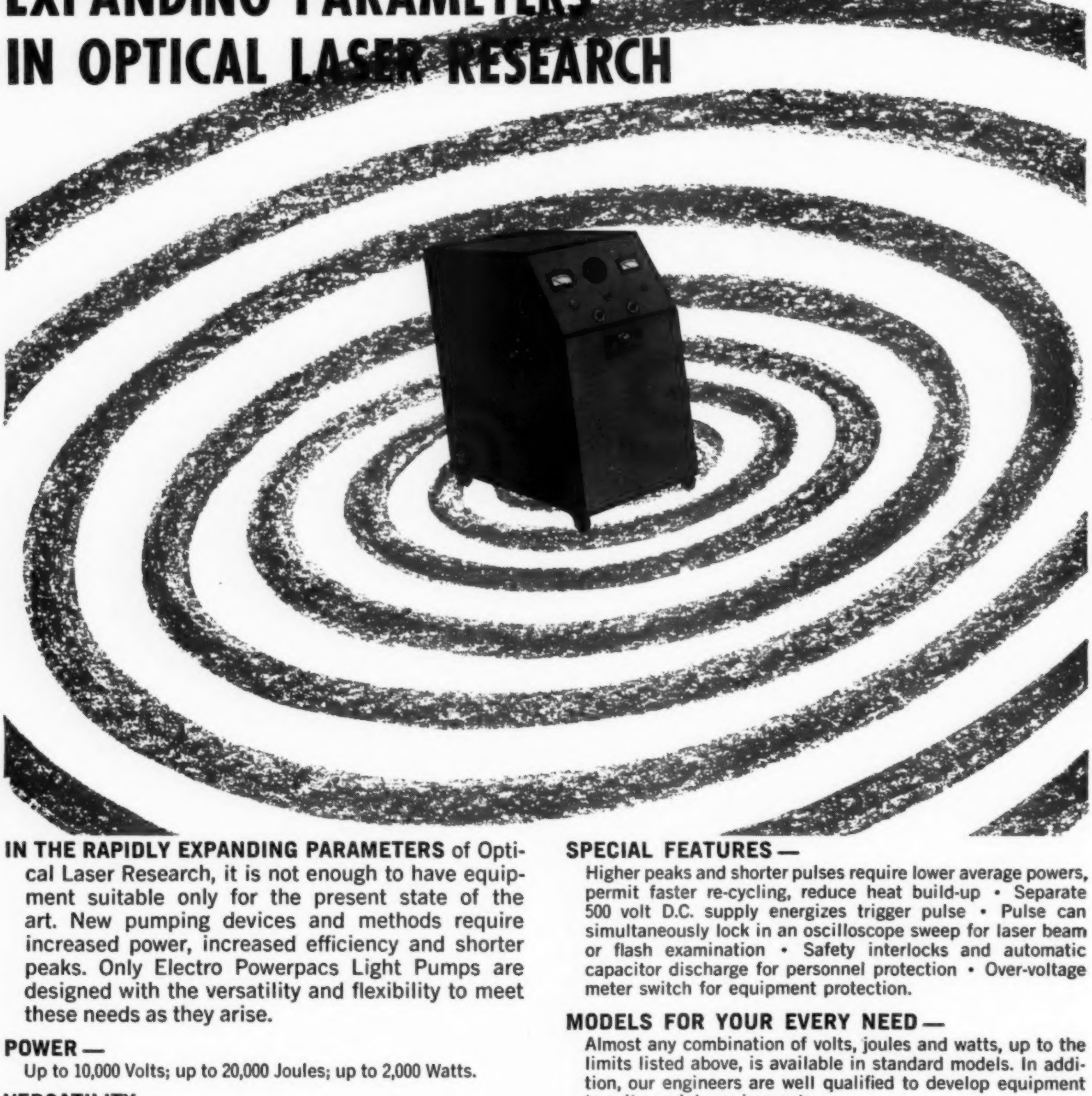

IN THE RAPIDLY EXPANDING PARAMETERS of Optical Laser Research, it is not enough to have equipment suitable only for the present state of the art. New pumping devices and methods require increased power, increased efficiency and shorter peaks. Only Electro Powerpacs Light Pumps are designed with the versatility and flexibility to meet these needs as they arise.

POWER —
Up to 10,000 Volts; up to 20,000 Joules; up to 2,000 Watts.

VERSATILITY —
Continuously variable voltages 0-10,000. Variable peak power and pulse length. Operates with all size rods. One mount for airblast or cryogenic cooling.

FLEXIBILITY —
100 to 20,000 joules, achieved by varying the voltage, the number of capacitor banks or the number of capacitors. Capacitors can be eliminated from circuit by merely removing a fuse.

SPECIAL FEATURES —
Higher peaks and shorter pulses require lower average powers, permit faster re-cycling, reduce heat build-up • Separate 500 volt D.C. supply energizes trigger pulse • Pulse can simultaneously lock in an oscilloscope sweep for laser beam or flash examination • Safety interlocks and automatic capacitor discharge for personnel protection • Over-voltage meter switch for equipment protection.

MODELS FOR YOUR EVERY NEED —
Almost any combination of volts, joules and watts, up to the limits listed above, is available in standard models. In addition, our engineers are well qualified to develop equipment to suit special requirements.

PARTIAL LIST OF LABORATORIES USING ELECTRO POWERPAC LASER EQUIPMENT:

American Optical Company
Bell Telephone Laboratories
General Telephone & Electronics
Lincoln Laboratory of M.I.T.
National Aeronautics & Space Adm.
Perkin-Elmer Corporation
Westinghouse Air Arm Division
International Business Machines
Radio Corporation of America
Avco Corporation
Harvard University
McMasters University
University of Dayton
University of Virginia

Be sure you get full information on Electro Powerpacs Light Pumps before you make your final selection.

ELECTRO POWERPACS, INC.
A Subsidiary of Hydra-Power Corporation
6 HADLEY STREET, CAMBRIDGE 40, MASS.

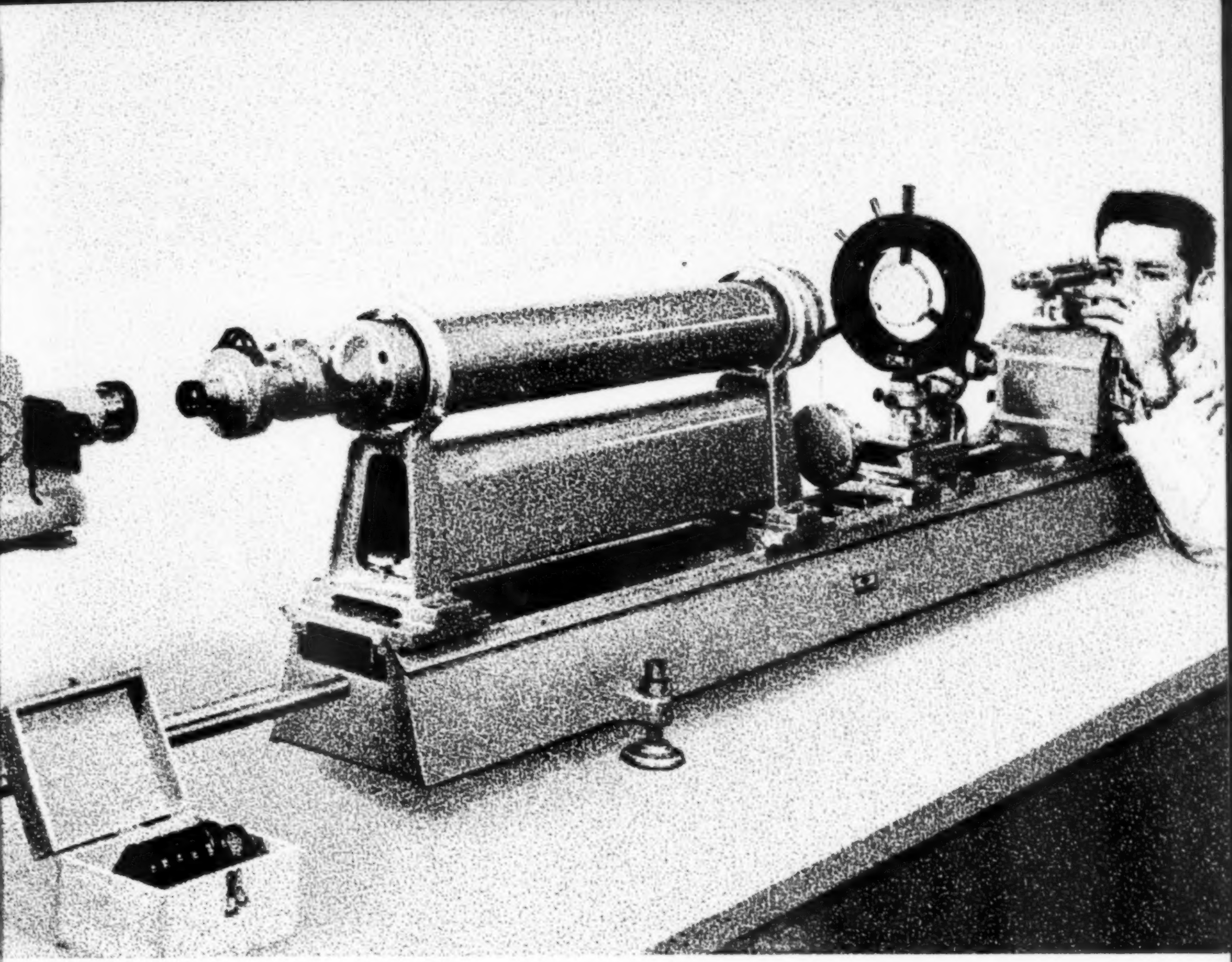

You owe it to your work . . .

You owe it to your work to avoid compromise in the selection of optical instruments. Equipment must be equal to your abilities and to the challenge of your work. Gaertner provides such instruments. For example, the lathe-bed-type optical bench owes its acceptence to its dependably permanent straightness, achieved by precision grinding of V and flat ways directly on a substantial casting of normalized meehanite. The complete assembly is widely used for measuring the focal lengths and aberrations of lenses and lens systems. The precision bed and carriages with rotary and three-way motions are available separately. These, together with a large selection of holders, diaphragms, slits and other accessories, provide versatile equipment for experimental setups where alignment and stability are important. Further, a number of beds can be bolted together end-to-end to provide a bench of any desired length. To meet unusual needs, Gaertner offers modifications of its wide range of precision optical and measuring instruments as well as special systems from your drawing or sketches. (Gaertner people have been doing this in Chicago since 1896.) For complete information on Gaertner optical and instrument benches, send for Bulletin 156-59. Find out why Gaertner instruments are the equipment of choice for the serious investigator. GSC-2-219

Inquire about employment opportunities for physicists and technical personnel

Gaertner

Gaertner Scientific Corporation 1294 Wrightwood Avenue Chicago 14, Illinois, U.S.A. Area Code 312, BUckingham 1-5335

OPTOVAC

HIGH QUALITY STANDARDS

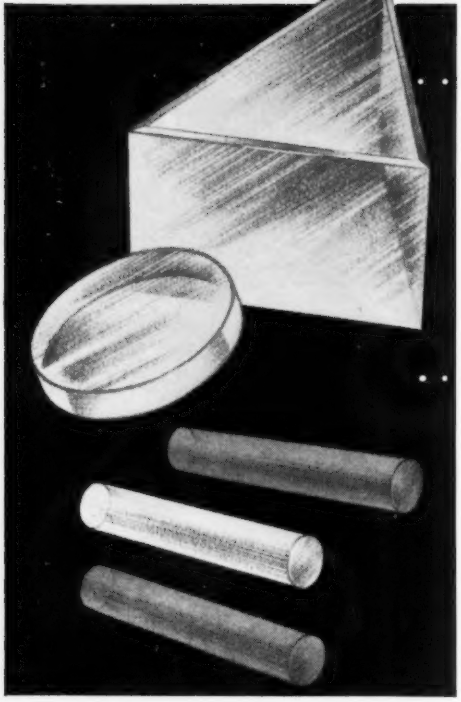

. . . . in Optical Crystal Blanks

Calcium Fluoride	Sodium Chloride
Barium Fluoride	Potassium Chloride
Lithium Fluoride	Potassium Bromide

• *Prompt Delivery* • *Large Size Availability*
• *Precision Cutting* • *Scattering Free*
• *Impurity Absorption Free* • *Strain Free*

. . . . in Optical Maser Crystals

Optovac offers a complete line of rare earth, transition element, and uranium doped crystals of calcium fluoride, barium fluoride, strontium fluoride, and cadmium fluoride, for optical maser research.

Indicative of Optovac quality is the table below which is a complete listing (to June 1962) of mased fluoride crystals, with many Optovac "firsts" as the crystal source. Included in the table are two units which can be supplied as guaranteed CW quality. All of the others in the table are available as guaranteed pulse maseable units.

	MASER	OUTPUT WAVELENGTH	MAX. TEMP.	FIRST MASING DATA
Fluoride Optical Maser Crystals	$U^{+3} \cdot CaF_2$	2.61 microns	295°K pulsed	pulse mased 1 *
		(also 2.51, 2.2)	77°K CW	CW operation 3 *
	$U^{+3} \cdot BaF_2$	2.55 microns	77°K	pulse mased 2 *
	$U^{+3} \cdot SrF_2$	2.40 microns	77°K	pulse mased 3 *
	$Nd^{+3} \cdot CaF_2$	1.05 microns	77°K	pulse mased 3 *
	$Nd^{+3} \cdot BaF_2$	1.05 microns	77°K	pulse mased 3 *
	$Nd^{+3} \cdot SrF_2$	1.05 microns	295°K	pulse mased 3 *
	$Sm^{+2} \cdot CaF_2$	7082. A	4°K	pulse mased 1
	$Sm^{+2} \cdot SrF_2$	6969. A	20°K	pulse mased 1 *
	$Tm^{+3} \cdot SrF_2$	1.97 microns	77°K	pulse mased 3 *
	$Tm^{+2} \cdot CaF_2$	1.11 microns	20°K	pulse mased 3 *
				pulse mased 4
	$Ho^{+3} \cdot CaF_2$	2.092 microns	77°K	pulse mased 3 *
	$Dy^{+2} \cdot CaF_2$	2.36 microns	77°K	pulse mased 4
				CW operation 3 *
				CW operation 4

First masing: 1-IBM 2-MIT (Miles) 3-BELL LABS 4-RCA
* — Denotes Optovac, Inc. as source of crystal used.

OPTOVAC, INC.

NORTH BROOKFIELD, MASSACHUSETTS

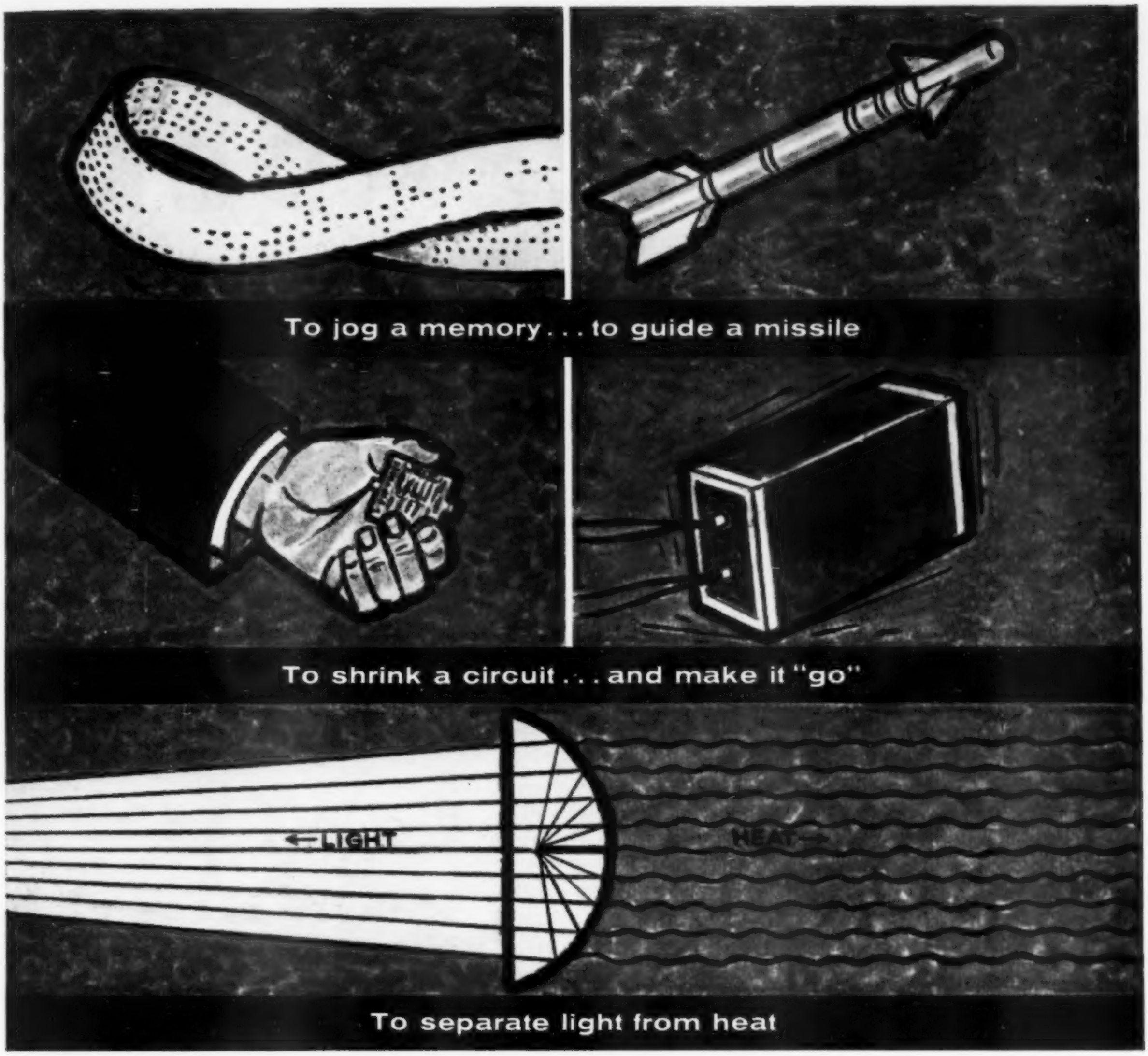
To jog a memory . . . to guide a missile
To shrink a circuit . . . and make it "go"
←LIGHT
HEAT→
To separate light from heat

. . . rely on Bausch & Lomb

MULTI-FILMS

First it was thin films, pioneered by Bausch & Lomb a generation ago. Now multi-films — perfected by Bausch & Lomb — usher in the "miracle" state of the art. From enhancing the speed and accuracy of computer memories . . . to protecting solar cells from harmful radiation . . . B&L Multi-Films control heat, light and wavelength to meet your most sophisticated design specifications.

We're now designing, producing and delivering multi-film components in five major classes: color filters, color separating filters, heat control filters, neutral beam dividers, first surface mirrors. And you can be sure of the precision and efficiency essential to end-product success . . . because you're dealing with the world's prime source, equipped with the world's most comprehensive facilities, staffed with the world's leaders in multi-film technology.

BAUSCH & LOMB

BAUSCH & LOMB INCORPORATED
77133 Bausch Street, Rochester 2, N. Y.

☐ Please send me B&L Multi-Film Handbook E-306.

Name..

Professional
Address...

....

....

Semi-Elements, Inc.

LASER LEADERS

The progressive organization and highly Specialized Facilities of Semi-Elements enable us to offer the largest variety of LASER and MASER single crystals available.

Most Complete—Highest Quality

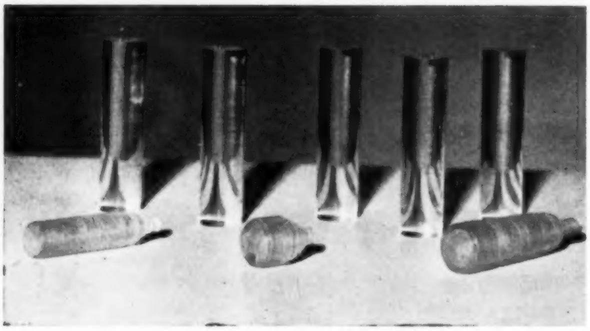

Research and Development

NOW AVAILABLE—

Sodium Terbium Borate

Cobalt Manganese Fluoride

Full Scale Production of

$CaWO_4$ SINGLE CRYSTALS

DOPED WITH RARE EARTHS AND TRANSITION ELEMENTS

GLASS LASERS
PLASTIC LASERS
LIQUID LASERS

doped with rare earths and transition elements.... available from stock. Special requirements and sizes quoted on request.

Single Crystal Chips
$15.00 to $40.00 each

STOCK LASERS

CaF_2, BaF_2, CdF_2, SrF_2, TiO_2, MgO, $RbMnF_2$, $CaWO_4$, Al_2O_3, $KMnF_2$, $SrWO_4$, $SrMoO_4$, $SrF_2 \cdot BaF_2$, $SrF_2 \cdot CaF_2$, $SrF_2 \cdot BaF_2 \cdot CaF_2$.

Write for Complete Literature—or Phone

SINGLE CRYSTAL DIVISION Dial 412-352-1548

SEMI-ELEMENTS, INC.

SAXONBURG BOULEVARD, SAXONBURG, PA., U.S.A.

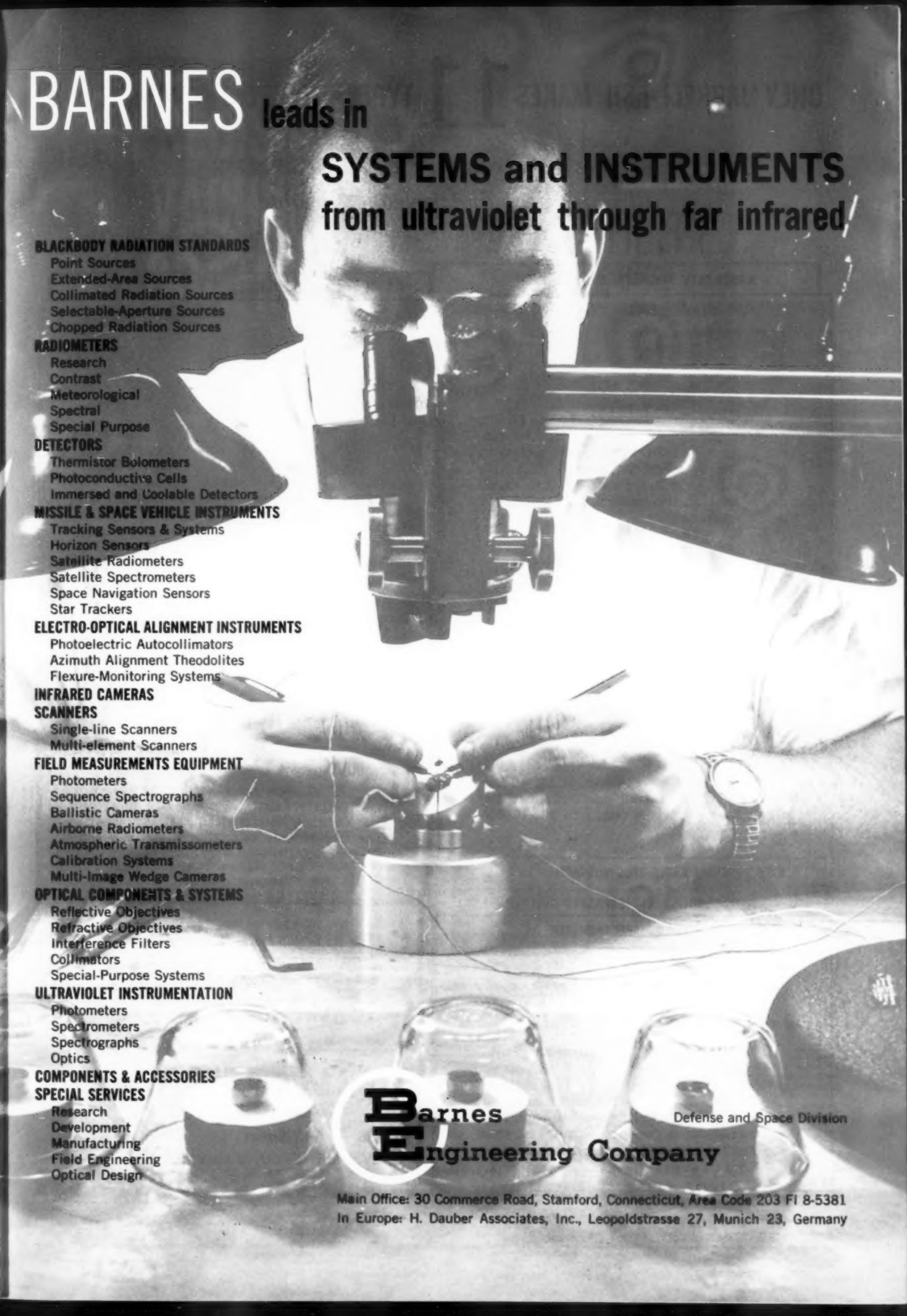

BARNES leads in

SYSTEMS and INSTRUMENTS
from ultraviolet through far infrared

BLACKBODY RADIATION STANDARDS
- Point Sources
- Extended-Area Sources
- Collimated Radiation Sources
- Selectable-Aperture Sources
- Chopped Radiation Sources

RADIOMETERS
- Research
- Contrast
- Meteorological
- Spectral
- Special Purpose

DETECTORS
- Thermistor Bolometers
- Photoconductive Cells
- Immersed and Coolable Detectors

MISSILE & SPACE VEHICLE INSTRUMENTS
- Tracking Sensors & Systems
- Horizon Sensors
- Satellite Radiometers
- Satellite Spectrometers
- Space Navigation Sensors
- Star Trackers

ELECTRO-OPTICAL ALIGNMENT INSTRUMENTS
- Photoelectric Autocollimators
- Azimuth Alignment Theodolites
- Flexure-Monitoring Systems

INFRARED CAMERAS

SCANNERS
- Single-line Scanners
- Multi-element Scanners

FIELD MEASUREMENTS EQUIPMENT
- Photometers
- Sequence Spectrographs
- Ballistic Cameras
- Airborne Radiometers
- Atmospheric Transmissometers
- Calibration Systems
- Multi-Image Wedge Cameras

OPTICAL COMPONENTS & SYSTEMS
- Reflective Objectives
- Refractive Objectives
- Interference Filters
- Collimators
- Special-Purpose Systems

ULTRAVIOLET INSTRUMENTATION
- Photometers
- Spectrometers
- Spectrographs
- Optics

COMPONENTS & ACCESSORIES

SPECIAL SERVICES
- Research
- Development
- Manufacturing
- Field Engineering
- Optical Design

Barnes Engineering Company

Defense and Space Division

Main Office: 30 Commerce Road, Stamford, Connecticut, Area Code 203 FI 8-5381
In Europe: H. Dauber Associates, Inc., Leopoldstrasse 27, Munich 23, Germany

ONLY JARRELL-ASH MAKES 11 TYPES OF SPECTROMETERS...

because no one spectrometer is versatile enough for all analytical and research problems

WADSWORTH STIGMATIC SPECTROGRAPH

HIGH APERTURE SPECTROGRAPHS

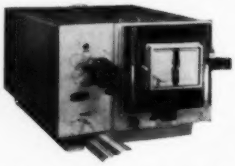

F/6.3 plane grating instruments for analysis of faint or short duration light sources as encountered in combustion studies, shock tube investigations, high temperature and free radical studies; time resolved spectroscopy. Photoelectric attachment available.

1M & 2M NORMAL INCIDENCE VACUUM SPECTROGRAPHS

1M & 0.5M SEYA-NAMIOKA VACUUM SPECTROMETERS

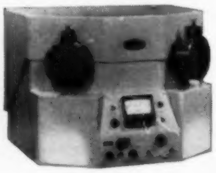

Vacuum Scanning Spectrometers, Seya-Namioka Model available in 1.0 or 0.5 meter models with optional camera and light sources and detectors for absorption and emission studies. Virtually universal monochromators, they offer a complete scanning range from 0 to 10,000A.

6.65M VACUUM EAGLE SPECTROGRAPH

1.8M EVACUABLE EBERT SCANNING SPECTROMETER

0.5M EBERT SCANNING SPECTROMETER

0.5 meter Ebert-type plane grating instrument is available with a variety of photomultiplier receivers and electronics systems. Also available as a flame spectrometer with full accessories. Applications include combustion and reaction studies, flame temperature measurement and atomic absorption spectroscopy.

5.0M VACUUM SPECTROGRAPH

1.0M EVACUABLE EBERT SCANNING SPECTROMETER

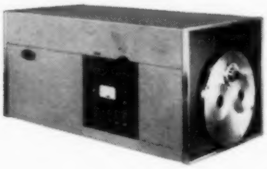

For direct measurement of relative line intensities . . . ultra high resolutions. Equipped with 12-speed precision linear wavelength scanning drive. High aperature (F/8.6). Very high photoelectric speed. Similar to 1.83M ultra high resolution spectrometer.

1.0M VACUUM GRAZING INCIDENCE SPECTROGRAPHS

3.4 and 2.25M EBERT SPECTROGRAPHS

These instruments may be fitted with multiple photomultipliers or adapted for precise scanning work. The Ebert, with order sorter, permits high resolution studies to be made with ease. Plasma sources, laser, crystal studies, high temperature measurements, combustion studies only hint at the spectrometer's full range of applications.

Let us bring your files up to date with complete information about all eleven. Write for literature or ask to have our analytical methods engineer visit your laboratory.

Jarrell Ash

JARRELL-ASH COMPANY

26 Farwell Street
Newtonville 60, Massachusetts

PRECISION VACUUM COATING

DESIGNED FOR

VERSATILITY

FOR TODAY'S NEEDS

The coating department of Kinney Vacuum has employed the vacuum deposition process to produce thin films to control light, heat and color for over fifteen years. They have developed many new techniques to meet customer requirements, such as coatings to provide high transmission in the infra-red on optics made from Germanium and Silicon, coatings on metal substrates to provide very low solar emmissivity, mirrors for solar collection or solar simulation, transparent films with high heat reflection properties; ultra-thin, virtually weightless coatings for use in orbital vehicles in the space program.

The most modern equipment designed and built by Kinney Vacuum measure film thickness during actual evaporation. Our Research and Development laboratory uses Spectrophotometers, Reflectometers, interferometer devices to measure each research problem. Highly trained research technicians constantly provide new methods and techniques to produce better product.

In new exotic techniques in Vacuum deposition of film or regular production of low or high reflection films, the coating department of Kinney Vacuum offers the ultimate.

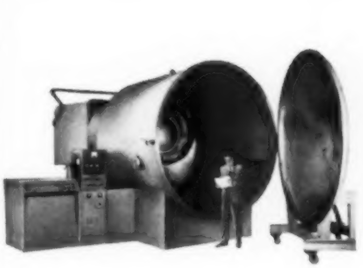

The facilities in the Coating Department incorporate coating equipment of the latest design. Coating chambers from the standard 18" dia. bell jar type to steel chambers 9 feet in dia. by 9 feet long are utilized. This equipment has been designed to produce many of the vacuum coatings that are commonly used today. Coating technicians have years of experience and proven ability in all phase of vacuum coatings.

KINNEY VACUUM
COATING DEPARTMENT

DIVISION THE NEW YORK AIR BRAKE COMPANY
3529 WASHINGTON STREET • BOSTON 30, MASS.

LASER COATINGS

99.6 Per Cent Reflectance

HIGH-EFFICIENCY DIELECTRIC COATINGS — obtained by Fabry-Perot vacuum-deposition techniques — are just one of the many capabilities of Infrared Industries, Inc. in visible and infrared optics. IRI products and services, presently contributing to MIDAS and other military infrared programs, include:

INFRATRON® INTERFERENCE FILTERS
In the visible: Standard 1% bandwidths corresponding to most widely used wavelengths from 4047Å (Hg) to 7698Å (K). In the infrared: dichroics and bandpass types (including 0.1% "spikes") from 0.8 out to 12 microns. Dielectric substrates; up to 8″ diameters; many available from stock.

LEAD SULFIDE IMMERSED OPTICS
Increased optical gain/angular coverage achieved by direct chemical deposition onto high-index optical substrates. Compatible materials include sapphire, strontium titanate, rutile, silicon, moldable IRTRAN II.

LEAD SULFIDE MOSAICS
For precise field-of-view resolution with highest detectivity in the near-IR.

OPTICAL ACCESSORY GLASSWARE
Gas cells; Dewars; glass-to-metal, glass-to-sapphire (or other IR-transmitting material) seals; special gas, liquid or vacuum "plumbing".

Send for catalogs and technical data.

IR INDUSTRIES, INC.

INFRARED INDUSTRIES, INC., P. O. Box 42, WALTHAM 54, MASS.

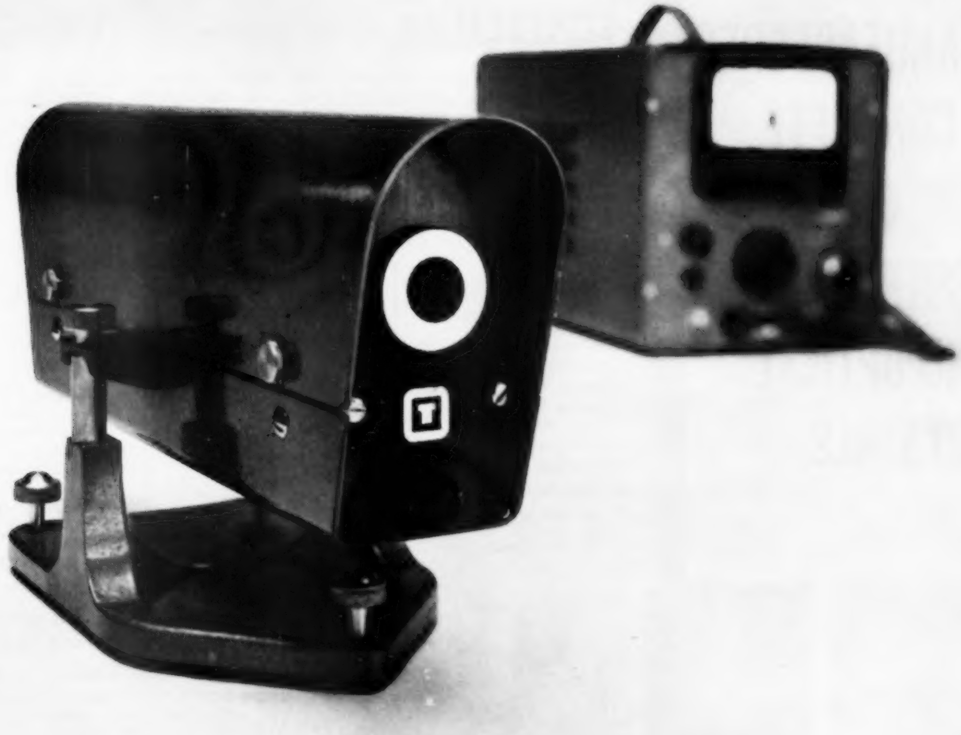

PRECISION LABORATORY LASER/$995

Now: A low-priced precision source of coherent pulsed light, complete with power supply, designed to accommodate a wide range of accessories for advanced research. The elliptical optical cavity gives high pumping efficiency, and is demountable for easy access to the Xenon lamp and LASER crystal holder. Standard accessories—a cryogenic cooling dewar, Fabry-Perot interferometer, optical bench mount, rubies with highly efficient multi-layer end reflectors—greatly extend experimental research capabilities.

Other new products

OPTICAL CALORIMETER/$650 Entirely new, measures CW or pulsed LASER energy from .05-200 joules, through the visible and infrared spectrum, independent of pulse length.

RUBY LASER INTERFERENCE FILTER SET/$350 includes seven *all dielectric* mirrors and beam splitters at several levels of attenuation, a MONOPASS filter at 694 millimicron ruby wavelength, and calibration curves.

OPTICS TECHNOLOGY, INC

248 HARBOR BOULEVARD
BELMONT, CALIFORNIA
LYtell 1-0358 (Area Code 415)

For additional information, write OTI or your nearest OTI representative: New England: H. J. Schuft Co.; New York, Metropolitan: RMC Associates: New York, Upstate: E. W. Stone Co.; Mid-Atlantic: C. E. Snow Co.; So. California: Abbott Instrument & Engineering; No. California: Charles Long Associates

HARSHAW MANUFACTURES A COMPLETE LINE OF SCINTILLATION AND OPTICAL CRYSTALS

SCINTILLATION *Mounted* NaI(Tl) *Crystals*

Crystal detectors designed for the most sophisticated counting problems. Our physics and engineering group are available to assist you in your special detector problems.

More detailed information is contained in our 32-page book, "Harshaw Scintillation Phosphors". We invite you to write for your free copy!

STANDARD LINE

(Hermetically Sealed Crystal Assemblies)

- The accepted standard of the industry
- Proven through years of service in research, medical and industrial applications
- unparalleled performance
- dependability
- consistent good quality

INTEGRAL LINE

(Crystal photo multiplier tube combination assembly)

- Improved resolution
- Ready to use plug-in unit
- Permanently light sealed
- Capsule design facilitates decontamination
- Close dimensional tolerances
- Harshaw guaranteed

Large Crystal MATCHED WINDOW LINE

(Designed primarily for crystals 4" dia. and larger)

- "Small crystal" performance achieved through improved optical design
- Low mass containers
- Available in standard aluminum or complete low background assemblies
- Convenient mounting flange
- Ready to use

Every Harshaw crystal is a product of our experience in crystal growing technology since 1936

Other Phosphors Available from The Harshaw Chemical Company

ROUGH CUT THALLIUM ACTIVATED SODIUM IODIDE CRYSTAL BLANKS • EUROPIUM ACTIVATED-LITHIUM IODIDE (NORMAL) • EUROPIUM ACTIVATED LITHIUM IODIDE (96% Li^6 ENRICHED) • THALLIUM ACTIVATED CESIUM IODIDE • THALLIUM ACTIVATED POTASSIUM IODIDE • ANTHRACENE • PLASTIC PHOSPHORS

OPTICAL *Crystals*

For Infrared and Ultra Violet Transmitting Optics

"HARSHAW QUALITY" INHERENT IN EACH HARSHAW-GROWN CRYSTAL GUARANTEES THE MOST EFFICIENT OPTICAL TRANSMISSION POSSIBLE THROUGH:

1) Negligible light scattering in crystals, permitting higher sensitivity and improved resolution
2) Freedom from absorptions caused by trace impurities in crystal optics
3) Minimum strain

"HARSHAW QUALITY" meets the demand for uniformity of optical properties such as dispersion and refractive index.

Prices, specifications, or other information will be sent in answer to your inquiry.

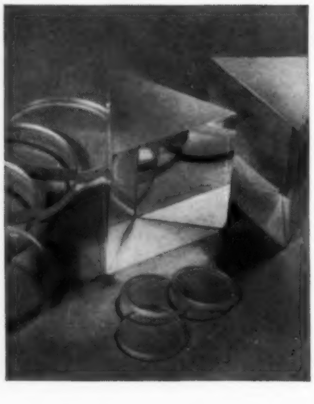

The following infrared and ultra violet transmitting crystals are available; others are in the process of development:

SODIUM CHLORIDE • SODIUM CHLORIDE MONOCHROMATOR PLATES • POTASSIUM BROMIDE • POTASSIUM BROMIDE PELLET POWDER (through 200 on 325 mesh) • POTASSIUM CHLORIDE • OPTICAL SILVER CHLORIDE • THALLIUM BROMIDE IODIDE • LITHIUM FLUORIDE • LITHIUM FLUORIDE MONOCHROMATOR PLATES • CALCIUM FLUORIDE • BARIUM FLUORIDE • CESIUM BROMIDE • CESIUM IODIDE

Additional information on the physical and optical properties of the above crystals is available in our 36-page booklet "Synthetic Optical Crystals". Send for your free copy.

HARSHAW

THE HARSHAW CHEMICAL CO.
Crystal Division • Cleveland 6, Ohio

Recent Developments in Infrared Technology

Stanley S. Ballard and William L. Wolfe

Developments in infrared technology are proceeding at a rapid pace. A sampling is given of advances made during the last three years. Illustrative items are taken from the categories of new instruments, components, and techniques.

Introduction

Basic research and applied technology supplement and complement each other in a manner that is beneficial to both. This statement, accepted today by many as a truism, is also an appropriate characterization of the way the phenomena and the applications peculiar to the infrared portion of the spectrum have broadened and have become better understood. The most recent and probably the most comprehensive review of the status of infrared physics and technology is contained between the covers of the September 1959 issue of the *Proceedings of the Institute of Radio Engineers*. Three years having passed since the time of preparation of that opus, it seems appropriate to review the status once again, and this is particularly appropriate in an issue of *Applied Optics* that features infrared techniques.

The three-year era was characterized by the appearance of new, rapid, sensitive detectors; novel and ingenious solutions to instrument problems; wider application of infrared equipments to the exploration of our earth and of space; and tremendous emphasis on the means by which infrared techniques can be utilized in the defense against intercontinental ballistic missiles. Most of the innovations in instrumentation have come from the fruits of basic research, but some have led in turn to a reconsideration of basic principles: The very practical problem of what radiations are emitted in the optical (0.2 to 2000 μ) part of the spectrum by ballistic missiles has led directly to frontier research in the nature of aerodynamic flow fields, the locations and density distributions in the missile plume of various atoms, molecules, and ions, their excitation states and the nature of the radiation they emit. Although it is not possible to relate all of the steps forward because of restrictions of both manuscript length and military security, we will attempt to draw attention to some interesting and representative results.

Prodded by the double spur of radiation physicists and military system designers, atmospheric physics has made bold strides. The physicists would like to have at hand reliable measurements of radiation values of missiles after correction for atmospheric absorption and scattering. The system designers would like to have both the true radiation values and the atmospheric transmission data, so they could calculate the irradiance from a specified target at any range. Elsasser[1] provided the first, albeit somewhat restricted, method of calculation for obtaining band transmission, and he has been followed by Goody,[2] Zachor,[3] Plass,[4,5] and others. To date, the best methods of calculating atmospheric transmission of infrared radiation over long slant paths seem to be those of Altshuler,[6] Carpenter,[7] Green,[8] and Plass.[4,5] Recently, John N. Howard, of Geophysics Research Directorate, gathered a group of people together to assess these models. They found wild disagreement, but mostly due to differing assumptions about the constituents of the atmosphere. It is to be expected that this group will come to agreement within the next few months, and the scientific community will be the better for it; a best, if not absolutely correct, model for atmospheric transmission is the key step to many unsolved problems today.

In a parallel and equally important undertaking, the great complexities of the nature of radiation from powered missiles and reentering nose cones are being unraveled. The powered rocket has behind it a great trail of combustion products such as CO_2 and H_2O blanketed within a turbulent boundary wave and distributed among Mach diamonds and regions of high and

---

Stanley S. Ballard is in the Department of Physics, University of Florida, Gainesville, Florida; William L. Wolfe is at the Institute of Science and Technology, The University of Michigan, Ann Arbor, Michigan.

Received 15 June 1962.

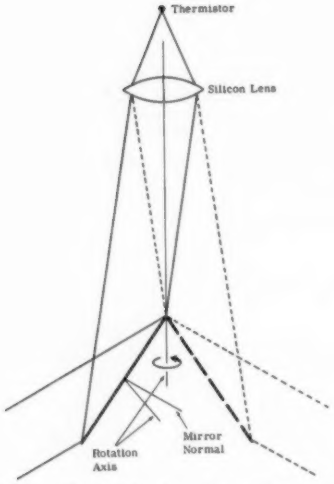

Fig. 1. Typical horizon sensor, schematic.

low pressure. The volume of this plume is not isotropic, or homogeneous, or stationary. As the missile rises, a great bow wave develops, the turbulent layer becomes less dense on expansion, and the internal structure of the plume redistributes itself. The description of reentry radiation phenomena is hardly less complex—but there has been encouraging progress on these tasks.

The maturity—or possibly the advanced state of maturation—of what is usually called the infrared field is indicated in part by the increasingly large number of "off the shelf" instruments, which not long ago were the pride and joy of some graduate student or a laboratory technician. These instruments, to repeat our theme, are the product of technology but they immensely assist the pursuit of basic research. From any of five to ten companies one can now purchase such items as carefully controlled blackbody sources ranging in temperature from ambient to over 1000°C and with a large variety of aperture sizes; trackers with 0.01 mrad static accuracy; and radiometers in many shapes, sizes, and with different focal ratios and degrees of optical perfection.

No introduction to a paper on instrumentation would be complete without a reference to optical masers. Our duty in this respect is discharged simply by referring to the many articles on masers and lasers that have already appeared in the literature, including *Applied Optics*.

Horizon Sensors

One of the most spectacular applications of infrared devices is that of using the infrared horizon to determine the local vertical in a satellite reference system. Present horizon sensors may be divided into two groups: those which scan and those which do not. A typical instrument of the latter type has four thermistor flakes and an image of the earth in the focal plane, so that the detectors are placed at 90° intervals around the earth circle. If the optical axis is coincident with the local vertical, all detectors should give the same output signal; but if the optical axis deviates from the local vertical, one thermistor flake senses a higher power level while the level on the opposite detector diminishes. When the two signals are subtracted, the deviation from zero is proportional to the error—*if* the irradiance due to the earth is uniform in the focal plane. When deviations are noted on all detectors, a slightly more complicated comparison between detectors is required. This simple device is subject to errors too numerous to discuss; important among them are the aberrations of the wide field and the variability of the earth's irradiance at the instrument exit pupil.

Scanning horizon sensors may be grouped according to the way they scan. Only one type of scanning horizon sensor will be described here, the tracking scanner, which is probably the most accurate type.

A typical tracking sensor is shown schematically in Fig. 1. The scanning technique is the familiar hypocycloidal scan obtained by superimposing two circular scanning motions on a single mirror. One motion governs the rate at which the entire horizon circle is scanned—the revolution rate—the other determines the number of times the field of view crosses the horizon per revolution—the cycle rate. The scanning mirror is usually set at an angle that corresponds to the average position of the horizon circle; the excursion of the other motion is then set to include the total uncertainties so that the actual horizon circle *will* fall within the scan excursion. This traverse is usually about 10°; there are usually about 10 cycles per revolution and the field of view of the instrument is 0.2 to 1.0°.

There are two types of errors associated with horizon sensors, although in some cases it is difficult to differentiate between them. One may be classified as system errors, denoting those unavoidable inaccuracies when an imperfect equipment is viewing a perfect target. The other, called natural errors, are errors which exist when a perfect equipment looks at an imperfect target—the real horizon. The same natural errors can be reduced by appropriate signal processing, so it is not advisable to call them inherent errors. The earth is an oblate spheroid rather than a perfect sphere, and the degree of oblateness contributes an error which is usually not corrected by the horizon sensor. It is probable that in no part of the optical spectrum is the actual surface of the earth visible from space, so some equivalent horizon must be used as a reference. The double difficulty here is that no one has yet found the perfect discontinuity which can be used (although the tropopause seems best at the moment), and it is not possible to relate the position of this discontinuity with adequate precision to the surface itself. The last of the natural errors is the frequent occurrence of very high altitude, very cool clouds which can mask the warmer temperature signal from the tropopause horizon.

The nonscanning sensor is limited to some extent by its large field of view. The integrating effect of such a field of view can in the presence of cold clouds cause errors up to 5° at the nadir at 480 km altitude, due to the masking effect of these clouds near the horizon. This device is less sensitive to the effect of oblateness because of the smoothing effect of the optical system; errors of approximately 0.1° will be common at 480 km. Other effects such as nonuniform sensitivity over the thermistor surface and the presence of the sun will cause more serious problems in this device than in the scanning sensors due to the large area in the image plane seen by one detector. The nonscanning devices have an extremely low instrument noise because of their simplicity of design and would sense the local vertical of an ideal planet to within 0.1°; however, the earth being extremely nonideal will induce average errors greater than 1° at 480 km. At altitudes of above 8000 km the system accuracy should approach the instrument accuracy.

The scanning sensor, which is essentially a scanning or tracking telescope, is characterized by relatively high angular resolution and high instrument accuracy. Consequently, the detection of finely resolved points near the horizon may be used to compute the apparent vertical more accurately after bad points have been discarded, and the oblateness error can be minimized if the approximate position of the platform relative to the earth is known. If the computer has proper system logic and a sufficient memory, the effects of cold clouds may also be minimized. However, for many horizon sensors of this type, system noise is presently the limiting accuracy, although it should be possible to reduce the typical errors of 0.5 to 1.0° by using more sensitive detectors.

The uncertainties which presently exist in the design and evaluation of horizon scanners are due to the paucity of data about the physical properties of the atmosphere, particularly the radiative properties of the horizon, and although they were satisfactory for stabilizing Liberty Seven, Tiros, and other satellites, they can be improved only after the fundamental research has been done.

The Germanium Modulator

A wedding of the ideas of solid-state physics and infrared communications has resulted in the conception of a new method for modulating an infrared beam. Infrared radiation from a suitable source is collimated by a lens or mirror, and the collimated beam passes through a plate of germanium; then, as the free carrier concentration is varied, the resultant change in absorption provides the modulation.

According to the modern version of the Drude electron theory, the extinction coefficient of the germanium is proportional to the density of free carriers; the absorption coefficient is proportional to the extinction coefficient and therefore the density of carriers, but the absorptance is related exponentially to these quantities. Thus the transmitted power is a sensitive function of the carrier density. The free carriers are generated by using a germanium diode as an optical filter. Figure 2 illustrates such a diode; the electric current i passes through from top to bottom while the infrared radiation passes from left to right. The percent modulation of such a device can be defined as $(I_T - I_T')/I_T$, where I_T is the radiation intensity transmitted by the diode when no current is applied and I_T' is the same quantity when current is applied. The modulation efficiency can be defined in a similar way, as $(I_T - I_T')/I_o$, where I_o is the input radiation intensity. Experimental values given[9] are that modulations of 50% at $6\ \mu$ and 95% at $12\ \mu$ were obtained with less than 1% phase distortion. Although germanium when used as a photodetector—with or without impurities—has a time constant of about 10 μsec, the modulator does not respond to 17,500 cps, but to about 1750 cps—an order of magnitude less. The reasons for this effect are not yet clear and presently are stimulating additional research in this new realm of solid-state physics.

An earlier application of this technique by Lasser *et al.*,[10] called Filterscan utilized a piece of silicon through which infrared could pass. An electron beam was scanned across this material, generating free carriers where it struck and thereby causing a portion of the incident radiation to be "blanked out." The result of such a negative scanning process could be sensed electrically. This device proved to have considerable noise and of course required wide-angle optics which even today are at a premium.

Interferometric Spectrometry

The renaissance of interferometric spectroscopy has a lively application in military infrared instrumentation,

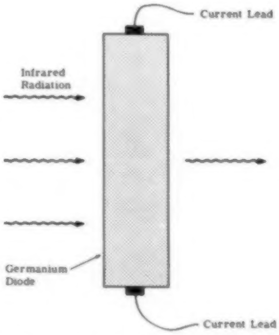

Fig. 2. Germanium modulator.

and the growth has been rapid. The advantages, usually given in terms of "through-put" and "finesse," amount to the fact that an interferometer, which by most reasonable standards (size, or area of foreoptics' entrance pupil) is equivalent to a dispersing instrument, can obtain a spectrum of given resolution many times as fast as the disperser, or it can take the same amount of time to obtain a much better spectrum. Such interferometric instruments have been used as delicate laboratory devices for obtaining the ultimate in precision and resolution, and there has been a great deal of discussion concerning the pros and cons of the disperser with its inherent or "built in" data processing system and the interferometer which requires a more than insignificant amount of auxiliary apparatus. But the advantage is all with the interferometer in many military applications which impose stringent requirements on response time, simplicity, and size. The understanding of rocket plume radiation has already been mentioned as a most pressing problem. Measurements made from the ground incorporate the ambiguities due to the atmosphere, and even high-flying aircraft need air, so that it was natural to suggest an experiment using an instrument carried aloft by a rocket. Here a small interferometer has been used to obtain the spectrum in the same time and with the same resolution that a larger spectrometer would. The processing can be done any time, but the instrument must be small for this application.

The arrangement which has often been used is just a small-size Michelson interferometer—small compared with the roomfuls of apparatus used by Chabal, Gebbie, Jacquinot, and others—weighing about 2 kg and displacing about 910-cm cube. The device has been placed on board some of the larger missiles and has made measurements from that vantage point. Quite naturally, the most serious problems center around the establishment of a uniform drive which is not affected by the tremendous vibration encountered near the rear of a missile as it roars from the launching pad and as it continues into the air with hundreds of thousands of kilos of thrust.

Present-day devices are by no means satisfactory on all counts; experience is still teaching the lesson of how to make the drive impervious to environmental effects, how compensator plates and other materials are affected by intense radiation, and how the microphonics and vibrations influence the calculated spectrum. But interferometric spectroscopy seems to have "arrived" as a field technique.

Airborne Spectrometers

Airborne interferometers have the advantages of small size and weight just mentioned, but on the ground there must be a considerable amount of data-processing equipment, and the time involved in analyzing the data may be lengthy. The other attack on the problem is to put a complete spectrometer in the air and record the final spectral data there. This results in heavier and bulkier airborne instrumentation, but the data extraction is rapid. Three types of modern airborne spectrometers are mentioned briefly to illustrate possible methods:

Balloon-borne instruments can be larger and heavier than rocket-borne gear, and they have the advantage that they work in a relatively stable environment. For some years the University of Denver has had a team engaged in high-altitude studies of atmospheric transmission in the near infrared.[11] These studies have been conducted using a small, automatic-scanning balloon-borne spectrometer to measure solar spectra at various altitudes up to 30 km. Their first instrument was equipped with a PbS detector and a quartz prism and was limited to wavelengths shorter than 2.7 μ. The wavelength range was subsequently extended to beyond 4.3 μ by using an LiF prism and an uncooled PbSe detector. Since it was desired to extend the range so as to include the water-vapor band at 6.3 μ and the ozone band at 9.6 μ a new single-beam Littrow-type instrument was designed, using basic optical elements of the type employed in the single-beam Perkin-Elmer spectrometers. With a rocksalt prism and a thermistor-bolometer detector, solar spectra can now be obtained throughout the entire infrared region of interest. The important auxiliary piece of equipment is a sun-seeker which maintains the sun's image on the slit of the spectrometer. The spectra, as well as information on time, altitude, temperature, and relative humidity, are recorded on magnetic tape and the records are retained in the balloon, so that telemetry data links are not necessary.

Two different systems can be used in a spectrometer to cover the wavelength range of interest. The prisms can be rotated in a Littrow arrangement and a single detector employed, as is done in the Denver instruments and also in the Bendix device described below, or there can be a multiplicity of detectors arranged around the focal plane of the "camera" portion of the spectrograph so that all parts of the spectrum are recorded at all times. The latter arrangement results in a less completely continuous spectral coverage but avoids the possibility that an event may be recorded at some wavelengths but missed at other wavelengths because of the time sequencing inherent in a single-detector, wavelength-scanning device.

The airborne spectrometer system designed and built at the Lockheed Aircraft Corporation, California Division,[12] under the sponsorship of the USAF Aeronautical Systems Division, is of the multiple-detector type. It is designed to be installed and flown in a C-130 aircraft. The external optics are a 55-cm diameter, *f*/4 Cassegrain system. A 2500 cps chopper disk also separates the incoming beam into two beams, each of which goes through a three-prism, single-pass spectrometer. Each spectrometer is equipped with 20 separate detectors, each covering a prescribed wavelength band. One spectrometer (LiF prisms) covers the region 2 to 5 μ and uses cooled PbSe cells; the other (NaCl prisms) covers the region 5 to 15 μ and uses cooled, copper-doped germanium-silicon-alloy detectors. There is an internal blackbody calibration source that can be employed prior to data runs. Following the 40 channels of preamplifiers there is a commutator which multiplexes the detector signals, after which they are tape recorded for later analysis on the ground. Another feature is a small radiometer which receives and records total radiation from the target source—this information, along with an oscilloscope presentation of the outputs from the 40 channels, is useful to the operator in monitoring the system from his console. The spectrometer is equipped with an auxiliary tracker with 15 cm diameter, *f*/5 optics and a 1° field of view.

The airborne spectroradiometer developed at the Bendix Systems Division for the Air Force Cambridge Research Laboratories is of the wavelength-scanning type.[13] This large instrument is installed in a KC-135 aircraft for data collection at altitudes up to 12 km. It covers the spectral range 0.25 to 15 μ. Through the use of reflective choppers, dichroic filters, and multiple exit slits, five types of data are acquired simultaneously: spectral data in the regions 0.25 to 0.6 μ, 0.6 to 5 μ, and 5 to 15 μ; radiometric data in the regions 0.25 to 0.6 μ and 0.6 to 15 μ. The entrance optics are of 51 cm aperture and *f*/5 focal ratio. A high-resolution optical tracker is built into the instrument to assure a tracking accuracy of 0.1 mrad; the field of view of the spectrometer–radiometer is 0.2 mrad. The detectors used are S-13 response multiplier phototubes for the ultraviolet and visible regions, cooled PbSe for the short-wavelength infrared, and copper-doped germanium cooled to 17°K for the long-wavelength region. The two spectrometer systems employ single Littrow prism arrangements with LiF for the short-wavelength region and NaCl for the long-wavelength region. The spectral scanning rate can be set at 0.5, 4, 30, or 240 scans per minute, depending on the target strength. The radiometers receive part of the incoming radiation from reflecting choppers and analyze it by means of rotating filter wheels or multiple exit slits and appropriate detectors.

More information on "Project Skyscraper" than is given in the reference can be obtained from D. S. Lowe of the Bendix Laboratories in Ann Arbor, Michigan; this should include information on results of flight tests conducted during the past summer.

Lopair

An unusual field application of infrared is the detection of highly toxic chemical warfare agents such as the so-called nerve gases. This detection problem comes within the cognizance of the U.S. Army Chemical Research and Development Laboratories, located at the Army Chemical Center in Maryland.[14] The detection is based on the fact that the chemical linkage P-O is common to the nerve-gas compounds, and this stretching vibration produces a characteristic absorption band centered at 9.8 μ.

The name Lopair comes from the phrase **lo**ng-**pa**th **i**nf**r**ared and suggests that the detection is effected by measuring the absorption over a considerable path length, say a few hundred meters. As would be imagined, the detecting device can be either an infrared spectrometer which is equipped with external telescopic optics so as to receive radiation from a distant infrared source such as a Nernst glower, or it can perhaps be a simpler, less expensive, filter photometer. In either case, the analytical beam is filtered so that it passes a wavelength band centered at 9.8 μ, and this is compared against a reference beam usually with passbands at around 9 and 11 μ, where the nerve-gas compounds have only slight absorption. The instrument is adjusted so that the detector response for these two beams is balanced. Then if some of the chemical agent is introduced into the path of sight of the instrument, there will be absorption at the 9.8-μ wavelength but not at the reference wavelengths, the instrument will be put out of balance, and a warning signal will be given.

Several different types of instruments have been developed to perform this particular, specialized analytical task. One of them uses a grating spectrometer; another employs a double-beam arrangement between the external optics and the thermistor bolometer detector, with appropriate interference filters in the two arms. Another uses a spinning filter wheel and simpler optical filters. These are "active" instruments which must have a light source located at a distance or perhaps located next to the transceiver, in which case a retroreflective mirror is located at the end of the working range. It would be highly desirable if one could use a "passive" system in which the infrared source was some terrain feature selected by the operator. Such passive detectors have indeed been built and have been found to show promise. With them, the test range can be selected simply by pointing the passive receiver at any convenient object whether on land or water, or perhaps at the sky, thus determining the path over which the absorbing gas may be detected. Of course this path must be free of foreign gas pollution at the time the instrument is balanced. Advances in technique will probably go in the direction of such a one-station system.

Present systems give a sensitivity of detection of a few parts per billion nerve gas over a 400-m path; a concentration of 1 part per million is fatally toxic, and lower concentrations may be incapacitating. Among the major sources of error are atmospheric scintillation or "shimmer" when the path is over the heated surface of the earth, and various means are being examined for reducing the effect of this shimmer. The problems of reliability of operation under varying atmospheric conditions and of low false alarm rate must be faced, as with any detection-alarm system.

Measurements of Missile Radiation

We have referred to the importance of making both spectral and total energy measurements on the radiation from missiles, both during the launch phase and during reentry. In this connection, much specialized, highly sophisticated equipment has been designed and built for use on the several missile ranges in the free world. Some of the devices are carried in balloons, aircraft, or rockets, some are installed on shipboard, and some are ground-based. This subject was reviewed at a conference of the International Commission of Optics held in London in July 1961, by S. S. Ballard and D. C. Marquis in their paper "Optical and Infrared Systems on the Atlantic Missile Range"; the proceedings of this second London conference on optical instruments are being published in book form by Chapman & Hall. The paper described the instrumentation being procured for Stations 1 and 12 of the Atlantic Missile Range, respectively, a station at Cocoa Beach near the launch area at Cape Canaveral, and a station on Ascension Island, in the 8000-km ICBM impact area. The two infrared systems consist of the same type of instrumentation, the main differences being in the sensitivities prescribed and the fields of view employed. Whereas the instruments appear to be fairly conventional in construction, they utilize the latest developments of the various techniques involved and are true state-of-the-art instruments for the time period for which they were designed and built.

There are special problems in missile radiometry which may not apply to all other types of radiometric measurements. One of the most important is the problem of background discrimination or cancellation—that is, the removal of the effects of the background radiation so that the recorded signal represents true target radiant intensity (after correction for atmospheric absorption). This calls for instruments with small fields of view which will just cover the target at its shortest range from the measuring device. The radiometric instruments on the Atlantic Missile Range have fields of view of 1, 3, and 8 mrad. These small fields necessitate extremely accurate tracking, so the infrared tracker and its pedestal should have a combined dynamic accuracy as small as 0.1 mrad. Another requirement is for wide dynamic range, since fluctuations in the target signal of many orders of magnitude may occur in time intervals of only milliseconds. Dynamic ranges of 10^5 or more, automatically controlled electronically, are required. In order to accommodate the various types of measurements, several different instruments are mounted on a common pedestal and are accurately boresighted together and to the tracker.

It is of greatest practical importance to reduce the time interval between data acquisition and data dissemination. Thus an automatic data reduction program using large computers is a necessity. Data should hence be collected in an appropriate fashion, such as on magnetic tape, and should be capable of being processed, reduced, and tabulated by a computer such as the IBM 7090 and its associated equipment. These requirements impose the need for additional equipment such as analog-digital convertors, but they result in an enormous saving of time and subsequently in making the data all the more valuable on a timely basis. Finally, the importance of atmospheric transmission correction cannot be overlooked, especially for ground-based equipments or equipments mounted on shipboard, where the infrared radiation has passed through substantially the entire earth's atmosphere on its way from the high-altitude target to the radiometric instrument. The general problem of atmospheric transmission in the infrared is referred to several times in the present issue and will not be discussed further here, except to say that it is necessary to reduce the atmospheric transmission calculation routine into a form which is compatible with the rest of the data-reduction technique.

The four major instruments used at Stations 1 and 12 of the Atlantic Missile Range for obtaining radiometric data are the infrared tracker, the infrared radiometer, the ultraviolet-visible photometer, and the infrared scanner.

The infrared trackers and radiometers were built by the Barnes Engineering Company. Each of them comprises two identical optical systems, each a 30.5-cm aperture, $f/3$ Cassegrain collecting system. The dual systems are provided in the radiometer to make available four detector channels. The present devices have cooled PbS and two thermistor-bolometer channels, one limited by filters to 6 μ and one extending to 15 μ. Other detectors may be substituted at a later date, and another channel can be added. Specifications call for a noise equivalent power density of 10^{-14} watts/cm^2. One of the two optical systems of the tracker is utilized for coarse acquisition and the other for fine-field tracking; the fields of view are 4° square and 4 mrad square, respectively. The detectors are PbS, run at ambient temperature.

The ultraviolet-visible photometer, built by I.T.T. Federal Laboratories, uses a filter wheel arrangement so as to make radiometric measurements in six spectral intervals in the range 0.24 to 1.00 μ. The optical telescope is a 25-cm aperture, $f/8$ parabolic Newtonian system. The detectors are multiplier phototubes with the S-1 and S-13 surfaces. The entire spectral region is covered in 1 sec.

The multi-element scanner is a wide-field-of-view device built by the ACF Electronics Corporation. It is capable of gathering radiometric data from each of multiple targets and thus establishes radiance ratios among all targets in the field of view. The primary parabolic mirror is of 28-cm diameter and $f/2$ focal ratio. As shown in Fig. 3, the secondary mirror, which is of 11.4-cm diameter, is wobbled in one plane so as to translate the final image back and forth across a vertical linear array of 28 PbS detectors, at a rate of 10 complete frames per second. The noise equivalent power density of the PbS system is specified at 10^{-13} watt/cm^2. The effect of the mirror scan is that each individual detector sweeps out in the horizontal plane a field 28 times as wide as its own dimension. Thus the information given is for a field 2.8 mrad square for the Station 1 instrument and 28 mrad square for the Station 12 scanner. This permits plotting the intensity distribution in the missile plume when the missile is close to the Station 1 scanner, or plotting the reentry complex of objects in the Station 12 area. Since the associated, narrow-field radiometer gives quantitative information on one of the objects in the field of view, data from the scanner permit extension of quantitative measurements to the other objects.

Optical Materials and Optical Components

Developments have continued during the three years since we prepared our paper "Optical Materials, Films, and Filters for Infrared Instrumentation."[15] Investigations of infrared-transmitting glasses are proceeding in several laboratories. It is now possible to obtain calcium aluminate glass with substantially level transmission across the broad water band centered at 2.8 μ, where formerly there was a considerable absorption. Glasses containing arsenic, tellurium, and selenium transmit up to the important wavelength of 15 μ but are still likely to have unduly low softening temperatures. There has been some work on amorphous semiconductors—infrared-transmitting glasses containing silicon, tellurium, arsenic, etc., with softening points above 500°C. For the single-crystal and polycrystalline materials, larger blanks of silicon, germanium, and sapphire are available than formerly. The widespread interest in optical masers has brought forth accelerated development, especially for materials from which laser rods can be made. This has resulted in producing more homogeneous sapphire samples and in bringing out glasses and crystals doped with rare earth elements; also it has introduced some new companies into the optical materials field.

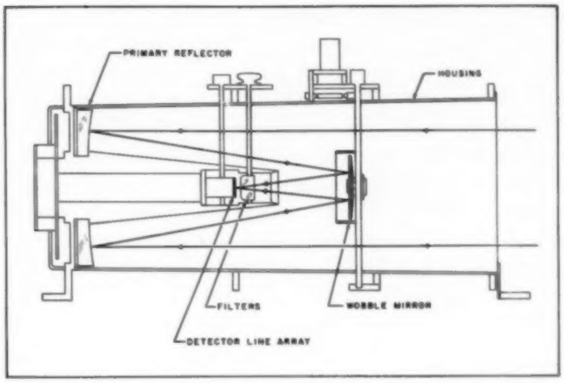

Fig. 3. Optical schematic of 28-element scanner.

Outstanding among the optical materials that have recently become available are the so-called Irtran (infrared-**tran**smitting) materials developed by the Eastman Kodak Company.* To date there are four of these, each of which is a pressed, sintered compact of a familiar material. Irtran-1, which is predominantly magnesium fluoride, transmits in a 2-mm thickness to about 8 μ. (The wavelength for 10% external transmittance is quoted, in accordance with our usual practice.) The short-wavelength cutoff of this material occurs at around 1 μ and shows a form characteristic of scattering rather than absorption limit. Its refractive index at 4 μ is 1.35. Irtran-2 is a pressed, sintered compact of zinc sulfide; it transmits from about 1 μ to beyond 14 μ. Its refractive index at 4 μ is 2.25. Irtran-3 transmits to about 12 μ; Irtran-4 to beyond 20 μ. These materials have attractive physical and chemical properties, as would be expected from the compounds from which they are made and the physical processes to which they have been subjected. The first two are more fully developed; blanks up to 16.5-cm diameter can be furnished. A line of standard meniscus-type lenses, some with spherical surfaces and some with one aspheric surface, are now available as standard items.

Another well-known crystal which has found some application as a window material is diamond. It transmits throughout the entire infrared region of interest (from 0.25 μ to more than 80 μ) but has rather broad and deep absorption bands centered at about 5 and 8 μ. The admirable physical properties of diamond are well known.

At the other end of the optical spectrum there is interest in materials transmitting in the deep ultraviolet. Lithium fluoride has always been the crystal which transmits to the shortest wavelengths, but there has been a problem of uniformity of transmission from crystal to crystal, especially in the Schumann region.[16] The purity of the basic salt is of great importance, but soft crystals may be produced from superpure materials. Experiments are underway at the Harshaw Chemical Company and elsewhere on methods to insure a supply of samples of lithium fluoride with acceptable physical properties and transmission to the Lyman alpha line. Crystal quartz is of course useful down to at least 0.18 μ, and the success in producing cultured quartz so as to obtain larger crystals and hence larger optical elements is of particular interest.

---

* See article by S. E. Hatch, p. 595 of this issue.

Efforts continue to develop suitable fiber optics bundles for use throughout the infrared region.[17] For latest information on the progress on this important front one should consult the pages of the current issues of the *Journal of The Optical Society of America* and of *Applied Optics*.

Interference filters are now available out to longer wavelengths than was previously the case, so that one can obtain long-wavepass, short-wave pass, or bandpass filters operating from the ultraviolet out to about 15 μ.

Optical instruments had their birth in laboratories and have been largely used in laboratory environments with the exception of the field use of telescopes, binoculars, and the like, until relatively recently. Now that they are carried aloft in missiles so that aerodynamic skin heating is encountered, and then are taken up into space where the ambient temperature is very low, there is more than an academic interest in the properties of optical materials at temperatures considerably higher and considerably lower than ordinary room temperatures. Thus, studies have been underway in several laboratories to determine the properties of materials useful in optical and infrared instrumentation, when the materials are taken to temperatures as high as 1000°C. The ordinary physical properties can be measured fairly easily, but it is more difficult to determine transmittance, reflectance, emissivity, and related properties. Even less is known about changes in the optical properties of the common materials as the temperature is lowered from 300°K (ordinary room temperature) to temperatures approaching that of outer space. Here is an area where much remains to be done. It may not be exciting work to an experimental physicist or an engineer, but the data produced will be of great practical importance. For example, now that high-quality optical instruments are being taken into space by rockets and satellites, and will be at temperatures considerably below that on the surface of the earth, the designer must know whether the refractive index of the materials will change enough to throw the instrument off focus, or in spectroscopic instruments enough to cause unexpected deviations of the light beam. Presently available data on the temperature coefficient of refractive index are confined to a range very close to ordinary room temperatures, alas.

The whole question of the quantitative effects on engineering materials when they are carried in spacecrafts must now be investigated in detail. The space environment differs from that on the earth's surface because the pressure is much lower than any encountered on earth except perhaps in the very highest laboratory vacuums, and the ambient temperature may be very high when direct sunlight is being absorbed or very low when the object is radiating into cold outer space. Thus the effects of vacuum plus very high and very low temperatures must be considered for all materials to be used in space instrumentation. To be sure, the problem is much more extreme for such materials as organic materials, lubricants, and paints than it is for the usual optical glasses and crystals, which are substantially stable materials. Another factor to consider, however, is the bombardment by the particles in the earth's radiation belts and by radiations from the sun—perhaps charged particles, and certainly short ultraviolet and x-rays. Finally, the erosion by meteoroids may be significant at some lower altitudes. This whole subject has been reviewed in an excellent report published by the Jet Propulsion Laboratory of California Institute of Technology.[18] Their survey does not indicate that optical materials are particularly vulnerable to the special conditions of the space environment. Selenium as used in photocells may sublime; oils and greases may creep over the clean optical surfaces. Glass covers of solar cells may discolor because of the short-wavelength radiation incident on them. This same coloring effect may also be produced in some crystalline materials if they are exposed to ultraviolet light. At the low pressures and high temperatures, some semiconductors such as germanium and silicon may sublime slightly. Some effect may be caused, especially in semiconductors and organic materials, by the short-wavelength ionizing radiation from sunlight, especially as the irradiation may continue so as to produce large total doses. Special optical glasses have been developed for their resistance to discoloration as produced by neutrons and gamma rays, and high-purity fused silica is also less susceptible to discoloration by this type of radiation. More information on the whole subject of the reaction of optical materials to the space environment will soon be forthcoming as a result of the acceleration of the space effort.

Immersion Lenses

One of the more interesting developments in infrared optics which has occurred in recent years is the application of techniques analogous to those of immersion microscopes to telescopic systems. Although it is not

Table I. Gains to be Expected with Immersion Lenses Calculated by Wolfe and Duncan (n is Refractive Index, o is Object Distance of the Immersion Lenses, f is Focal Length of the Primary Optical System, r is Radius of the Immersion Lenses)

	Subaperture source		Extended source	
Lens	Constant area	Constant position	Constant area	Constant position
Hemisphere	1	n	$\left(\frac{nf}{o}\right)^2$	n
Hyperhemisphere	1	n^2	$\left(\frac{nf}{o + (r/n)}\right)^2$	1

Table II. Gains to be Expected with Immersion Lenses Calculated by Jones

			Internal noise		Radiation noise	
Lens	A	Ω	D^*	D^{**}	D^*	D^{**}
Hemisphere	n_s^2	n^2/n_s^2	n_s	n	n_s/n	1.0
Hyperhemisphere	n_s^4	n^2/n_s^4	n_s^2	n	n_s^2/n	1.0

clear who first used immersion lenses for infrared detectors, S. M. MacNeille, then of the Eastman Kodak Company, and R. DeWaard and E. Wormser of the Barnes Engineering Company are certainly among the first.[19,20] Until 1960, the lenses have usually been simple hemispheres of a high-refractive-index material brought into optical contact with a detector surface, and the reduction of the image size has been proportional to the square of the refractive index. Since that time, however, Strong and Wormser,[21] Wolfe and Duncan,[22] and Jones[*,23] have improved upon the technique. The essence of these recent works is given in Tables I and II.

The specification or gain for an immersion lens can be given either in terms of detectivity D or of either of the normalized detectivities D^* or D^{**}. Wolfe and Duncan chose to define gain as follows:

$$G = \frac{P'D'}{P\,D},$$

where P is radiant power, primes indicate quantities for an immersed detector, and unprimed quantities are for an unimmersed detector. Their results include sources which are much smaller, equal to, and larger than the field of view of the system; they also provide calculations for systems which are modified by either holding the detector area constant (and changing the detector position in the optical system) or retaining the position (and changing the detector area) after an immersion lens of either a hemispherical or hyperhemispherical type is used. Their results are summarized in Table I.

Jones chose to evaluate gain by utilizing an interesting and general method, the optical invariant $n^2A\Omega$, where n is the refractive index, A is the area, and Ω is the solid angle. He found ratios for x'/x as indicated in Table II, where x is any variable of the system. It might be noted that in Table II, n_s is the refractive index of the immersion lens and n is the refractive index of any coatings, lenses, or adhesives—the limiting index of the system. The cases to compare in Tables I and II are those for D^* and subaperture sources, constant position.

The two analyses provide complementary information about these lenses: D^{**} cannot be improved by immersion techniques when the detector is limited by radiation noise; both types of lenses provide a gain when the detector is limited by other noises; for subaperture sources it is best to reduce the area of a detector and use a hyperhemisphere; for extended sources, the hemisphere seems superior. There are other desiderata, but the value of the immersion lenses is attested by these analyses and by the use of the lenses by prominent manufacturers of thermistor bolometers and lead sulfide detectors.

Applications to Geophysics

A very direct application to infrared technology is the utilization of infrared sensing equipment in determining the absolute or relative distribution of thermal energy over the earth's surface and within the atmosphere. The data so acquired with these infrared devices can then be interpreted in terms of their implications to a particular geologic, oceanographic, or atmospheric environment. Some of the applications of infrared technology to geophysics are quite straightforward, while others are more subtle and require more refined data analysis techniques.

Two types of infrared sensing devices in use today are the infrared radiometer and the scanner, the latter of which generates maplike presentations of the thermal characteristics of objects being scanned. (See the cover picture of *Proc. IRE* for September 1959.) The imagery generated in the scanning process represents the relative values of the emitted and reflected radiation within the spectral region to which the detector responds; the data acquisition rate is similar to the acquisition rate for aerial photography. The infrared scanner can be used solely for its unique information content or with the mutually corroborative information of thermal maps and visual photographs which can provide the geophysicist with valuable mensural information and the location of thermal anomalies that may be indicative of subsurface activities.

---

[*] See p. 607 of this issue.

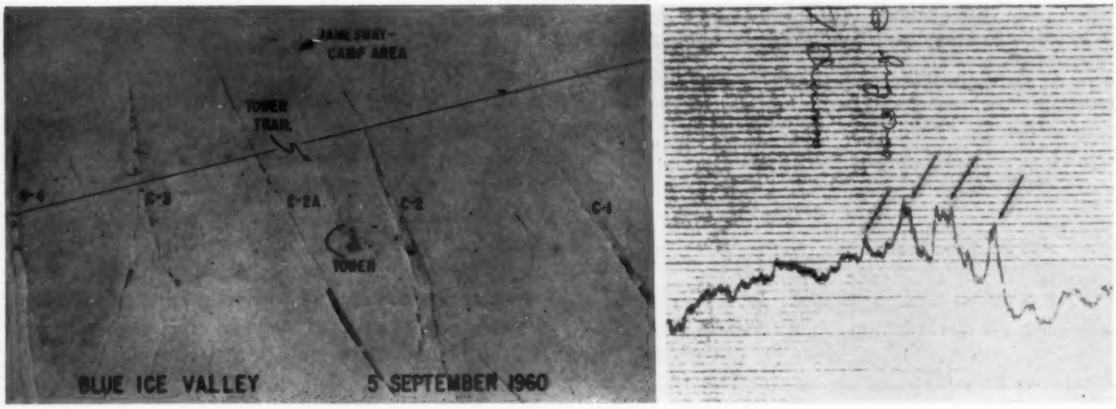

Fig. 4. Panchromatic photograph and radiometer line scan.

The use of absolute and net radiometers to obtain useful geophysical data requires refined data reduction and analysis techniques. These equipments are point or line samplers depending upon how they are used, and thus do not furnish the maplike presentation of the infrared scanner. When used in an airborne role, they measure the absolute values of the incoming and outgoing radiation (or the net radiation, if desired) along the line over which the carrying vehicle is traveling. Thus, radiation exchange variations with altitude, time of day, time of year, latitude, and weather can be studied. The use of these devices in satellites can furnish global information which can be used in assessing the total heat budget for the earth as well as in the fields of meteorology and climatology.[24]

To date, only the briefest explorations have been made of the possibilities and potential of the use of these devices alone or in combination. With further refinements of equipment and of data storage and retrieval techniques, infrared sensing devices should continue to find further applications in the geophysical field in both earth satellites and air-breathing aircraft.

A more applied but no less important use is the detection of crevasses. Figure 4 shows a panchromatic photograph of snow in Greenland with a radiometer trace on it. The radiometer output, as the radiometer scans across the trace, is shown next to the picture; the maxima in the output are indications of snow-bridged crevasses in the snow field—an ever-present danger on ice caps which is completely undetectable by photographic means. The panchromatic-film picture was taken in the summer, during which time the snow bridges had slumped and crevasses were visible by resulting shadows. The radiometric traces were taken during March, when visual observers saw nothing but white snow. It might be added that more confidence is obtained when several radiometric scans are laid side by side, or a vastly more useful display would be a thermal map.

We should like to express our appreciation to several of our colleagues who provided useful information; they are John Duncan and Carl Miller of the Institute of Science and Technology, University of Michigan, and Dennis Marquis of Pan American World Airways, Guided Missiles Range Division, and also to acknowledge the partial support of the Office of Naval Research, Physics Branch.

References

1. W. Elsasser, Phys. Rev. **54,** 126 (1938); also *Harvard Meteorological Studies,* No. 6 (Harvard U. Press, Cambridge, Mass., 1942).
2. R. M. Goody, Quart. J. Royal Meteorol. Soc. **78,** 165 (1952); also *The Physics of the Stratosphere* (Cambridge U. Press, Cambridge, England, 1954).
3. A. S. Zachor, Report R-328, Vol. 2, M.I.T. Instrumentation Laboratory (July 1961).
4. G. N. Plass, J. Opt. Soc. Am. **50,** 868 (1960).
5. P. J. Wyatt, V. R. Stull, and G. N. Plass, Aeronutronic Report U1504. Final Report Contract No. AF 19(604)–7479, AFCRL 62-210 (15 July 1962).
6. T. L. Altshuler, General Electric Co. MSVD Document 61 SD 199, Valley Forge, Pa.
7. R. O'B. Carpenter, J. A. Wright, A. Quesada, and R. E. Swing, Report No. 1 on Contract AF19(604)-2405, Baird-Atomic, Inc. (Nov. 1957).
8. A. E. S. Green and M. Griggs, General Dynamics Astronautics Report, San Diego, Calif. (Mar. 1962).
9. M. L. Chatkoff, Proc. IRIS **7,** 63 (Jan. 1962).
10. M. E. Lasser, P. H. Cholet, and R. B. Emmons, Proc. IRE **47,** 2069 (1959).
11. D. G. Murcray, J. N. Brooks, F. H. Murcray, and W. J. Williams, J. Opt. Soc. Am. **50,** 107 (1960); D. G. Murcray, F. H. Murcray, W. J. Williams, and F. E. Leslie, J. Opt. Soc. Am. **51,** 186 (1961). See also F. Stauffer and J. Strong, Appl. Opt. **1,** 129 (1962).
12. E. W. Kutzscher, O. LaPlant, and E. S. Brumfield, Proc. IRIS, No. 3, 81 (1959).
13. L. G. Mundie, D. E. Brown, P. G. Hasell, Jr., and D. S. Lowe, J. Opt. Soc. Am. **50,** 1187 (1960).
14. H. Tannenbaum and H. R. Carlon, Proc. IRIS **7,** No. 1, 131 (Jan. 1962).
15. W. L. Wolfe and S. S. Ballard, Proc. IRE **47,** 1540 (1959).

16. S. S. Ballard, L. S. Combes, and K. A. McCarthy, J. Opt. Soc. Am. **41**, 772 (1951).
17. D. A. Pontarelli and N. S. Kapany, J. Opt. Soc. Am. **50**, 1178 (1960).
18. L. D. Jaffee and J. B. Rittenhouse, "Behavior of Materials in Space Environments," Jet Propulsion Laboratory Report No. 32-150 (Nov. 1961).
19. R. W. Astheimer and E. M. Wormser, J. Opt. Soc. Am. **49**, 179 (1959).
20. R. DeWaard and E. M. Wormser, NAVORD Report 5495, Barnes Engineering Co. (April 1958).
21. E. M. Wormser, (private communication).
22. W. L. Wolfe and J. Duncan, Proc. IRIS **6**, No. 2, 25 (May 1961).
23. R. C. Jones, Appl. Opt. **1**, 607 (1962).
24. V. T. Suomi, "Earth's Thermal Radiation Balance, Preliminary Results from Explorer VII," IGY Bulletin No. 52 (October 1961).

ANNOUNCEMENT OF PROGRAM
MANGER HOTEL, ROCHESTER, NEW YORK
OSA 47TH ANNUAL MEETING, OCTOBER 2 TO 5, 1962

Invited Papers. There will be six invited papers by acknowledged authorities on a wide variety of subjects, including the Purcell effect, space optics, light waves in nonlinear media, and optical glass. Many **contributed papers** will be offered on these as well as other topics of interest to OSA members. The dinner speaker will be **Crawford Greenewalt,** President of Du Pont, who will show slides of humming birds and high-speed motion pictures of birds and insects in flight.

Rochester, New York, is the home of the Institute of Optics and of many industries of an optical and general scientific nature. October 2nd therefore has been assigned to plant and other visits. Three full days of invited and contributed paper sessions will follow. A choice of full-day and half-day trips to other points of interest will be offered on Saturday, October 3rd.

Institute of Optics will hold an open-house all day on Tuesday, October 2nd, with a lecture and program related to education in optics in the evening.

Ladies' Program. A varied and complete program is planned, including leisurely local and day trips to the Naples Wineries or the Syracuse China Works.

Hotel. Headquarters will be located in the Manger Hotel, but downtown motel and other hotel accommodation is available. Midtown Plaza, just opened with national acclaim, is adjacent to the Manger Hotel and provides unusual facilities for shopping, meals, and parking.

Applied Optics semiannual meeting of Editors, Reporters, and Patents Panelists will be held at **noon on Thursday, October 4th in the Green Room of the Manger.**

Annual Business Meeting. The Annual Business Meeting of the Society will be held on Friday, October 5th.

George Eastman House. Plan to stay Friday evening for an event at George Eastman House, including showing of early movies and viewing of the recently opened Mees Gallery.

NO POSTDEADLINE PAPERS CAN BE ACCEPTED FOR THIS MEETING.

Optical Society of America
Mary E. Warga, Executive Secretary
1155 Sixteenth Street, N.W.
Washington 6, D.C.

Meetings Calendar

September

—	Relativity and Gravitation, internatl. IUPAP conf., Poland *P. Fleury, 3, blvd. Pasteur, Paris 15, France*
—	Tashkent Conf. on Spectral Analysis *B. M. Gandel'sman, St. Comm. on the Coordination of Scientific Research, Bratskaya Ul., 29, Tashkent, USSR*
—	Volograd Conf. on Spectral Analysis *B. G. Voronov, 11, Vniitmash, Volograd, USSR*
—	Conf. on Plasma Spectroscopy, USSR *N. A. Prilezhaeva, TGU, pl. Revolyutsii, 1, Tomsk, USSR*
—	British Assoc. Advancement Science Internatl. Mtg., Manchester *G. Allen, Burlington House, London W. 1, England*
3–7	Internatl. Symp. on Information Theory, Brussels *M. Selleslags, U. Libré, 50, ave. Franklin D. Roosevelt, Brussels, Belgium*
7–12	Internatl. Conf. on Crystal Lattice Defects, Kyoto *R. R. Hasiguti, U. of Tokyo, Bunkyo-ku, Tokyo, Japan*
9–14	Illuminating Engr. Soc. Technical Conf., Statler Hilton Hotel, Dallas *H. M. Walne, Dallas Power and Light Co., Dallas, Tex.*
9–14	Am. Soc. of Photogrammetry, semi-ann. mtg., Chase and Park Plaza Hotels, St. Louis, Mo. *C. E. Palmer, 1515 Mass. Ave., N.W., Washington 5, D.C.*
10–15	Molecular Structure and Spectroscopy, internatl. IUPAC symp., Tokyo *Science Council of Japan, Ueno Park, Tokyo, Japan*
10–15	Technical Forum on Forming Bonds in and with Fibers, Berkhamsted *Gen. Secy., Soc. of Dyers and Colourists, Dean House, 19 Piccadilly, Bradford, Yorkshire, England*
16–20	Electrochemical Soc. Mtg., Statler Hilton Hotel, Boston, Mass. *Electrochem. Soc., 30 E. 42 St., New York 17, N.Y.*
16–22	Low Temperature Physics, 8th internatl. conf., Queen Mary Col. *G. O. Jones, Queen Mary Col., U. of London, Mile End Rd., London, E. 1, England*
17–19	9th Ottawa Symp. on Applied Spectroscopy *B. Farrar, J. T. Donald & Co. Ltd., 1181 Guy St., Montreal 25, Que., Canada*
17–22	6th Internatl. Congress on High Speed Photography, Scheveningen *J. G. A. de Graaf, 14, Burgemeester de Monchyplein, The Hague, Netherlands*
20–23	Symp. on Rockets and Space Flight, 11th, Coblenz *Deutsche Raketen-Gesellschaft, Fritz-Beindorf-Allee 9, Hanover, Germany*
24–28	Union of German Physical Societies, Stuttgart *H. Franke, Verband Deutscher Physik. Gell, Gänseheide 15A, Stuttgart, Germany*
30–Oct. 5	ASTM Pacific Area Mtg., Statler Hilton Hotel, Los Angeles *ASTM, 1916 Race St., Philadelphia 3, Pa.*

October

—	Symp. on the Question of Introducing Molecular Spectroscopy, USSR *V. M. Chulanovskii, Comm. on Spectroscopy, Akad. Nauk USSR, proezd Sapunova, 13/15, Moscow, USSR*
—	Belorussian Conf. on Spectral Analysis *B. I. Stepanov, Inst. Fiz. Akad. Nauk BSSR, Leninskii Prospekt, 70, Minsk, USSR*
—	Gen. Conf. of Photography, London *A. E. Smiles, Inst. of British Photographers, Queen Mary Col., Mile End Rd., London, E. 1, England*
—	Infrared Information Symp., Eastern States Fall Mtg.
—	URSI Mtg., Montreal *M. G. George, Thayer School of Engr., Dartmouth Col., Hanover, N.H.*
2–4	Space Electronics and Telemetry, 7th ann. symp., Fontainebleau Hotel, Miami Beach, Fla. *E. J. Cottrell, Martin Co., Orlando, Fla.*
4–6	**Optical Society of America Annual Meeting, Manger Hotel, Rochester** *Hilda Kingslake, 56 Westland Ave., Rochester, N.Y.*
10–12	The Fiber Soc. Fall Mtg., Boston, Mass. *J. S. Jacobs, P.O. Box 405, Athens, Ga.*
12–13	SPSE Symp. on Photography of Electronic Display, Shoreham Hotel, Washington, D.C. *E. S. Cobb, P.O. Box 1609, Main P.O., Washington, D.C.*
15–19	ISA 17th Ann. Instrument-Automation Conf. and Exhibit *W. H. Kushnick, 313 6th Ave., Pittsburgh 22, Pa.*
18–19	Applied Spectroscopy and Analytical Chemistry Mtg., Pasadena. *W. F. Ulrich, Beckman Instrument Co., 2500 Harbor Blvd., Fullerton, Calif.*
22–24	10th Detroit ANACHEM Conf., McGregor Memorial Conf. Center, Wayne State U. *D. F. Boltz, Wayne State U., Detroit 2, Mich.*
22–26	SMPTE Semi-Ann. Convention, Chicago, Ill. *C. S. Stodter, 55 W. 42 St., New York 35, N.Y.*
23–24	Optical Processing of Information Symp., Dept. of Interior Auditorium, Wash., D.C. *B. A. Novy, ONR, Code 437, Wash. 25, D.C.*

November

14–16	4th Ann. Eastern Analytical Symp., Statler Hilton Hotel, NYC *P. Lublin, Gen. Telephone & Electronics Labs, Bayside, N.Y.*
23–24	APS, Cleveland, Ohio *K. K. Darrow, 538 W. 120 St., New York 27, N.Y.*

December

—	Am. Astronomical Soc. Mtg., U. of Ariz. and Kitt Peak Natl. Observatory, Tucson *H. Smith, Yale U. Observatory, New Haven, Conn.*
3–7	19th Internatl. Ophthalmological Cong., New Delhi *Y. K. C. Pandit, Bombay Mutual Bldg., Sir Pherozeshah Metha Rd., Bombay 1, India*
26–29	APS, Stanford *H. A. Shugart, U. of Calif., Berkeley, 4, Calif.*

1963

January

22–25	APS, New York City *K. K. Darrow, 538 W. 120 St., New York 27, N.Y.*

February

—	1st Australian Conf. on Electrochemistry, Sydney and Hobart *F. Gutmann, U. of New South Wales, P.O. Box 1, Kensington, N.S.W., Australia*
11–15	3rd Quantum Electronics Conf., Paris *Mme. Cauchy, 7 rue de Madrid, Paris 8, France*
20–22	Internatl. Solid-State Circuits Conf., 10th ann., U. of Pa. and Sheraton Hotel, Philadelphia *S. K. Ghandi, Philco Scientific Lab, Blue Bell, Pa.*
28–Mar. 2	APS, Houston, Tex. *K. K. Darrow, 538 W. 120 St., New York 27, N.Y.*

March

16–29	IAU Symp. No. 20, The Galaxy and the Magellanic Clouds, Canberra and Sydney, Australia *D. H. Sadler, c/o Royal Greenwich Observatory, Herstmonceux Castle, Hailsham, Sussex, England*
25–28	APS, St. Louis, Mo. *K. K. Darrow, 538 W. 120 St., New York 27, N.Y.*

April

22–25	APS, Wash., D.C. *K. K. Darrow, 538 W. 120 St., New York 27, N.Y.*

May

—	2nd Hungarian Optical Conf., Budapest *Soc. of Optics, Acoustics and Film Technics, Szabadság-tér 17, Budapest 5, Hungary*

June

10–14	Molecular Structure and Spectroscopy, 18th symp., Columbus *H. H. Nielsen, Ohio State U., 174 W. 18 Ave., Columbus 10, Ohio*
23–28	ASTM Ann. Mtg., Chalfonte-Haddon Hall, Atlantic City, N.J. *ASTM, 1916 Race St., Philadelphia 3, Pa.*

July

2–5	Internatl. Symp. on Free Radicals, 6th, Cambridge *A. B. Callear, U. of Cambridge, Lensfield, Rd., Cambridge, England*
11–14	IUPAC, 22nd conf., London *R. Morf. c/o F. Hoffmann-La Roche & Co., Ltd., Basel 2, Switzerland*

August

4–9	Internatl. Conf. and Exhibit on Aerospace Support, Wash., D.C. *Box 6635, Wash., D.C.*

continued on page 654

University Research in Infrared Physics

John S. Garing and John N. Howard

A short review is presented of the academic research of the past five years in infrared physics. The principal areas included are studies of molecular spectra under very high resolution, infrared studies of the atmosphere, and the development of novel techniques of measuring and analyzing spectra, such as interferometric techniques, particularly in the region of the far infrared.

To cover all the current academic studies involving infrared radiation or the application of infrared spectrometers would require writing a small book. We will limit our present survey to some of the physics applications of infrared as contrasted to the widespread use of commercial infrared spectrometers as analytical tools for assistance in the study of large molecules or for chemical problems. This review emphasizes three main areas of study: studies of molecular spectra under very high resolution (i.e., with "home-made" spectrometers of higher spectral resolution than is generally available in commercial instruments); infrared studies of the atmosphere, which crosses the disciplines of physics and meteorology; and the development and use of novel techniques for measuring and analyzing infrared spectra, particularly in the region of the far infrared. The emphasis will be on research in the United States as many of the research efforts in other countries were adequately discussed in a previous issue of *Applied Optics*. In spite of the title some academic-type research in government and nonprofit laboratories is included.

There are several universities which can be considered as the focal points of infrared research in the United States, as they turn out the bulk of the trained personnel in infrared physics and molecular spectroscopy. The University of Michigan (which is not doing so much in this field today as it did in its heyday of the 1920's and 1930's), Ohio State University, Johns Hopkins University, Pennsylvania State University, and the University of Tennessee, are particularly active.

At Ohio State University, H. H. Nielsen and K. N. Rao have constructed and are operating two large spectrometers (one using a Pfund arrangement and the more recent a six-meter Ebert for the nearer infrared) to obtain high-resolution spectra of small polyatomic molecules, particularly of the ammonia type, including the deuterated and tritiated forms.[1] These spectra are being analyzed to study the higher-order interactions such as those derived by H. H. Nielsen and G. Amat (of CNRS, Paris) who have extended the theory of molecular energies to fourth-order interactions.[2] D. Williams, J. Shaw, and co-workers are continuing their several studies on atmospheric infrared phenomena, including a recently completed extensive set of measurements of long path transmission through various atmospheric gases under reduced pressure conditions by D. E. Burch and D. Williams (which is described elsewhere in this issue).[3] These data, together with earlier results taken at OSU,[4] have provided the basic experimental data for most of the calculations of atmospheric transmission in the infrared. Other efforts include the determination of atmospheric abundance of the minor constituents as a function of season and time of day and geographical location,[5] and the experimental study of the total absorption by two samples of a gas, as their total pressures and concentrations are independently varied.[6] In addition, this group is now completing a large Ebert-type spectrometer optimized for the four-micron spectral region for use in further atmospheric studies.

Another group at Ohio State University, under E. E. Bell and R. A. Oetjen, is reconstructing their far-infrared grating spectrometer.[7] In the new instrument they make use of a rapidly oscillating lamellar interferometric modulator similar to one developed by L.

The authors are at the Geophysics Research Directorate, AFCRL, Bedford, Massachusetts.

Received 4 June 1962.

Genzel at the University of Freiburg[8] as a wavelength order sorter or premonochromator. F. P. Dickey has developed methods for observing the infrared emission of radicals (such as OH) in flames even in wavelength regions where the principal combustion products (such as CO_2 or H_2O) also have intense emission bands.[9] One method involves injection pumping excess fuel into the flame through a pulsating needle valve at, say, 13 pulses a second and then phasing the detector-amplifier output to this pumping cycle so that only the effect of the added fuel is observed. A second method utilizes a rotating mirror arrangement for looking alternately at two flames matched so that there is no net signal. An excess of fuel, oxidizer, or diluent is then introduced into one of the flames and only the emission of the additional molecules or radicals is observed. More recently Dickey has used an electrical discharge through a gas at low pressure to observe the emission from radicals such as CN in the near infrared.

At the University of Michigan, D. M. Dennison and K. T. Hecht are active in theoretical molecular studies, including inversion calculations in NH_3 and the study of hindered rotation in molecules.[10] The development and use of a number of interesting experimental techniques have been carried out by C. W. Peters. These include, for example, the modification of a monochromator so as to produce an output signal from the detector that is directly proportional to the first derivative of the spectrum being examined.[11] In another study by this group, vibration-rotation absorption in H_2 and D_2 (ordinarily a forbidden dipole radiation because of the molecular symmetry) has been observed at high resolution by placing the gas in a modulated high electric field (100,000 V/cm maximum) at pressures up to 30 atm.[12] This same one-meter-long Stark cell has been used to observe Stark effects in the vibration spectra of several simple polar molecules (HCN, CH_3F, CH_3I, NH_3, and H_2O).[11] At present Peters and P. A. Franken are studying such phenomena as harmonic generation in optical masers.

One of the original pioneers of infrared physics, Prof. H. M. Randall, who established the infrared laboratory at Michigan, is still extremely active in infrared research 22 years after his "retirement" from academic work. His present interest is in the area of biochemistry where he is using his knowledge of infrared spectroscopy in the study of bacteria. Indeed, to quote H. H. Nielsen[13] (one of his students) "Since his retirement, he has made a more distinguished contribution than many scientists have in an entire lifetime." Many readers will no doubt remember that the December 1960 issue of *J. Opt. Soc. Am.* was a salute to the 90th birthday of H. M. Randall, and consisted of contributions from his many students and grandstudents.

There is another active infrared group at the University of Michigan in the Department of Electrical Engineering (Wolfe, Zissis). The activities of this group are described elsewhere in this issue.

At the National Bureau of Standards, W. W. Coblentz, also nearing his 90th birthday, and another of the great pioneers in radiometry and infrared studies, continues to be active in retirement. E. K. Plyler of the National Bureau of Standards can also be considered one of the "fathers" of infrared in the United States, both at NBS and for many years prior at the University of North Carolina. His contributions to molecular studies, infrared flame studies, far-infrared development, wavelength calibration techniques, and high-resolution spectrometry are too numerous to detail here.[14] With his high-resolution spectrometer for the 1–5 μ spectral region, he has obtained detailed spectra, for example, of the ammonia and water vapor molecules (including their deuterated forms) as well as of the nitrous oxide and nitrogen peroxide molecules.[15]

Many of these experimental spectra taken at NBS have been thoroughly classified and analyzed at Johns Hopkins University by W. S. Benedict. Benedict, in collaboration with others (Silverman, Migeotte), is also studying the strengths, widths, and shapes of absorption lines (in particular HCl, DCl, and recently CO) and how these factors affect the infrared transmission through gases.[16]

The very active group at Johns Hopkins University under John Strong has pioneered many novel experimental techniques in the infrared. In 1959 he planned and directed a manned high-altitude balloon flight in order to observe the near infrared spectrum of Venus from above the major portion of the earth's atmosphere. The goal of the study was to determine how much water vapor is present in the atmosphere of Venus above its cloud layer. Professor Strong is now preparing an additional series of unmanned balloon-borne infrared-spectrometer-telescope observations of the planets beginning this fall (with Venus and Mars as the first targets). In another current program at Johns Hopkins University a balloon-borne scanning spectrometer for the 5–25 μ region has been constructed which "looks," by means of a rotating mirror, alternately above and below the balloon in order to measure the infrared flux divergence in the atmosphere as a function of altitude.[17] In yet another study a rock salt monochromator was carried up to 20 km in a U-2 aircraft to obtain the solar spectrum for various altitudes.[18] Laboratory studies at Johns Hopkins University have included the development of lamellar interferometric modulators for the far infrared.[19] Also, under Professor Strong, a large grating spectrometer was constructed and used to study the absorption line strengths and widths due to individual lines and Q-branches of CO_2 bands in the 15–18 μ spectral region (by R. P. Madden)[20] and the absorption due to individual pressure-broadened lines in the 15–20 μ region of the H_2O pure rotation spectrum (by J. R. Izatt).[21] The experimental transmission data for mixtures of water vapor and nitrogen for the 20–50 μ region of the pure rotation band of water vapor were obtained by C. H. Palmer, Jr., using a long path (up to 200 m) absorption cell.[22]

D. H. Rank and his co-workers at Pennsylvania State University have developed several methods, including the "sliding wedge" wavelength scanning system and combination of grating spectrometer and Fabry-Perot interferometer, to obtain extremely precise measurements and accurate measurements of absorption line wavelengths and their shift with pressure.[23] For example, by comparing the values for the rotational constant B_0 obtained from these measurements with those obtained in the microwave region of the spectrum for DCl^{35}, Rank was able to compute a value for the velocity of light of 299,793.1 ± 0.65 km/sec.[24] This group has also recently used very long absorption paths to obtain infrared spectra of some "forbidden" transitions in simple molecules.[25] T. K. McCubbin has constructed a spectrometer using a hind prism instead of the more conventional fore prism,[26] as well as using the grating in an echelle fashion. He has obtained some of the best spectral resolution to date on the 10 μ spectral region and is presently studying the possibility of adding a Fabry-Perot interferometer to improve this resolution further.

At the University of Tennessee, A. H. Nielsen and co-workers (W. E. Deeds, N. M. Gailar, R. J. Lovell) have used a recently completed high-resolution spectrometer to carry out a detailed study of the intensities and shapes of the individual absorption lines in the fundamental vibrational band of hydrogen fluoride.[27] A small, far infrared spectrometer is also being used to measure pure rotational lines of HF.[28] Detailed experimental studies of the 4.3 μ CO_2 bands and the CH_3Cl fundamental bands are also under way.

The group at Michigan State University under T. H. Edwards has recently obtained some very high-resolution spectra of many of the absorption bands of molecules with symmetry C_{3v} (primarily the methyl halides). Several of these bands provide excellent illustrations of the interaction perturbations predicted and studied by G. Amat and H. H. Nielsen.[2]

W. M. Benesch at the University of Pittsburgh has introduced a hydraulic wavelength drive interferometrically controlled in his spectrometer. He has measured with this instrument the equivalent widths of collision broadened lines of the P-branch of the 3.5 μ band of HCl and deduced the optical collision cross sections for collisions between HCl and several foreign gases as well as for self-broadening of HCl.[29] He is at present modifying this apparatus to permit extension of his data into the wings of the HI fundamental band and to permit the taking of data on the overtone band as well.

At the Weizmann Institute of Science, Rehovoth, Israel, J. H. Jaffe has combined a high-resolution spectrometer with a hollow-prism refractometer to measure the optical dispersion of molecular lines in the infrared, including a detailed study of the first overtone band of HCl.[30] This group has developed techniques which permit them to measure and calculate the intensity and line widths of individual rotation lines. The results obtained here, as well as at Pittsburgh (W. M. Benesch) and at Pennsylvania State (D. H. Rank), have been analyzed in an attempt to obtain some understanding of intermolecular forces. The groups at Penn State (Rank), Pittsburgh (Benesch), Toronto (Welsh), Princeton (Hornig), the Weizmann Institute (Jaffe), and the National Bureau of Standards (Plyler) have had very closely related interests in line shape studies and maintain a vigorous program of exchange of personnel between groups.

Activities in molecular spectroscopy are not confined to the major universities. As an example of a small group active in such studies, E. K. Gora of Providence College, R. I., has made a complete theoretical analysis of the pure rotation bands of SO_2 and O_3 as part of his more general theoretical study of line shapes.[31]

Several universities are active in atmospheric infrared studies. The efforts at Ohio State and Johns Hopkins have already been discussed. Another very active group is that of M. V. Migeotte and his co-workers (L. Delbouille and G. Roland) at the University of Liège, Belgium. This group has published a high-resolution atlas of the solar spectrum (the radiation from the sun as observed through the earth's atmosphere) from 2.7 μ to 23 μ.[32] These measurements were obtained at the International Scientific Station at the Jungfraujoch, Switzerland, at an elevation of 3573 m. More recently this atlas has been extended to include the spectral region 8000–12,000 Å and the PbS spectral region (1.2–2.7 μ) will soon be completed. Professor Migeotte and his co-workers also work closely with H. A. Gebbie of the National Physical Laboratory, England, in an effort to measure night airglow by interferometric techniques at the Joch and also to obtain the infrared absorption spectrum of Venus and other planets using the 2-m telescope at the Observatory of Haute Provence, France.[33]

At the University of Denver, D. G. Murcray is continuing his measurements of sky emission and solar spectra with infrared instruments carried up to altitudes of 30 km on balloons.[34] From the water vapor absorption bands observed in the solar spectrum, he has calculated the total amount of water vapor above 15 km and 30 km in the earth's atmosphere. He has attempted to determine the pressure correction required to fit the observed slant path absorption to constant pressure laboratory data. In addition, these and other flights carry radiometers to measure upward flux and terrestrial emission as seen from above as a function of azimuth and elevation. More recent flights also carry auxiliary humidity measuring devices such as frost point hygrometers in an effort to check the accuracy of the spectroscopic techniques.

Several groups are actively pursuing infrared studies for the meteorological satellite program. These include W. Stroud and R. Hanel of NASA who were responsible for the original design of the TIROS satellites[35] and S. Fritz, D. Wark, D. Hilleary, and S. Manabe of the U.S. Weather Bureau, who have been developing advanced designs for radiation experiments to function on the Nimbus Satellite.[36] Such well-known experts on atmospheric heat balance as F. Möller of the University of Munich[37] and G. Yamamoto of Tohoku University[38] have worked closely with the Weather Bureau in developing techniques for meteorological satellite data analysis and interpretation.

At the National Bureau of Standards laboratories at Boulder, Colorado, the groups of D. Gates and R. Megill are engaged in studies of the slant path transmission of the atmosphere, with particular emphasis on high-altitude (up to 30 km) infrared behavior of the atmosphere.[39]

At the University of Munich, H.-J. Bolle and F. Möller are analyzing the emission spectrum of the atmosphere and the ground measured at Munich, at the Jungfraujoch, Switzerland, and at St. Agata, Italy.[40] W. Zdunkowski has just completed a series of calculations involving a comparison of radiation equilibrium temperatures as obtained by black ball measurements and as calculated by means of a radiation diagram constructed for a spherical receiver.[41]

Recently D. K. Edwards (while at University of California, Berkeley) has obtained experimental data and empirical correlations for the total absorptance of the infrared bands of carbon dioxide in nitrogen at total pressures from 0.5 to 10 atm, temperatures from 294° to 1390°K and mole fractions from 0.05 to 1.00.[42]

P. A. Sheppard's group at Imperial College, London, has also been measuring horizontal path transmission in the ten-micron spectral region as well as atmospheric emission in order to derive better data for determining vertical ozone distribution from ground-based measurements.[43] A. Adel at Arizona State has been carrying out such studies of vertical ozone distribution for a number of years by measuring the $9.6\ \mu$ band in absorption (using the sun or the moon as the radiation source) and comparing this with the ozone emission of the atmosphere.[44] In addition, he has been measuring atmospheric scattering of infrared radiation as a function of angular distance from the edge of the sun's disk.[45] E. Vigroux of the Institut d'Astrophysique, Paris, is setting up a station at Montlouis in southern France to make additional ozone measurements utilizing infrared techniques.[46]

Studies of the attenuation of infrared radiation by atmospheric scattering are being carried out at the University of Mainz by K. Bullrich, at UCLA by Z. Sekera, and at Harvard by R. M. Goody. One of Sekera's former students, D. Diermendjian, of the Rand Corporation, continues to publish extensive treatments of Mie scattering in real atmospheres.[47]

N. Ginsburg at the University of Syracuse has built a vacuum grating high-resolution far-infrared spectrometer which he is presently using for the study of pressure broadening effects in water vapor pure rotational absorption lines and also for studies of the optical properties of crystals.[48] Professor Ginsburg with R. Paulson has been measuring the characteristics of the noise in the transmission of infrared radiation over horizontal paths near the ground caused by atmospheric turbulence.[49]

A substantial effort is under way in the Soviet Union on the application of infrared techniques to meteorological problems and to basic studies of the atmosphere. The principal effort is at Leningrad State University under K. Ya. Kondrati'ev.[50] As part of their albedo studies, this group has constructed apparatus to measure the spectral reflectance of terrain in the near infrared.[51] A portable near-infrared spectrometer has been built to measure the solar spectrum and sky emission in the $1\text{–}15\ \mu$ region from a field station at the 4000-m level of Mt. Elbrus in the Caucasus Mountains.[52] The principal activities of Kondrati'ev himself are flux divergence studies of the atmosphere. An active group under K. S. Shifrin studies Mie scattering of infrared radiation and the reflectivity of clouds.[53] M. Budyko of the Main Geophysical Observatory is concerned with the radiation balance in arid regions and related climatological problems.[54]

In Moscow, an active group under G. V. Rozenberg at the Institute of the Physics of the Atmosphere is engaged in infrared scattering studies and the development of balloon-borne spectroscopic equipment for the determination of the water vapor content of the stratosphere.[55]

Several groups not yet mentioned are concerned with far-infrared studies (beyond $50\ \mu$) or the application of interferometric techniques to infrared studies.

At the University of Nancy, France, A. Hadni has built up a remarkable collection of far-infrared spectrometers and team of workers.[56] For example, one instrument is completely automated so that the complete spectra of several samples (thin films, for example) can be obtained during an overnight run. He has been interested in the study of solids at low temperatures, thin films, far infrared filters, properties of gratings, luminance of mercury arcs, and the emission of argon plasmas. More recently he obtained spectra of NH_3 and H_2O by replacing the argon gas in a Golay pneumatic detector with the absorber gas under study.

At Osaka University, Japan, H. Yoshinaga is designing and constructing a far-infrared interferometric spectrometer.[57] Moire fringe techniques will be used to measure the displacement of the movable component. This group has also designed a computer which calculates the Fourier transform of the interferogram as it is being measured, thus providing the frequency spectrum as soon as the interferogram is completely scanned.

At MIT, G. R. Harrison and G. W. Stroke have constructed an interferometrically controlled grating engine with which they have ruled excellent gratings of up to 30 cm of ruled surface.[58] The gratings for the visible and near ultraviolet are close to being usable for spectroscopic applications in the 10^6 resolving-power range. At this resolving power these gratings perform as well as the Fabry-Perot interferometer for many applications and with a much larger free spectral range. Modification of this ruling engine and control system in the last two to three years have resulted in improvement of the order of factors of 4 to 9 in the spectral quality of the high-angle 25-cm gratings when compared to earlier gratings ruled on the same engine.

H. W. Babcock has recently added a similar interferometric control system to the smaller ruling engine of the Mount Wilson Observatory.[59] This 25-cm ruling engine with interferometric control has produced several gratings of high quality in sizes up to 13 × 20 cm.

J. Ring and R. Beer at the University of Manchester[60] have constructed a high-pressure scanning Fabry-Perot interferometer for the range 1–18 μ and have obtained a resolving power of at least 240,000. H. P. Gush at the University of Toronto has constructed a rugged interferometer designed for the 6-μ region which is to be flown by C. Cummings and others of the C.A.R.D.E. group in a balloon to observe infrared sky emission at altitudes of up to 30 km.[61]

At Air Force Cambridge Research Laboratories, the development of interferometric techniques, particularly the use of the lamellar grating (of the type originally developed at Johns Hopkins University), is continuing under G. A. Vanasse and E. V. Loewenstein.[19] R. G. Walker is using a small Michelson type interferometer at the focus of a 2-m telescope to measure the near-infrared spectra of the stars and planets. A high-resolution prism grating spectrometer is being used to study molecular absorption in the 5–10 μ region with present interest in the 9 and 9.6 μ bands of ozone.[62] In this spectrometer the fringes from an interferometer with the movable mirror mounted on the nut of the precision screw which drives the grating spectrometer are used as a "ruler" for interpolating the unknown wavelengths of absorption lines between the wavelengths of higher-order neon emission lines.

B. Schurin has obtained the intensity of the NO fundamental band by pressure broadening the lines to minimize slit corrections and is presently measuring the overtone band intensities.[63] An interferometer will be used next with a Beckman IR-7 to measure the anomalous dispersion of absorption bands to determine the band intensities. These intensity studies are related to earlier studies carried out at the University of Wisconsin by Rollefson's group.

At the University of Freiburg, Germany, L. Genzel is continuing the traditions of the well-known far-infrared laboratory of M. Czerny at the University of Frankfurt, with whom Genzel was associated for a number of years. Particular emphasis is on the application of interferometric techniques to far-infrared studies.

Far-infrared molecular studies are being carried out at Johns Hopkins by D. W. Robinson[64] and at MIT by R. C. Lord.[65] E. D. Palik has been studying cyclotron resonance in solids in the far infrared at the Naval Research Laboratory, Washington, D.C., and has written a comprehensive bibliography of publications in far-infrared studies.[66] The reader is referred to this for a much more comprehensive listing of present efforts in the far infrared.

In astronomy, the study of the planets and stars in the infrared is increasing. Several infrared telescopes or programs are in progress or being planned both at existing observatories and for new observatories.

Some of the present efforts include the interesting well-known spectra of Mars and Venus obtained by W. Sinton of Lowell Observatory who is presently constructing a polarization-type interferometer to continue such measurements.[67] At Lick Observatory, C. Sagan is constructing an interferometer to be used with the Schwarzchild balloon-borne spectrometer to obtain planetary infrared spectra, while at the Jet Propulsion Laboratories of CIT, infrared radiometers and spectrometers are being developed for obtaining emission measurements of Venus and Mars from satellites launched to fly close to the planets.

In addition to molecular studies, atmospheric studies, and far-infrared studies there are several other studies underway of infrared radiation properties. These include, for example, the studies of hot gases or flames (F. P. Dickey at Ohio State University, S. S. Penner at CIT, U. Oppenheim at Technion, Israel); studies of infrared optical materials (W. Wolfe, Michigan; S. S. Ballard, Florida) as well as many infrared detector studies which are reviewed elsewhere in this issue. The infrared properties of solids and crystals including semiconductors are much studied. Many lasers function in the infrared. Laser studies in turn have intensified the interest in studies of coherence properties of infrared radiation. All of these areas in infrared are actively pursued in universities but it is not possible to include them in this brief review.

References

1. K. N. Rao, W. W. Brim, J. M. Hoffman, L. H. Jones, and R. S. McDowell, J. Mol. Spectroscopy **7,** 362 (1961).
2. G. Amat and H. H. Nielsen, J. Chem. Phys. **36,** 1859 (1962).
3. D. E. Burch, E. B. Singleton, and D. Williams, Appl. Opt. **1,** 359 (1962). A series of further papers is in publication in Applied Optics.
4. J. N. Howard, D. E. Burch, and D. Williams, J. Opt. Soc. Am. **46,** 186, 237, 242, 334, 452 (1956).
5. J. W. Birkeland, R. L. Bowman, D. E. Burch, R. R. Patty, K. N. Rao, J. H. Shaw, and D. Williams, Ohio State Univ., Final Report, Contract No. AF19(604)-2259, GRD-TR-60-285 (April 1960).
6. D. A. Grynak and J. H. Shaw, J. Opt. Soc. Am. **52,** 539 (1962).
7. E. E. Bell and R. L. Brown, Sci. Rept. 2 Contract No. AF19(604)-4119, AFCRC-TN-60-260, Ohio State Univ. (November 1959).
8. H. Happ and L. Genzel, Infrared Phys. **1,** 39 (1961).
9. W. H. Rogge, F. L. Yarger, and F. P. Dickey, J. Chem. Phys. **33,** 453 (1960).
10. W. T. Weeks, K. T. Hecht, and D. M. Dennison, J. Mol. Spectroscopy **8,** 30 (1962).
11. C. H. Church, R. Hunt, P. Maker, and C. W. Peters, Univ. of Michigan, Final Report Contract No. AF19(604)-2071, AFCRL-TR-60-433 (August 1960).
12. C. H. Church, Univ. of Michigan, Technical Rept. 1, Contract No. AF19(604)-2071, AFCRC-TN-59-237 (January 1959).
13. H. H. Nielsen, J. Opt. Soc. Am. **50,** 1147 (1960).
14. These papers have been largely published in J. Research Natl. Bur. Standards.
15. E. D. Tidwell, E. K. Plyler, and W. S. Benedict, J. Opt. Soc. Am. **50,** 1243 (1960).
16. R. Herman, W. S. Benedict, G. E. Moore, and S. Silverman, Astrophys. J. **135,** 277 (1962).
17. J. Strong, Johns Hopkins University, Sci. Rept. 1 Contract No. AF19(604)-2238, AFCRC-TN-58-608 (October 1958).
18. F. Stauffer and J. Strong, Appl. Opt. **1,** 129 (1962).
19. J. Strong and G. Vanasse, J. Opt. Soc. Am. **59,** 113 (1960).
20. R. P. Madden, J. Chem. Phys. **35,** 2083 (1961).
21. J. R. Izatt, Johns Hopkins Univ., Progress Rept. Contract No. Nonr 248 (01) (15 August 1960).
22. C. H. Palmer, J. Opt. Soc. Am. **50,** 1232 (1960).
23. D. H. Rank; paper presented at Conf. on Spectral Line Shape, Weizmann Institute, Rehovoth, Israel, September 1961.
24. D. H. Rank, D. P. Eastman, B. S. Rao, and T. A. Wiggins, J. Opt. Soc. Am. **52,** 1 (1962).
25. D. H. Rank and T. A. Wiggins; paper presented to Symposium on Mol. Spectroscopy, Columbus, Ohio, June 1962.
26. T. K. McCubbin, R. P. Grosso, and J. D. Mangus, Appl. Opt. **1,** 431 (1962).
27. W. F. Herget, N. M. Gailor, and A. H. Nielsen, University of Tennessee, Sci. Rept. 1, Contract AF19(604)-7981, AFCRL-62-253 (March 1962).
28. A. A. Mason and A. H. Nielsen; paper presented at Southeastern Section of APS, Tallahassee, Florida, April 1962.
29. G. Ameer and W. Benesch, J. Opt. Soc. Am. **51,** 303 (1961).
30. A. Ben-Reuven, S. Kimel, M. A. Hirshfeld, and J. H. Jaffe, J. Chem. Phys. **35,** 955 (1961). Also J. H. Jaffe, J. Meison, and N. Jacobi, J. Opt. Soc. Am. **52,** 8 (1962).
31. E. K. Gora, J. Mol. Spectroscopy **3,** 78 (1959). Also Final Report Contract AF19(604)-8603, AFCRL-62-445 (February 1962).
32. M. Migeotte, L. Neven, and J. Swenson, University of Liège, Final Rept. Contract AF61(514)-432 (1956).
33. H. A. Gebbie, L. Delbouille, and G. Roland, Report B. P. 11, National Physical Laboratory, Teddington (23 November 1961).
34. D. G. Murcray, J. N. Brooks, N. J. Sible, and H. C. Westdahl, Appl. Opt. **1,** 121 (1962).
35. R. A. Hanel and D. Q. Wark, J. Opt. Soc. Am. **51,** 1394 (1961). Also R. A. Hanel and W. G. Stroud, Tellus **13,** 486 (1961); J. Geophys. Research **66,** 3169 (1961).
36. M. G. Dreyfus and D. T. Hilleary, Aerospace Eng. **21,** 42 (1962).
37. S. Manabe and F. Möller, Monthly Weather Rev. **89,** 503 (1961).
38. G. Yamamoto and T. Sasamori, Sci. Repts. Tohoku Imp. Univ., Fifth Ser. Geophysics **10,** 37 (1958). Also G. Yamamoto, J. Meteorol. **18,** 581 (1961); J. Atmospheric Sci. **19,** 182 (1962).
39. D. M. Gates, J. Opt. Soc. Am. **50,** 1299 (1960); D. M. Gates and C. C. Shaw, J. Opt. Soc. Am. **50,** 876 (1960); also L. R. Megill and P. M. Jamnick, J. Opt. Soc. Am. **51,** 1294 (1961).
40. H.-J. Bolle, F. Möller, and H. Quenzel, Univ. of Mainz, Tech. Report Contract AF61(052)-246 (December 1961). Also Technical Report Contract AF61(052)-488 (March 1962).
41. F. Möller and W. Zdunkowski, Tech. Rept. 1 Contract AF61-(052)-357 (January 1961).
42. J. T. Bevans, R. V. Dunkle, D. K. Edwards, J. T. Gier, L. L. Levenson, and A. K. Oppenheim, J. Opt. Soc. Am. **50,** 130, 617 (1960).
43. F. Saiedy, Quart. J. Roy. Meteorol. Soc. **87,** 578 (1961).
44. A. Adel, Scientific Rept. HB-5, Contract No. AF19(604)-2177 (9 April 1958).
45. A. Adel, Scientific Rept. HB-9, Contract No. AF19(604)-2177 (31 January 1961).
46. E. Vigroux, University of Liège, Tech. Note, Contract AF61(514)-962 (in preparation 1962).
47. D. Diermendjian, J. Opt. Soc. Am. **51,** 620 (1961).
48. N. Ginsburg, Final Report, Contract AF19(604)-2443 (20 December 1961).
49. R. Paulson, E. Ellis, and N. Ginsburg, J. Opt. Soc. Am. **51,** 484 (1961).
50. K. Ya. Kondrati'ev, *Thermal Processes in the Atmosphere* (Hydrometeoizdat, Leningrad, 1960). See also K. Ya. Kondrati'ev and H. I. Niilisk, Geofis. pura e appl. **46,** 216, 231 (1960).
51. K. Ya. Kondrati'ev (private communication).
52. K. Ya. Kondrati'ev, "The Soviet Field Station on Mt. Elbrus," Weather (1961).
53. K. S. Shifrin, *Actinometry in Atmospheric Optics* (Hydrometeoizdat, Leningrad, 1961). See also K. S. Shifrin and O. Avaste "Short-wave Fluxes in the Cloudless Atmosphere," Estonian Academy of Sciences, Tartu (1960).
54. M. I. Budyko, "The Radiation Climate of the Arid Zones"; paper presented at Symposium of Radiation Commission; IAMAP, Vienna (August 1961).
55. E. Feigelson, Ph.D. Thesis, Moscow 1961 (in publication). Also G. V. Rozenberg, Uspekhi Fiz. Nauk **69,** 57 (1959); ibid. **71,** 173 (1960).
56. A. Hadni, J. M. Munier, C. Janot, and P. Poinsot, Abstracts, Fifth European Congr. Mol. Spectroscopy, Amsterdam, 1961.

57. A. Mitsuishi, Y. Yamada, and H. Yoshinaga, J. Opt. Soc. Am. **52,** 14, 17 (1962).
58. G. R. Harrison and G. W. Stroke, J. Opt. Soc. Am. **50,** 1153 (1960). See also G. W. Stroke, J. Opt. Soc. Am. **51,** 1321 (1961).
59. H. W. Babcock, Appl. Opt. **1,** 415 (1962).
60. R. Beer and J. Ring, Infrared Phys. **1,** 94 (1961).
61. H. P. Gush (private communication).
62. S. A. Clough; paper presented at Symp. Mol. Struct. and Spectros., Columbus, Ohio, June 1962.
63. B. Schurin and S. A. Clough; paper presented at APS meeting, New York City, February 1962.
64. D. W. Robinson, J. Chem. Phys. **36,** 83 (1962); ibid. **35,** 1045 (1961).
65. J. R. Durig and R. C. Lord, also B. Krakow and R. C. Lord; papers presented at Symposium on Mol. Spectroscopy, Columbus, Ohio, June 1962.
66. E. D. Palik, J. Opt. Soc. Am. **50,** 1329 (1960). A later version of this bibliography may be obtained from E. D. Palik of NRL.
67. W. M. Sinton, Appl. Opt. **1,** 105 (1962).

Applied Optics Patents

Reviewing panel

C. Shepard (Chairman) *Rochester*
R. Anwyl *Rochester*
G. W. Cleek *National Bureau of Standards*
A. Danti *Texas A & M*
J. Fitzmaurice *Baird-Atomic*
F. F. Hall, Jr. *ITT Federal Labs*
W. L. Hyde *Fecker*
R. Kingslake *Eastman Kodak*
D. J. Lovell *University of Michigan*
D. L. MacAdam *Eastman Kodak*
A. Mann *Spectrolab*
T. K. McCubbin *Penn. State University*
R. K. McDonald *Boeing*
J. R. Meyer-Arendt *Utah State University*
G. W. Stroke *University of Michigan*
D. E. Williamson *Cordis*

The patents reviewed below have been issued by the U.S. Patent Office on the dates quoted except where otherwise mentioned. The patent number, date of issuance, and classification number are quoted in the first line. The filing date is that of the earliest patent application. The opinions stated in the reviews are those of the reviewers and are not meant to express the thinking either of the organizations with which members of the panel are associated, of the Optical Society of America, or of this journal. Normally, statements of fact are based upon the patents and not independently verified. Printed copies of American patents may be ordered from the Commissioner of Patents, Washington 25, D.C., for 25¢ each. A weekly subscription service to any selected subclass is also available from the Patent Office.

3,015,249 Jan. 2, 1962 (Cl. 88-1)
Tracking telescope.
P. H. Taylor. Assigned to Northrop Corporation. Filed Mar. 14, 1949.

An early patent in the now popular field of star trackers. The field is scanned with a narrow wedge slit, the scanning frequency and low harmonics are discarded, the noise is clipped, and the resulting pip drives a high-Q circuit at the fundamental frequency. The phase then shows the angular position of the star in the field of view (though not its distance from the center). The telescope is vertical, and elevation is adjusted with a prism while the whole unit rotates in azimuth to point at the star. It is the telescope which is claimed, not the scanning technique. W.L.H.

3,016,464 Jan. 9, 1962 (Cl. 250-219)
Apparatus for determining the location and thickness of a reflecting object.
E. M. Bailey. Assigned to Daystrom Inc. Filed June 10, 1959.

A narrow beam of radiation is oscillated over a surface. A detector with a narrow receiving pattern detects the coincidence of the "beams" at the surface. The angular relationships involved are read out in any of several ways to indicate the relative location of the surface. D.E.W.

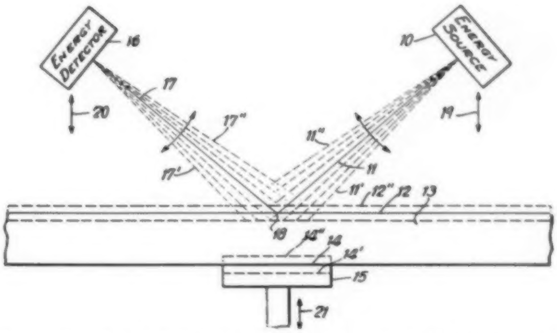

Apparatus for determining the location and thickness of a reflecting object.

3,016,785 Jan. 16, 1962 (Cl. 88-1)
Method and means for transmitting images through a bundle of transparent fibers.
N. S. Kapany. Filed May 20, 1957.

This is a generic patent for the principle of wobbling or vibrating the two ends of an image-transmitting fiber bundle synchronously so the image stands still while the fibers blur out. Any receiver with a finite time constant such as a human observer or photographic film will record the invariant portion (the image) and not the fibers themselves so the effective resolving power is improved over the static case. Several mechanical schemes to accomplish this are shown. W.L.H.

3,016,788 Jan. 16, 1962 (Cl. 88-14)
Methods and apparatus for color grading of fruits and vegetables.
T. J. Smith, assignor, by mesne assignments, of one-half to Genevieve I. Magnuson and one-half to G. I. Magnuson, R. Magnuson, and Lois J. Fox, as trustees. Filed May 24, 1952.

A photoelectric reflectometer for reading directly the average diffuse reflectances in the blue (436 μ) and red (640 μ) of both cut surfaces of a halved tomato, illuminates the halves separately and simultaneously with two sets of small mercury and neon arc lamps, filters the reflected light so as to confine the measurements to the stated wavelengths and receives the light on two photocells. Optical and electronic provisions are made for calibration and standardization. D.L.M.

3,016,789 Jan. 16, 1962 (Cl. 88-14)
Polarimetric apparatus.
A. S. Keston. Filed Jan. 3, 1958. (Division of Application filed Aug. 6, 1951, now patent 2,829,555.)

A number of split-field polarimeters are described for the measurement of small rotations. Balance is not restored; instead the intensity ratio of the two fields is measured to deduce the rotation of the sample. W.L.H.

3,016,795 Jan. 16, 1962 (Cl. 88-40)
Substage lighting means for microscopes.
C. J. de Grave, Jr., and H. W. Straat. Assigned to Bausch & Lomb, Inc. Filed Dec. 28, 1959.

A mechanical arrangement is described which allows a conventional Abbe condenser to be changed into a variable focus condenser by separating the two elements, clamping the upper one, and moving only the lower lens. W.L.H.

3,017,801 Jan. 23, 1962 (Cl. 88-14)

Device for measuring the width or diameter of fixed or movable tapes and wires.

O. H. INGBER. Filed Nov. 25, 1958 (in France Nov. 29, 1957).

A simple system is claimed consisting of a light source, a lens focusing an image of the tape on a diaphragm, and a photocell to detect the transmitted light. A servo system adjusts the diaphragm to maintain the light constant, and read out the desired dimension. A variation uses a reference beam and chopper. This patent has unusually complete description with variations in technique including choppers with teeth of varying width. The 41 figures include circuit diagrams with component values. D.E.W.

3,017,805 Jan. 23, 1962 (Cl. 88-26)

Projector.

R. KREMP AND P. FROST. Assigned to Agfa Aktiengesellschaft. Filed Dec. 4, 1958 (in Germany Jan. 11, 1958).

Provides a small lens which can be introduced between the picture and the projection lens and positioned to magnify a portion of the picture selectively, and a corresponding movable condenser lens. No provision is made to restore the focus, or to reorient the projection angle toward the screen. W.L.H.

3,018,686 Jan. 30, 1962 (Cl. 88-27)

Tachistoscope.

K. F. KURZ. Assigned to Sawyer's Inc. Filed Jan. 10, 1961.

A detailed scheme to feed transparencies into a projector, to shutter the aperture, and to adjust the framing of the aperture. W.L.H.

3,019,135 Jan. 30, 1962 (Cl. 117-211)

Method of producing coated glass articles.

L. E. ORR. Assigned to Pittsburgh Plate Glass Co. Original application May 19, 1955, divided and this application Oct. 17, 1957.

Describes a method of depositing electrical conductive transparent coatings of nonuniform thickness on glass windows or viewing closures of irregular shape. The use of "split" or "dumbbell" spray patterns makes it possible to obtain nonuniform surface resistivity in the coatings, which in turn control the temperatures produced when a current is passed through the coating. The method is applicable to curved surfaces as well as flat surfaces and to cases where the bus bars are not parallel. The coating material is primarily tin oxide, but mixtures containing other metals may be used. Oxide films of metals, such as cadmium, zinc, indium, etc., may also be produced. G.W.C.

3,019,692 Feb. 6, 1962 (Cl. 88-14)

Condensation nuclei optical measuring apparatus.

G. F. SKALA. Assigned to General Electric Co. Filed Aug. 30, 1957.

Apparatus for measuring the concentration of condensation nuclei in a gaseous sample is described. The device comprises an electronic circuit for differentiating, with respect to time, the electrical output signal of a sensitive detector positioned to intercept radiation scattered by nuclei-induced droplet clouds formed in an expansion chamber traversed by a beam of radiant energy. The resulting electrical output, measured by a peak-reading voltmeter, is a linear function of nuclei concentration which, it is claimed, yields increased sensitivity at high concentrations over previous nonlinear devices. R.D.A.

3,019,703 Feb. 6, 1962 (Cl. 88-24)

Photographic colour reproduction apparatus.

A. R. KILMINSTER. Assigned to Hunter-Penrose Ltd. Filed Sept. 18, 1958 (in Gt. Britain Sept. 24, 1957).

Color originals are illuminated for photographic preparation of color separation negatives by a scanning spot of white light, the intensity of which is controlled by a complex photoelectric sensing and feedback system designed to compensate for all the characteristics of the photographic and printing media. Four-color separations are made by successive uses of the device with manually switched correction parameters. D.L.M.

3,019,705 Feb. 6, 1962 (Cl. 88-39)

Coarse and fine adjustment mechanism for microscopes.

L. A. WILKINSON. Assigned to American Optical Co. Filed Dec. 13, 1957.

A scheme for a coaxial coarse and fine adjust mechanism using planetary gears and a single set of ways. W.L.H.

3,019,706 Feb. 6, 1962 (Cl. 88-39)

Fine adjustment mechanism for microscopes.

T. UENO. Assigned to Nippon Kogaku K. K. Filed Feb. 25, 1958.

The objective turret is tilted on a leaf spring by a lever arm for the fine focus. The coarse focus is entirely separate. W.L.H.

3,019,707 Feb. 6, 1962 (Cl. 88-39)

Fine adjustment mechanism for microscopes.

H. W. STRAAT. Assigned to Bausch & Lomb, Inc. Filed May 13, 1959.

A single long claim describes a particular arrangement of gears for putting the fine adjustment concentric with the coarse. W.L.H.

3,020,793 Feb. 13, 1962 (Cl. 88-14)

Automatic photoelectric colorimeter.

D. A. NEUBRECH AND M. A. CATTARO. Assigned to Gardner Laboratory, Inc. Filed Apr. 20, 1960.

An improved circuit for the Hunter (U.S. Pat. 2,696,750) automatic photoelectric colorimeter employs electrically independent networks for the photocells and servos controlling the vertical and horizontal coordinate indicators. This separation is said to facilitate calibration and continuous self-standardisation. D.L.M.

3,024,692 Mar. 13, 1962 (Cl. 88-14)

Chart readers and comparators and method of translating light transmittance values of colorimeter recordings into concentration values.

L. T. SKEGGS. Assigned to Technicon Instruments Corp. Filed June 12, 1958.

A laminated, optically clear plate with vertical, spaced-line segments marked on one of the laminated surfaces, and a matte upper surface receptive of pencil or ink markings is designed to be placed over strip-chart records so as to facilitate the application of nonlinear calibrations, such as concentration versus photocell response in optical assay. D.L.M.

3,025,744 Mar. 20, 1962 (Cl. 88-14)

Spectrometer.

P. W. COLLYER AND R. B. BARNES. Assigned to Barnes Engineering Co. Filed Jan. 6, 1961. Division of application filed Jan. 20, 1960.

A compact in-line spectrometer for measurements of the spectra of distant objects is described. Cassegrainian mirror systems serve as condenser, collimator, and telescope. Parts 3 and 4 are a filter holder and a neutral density filter. A wedge in contact with the transmission grating, 8, cancels the deviation. Parts 11 and 12 are a field lens and a photographic film. It is claimed that the spectrometer is low in cost, high in light gathering power, rugged, and capable of easily being set up and aimed in the field by semiskilled personnel. T.K.M.

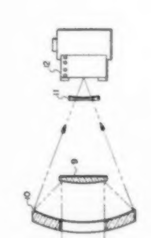

Spectrometer.

3,031,917 May 1, 1962 (Cl. 88-14)

Recorder means for fluid examination apparatus.

M. H. PELAVIN. Assigned to Technicon Instruments Corp. Filed July 10, 1958.

A thermistor temperature compensator for continuously recording photoelectric colorimeters. Alternatively a variable-tap function-generating potentiometer coupled to the recording member of a colorimeter to convert from transmittance to a linear concentration scale. D.L.M.

NEW SUBSCRIPTION ORDER

APPLIED OPTICS

Please enter my/our subscription* and continue until countermanded:

☐ OSA member rate $6.00 per year
☐ Other AIP Societies' rate $8.00 per year
☐ Regular rate $10.00 per year
☐ Please send OSA membership information
☐ check enclosed ☐ bill me
☐ Single copy of issue $2.00
☐ **MASERS Supplement** published December 1962 .. $5.00

Name .... Membership No. ....

Address ....

....

*Subscriptions entered for calendar year only.

NEW SUBSCRIPTION ORDER

APPLIED OPTICS

Please enter my/our subscription* and continue until countermanded:

☐ OSA member rate $6.00 per year
☐ Other AIP Societies' rate $8.00 per year
☐ Regular rate $10.00 per year
☐ Please send OSA membership information
☐ check enclosed ☐ bill me
☐ Single copy of issue $2.00
☐ **MASERS Supplement** published December 1962 .. $5.00

Name .... Membership No. ....

Address ....

....

*Subscriptions entered for calendar year only.

FIRST CLASS
Permit No. 18297
New York, N. Y.

BUSINESS REPLY MAIL
No postage stamp necessary if mailed in the U. S. A.

POSTAGE WILL BE PAID BY

APPLIED OPTICS
American Institute of Physics
335 E. 45th Street
New York 17, N. Y.
Attention Miss J. Raimondi, Circulation

FIRST CLASS
Permit No. 18297
New York, N. Y.

BUSINESS REPLY MAIL
No postage stamp necessary if mailed in the U. S. A.

POSTAGE WILL BE PAID BY

APPLIED OPTICS
American Institute of Physics
335 E. 45th Street
New York 17, N. Y.
Attention Miss J. Raimondi, Circulation

Infrared Photodetectors: A Review of Operational Detectors

R. F. Potter and W. L. Eisenman

A comparison is given, in terms of D^*, of the characteristics of most of the photodetectors of both quantum and thermal types, which are available for operational use at the near and intermediate infrared. A discussion of detectors for use at longer wavelengths (up to the mm range) includes two quantum types as well as the cooled bolometers and the pneumatic cell. The review of thermal detectors emphasizes noise limitations as well as spectral characteristics. The need for gray body detectors for use in spectral response measurements is discussed. It is pointed out that a complete noise power spectrum is essential in order to evaluate effectively a detector and determine the operational limitations.

Introduction

Infrared radiation detectors have been the subject of several comprehensive reviews as is needed in a rapidly developing technology. However, the emphasis has been on the class known as quantum photodetectors. With the rapid developments in semiconductor technology in the past decade and a half, an imposing array of such detectors is available for a wide variety of applications. The theory of operation and description of the parameters has an extensive literature.[1] More recently Levinstein and co-workers[2] have given a review of the status of quantum photodetectors including a discussion on the figure of performance known as D^*.

There has been a resurgence of interest in another class of detectors which we call thermal photodetectors, i.e., the detector material absorbs photons and the resulting change in temperature is measured. This is usually detected using an intrinsic property but not always so. An expanding interest in detecting radiation at long wavelengths ($\lambda > 50\ \mu$) has brought about the development of a series of bolometer elements operated at extremely low temperatures ($T < 5.0°\text{K}$). There are also a growing number of requirements for detectors capable of operating at considerably higher temperatures (200°K–350°K) and this has given new emphasis to thermistor bolometer elements. It will be the purpose of this review then to emphasize the long-wavelength quantum detectors, to provide recent data on the thermal detectors, to provide a comparison where applicable, and to discuss some special topics in connection with certain parameter measurements that are necessary to provide a quantitative evaluation on a photodetector.

In Table I of Appendix A we list the symbols, definitions, and terms in common use for describing photodetectors and their capabilities. In Appendix A the functional relationships are also given for those figures of performance which are in general modern use in describing photodetectors, including $NEP(P_N)$ and D^*.[3]

Because many detectors have an $A^{-1/2}$ dependence on their detectivity the importance of D^* is that it permits comparison of most detectors of the same type but of different areas.

Note that with D^* or NEP it is not possible to predict the responsivity of any detector of the same type; however, it is possible to predict the signal-to-noise ratio of any detector of the same type. Unfortunately, the manufacture of detectors has not reached the point where this theoretical reproducibility is achieved, and the relationship between different detectors of the same type is complicated by factors that evidently cannot yet be controlled. However, with D^*, an approximation may be made of what is to be expected from different detectors of the same type. For background noise limited detectors, Jones has defined D^{**} which normalizes to unit solid angle.[4] In Figs. 2 and 3 we indicate the detector field of view as well as the operating temperature.

Detailed discussions of the theory of photoconductive, photovoltaic, etc., detectors are available in the literature.[1, 2] Because small signal and noise theory are treated so extensively elsewhere we limit our-

---

The authors are in the Infrared Division, U.S. Naval Ordnance Laboratory, Corona, California.

Received 6 March 1962.

This work was performed by the Joint Service Infrared Sensitive Element Testing Program at the U.S. Naval Ordnance Laboratory, Corona, California. This program is supported by the Army, Navy, Air Force, and NASA.

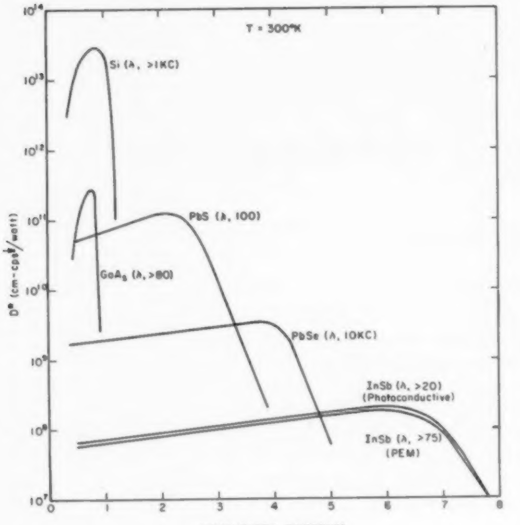

Fig. 1. A comparison of room temperature quantum photodetectors. Parenthesized data indicate spectral data and the optimum operating modulation frequencies. Data are representative of detectors reported in the Photodetector Series Reports, NOLC 474, 527, 557, and 561.

selves to a parametric description. In all the data presented here the measurements are limited in detectivity by the detector noise which in most instances comprises in part or entirely the three noise components described in Appendix B.

Near and Intermediate Infrared Quantum Photodetectors

By quantum photodetectors we mean those devices which operate by photon excitation of an electron state, such an excitation resulting in a detectable change of an intrinsic property, i.e., conduction, electron emission, etc., with the exclusion of a change of temperature. Several classification schemes have been proposed for characterizing detectors in a general way (see R. C. Jones[5]) but we will group detectors according to the operating temperatures. Thus we have four such groups:

(a) 25°C (so-called room temperature) (Fig. 1),
(b) −78°C (so-called dry ice temperature) (Fig. 2),
(c) −196°C (so-called liquid nitrogen temperature) (Fig. 2), and
(d) all lower temperatures (Fig. 3).

Most of these curves are representative of the best detectors which have been measured at Corona, and all detectors of these types are available from commercial sources. Many curves in these figures can be compared with similar curves of 1959[3] and it will be seen that substantial over-all performance improvement has been made. We have also indicated for each respective detector the frequency or the range of frequencies at which the detector can be modulated or "chopped" without reducing its detectivity from optimum.

There are several features out of the ordinary to note in these figures. The room temperature InSb has the same detectivity for the photoconductive as that for the *PEM* mode. Of more general interest are the operating temperature characteristics of the PbS and PbSe film detectors. Each type can be made to peak at or near "dry ice" temperature which is a most important consideration in view of modern cryogenic techniques. Of course if one requires the longer wavelength capabilities he would use a detector designed for operation at a cooler temperature.

Levinstein includes spectral data for several extrinsic germanium detectors in his review.[2]

Long-Wavelength Infrared Quantum Photodetectors

The quantum photodetectors in Fig. 3 which function beyond 7–10 μ are of the impurity photoconductor type, and are semiconductors. The semiconductor absorbs photons of sufficient energy that electrons are excited to the conduction bands and contribute to the conductivity (a similar situation of course holds for hole processes). For operation out to 40 μ these levels

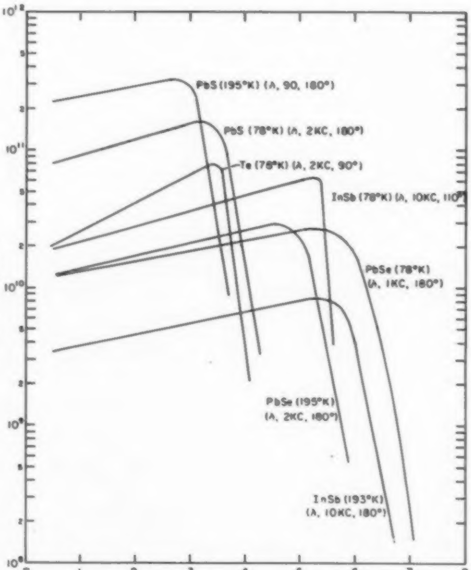

Fig. 2. A comparison of quantum photodetectors operated at dry ice and liquid nitrogen temperatures. The first set of parentheses includes the refrigerant temperature. The second set of parentheses includes an indication of spectral data, optimum modulation frequency, and the field of view in degrees. Data are representative of detectors reported in the Photodetector Series Reports, NOLC 474, 551, 557, and NavWeps 7181.

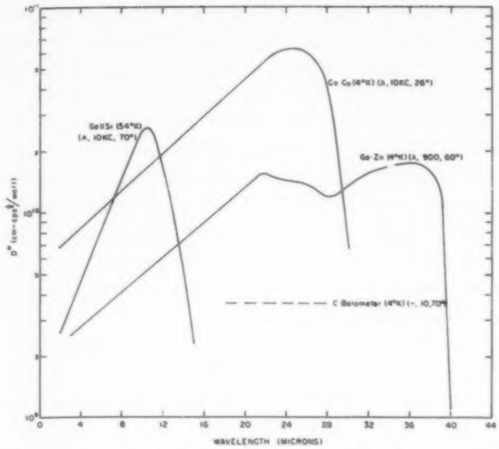

Fig. 3. A comparison of quantum photodetectors operated at $T < 77°K$. The temperatures in parentheses are those of the refrigerants to which the detector heat sink is attached. Spectral characteristics, optimum modulation frequency, and field of view are included in the second set of parentheses. Data are included for a carbon resistor bolometer mounted on a heat sink attached to a 4°K bath in a commercial cryostat. Photodetector Series Reports, NOLC 527 and NavWeps 7181 give further data on the Ge:Cu and the Ge:Si detectors, respectively. The Ge:Zn detector is as reported in ref. 2.

are required to be of the order of 0.03 ev. In order to extend the response to longer wavelengths impurity levels closer to the band must be found.

Putley[6] has described such a detector which can be used in the mm and sub-mm region of the spectrum. The photoconduction is based on the fact that shallow impurity levels are evident in the presence of magnetic fields of strengths, B, *ca* 5000 gauss. These levels appear in relatively pure InSb ($N_0 \simeq 5 \times 10^{13}$ cm^{-3} at 77°K) and have values between 2 and 8×10^{-4} ev.

As can be seen from Fig. 5, there exists an optimum field strength for the effect. Putley suggests that the effect is due to a conventional photoconduction process plus an "electronic bolometer" behavior wherein the radiation is absorbed by the electron gas with a resultant change of mobility. This detector has been used at wavelengths as long as 8 mm. A $D^* = 2 \times 10^{11}$ cm cps$^{1/2}$ watt^{-1} at 1.0 mm was measured in a system considered to be amplifier noise limited.

Another long-wavelength electronic bolometer has been suggested by Goodwin and Jones.[7] Their suggestion is to increase the optical absorption at the cyclotron resonance frequency [$\omega_c = (eB/m^*)$]. This raises the electron gas temperature with a resulting change in conductivity. Measurements on n-type Ge at 4.2°K at $\lambda = 9$ mm, $m^* = 0.13\, m_e$ gave a value of $D^* = 10^{11}$ cm cps$^{1/2}$ watt^{-1}, the detector being Nyquist-Johnson noise limited (see Appendix B). The inventors expect that this could be substantially improved. Whereas the Putley detector has a broad spectral band, the Goodwin-Jones detector has a narrow bandpass. One tunes the center of the bandpass by varying the magnetic field. Detectors of these types, if highly developed, will enable a wholesale exploration of the far infrared spectrum to begin.

Thermal Photodetectors

An excellent source and reference book by Smith *et al.*[8] gives a comprehensive review of all types of thermal photodetectors, including a discussion of the pertinent theory. The present section is limited to a discussion of recent developments.

Thermistor Bolometer

There has been a renewed interest in this type of photoelement, both as a single element and as an array

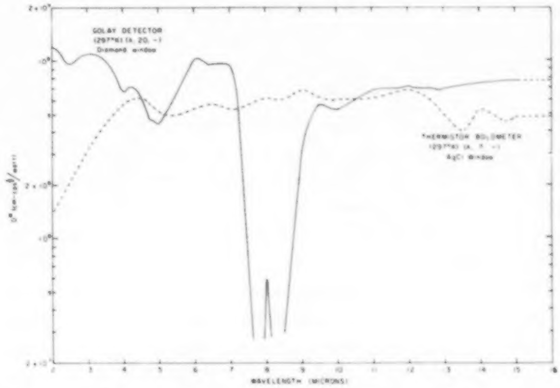

Fig. 4. Spectral detectivity for two thermal photodetectors operated at room temperature. D^* is not a proper figure of performance for the Golay cell, and the values shown here should be multiplied by a factor of 3.6 to give $D = NEP^{-1}$. These data are representative of detectors reported in Photodetector Series Report, NOLC 561.

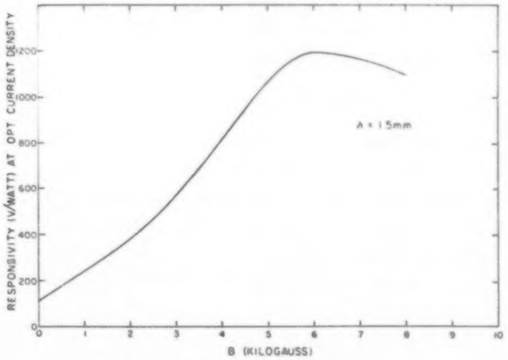

Fig. 5. The responsivity of the Putley detector at $\lambda = 1.5$ mm is shown as a function of the field strength B. The use of a superconductor-wound electromagnet will permit a relatively compact package size. The data given here are taken from that of ref. 6.

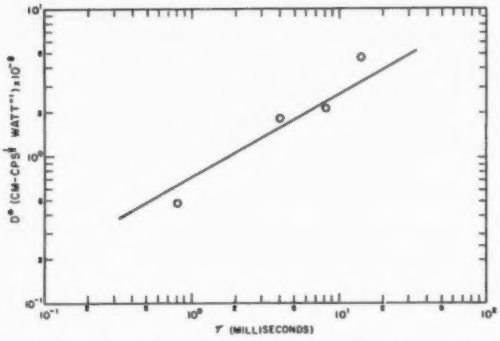

Fig. 6. Optimum detectivity for several thermistor bolometer elements as a function of their response time constant. The four detectors approximately follow the solid line which has a slope of $^1/_2$.

of elements. This interest, of course, stems from their capabilities at longer wavelengths while operating at a temperature near ambient. A spectral curve for D^* is shown in Fig. 4. Thermistor bolometers are among that class of detectors whose D^* exhibits a $\tau^{1/2}$ dependence. In Fig. 6 are shown the detectivities of four such bolometers made up of thermistor material composed of oxidic mixtures of manganese, nickel, and cobalt.[9] It can be seen that one does indeed sacrifice detectivity to obtain a bolometer having a faster response time.

Thermistor bolometers have generally been considered to be limited by the Nyquist-Johnson noise which is frequency independent. Recently, however, improvements in techniques for measuring low-noise power levels at low frequencies have permitted measurements on thermistor bolometers down to 1 cps.[10] In Fig. 7 are shown a family of curves for a bolometer element with a time constant of 8 msec. One can see that an f^{-1} component of noise has set in at 30 cps, and at lower frequencies this type of noise limits the detector. In the same figure are shown a family of curves for $D^*(\lambda_{\max})$. One sees that at the higher frequencies the detector is Nyquist-Johnson noise limited.

Cooled Bolometers

The same theoretical conditions hold for bolometers at temperatures other than ambient, the primary considerations being that of thermal conductance and the temperature coefficient of resistivity of the material.

Carbon resistor bolometers and suitably doped germanium elements have been successfully developed for operation at 4.2°K and less.

Carbon composition resistor bolometers operated at 1.5°K have been used extensively by Tinkham and coworkers[11] in their investigation at mm wavelengths. It would be expected that semiconductor bolometers of the type described by Low[12] will come into use in future research at these very long infrared wavelengths. Low estimates that a gallium-doped germanium bolometer operated at 4.2°K with a 180° field of view of 300°K background will be background noise limited and have an *NEP* of 2.7 × 10^{-12} watts. Substantial improvements can be achieved by lowering the operating temperature and narrowing the field of view. Selective filtering will also aid in this respect. Low reports that he achieved an *NEP* of 5 × 10^{-13} watts operating at 2.15°K with a time constant of 400 μsec. It should be noted that Low's bolometer is operated so that the thermal coupling is through the leads; hence it should have no area dependence.

In reading the literature one cannot but note the variety of conditions under which the low-temperature carbon resistor bolometers have been measured and reported. Boyle and Rodgers[13] report an *NEP* of 10^{-11} watts for a carbon bolometer operated at 2°K with an unspecified but evidently very narrow field of view and filtered background radiation. A similar bolometer, fashioned at NOLC, mounted in a commercial liquid helium dewar with a wide field of view and a minimum of filtering, had an *NEP* of 6 × 10^{-10} watts when operated at 10 cps. This detector is shown for comparison in Fig. 3 although no spectral measurements were made.

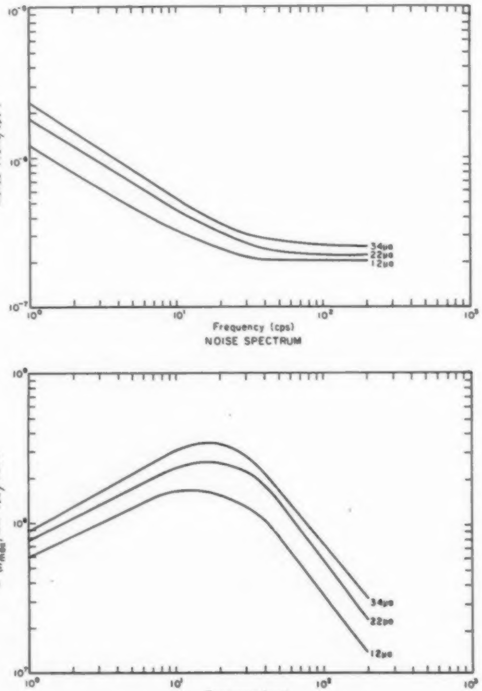

Fig. 7. The low-frequency noise spectrum of a thermistor bolometer is shown in the upper curve. It shows the detector to be f^{-1} noise limited at the lower frequencies. As a result the detectivity peaks at approximately 20 cps.

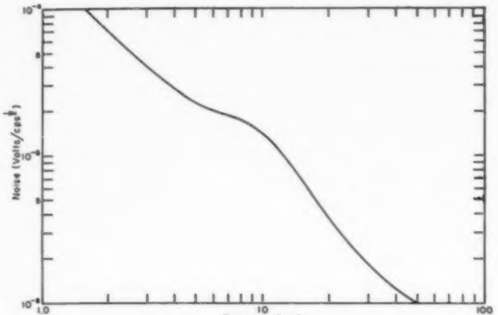

(A) NOISE SPECTRUM

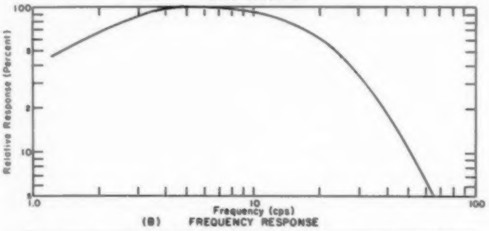

(B) FREQUENCY RESPONSE

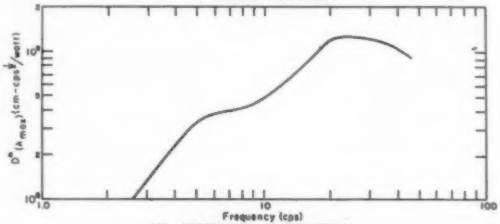

(C) DETECTIVITY VS FREQUENCY

Fig. 8. The low-frequency noise spectrum for a Golay pneumatic detector is shown in the upper curve. The detector is limited by a mixture of the f^{-1} noise of the optical system and response noise. The middle curve shows the effect of ballasting and diaphragm response time on the frequency response. The bottom curve shows the resulting effect on the detectivity. If the detector could be made to be response noise limited, not only would the gouge be eliminated but the detectivity value would be higher.

The authors are not aware of any recent developments for metal strip bolometers and superconducting bolometers; the reader is referred to ref. 8 for a discussion of the known characteristics of these detectors.

Pneumatic Detector

The Golay detector is a widely known detector but somewhat less widely used. There exists an extreme paucity of quantitative information concerning the operating characteristics. In some literature it is described as having a frequency response of the form $r = r_0\ (1 + \omega^2\tau^2)^{-1/2}$ which is directly contradictory to the description of the cell operation. Also, many descriptions assume the detector to be response noise limited [Brownian motion of the membrane and power fluctuations (see Appendix B)] with the result that detectivity is expected to have little or no frequency dependence over a wide frequency range. Failure in achieving these conditions, of course, leads (in many instances) to disappointment in the use of the detector.

The Golay cell utilizes the mechanical energy of a pneumatic circuit coupled with an optical system for measuring the mechanical displacement caused by the incoming radiation signal.

In commercial units the optical system operates with a photoemissive tube; thus there are two dominant sources of noise present (Appendix B): (1) The flicker noise (f^{-1}) of the photoemissive cell, and (2) the response noise of the detector.

In order to avoid thermal drift the pneumatic cell is suitably ballasted, resulting in a low-frequency fall-off in the responsivity. There is an additional fall-off occurring at higher frequencies caused by the natural response time of the diaphragm. Apparently no detailed information on these detectors has been made available since the original paper by Golay.[14]

A refurbished detector equipped with a diamond window recently became available for evaluation as it came from the factory. The detectivity as a function of wavelength in the intermediate infrared is shown in Fig. 4 (the strong absorption lines indicate that the window was made from type I diamond). In Fig. 8 are shown the frequency response and noise spectrum. These reflect the presence of thermal ballasting (low-frequency cutoff), natural time constant of the diaphragm, flicker noise of the photocell, and the response noise due to Brownian motion of the diaphragm and power fluctuations. All of these effects are reflected in the frequency spectrum of the detectivity. It is seen that this detector is not quite response-noise limited and that one gains a factor of approximately 2.5 by operating at 20 cps rather than the usual 10 cps. This demonstrates the need of information of the type of Fig. 8 when use of this detector is considered.

Special Considerations

Gray Detectors

Most detectors, as commercially fabricated, have color characteristics due to bulk properties, surface properties, and/or window properties. This becomes a critical problem when one considers the need for a standard gray reference for spectral response measurements. The Golay detector receptor film is hypothetically gray, the film being designed to have a reported impedance of 270 Ω/sq but verification of grayness has evidently never been reported beyond 15 μ. Radiation thermocouples and thermopiles with "blackened" surfaces have long been used as transfer standards. Preliminary measurements carried on at NOLC indicate that the emittances of such surfaces begin to decrease between 10 and 12 μ.

The use of blackened radiation thermocouples as gray body reference standards in the infrared is undoubtedly

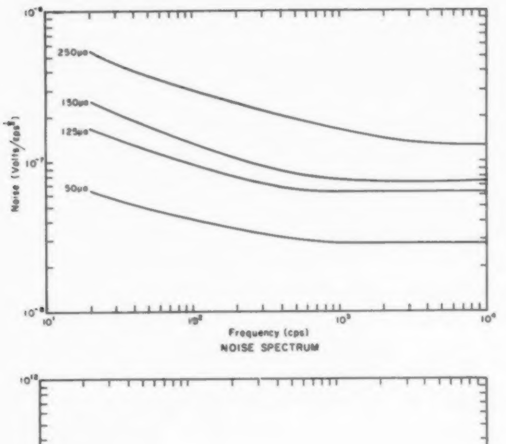

Fig. 9. Frequency spectra of the noise for a liquid nitrogen cooled InSb photoconductor. At higher frequencies the detector is response noise limited (G-R). The detectivity spectra are shown in the lower curve.

a relatively safe procedure out to wavelengths of approximately 15 μ. However, the unsubstantiated assumption of grayness of these detectors beyond this wavelength may lead to serious difficulties for any extension of radiometry to longer wavelengths.

If the Golay detector is indeed gray, then its use in this connection could be very fruitful over wide spectral ranges, provided one knows the spectral transmittance of the windows used. Parenthetically, several developers of long-wavelength detectors have been using this as a standard. One can find such statements as "the response..." or "the sensitivity is X times that of a Golay detector," but no further reference to the standard is given. The Golay needs further study in this regard, but it may well turn out that, as a standard, it will be a most important link in the radiometric exploration of the far infrared spectrum.

Another approach to this problem has been taken at NOLC. A calorimeter in the shape of a 15° cone, blackened on the inside, total weight 0.25 mg, wall thickness before blackening *ca* 2 μ, has been fabricated and mounted as the receiver for a Bi-BiSn thermocouple. The thermal inertia is such that it can be operated at 1 cps. The geometrical shape and blackening permit a reasonable assumption that this is a black detector. The spectral response of a suitable transfer standard detector (e.g., radiation thermocouple) is compared with that of the assumed blackbody detector. Keeping the transfer standard in the same optical position, the blackbody detector is replaced by the unknown and the spectral comparison made. In this manner, the unknown spectral response can be referred back to that of the blackbody detector. The geometry of the blackbody detector will limit the spectral region for the validity of the blackness assumption.

Although other possibilities suggest themselves, these two detectors seem to be the best available for the near future as gray body standards.

Noise Measurements

Many comparisons of detectors define and use various performance figures which are meant as guides for use by those carrying on detector development. While the user should know and be aware of the limits of the "ideal detector," he cannot rely on *NEP* and D^* alone. These are often given for optimum conditions assuming detector limited conditions only. If he has other empirical information at hand, he may choose to operate the detector in a condition other than "optimum." A case in point is that of the noise characteristics. We have seen how noise departs from the ideal in the case of bolometers and the Golay cell. In Fig. 9 we show the detectivity and noise spectra of a very good photoconductive InSb detector operated at 77°K. Two types of current noise are evident; an f^{-1} component, followed by response noise component (G-R, see Appendix B) for each bias current (at frequencies > 100 Kcps these noise curves would fall off to the Nyquist-Johnson noise level). The optimum bias is 125 μamp but this detector requires an extremely low-noise amplifier to realize this optimum detectivity. From the curves one can determine that by operating at 250 μamp he suffers a 20–30% loss in detectivity but this is offset by being able to relax the noise voltage requirements of his amplifier by a factor of 2.5 or more. Thus there are empirical as well as theoretical reasons for reporting complete pertinent data on detectors. As discussed in Appendix B a complete noise spectrum determines what type of noise is limiting the detector.

The Corona "Detector Series" now reports noise spectra from 1 cps to 10^4 cps (in the pertinent ranges) with a bandpass of 0.3 cps, 1–40 cps and 20 cps–10^4 cps with a 5-cps bandpass for impedances from a few ohms to 100 megohms. Using this capability the noise spectrum of a radiation thermocouple was measured 1 cps to 40 cps, and it was found to be Nyquist-Johnson noise limited down to 1 cps (15-Ω impedance).

Summary

In this review we have attempted to provide a quantitative comparison of most photodetectors in use today (and most are available); these include the intrinsic and extrinsic semiconductor quantum photodetectors as well as several thermal photodetectors. Because of the increasing interest and opportunity in the exploration of the far infrared spectrum by radiometric techniques we have emphasized the recent developments in semiconductor bolometers, and novel far infrared semiconductor detectors. It is our opinion that we will see some most exciting developments in this field (including masers). We have also mentioned two special topics which are generally not covered in detector reviews: (1) Continuing need for standard references for spectral response, and (2) measurement of noise spectra from low to high frequencies.

In conclusion we acknowledge with pleasure the contribution and effort of J. D. Merriam, A. B. Naugle, P. C. Caringella, and R. L. Bates in making the detector evaluation program a success; they are responsible for much of the data drawn upon for this report. We also wish to thank E. H. Putley for furnishing us a preprint of his paper presented before the 1961 International Photoconductivity Conference.

Appendix A

Because the requirements are so diverse, several figures of performance have been developed for use in comparing one detector with others of the same or similar type. The following definitions and functional relationships are given for those which are considered to be the most pertinent in modern day use. They are summarized in Table I.

Responsivity

The responsivity is defined as

$$R = \frac{V}{JA}\,\frac{\text{volts}}{\text{watts}}. \tag{A1}$$

Responsivity, the ratio of the rms value of the fundamental component of the signal voltage to the rms value of the fundamental component of the incident radiation power, is written in functional notation as

$$R = R(b,\lambda,f).$$

The absolute responsivity as a function of wavelength and modulation frequency is given by

$$R(\lambda,f) = R_{\text{bb}}\,\frac{V_\lambda(\lambda)P_{\text{rms}}}{V_\lambda(\lambda)P_{\lambda,\text{rms}}d\lambda}\,\frac{V_f(f)}{V_f(f)_r}, \tag{A2}$$

where

R_{bb} = responsivity to a blackbody source (or other suitable source having a known spectral content),

f_r = frequency at which R_{bb} is measured,

$P_{\text{rms}} = \int_0^\infty P_{\lambda,\text{rms}}\,d\lambda$ total rms radiation source power flux.

The term $V_f(f)/V_f(f_r)$ gives the frequency characteristics of the detector, and the term

$$E(P) = \frac{\int_0^\infty V_\lambda(\lambda)P_{\lambda,\text{rms}}d\lambda}{P_{\text{rms}}} \tag{A3}$$

gives the spectral power efficiency; that is, it indicates how effective the detector is compared to a "black" or "gray" detector (detectors with constant response at all wavelengths).

The wavelength dependence of the responsivity can now be written

$$R(\lambda) = \frac{R_{\text{bb}}}{E(P)}\,V_\lambda(\lambda). \tag{A4}$$

Since $V_\lambda(\lambda_{\max}) = 1$, the term $R_{\text{bb}}/E(P)$ gives the maximum response of the detector at the spectral peak.

Noise Equivalent Irradiance

The noise equivalent irradiance is defined as

$$H_N = \frac{NJ}{V(\Delta f)^{1/2}}\,\frac{\text{watts}}{\text{cps}^{1/2}\,\text{cm}^2}. \tag{A5}$$

H_N is the minimum radiant flux density necessary to produce a signal-to-noise ratio of 1 when the noise value is normalized to a unit bandwidth. In functional notation

$$H_N = H_N\,(b, \lambda, f, A).$$

Since the area of the detector is not taken into account in H_N, the figure describes the performance of a detector of a specific area.

Noise Equivalent Power

The noise equivalent power is defined as

$$NEP = P_N = \frac{NJA}{V(\Delta f)^{1/2}}\,\frac{\text{watts}}{\text{cps}^{1/2}}. \tag{A6}$$

P_N is the minimum radiant flux necessary to produce a signal-to-noise ratio of 1 when the noise value is normalized to unit bandwidth. In functional notation

$$P_N = P_N\,(b, \lambda, f).$$

D-Star

D-Star, or D^*, is defined as

$$D^* = \frac{A^{1/2}}{P_N}\,\frac{\text{cm-cps}^{1/2}}{\text{watts}}. \tag{A7}$$

D^* is the detectivity normalized to unit area and unit bandwidth. Detectivity is the signal-to-noise ratio produced with unit radiant flux incident on the detector. Since the area dependence of the signal-to-noise ratio has been taken into account, D^* describes the general detector type rather than a detector of some particular area.

In functional notation

$$D^* = D^*(b, \lambda, f).$$

Table I. Figures of Performance

Symbol	Definition in terms of observables	Figures of performance and units
R	$R = V/JA$	Responsivity in volts per watt
NEI	$NEI = JN/V\Delta f^{1/2}$	Noise Equivalent Irradiance in watts/(cm^2 cps$^{1/2}$)
$NEP = P_N$	$NEP = JNA/V\Delta f^{1/2}$	Noise Equivalent Power in watts/cps$^{1/2}$
D^*	$D^* = A^{1/2} (\Delta f)^{1/2}/P_N$	The detectivity normalized to unit area and unit bandwidth in cm-cps$^{1/2}$ watt

Symbol Definitions

A = area of the detector in cm^2,
b = bias applied to the detector,
f = modulation frequency of the radiation incident on the detector,
Δf = frequency bandwidth of the electrical measuring system in cps,
J = radiation flux density in watts/cm^2,
N = noise of the detector in volts,
$P_{\lambda,\mathrm{rms}}$ = rms spectral distribution of radiant power flux,
V = signal of the detector in volts,
$V_b(b)$ = bias dependence of the detector signal,
$V_f(f)$ = frequency dependence of the detector signal,
$V_\lambda(\lambda)$ = spectral dependence of the detector signal,
λ = wavelength, in vacuum, of the radiation incident on the detector.

Appendix B

Fluctuations in the observable parameters or "noise" are what essentially limit the detectivity of detectors. While the several performance figures perform an important and valuable function for comparison and tabulation of large varieties and quantities, the noise power spectrum should be considered no less important. The noise spectra of the detectors included in the report were dominated by some or all of the following three types:

1. $\overline{N^2}_{f^{-1}}$ α $(i^x/f^y)\Delta f$ where $x = 2$ generally and $y = 1$ although variations from these values have been noted. This noise is commonly called "one over f" noise and is generally attributed to surface effects and faulty contacts.[2]

2. $\overline{N^2}_{\mathrm{N\text{-}J}} = 4kTR\Delta f$ where k is the Boltzmann constant, T is absolute temperature, and R is the resistance of circuit. Electrical fluctuations in element occur at thermal equilibrium, hence known as thermal noise, better known as Nyquist-Johnson noise. This type of noise has no frequency dependence except at high frequencies when R should be replaced by the circuit impedance.

3. $\overline{N^2}_r$ $\alpha b^x r^2 \Delta f$ where b is an applied bias and r is the detector response. This general type of noise could well be known as signal noise but we prefer to call it response noise because it is caused by fluctuations in the incident radiation or in the fundamental mechanism of the detector and will, therefore, be proportional to responsivity and have the same frequency characteristic [in most cases $r = r_0/(1 + \omega^2 \tau^2)^{1/2}$].

Detectors in the range where they are response noise limited will have a flat detectivity frequency spectrum.

The general class of response noise includes the following:

1. That due to Brownian motion of a diaphragm or similar element.

2. That due to fluctuation in power flowing to and from the sensitive element.

3. Generation-recombination noise (G-R) which includes fluctuation in carrier concentrations caused by emission and absorption of lattice phonons and by absorption of background radiation photons. (If the latter noise is limiting the detector is said to be background limited.)

4. That due to fluctuations in the incident radiation signal (the ultimate limiting noise).

Response noise indicates the fundamental limitation on detectivity for the particular detector considered. When this condition prevails, such action as cooling the lattice, restricting the field of view, or modifying the thermal conductance path etc., can result in performance improvement.

References

1. The reader is referred to "Infrared Issue" Proc. IRE **47**, No. 9 (1959) for several such review articles; P. W. Kruse, L. D. McGlauchlin, R. B. McQuistan, *Elements of Infrared Technology* (John Wiley and Sons, New York, 1962), Chap. 7–10; Proc. Int. Photoconductivity Conference, Ithaca, N.Y. (1961) (in press).
2. P. Bratt, W. Engeler, H. Levinstein, A. MacRae, and J. Pehek, Infrared Physics **1**, 27 (1961).
3. R. C. Jones, Proc. IRE **47**, 1496 (1959).
4. R. C. Jones, J. Opt. Soc. Am. **50**, 1058 (1960); Appl. Opt. **1**, 607 (1962).
5. R. C. Jones, in *Advances in Electronics*, L. Marton, ed. (Academic Press, New York, 1953), Vol. 5, p. 2.
6. E. H. Putley, Proc. Int. Photoconductivity Conference, Ithaca, N.Y. (1961) (in press).
7. D. W. Goodwin and R. H. Jones, J. Appl. Phys. **32**, 2056 (1961).
8. R. A. Smith, F. E. Jones, R. P. Chasmar, *The Detection and Measurement of Infrared Radiation* (Clarendon Press, Oxford, 1957).
9. W. H. Brattain and J. A. Becker, J. Opt. Soc. Am. **46**, 354 (1946).
10. P. C. Caringella and W. L. Eisenman, Rev. Sci. Instr. (in press); "System for Low-Frequency Noise Measurements," NOLC Tech Memo 43-9.
11. P. L. Richards and M. Tinkham, Phys. Rev. **119**, 575 (1960).
12. F. J. Low, J. Opt. Soc. Am. **51**, 1300 (1961).
13. W. S. Boyle and K. F. Rodgers, J. Opt. Soc. Am. **49**, 66 (1959).
14. M. J. E. Golay, Rev. Sci. Instr. **18**, 347, 357 (1947); **20**, 816 (1949).

Quelques Resultats Nouveaux dans la Mesure des Indices de Refraction (Liquides et Solides) dans l'Infrarouge

Josette Vincent-Geisse et Jean Lecomte

During these last years, fairly extensive research has been performed on the study of dispersion in the infrared. In the present paper an account is given of the work carried out in the Laboratoire des Recherches Physiques and of the results recently obtained in the case of transparent substances by the method of the prism at minimum deviation and critical angle refractometry, and also for the case of absorbing substances by reflection methods. We have improved existing devices and evolved new techniques.

Dans un article récent,[1] relatif à la mesure des indices de réfraction dans l'infrarouge, nous avons donné un résumé des méthodes utilisées et des résultats obtenus en montrant l'intérêt de ces mesures et leur extension progressive des corps transparents aux corps absorbants dans le domaine étudié.

Notre laboratoire a fourni une contribution importante à ces travaux et nous en avons donné, il y a quelques temps, une vue d'ensemble.[2] Notre but, dans cet exposé, est de reprendre la question: nous passerons rapidement sur les procédés classiques et bien connus et nous insisterons plus longuement sur les méthodes nouvelles utilisées dans notre laboratoire et sur les résultats nouveaux qu'elles nous ont permis d'obtenir. Nous avons été aidés dans ce travail par un certain nombre de collaborateurs de notre équipe, parmi lesquels nous devons citer Mme. Cameo, Mlle. Dayet, M. Gans, M. Nguyen Tan, Mlle. Raginel, M. et Mme. Vagner.

I. Géneralités

Quand on aborde la mesure des indices de réfraction dans l'infrarouge, le problème fondamental, qui se présente avant tout autre, est l'obtention de matériaux transparents aux radiations considérées et la détermination de leurs caractéristiques optiques. Le nombre de substances, répondant à la question, est très limité, puisque le domaine infrarouge représente précisément celui dans lequel s'effectuent des vibrations moléculaires. Ces dernières années ont vu toutefois l'apparition de nouvelles substances d'indices très variés et transparentes dans un grand domaine de longeurs d'onde.

Une fois mises à part ces intéressantes substances, en nombre d'ailleurs très limité, toutes les autres présentent des bandes d'absorption plus ou moins nombreuses et plus ou moins intenses; autrement dit, *la mesure des indices de réfraction dans l'infrarouge, exige, pour être complète, sa détermination à travers des bandes d'absorption.* Plusieurs méthodes sont utilisables dans ce cas, chacune d'entre elles correspondant à un domaine d'absorption particulier; notre laboratoire ayant proposé et utilisé plusieurs procédés de ce genre, nous insisterons tout spécialement, dans ce qui suit, sur ces déterminations.

Donnons d'abord quelques définitions:

La propagation, dans un milieu isotrope, d'une onde électromagnétique plane et polarisée rectilignement se représente, en notation complexe, par la fonction

$$\psi = \psi_0 e^{j(\omega t - Kx)}.$$

Si ω et K sont réels, il y a propagation sans amortissement. $\omega = 2\pi f$, $K = 2\pi a$, ω pulsation, f fréquence, K module du vecteur onde, a nombre d'ondes. La phase se propage avec une vitesse $W = \omega/K = f/a$, et on définit un indice de réfraction n réel: $n = c/W = cK/\omega$.

Si K est complexe, il y a propagation avec amortissement. $K = k' - jk''$

$$\psi = \psi_0 e^{-k''x} e^{j(\omega t - k'x)}.$$

On définit maintenant un indice de réfraction complexe $N = n - j\kappa$

$$N = \frac{cK}{\omega} = \frac{c}{\omega}(k' - jk'')$$

n, indice de réfraction réel, κ indice d'absorption.

The authors are in the Laboratoire des Recherches Physiques (Sorbonne), Paris, France.

Received 30 March 1962.

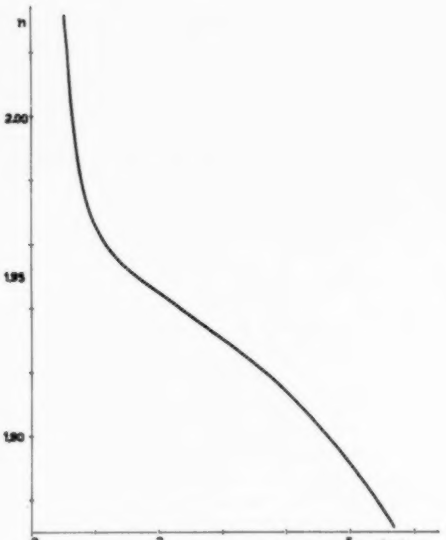

Fig. 1. Indice de réfraction du verre Parra-Mantois VIR 2.

La phase se propage encore avec la vitesse $W = \omega/k' = n/c$ tandis que l'amplitude de l'onde s'amortit suivant le facteur $e^{-k''x} = e^{-2\pi(\kappa\nu/c)x}$. L'intensité s'amortit suivant le facteur $e^{-4\pi(\kappa\nu/c)x}$ ou encore $e^{-4\pi(\kappa x/\lambda)}$, λ désignant la longueur d'onde dans le vide. L'application numérique de cette relation montre que l'intensité se trouve divisée par 2 environ après traversée d'une épaisseur

égale à 500 λ si $\kappa = 10^{-4}$,
égale à 5 λ si $\kappa = 10^{-2}$,
égale à $\lambda/20$ si $\kappa = 1$,

et ainsi de suite. Dans le dernier cas, on voit d'ailleurs qu'il n'y a plus propagation à proprement parler, tellement l'absorption est forte.

En pratique, et dans l'infrarouge, le coefficient κ varie dans de très larges limites. Inférieur à 10^{-6} dans les régions de transparence, il atteint quelques unités au milieu des bandes fortes de certaines substances, et tend vers l'infini dans le cas d'un métal parfaitement conducteur.

Dès que κ n'est plus très petit, la mesure de l'indice de réfraction n ne peut plus se faire en négligeant κ, et nous déterminerons alors simultanément n et κ. La mesure de l'indice d'un corps, dans un domaine étendu de longueurs d'onde, exigera la mise en oeuvre de plusieurs méthodes, chacune d'entre elles n'étant valable et applicable que dans des conditions déterminées d'absorption. Le Tableau I résume ces différents procédés, correspondant chacun à un domaine d'absorption, dans lequel il se montre le plus précis ou le plus commode.

Tableau I. Résumé des Différentes Méthodes

$\kappa < 10^{-6}$	Très grande transparence	Prisme
$10^{-6} < \kappa < 10^{-4}$	Absorption faible	Prisme; réfraction limite
$10^{-4} < \kappa < 10^{-2}$	Absorption moyenne	Réfraction limite; spectres cannelés
$10^{-2} < \kappa < 10^{-1}$	Absorption forte	Spectres cannelés; reflexion
$\kappa < 10^{-1}$	Absorption très forte	Reflexion

Cette classification sommaire ne prétend pas limiter l'utilisation de ces méthodes à un domaine déterminé. On sait, par exemple, que la méthode du prisme a permis de mesurer l'indice de métaux et nous en verrons d'autres exemples plus loin. Elle montre simplement le domaine d'utilisation le plus favorable, celui dans lequel nous avons effectué nos mesures. Nous allons maintenant étudier séparément chacun des procédés précédents; nous parlerons, en dernier lieu, des filtres de Christiansen et de leur application, dans des cas particuliers, à la mesure des indices de réfraction.

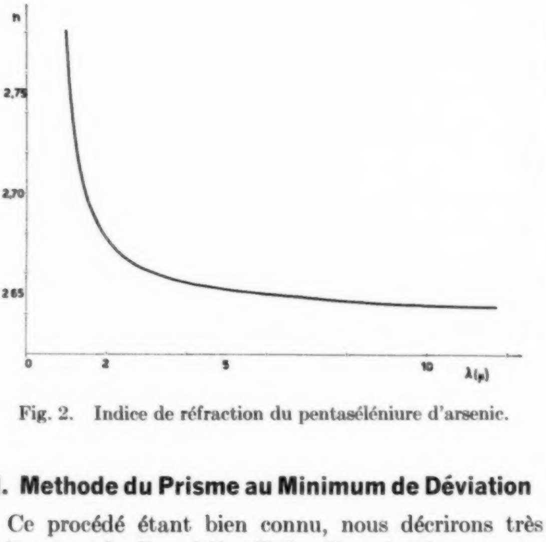

Fig. 2. Indice de réfraction du pentaséléniure d'arsenic.

II. Methode du Prisme au Minimum de Déviation

Ce procédé étant bien connu, nous décrirons très brièvement le dispositif utilisé. Une plateforme, avec cercle gradué, porte le prisme (taillé dans la substance à étudier) et un miroir plan; l'ensemble fonctionne à déviation constante, et on le place entre la fente de sortie et le récepteur d'un spectrographe Perkin-Elmer simple faisceau, à prisme de fluorure de lithium ou de chlorure de sodium. De nombreux verres, fabriqués par la firme Parra-Mantois, ont été étudiés de cette manière.[3] La précision des mesures atteint 10^{-4} en valeur relative. La Fig. 1 présente les résultats relatifs à l'un d'entre eux, le VIR 2, particulièrement intéressant dans l'infrarouge, puisqu'il transmet les radiations jusqu'à près de 6 μ. La Fig. 2 donne les résultats relatifs au pentaséléniure d'arsenic; ce matériau, préparé par l'une d'entre nous,[4] se présente sous forme de verre, à la température ordinaire, et transmet le rayonnement infrarouge entre 1 et 18 μ. La mesure de son indice présentait quelques difficultés supplémentaires, à cause de son absence de transparence dans le visible. La mise au minimum de déviation, pour une radiation visible, se montrant donc impossible, nous avons fait mesurer l'indice pour quatre raies du mercure dans le proche infrarouge au moyen d'un convertisseur d'images,* et c'est l'une de ces raies, à 1,014 μ, qui nous a servi de point de départ pour nos mesures dans l'infrarouge. La dispersion de cette substance, très grande dans le proche infrarouge, devient ensuite très faible, entre 12 et 17 μ, où l'indice reste sensiblement constant. Ce matériau ne pourrait donc être utilisé pour faire des prismes dispersifs, mais il se montre, au contraire, très précieux, quand on désire disposer d'un indice constant; nous en verrons des applications dans la suite.

III. Methode de la Réfraction Limite

Cette méthode permet de mesurer l'indice de réfraction de liquides; le principe en a déjà été décrit dans des publications antérieures,[5,6] et nous le rappellerons rapidement.

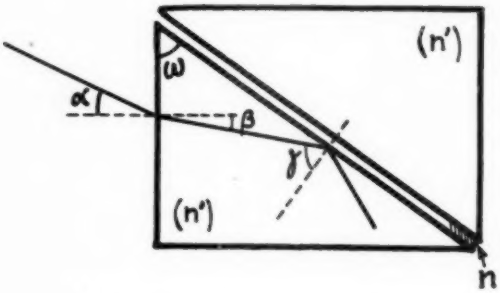

Fig. 3. Méthode de la réfraction limite.

On place sur la plate-forme précédente (paragraphe 2), l'ensemble de deux prismes rectangles identiques, accolés par leur face hypoténuse, avec un liquide d'indice n entre les deux (Fig. 3). Les prismes sont taillés dans une substance d'indice n', assez élevé; les mesures présentes ont été réalisées avec le verre VIR 2 (Fig. 1). On fait tomber sur la face d'entrée un faisceau parallèle et monochromatique. Tant qu'il y a transmission, le faisceau traverse l'ensemble sans déviation; on fait alors tourner la plate-forme, jusqu'à l'obtention de la réflexion totale sur la surface verre liquide. Pour cette valeur de l'angle γ, on a (Fig. 3): $\sin\gamma = n/n'$ et, de plus: $\sin\alpha = n' \sin\beta$ et $\gamma = \beta + \omega$ (α, β et γ, angles orientés). n' a été déterminé, en fonction de la longueur d'onde, par la méthode du prisme au minimum de déviation (Fig. 1). On mesure ω et α, on en déduit γ, puis n; la précision atteint 10^{-3} dans les meilleures conditions. L'angle ω est choisi de telle sorte que l'on ait $\alpha = \beta = 0$ pour un indice n moyen; ici nous avions $\omega = 45°$, avec $n' = 2.03$ pour la raie verte du mercure.

Le repérage de l'angle α, correspondant à la réflexion totale, se fait en traçant la courbe de l'intensité transmise en fonction de α. Pour des corps transparents et une radiation monochromatique, cette courbe présente un point anguleux à tangente verticale. Pour un corps faiblement absorbant et une radiation non rigoureusement monochromatique, cette courbe montre un point d'inflexion, dont la position nous donne encore la valeur de l'indice n (Fig. 4). Etant donné que l'épaisseur de liquide traversé reste relativement faible, de l'ordre d'une fraction de millimètre dans nos mesures, on conçoit qu'il soit possible de mesurer des indices de substances plus absorbantes que celles qui conviennent à la méthode du prisme au minimum de déviation (voir Tableau I). Si l'absorption augmente encore, le point d'inflexion disparaît,[7] et la méthode ne s'applique plus. Jaffé et ses collaborateurs l'ont toutefois transformée pour aller plus avant dans les bandes d'absorption au moyen de calculs correctifs assez compliqués;[8] dans ce cas la précision diminue d'ailleurs considérablement.

De notre côté, nous avons appliqué ce procédé à l'eau et à quelques alcools entre le visible et leur bande de 3 μ. La Fig. 9 en donne les résultats; au delà de 2 μ, les points correspondent à la méthode interférentielle, les deux procédés se recouvrant entre 2 et 3 μ.

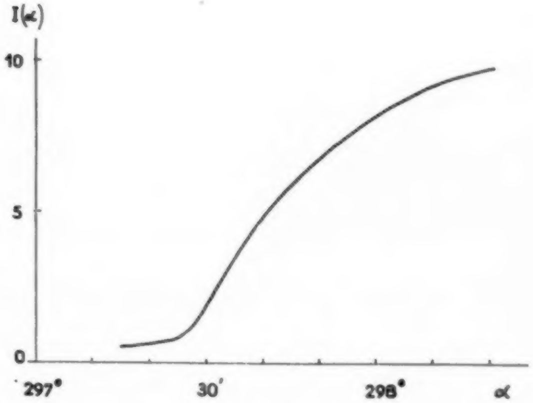

Fig. 4. Variation de l'élonga ion en fonction de l'angle d'incidence α (Méthode de la réfraction limite).

---

* Ces mesures ont été effectuées à l'Institut d'Optique de Paris.

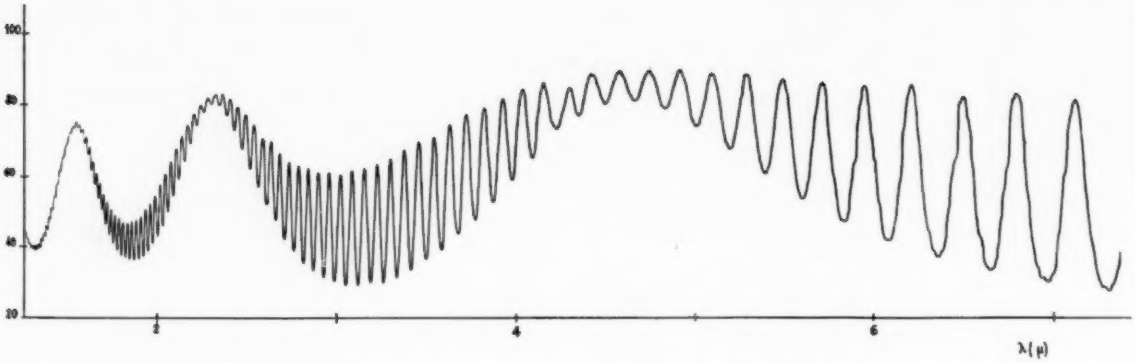

Fig. 5. Franges d'interférences entre lamelles de chlorure de sodium, recouvertes d'une couche mince de As_2Se_3 ($e = 71\ \mu$).

IV. Methode des Spectres Cannelés

Les deux méthodes précédentes, et surtout la première, se montrent les plus précises, mais ne s'appliquent d'une manière simple, que si le corps est relativement peu absorbant, et, en particulier, si la région de transparence s'étend jusqu'au visible. A partir de 3 μ, la plupart des substances présentent des bandes d'absorption nombreuses et, entre ces bandes mêmes, une absorption non négligeable; la méthode interférentielle se montre alors précieuse, parce qu'elle permet d'opérer sur des épaisseurs faibles (de l'ordre de quelques dizaines de microns) et donc d'obtenir l'indice de réfraction dans le voisinage même des bandes d'absorption (Tableau I).

Nous avons déjà décrit le principe de cette méthode et mesuré de cette manière l'indice de nombreux liquides,[2,9,10] en améliorant la technique de la manière suivante:

(a) En premier lieu, l'utilisation d'un spectrographe à double faisceau (Perkin-Elmer 112) présente un gros avantage, car elle permet de compenser l'absorption, à l'intérieur des bandes, au moyen d'une absorption égale du faisceau de référence (Fig. 7).

(b) En ce qui concerne les lamelles constituant les faces de l'interféromètre, nous avons essayé plusieurs substances. Une première solution a consisté à déposer par évaporation une couche mince de pentaséléniure d'arsenic ($n \sim 2{,}6$) sur des lamelles de sel gemme ou de bromure de potassium; on obtient ainsi (Fig. 5) des franges très contrastées dans certains intervalles, et peu contrastées dans d'autres. Ces franges sont malheureusement quelques peu perturbées,[11] ce qui diminue la précision, déjà faible, de la méthode. Une deuxième solution consiste dans l'utilisation de lamelles à haut indice de réfraction, soit de bromo iodure de thallium ($n = 2{,}5$), soit de germanium ($n = 4$). Le bromoiodure de thallium se montre commode, car il est transparent depuis le visible jusqu'à 40 μ, mais le germanium lui est supérieur, à cause de son polissage plus facile et de son indice plus élevé, ce qui donne des franges bien plus contrastées (Fig. 6). Son seul inconvénient provient de son absorption dans le visible et le proche infrarouge; on y remédie très

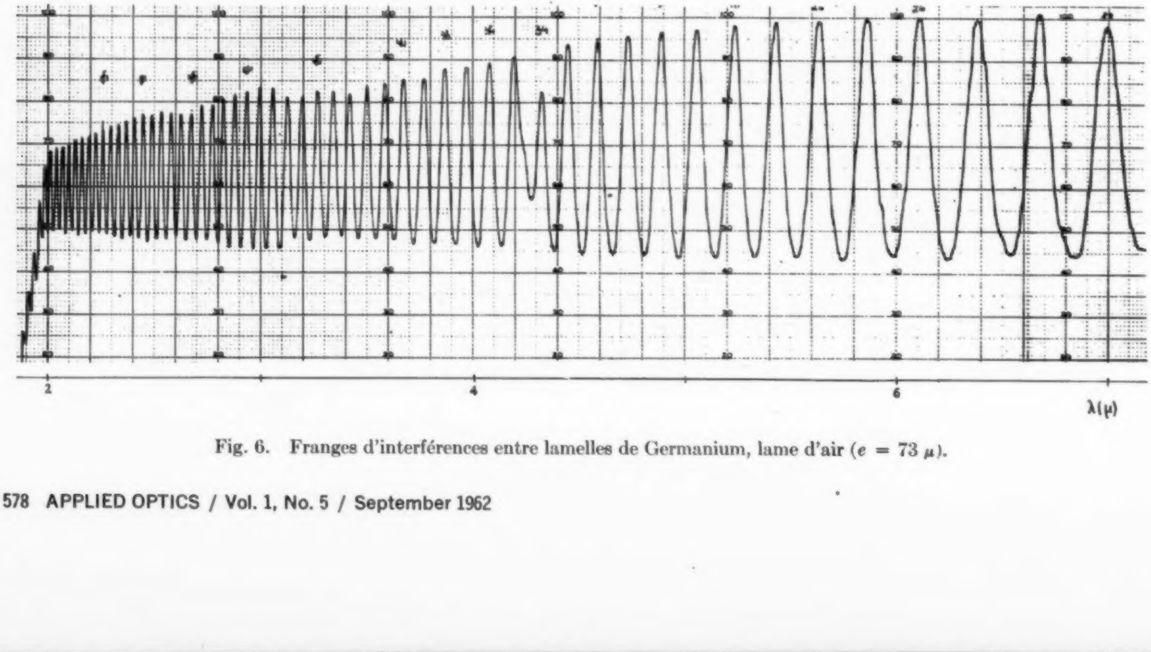

Fig. 6. Franges d'interférences entre lamelles de Germanium, lame d'air ($e = 73\ \mu$).

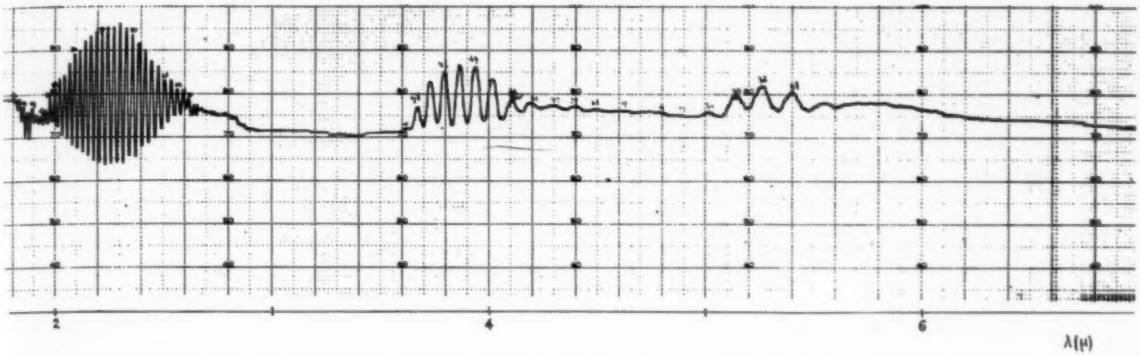

Fig. 7. Franges d'interférence entre lamelles de germanium, lame d'eau ($e = 64\ \mu$).

facilement en mesurant l'indice, en deçà de 2 μ, par la méthode de réfraction limite par exemple. L'utilisation du germanium a permis de mesurer l'indice d'un corps aussi absorbant que l'eau par exemple, entre 2 et 6 μ (Fig. 7).

(c) Enfin nous avons utilisé comme interféromètre, soit une cuve à épaisseur variable, dont le maniement, commode pour déterminer l'ordre d'interférence, se montre délicat pour le repérage de l'épaisseur, soit, quand on dispose de nombreuses lamelles, d'un jeu de plusieurs cuves d'épaisseurs variées. Le pointage des franges à vide donne l'épaisseur de la cuve; on la remplit alors du liquide étudié et les maximums du nouveau spectre cannelé correspondent aux valeurs entières de l'ordre d'interférence P dans la relation:

$$2\,ne = P\lambda. \tag{4.1}$$

La relation précédente n'est vraie, en toute rigueur, que pour des corps transparents. Toutefois, quand l'absorption devient assez grande pour qu'elle ne soit plus vérifiée, on observe en même temps, la disparition des cannelures (Figs. 7 et 8). On peut donc toujours admettre, avec une erreur bien inférieure à la précision des mesures, que l'ordre d'interférence P est entier aux maximums des franges, et le problème essentiel consiste dans la détermination de P. C'est ce problème qui avait arrêté de nombreux chercheurs. La difficulté principale vient de l'impossibilité de suivre par continuité la numérotation des franges à partir d'un ordre d'interférences connu, par exemple dans le visible. En effet la traversée des nombreuses bandes d'absorption infrarouge correspond à un saut de cet ordre d'interférences et il reste impossible de le prévoir.

Aussi avons-nous proposé pour ce calcul, une méthode rapide et sûre[10] qui rappelle celle des excédents fractionnaires, et que nous résumons en quelques mots. Le comptage des franges, entre les longueurs d'onde λ et $\lambda + \Delta\lambda$, nous donne la relation:

$$P = \frac{\Delta P}{\Delta\lambda}(\lambda + \Delta\lambda) + 2e\frac{dn}{d\lambda}. \tag{4.2}$$

Le deuxième terme $2e(dn/d\lambda)$ est inconnu, et on ne peut pas le négliger; on sait seulement qu'il est petit et négatif. On a donc:

$$P < P_l \text{ avec } P_l = \frac{\Delta P}{\Delta\lambda}(\lambda + \Delta\lambda).$$

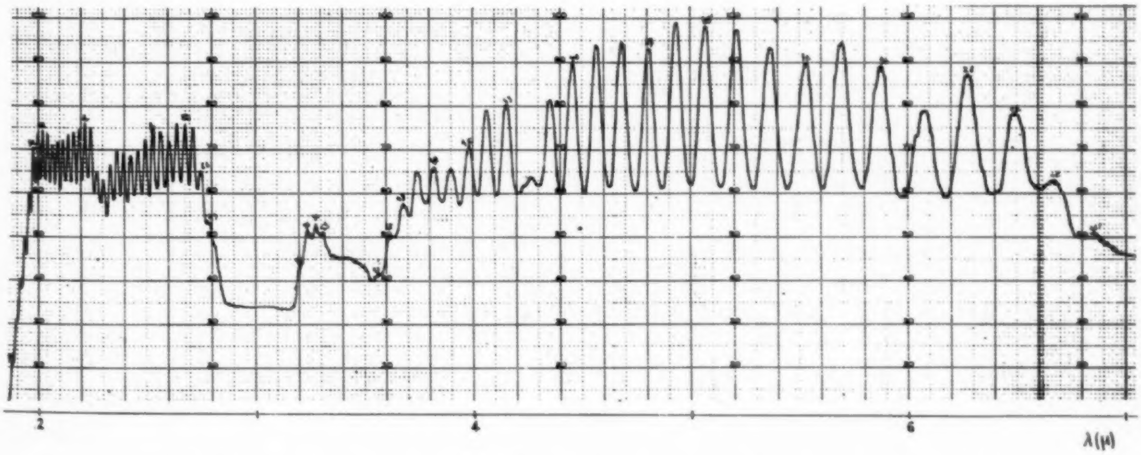

Fig. 8. Franges d'interférences entre lamelles de germanium, lame d'alcool t-amylique ($e = 64\ \mu$).

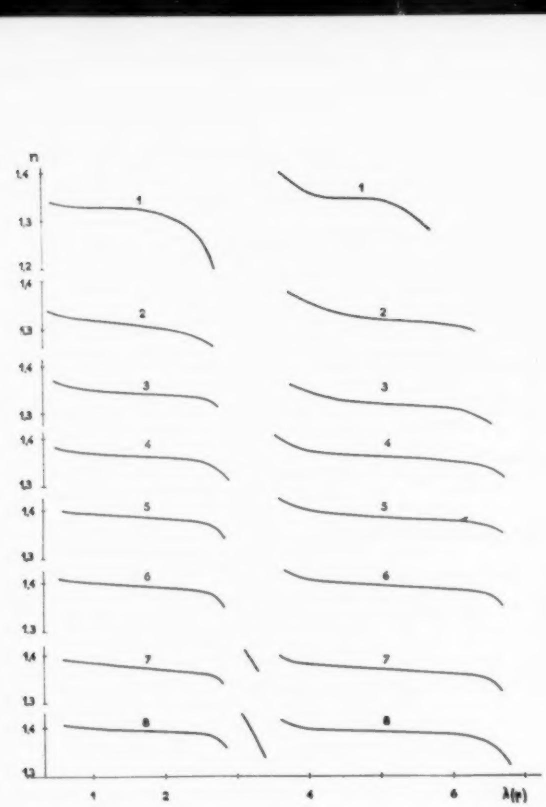

Fig. 9. Indices de réfraction de liquides: 1) Eau; 2) Alcool méthylique; 3) Alcool éthylique; 4) Alcool isopropylique; 5) Alcool n-butylique; 6) Alcool i-amylique; 7) Alcool t-butylique; 8) Alcool t-amylique.

On a donc pour P, à condition qu'il ne soit pas trop grand, le choix entre quelques entiers seulement; on dresse un tableau de ces valeurs possibles, on en déduit les valeurs correspondantes de P *pour la même longueur d'onde* λ et les autres épaisseurs, sachant que P est proportionnel à e, toutes choses égales d'ailleurs. L'examen de chaque spectre permet alors de distinguer les valeurs possibles de P de celles qui ne le sont pas; avec 4 ou 5 spectres, il ne reste en général aucune ambiguité sur P. Il faut remarquer que cette détermination de P doit se faire séparément pour une frange de chacun des intervalles, dans lesquels on observe un spectre cannelé (Figs. 7 et 8).

Le procédé est simple et rapide, mais la précision sur n ne dépasse guère une unité de la 2ième décimale, en raison de l'erreur commise sur l'épaisseur e, et de l'incertitude sur la longueur d'onde λ.

Les Figs. 7 et 8 montrent les franges relatives à une cuve de 64 μ d'épaisseur, remplie respectivement d'eau et d'alcool t-amylique; les franges sont beaucoup moins contrastées dans le cas de l'eau, à cause de sa très grande absorption. Les Figs. 9, 10, 11 montrent quelques résultats récents obtenus par cette méthode, au moyen de cuves à lamelles de germanium.[12] La Fig. 9 représente les courbes de dispersion de l'eau et de quelques alcools saturés aliphatiques, entre le visible et les bandes de 3 μ et entre les bandes de 3 et 7 μ. Pour deux d'entre eux, on obtient même quelques valeurs de n, entre les deux bandes OH et CH voisines de 3 μ, correspondant à des franges observées dans cette région (Fig. 8).

Les Figs. 10 et 11 représentent respectivement l'indice du benzène entre le visible et 14 μ, et celui du chloroforme au voisinage de sa très forte bande de 13 μ. Ces courbes avaient déjà été données auparavant,[9,10] mais l'usage de lamelles de germanium nous a permis d'augmenter la précision des résultats, et de rectifier quelques points douteux et, en particulier, de faire apparaître l'anomalie due à la bande de 15 μ du chloroforme dont l'influence se montre d'ailleurs restreinte.

V. Substances Absorbantes. Méthode par Réflexion

Aucune des méthodes précédentes ne permet de mesurer l'indice de réfraction jusque dans l'intérieur des bandes fortes des substances et, d'autre part, aucune, non plus, ne conduit à l'indice d'absorption κ, toutes supposant κ plus ou moins négligeable par rapport à n. *A l'intérieur des bandes fortes, n et κ ont des valeurs comparables, les propriétés optiques dépendent à la fois de n et κ, et tout procédé de mesure permettra la détermination simultanée des deux constantes.*

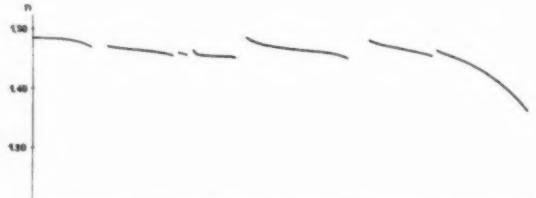

Fig. 10. Indice de réfraction du benzène.

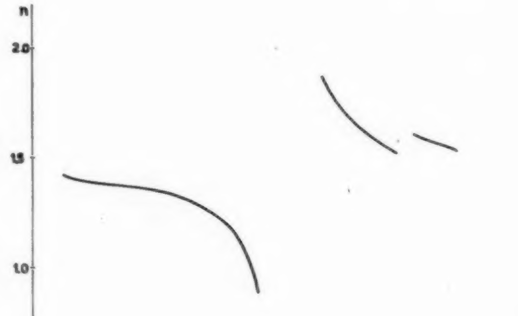

Fig. 11. Indice de réfraction du chloroforme.

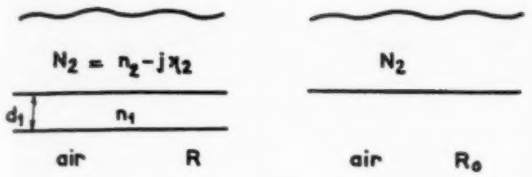

Fig. 12. Méthode par réflexion (principe).

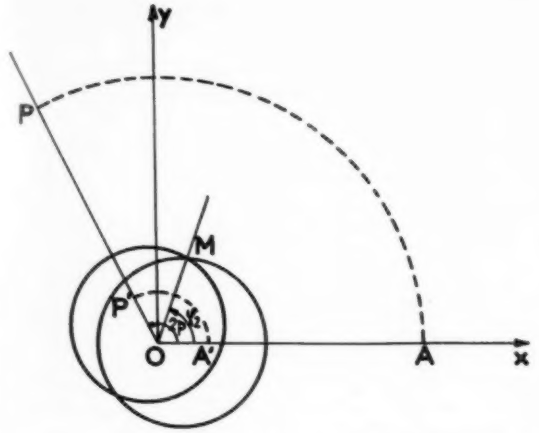

Fig. 13. Méthode par réflexion (construction graphique dans le plan complexe).

Une des meilleures méthodes, dans ce cas, repose sur la réflexion, puisque presque toute l'énergie incidente se retrouve ici dans le faisceau réfléchi. Plusieur procédés ont été proposés (voir bibliographie dans ref. 1). Nous avons, de notre côté, mis au point et appliqué à plusieurs solides une méthode simple et nouvelle,[13,14] fondée sur un principe rigoureux et ne nécessitant pas l'emploi d'une machine à calculer. Enfin, cette méthode peut s'étendre, avec quelques transformations, à l'étude des liquides.[15] Nous les reprendrons ici en détail, car quelques améliorations récentes nous ont permis d'en augmenter encore la rapidité.

A. Solides. Méthode de la Couche Mince

Principe

La substance étant ici très absorbante, nous désignerons son indice complexe par l'expression $N_2 = n_2 - j\ \kappa_2$ (voir paragraphe 1) et nous devrons, pour chaque longueur d'onde, déterminer deux grandeurs n_2 et κ_2.

On commence par tailler et polir avec soin une surface plane dans la substance considérée. Si le corps est anisotrope, il faut évidemment choisir convenablement la direction de ce plan et travailler en lumière polarisée. Dans ce qui suit, nous nous sommes limités toutefois à l'étude des substances isotropes, ou anisotropes uniaxes, le plan choisi étant, dans ce dernier cas, perpendiculaire à l'axe, et nous avons travaillé en lumière naturelle.

La détermination de n_2 et κ_2 est fondée sur la mesure du facteur de réflexion sous incidence normale, de la substance, d'abord nue, puis, ensuite, recouverte d'une couche mince d'un corps transparent, d'indice n_1 connu (Fig. 12).

Le pouvoir réflecteur en amplitudes, s'écrit, compte tenu de la phase, sous la forme complexe:

$$\mathcal{R} = \frac{r_1 + r_2\,e^{-2jp}}{1 + r_1r_2\,e^{-2jp}}, \tag{5.1}$$

où l'on a posé

$$r_1 = \frac{1 - n_1}{1 + n_1},\ r_2 = \frac{n_1 - N_2}{n_1 + N_2},\ 2p = \frac{4\pi n_1 d_1}{\lambda}. \tag{5.2}$$

En l'absence de couche mince, le rapport devient

$$\mathcal{R}_0 = \frac{r_1 + r_2}{1 + r_1r_2}. \tag{5.3}$$

Les facteurs de réflexion correspondants sont donnés par les expressions $R = \mathcal{R}\mathcal{R}^*$ et $R_0 = \mathcal{R}_0\mathcal{R}_0^*$, où $\mathcal{R}^*$ et $\mathcal{R}_0^*$ désignent, suivant la notation habituelle, les quantités complexes conjuguées de $\mathcal{R}$ et $\mathcal{R}_0$.

Le calcul algébrique de n_2 et κ_2, à partir des grandeurs mesurées R et R_0, conduit à un système de deux équations à deux inconnues facilement résoluble. Toutefois, la précision des mesures étant faible, inférieure à 1%, et étant donnée la forme simple des équations (5.1) et (5.2) en termes complexes, nous proposons une solution graphique facile et rapide. Cette méthode s'inspire d'ailleurs, en partie, de remarques géométriques relatives aux couches minces.[16] Revenons aux expressions complexes (5.1) et (5.2), r_1 est réel et négatif, r_2 complexe.

$$r_1 = -\rho_1,\ \ r_2 = \rho_2 e^{j\varphi_2}.$$

$\mathcal{R}$ et $\mathcal{R}_0$ s'écrivent de la manière suivante:

$$\mathcal{R} = -\frac{1}{\rho_1}\,\frac{\rho_1 e^{2jp} - \rho_2 e^{j\varphi_2}}{(1/\rho_1)\,e^{2jp} - \rho_2 e^{j\varphi_2}}, \tag{5.4}$$

$$\mathcal{R}_0 = -\frac{1}{\rho_1}\,\frac{\rho_1 - \rho_2 e^{j\varphi_2}}{(1/\rho_1) - \rho_2 e^{j\varphi_2}}. \tag{5.5}$$

Considérons le plan complexe et deux points A et A' sur l'axe réel et d'abcisses respectives $1/\rho_1$ et ρ_1 (Fig. 13). Les points P et P', d'affixes $(1/\rho_1)e^{2jp}$ et $\rho_1 e^{2jp}$, se déduisent de A et A' par une rotation d'un angle 2 p autour de l'origine et dans le sens positif. Soit enfin M le point d'affixe r_2; on a $OM = \rho_2$ et la demi droite OM fait un angle φ_2 avec l'axe réel positif. Des relations (5.4) et (5.5), on tire:

$$\mathcal{R} = -\frac{1}{\rho_1}\,\frac{\overrightarrow{MP'}}{\overrightarrow{MP}} \text{ et } \mathcal{R}_0 = -\frac{1}{\rho_1}\,\frac{\overrightarrow{MA'}}{\overrightarrow{MA}}.$$

Tableau II

Pouvoir réflecteur	Rayon du cercle	Abscisse du centre du cercle
0	0	43,7
0,20	37,6	36,4
0,40	55,4	28,4
0,60	70,7	19,8
0,80	85,3	10,4
1	100	0

Un pouvoir réflecteur de 1 correspond à une longueur de 100 mm. Les distances sont exprimées en mm.

On en déduit

$$\frac{MP'}{MP} = \rho_1\sqrt{R} \quad \text{et} \quad \frac{MA'}{MA} = \rho_1\sqrt{R_0}. \tag{5.6}$$

Le point cherché M partage *PP'* dans le rapport $\rho_1\sqrt{R}$ et AA′ dans la rapport $\rho_1\sqrt{R_0}$.

La construction graphique, tirée des relations (5.6), est très simple, à condition que les points A et A′ ne varient pas avec la longueur d'onde ou, autrement dit, que l'indice n_1 de la substance, constituant la couche mince, soit constant dans un domaine assez étendu de longueurs d'onde. On s'arrange pour qu'il en soit effectivement ainsi, comme nous le verrons plus loin. Nous avions ici n constant et égal à 2,55, à 1% près, entre 4 et 18 μ.

Sur un papier préparé pour une représentation en coordonnées polaires, on choisit donc les points fixes A et A′ et, pour une longueur d'onde donnée, on place *P* et *P′*, et on trace les deux cercles lieux des points qui partagent AA′ et *PP′* respectivement dans les rapports $\rho_1\sqrt{R_0}$ et $\rho_1\sqrt{R}$. Cette construction est rendue très simple par la construction préalable d'un tableau donnant pour chaque valeur du pouvoir réflecteur, R ou R_0, l'abscisse du centre et le rayon du cercle correspondant (R varie de 0 à 1 par valeurs de 0,01). Le Tableau II, qui en est extrait en montre quelques points.

Un graphique, tracé une fois pour toutes, et comportant un certain nombre de ces cercles, jouerait d'ailleurs le même rôle que ce tableau.

Le point M cherché, de coordonnées polaires ρ_2 et φ_2, est l'un des points de rencontre de ces deux cercles; on le détermine sans ambiguité sachant que l'on a $\varphi_2 < \pi$ et, par continuité, étant donné, qu'en dehors des bandes d'absorption, on a $\varphi_2 = 0$ (Fig. 13).

La connaissance de $r_2 = \rho_2 e^{j\varphi_2}$ permettrait le calcul de $N_2 = n_2 - j\kappa_2$, d'après la relation tirée de (5.2)

$$r_2 = \frac{1 - N_2/n_1}{1 + N_2/n_1}, \tag{5.7}$$

qui s'écrit aussi

$$\frac{N_2}{n_1} = \frac{1 - r_2}{1 + r_2}. \tag{5.7'}$$

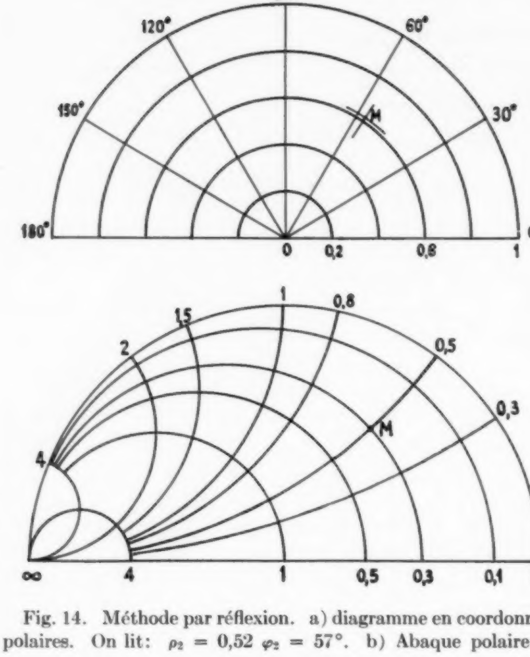

Fig. 14. Méthode par réflexion. a) diagramme en coordonnées polaires. On lit: $\rho_2 = 0{,}52$ $\varphi_2 = 57°$. b) Abaque polaire ou diagramme de Smith. On lit: $\frac{n_2}{n_1} = 0{,}3$ $\frac{\kappa_2}{n_1} = 0{,}5$.

Mais, là encore, une remarque simple évite tout calcul: les relations (5.7) et (5.7′) montrent que les points M et M′, d'affixes respectifs r_2 et N_2/n_1, se déduisent l'unde l'autre par une inversion de centre $(-1,0)$ et de puissance 2. Si l'on fait subir cette transformation, non plus au point M, mais aux axes de coordonnées rectangulaires eux-mêmes, on obtient l'abaque polaire, plus connue dans la théorie des lignes électriques, sous le nom de diagramme de Smith. Une simple superposition de la figure précédente (Fig. 13) et d'une telle abaque polaire nous permettra de lire, à la fois, ρ_2 et φ_2 sur l'un, n_2/n_1 et κ_2/n_1 sur l'autre.

La Fig. 14 nous montre ces deux diagrammes, non pas superposés, mais déplacés l'un par rapport à l'autre, pour plus de clarté.

Technique Expérimentale

Les mesures ont été effectuées sur un spectrographe Perkin-Elmer 112 à double passage et à prisme de chlorure de sodium. L'appareil utilisé pour les mesures par réflexion, construit par deux d'entre nous, a déjà été décrit[17] et permet d'avoir sur l'échantillon un angle d'incidence voisin de 0°; la précision des mesures se montre telle qu'une correction pour l'angle n'est pas nécessaire.

On mesure d'abord le facteur de réflexion R_0 sur une surface plane bien polie de la substance étudiée. On dépose ensuite, sur cette surface, par évaporation dans le vide, une couche mince du corps transparent d'indice constant n_1; à cet effet, nous avions essayé le germanium ($n \simeq 4$ entre 3 et 16 μ) et $As_2Se_5/n \simeq 2{,}65$ entre 5 et 15 μ); l'extraordinaire facilité de vaporisation de ce dernier corps nous l'a fait choisir pour effectuer nos mesures. Remarquons que l'indice n_1, utilisé dans notre construction, n'a pas été pris égal à 2,65, indice du corps à l'état massif, mais à 2,55, une série d'expériences ayant montré que l'indice du corps en couche mince, dans des conditions bien déterminées de température et de vitesse d'évaporation, était sensiblement constant et égal à 2,55, valeur légèrement inférieure à celle du même matériau pris à l'état massif. L'épaisseur de la couche déposée est voisine de 1 μ. Un dépôt identique, effectué en même temps sur une lame de chlorure de sodium, permet de déterminer l'épaisseur d_1 de la couche, d'après les franges d'interférence observées dans l'infrarouge.

On mesure alors le nouveau facteur de réflexion R, par rapport à un miroir étalon aluminé, dont nous prenons le facteur de réflexion égal à 0,98. En pratique, on dépose plusieurs couches successives, certaines valeurs de R étant plus propices que d'autres à une détermination facile de n_2 et κ_2; la construction graphique s'en trouve à peine allongée, et la précision des mesures s'accroît. Remarquons que les points de rencontre des courbe $R_0(\lambda)$ et $R(\lambda)$ présentent un intérêt particulier, car ils correspondent, soit à $2p$ multiple de 2π, soit à $\varphi_2 = p$ et permettent ainsi, dans ce dernier cas, de déterminer immédiatement φ_2 avec précision.

Resultats

Nous avons appliqué la méthode précédente à un certain nombre de verres et de cristaux. Nous donnons ici les résultats pour le flint extra dense de Parra Mantois F2021 (Fig. 15) et pour le quartz (Fig. 16), pour lequel nous avons amélioré la précision et étendu, par rapport à un travail antérieur,[13, 14] les mesures à la bande de 1160 cm^{-1}.

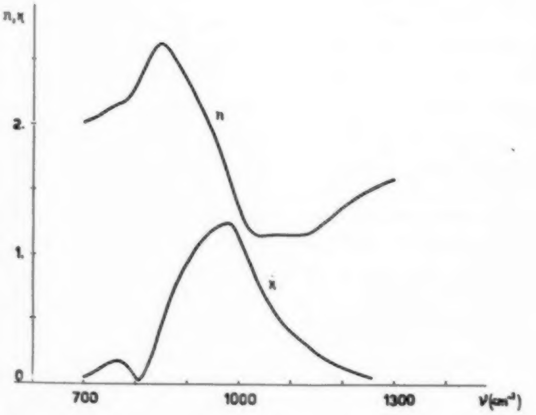

Fig. 15. Constantes optiques du verre Parra-Mantois F2021.

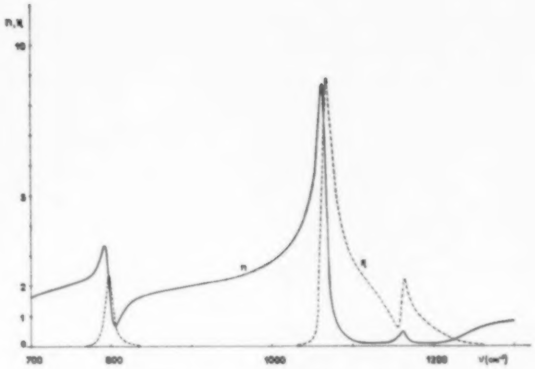

Fig. 16. Constantes optiques du quartz (echantillon perpendiculaire à l'axe).

En résumé cette méthode nous paraît présenter de grands avantages. Du point de vue expérimental, elle se montre très simple, car elle ne nécessite la mesure du pouvoir réflecteur que sous incidence normale et aux seules longueurs d'onde, pour lesquelles on désire obtenir effectivement les constantes optiques. L'interprétation des mesures se fait par un procédé exclusivement graphique. Enfin, elle ne fait appel a aucune hypothèse simplificatrice.

B. Liquides. Méthode de la Couche Épaisse

La méthode précédente a été étendue aux liquides par l'une d'entre nous[15] avec quelques modifications. La principale consiste dans le remplacement de la couche mince d'indice n_1, par une lame épaisse d'indice connu n_1.

La détermination de n_2 et de κ_2 est fondée sur la mesure du facteur de réflexion sous incidence normale, d'abord du liquide seul, si sa tension de vapeur se montre assez faible, puis du même liquide recouvert successivement de deux lames différentes.

Dans ce cas, on considère les pouvoirs réflecteurs en intensités, les phases étant distribuées au hasard, à cause de la grande épaisseur de la lame, de l'ordre du centimètre, et de la largeur du faisceau. Enfin les pouvoirs réflecteurs étant souvent faibles, on les mesure, non plus par rapport à un miroir aluminé, mais par rapport à la lame elle-même, d'indice n_1.

La détermination de n_2 et κ_2, à partir des pouvoirs réflecteurs mesurés, conduit à la résolution d'un système de deux équations du second degré. Chacune de ces équations étant celle d'un cercle, un procédé graphique, semblable au précédent, serait possible.

Cette méthode a été appliquée à l'étude de plusieurs liquides, à l'intérieur de très fortes bandes d'absorption.

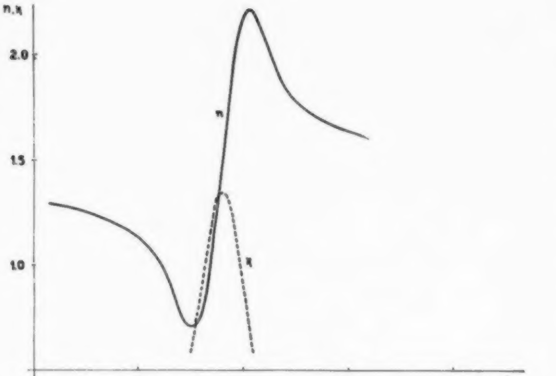

Fig. 17. Constantes optiques du chloroforme.

Les Figs. 17 et 18 représentent les résultats relatifs respectivement au chloroforme et au tétrachlorure de carbone, dans les bandes voisines de 750 cm^{-1}. Ces courbes se raccordent très bien à celles que nous obtenons à l'extérieur des bandes, par la méthode interférentielle (voir par exemple Fig. 11).

VI. Filtres de Christiansen

Ils ne constituent qu'une méthode accessoire pour la détermination des indices de réfraction, car ils ne fournissent que des points isolés de la courbe de dispersion, et parce que la précision ne dépasse pas quelques unités de la deuxième décimale.

Nous avons toutefois repris dernièrement cette méthode[2] car elle se montre utile dans quelques cas, principalement comme contrôle. Tout d'abord, elle n'exige pas de montage spécial, comme toutes les autres mesures d'indices de réfraction et elle permet, seule, l'utilisation de composés en poudre. Elle se montre particulièrement utile, par exemple, pour choisir ou tout au moins donner une valeur approchée de l'ordre d'interférence, dans la méthode des spectres cannelés.

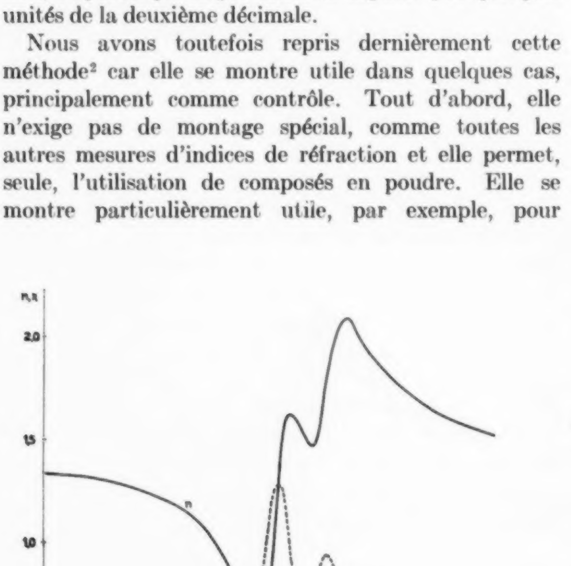

Fig. 18. Constantes optiques du tétrachlorure de carbone.

Nous avons déjà décrit la phénomène, dans le cas d'une poudre dans l'air, où, comme on le sait, l'on observe un maximum de transmission, lorsque l'indice du solide passe par la valeur 1, et dans le cas d'une poudre en suspension dans un liquide, où l'on observe un maximum de transmission, lorsque les courbes de dispersion du solide et du liquide se coupent. Nous n'y reviendrons pas. Nous allons montrer ici que ce phénomène se généralise encore, et qu'il se produit aussi, dans certaines conditions, entre deux solides.

Si les deux solides se présentent sous forme de poudre, l'un des deux n'est pas en suspension dans l'autre, mais tous deux en suspension dans l'air et il y a en réalité 3 constituants. Ce cas ne présente pas grand intérêt en pratique, la transmission restant en général très faible, avec cependant un ou plusieurs maximums dans certains mélanges. Plus intéressant est le cas où l'un des solides, sous forme de grains, se trouve en suspension dans un autre matériau homogène. On peut alors observer un véritable filtre de Christiansen, quand les deux indices deviennent égaux.

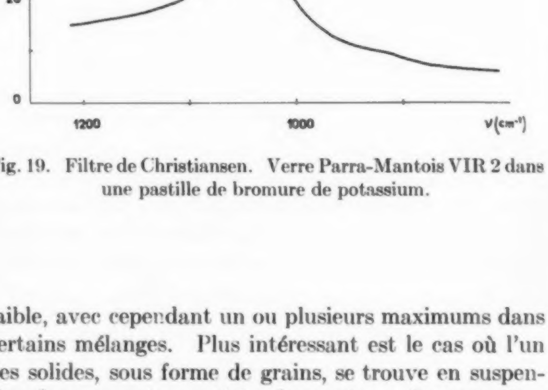

Fig. 19. Filtre de Christiansen. Verre Parra-Mantois VIR 2 dans une pastille de bromure de potassium.

On met en évidence ce phénomène, en mélangeant, par exemple, de la poudre de verre assez grossière et de la poudre de bromure de potassium, finement broyée, et en comprimant le tout suivant la méthode des pastilles. On observe un maximum de transmission bien marqué au point, s'il existe, où l'indice du verre devient égal à celui du bromure de potassium; il existe une grosseur optimum des grains de verre et une proportion optimum de verre dans KBr. La figure 19 montre un tel filtre de poudre de verre Parra-Mantois VIR 2 dans KBr. A 9,7 μ environ, l'indice de ce verre passe donc par la valeur 1,53.

VII. Conclusion

L'ensemble des méthodes précédentes permet ainsi de mesirer l'indice de réfraction, et accessoirement l'indice d'absorption, pour les solides et les liquides, dans un grand domaine de longueur d'onde, et dans les régions d'absorption faible ou importante. Ces mesures présentent un intérêt multiple. Tout d'abord, la connaissance de l'indice de réfraction se montre utile pratiquement pour les régions de transmission élevée, dans de nombreux cas: substances dispersives, solvants usuels, couches antiréfléchissantes, filtres interférentiels. A l'intérieur des bandes, la connaissance des constantes optiques se montre, théoriquement, très importante. Elle permet de déterminer la valeur exacte des fréquences d'absorption, ainsi que l'intensité d'absorption, et de relier ces grandeurs à celles prévues par la théorie.

Ces différentes applications ont pris un grand essor ces dernières années et nous y avons nous-mêmes fourni une contribution non négligeable[3,12,18,19] dont la description sortirait du cadre de cette étude.

En conclusion, nos recherches ont permis de compléter avec succès cet important chapitre de l'optique, qui comprend les propriétés de dispersion et d'absorption des substances, ainsi que leurs applications, et qui s'est trouvé étendu derièrement, d'une manière systématique, du visible au domaine infrarouge. Celui-ci, à cause de son grand nombre d'octaves, et à cause de la présence, dans son domaine, de nombreuses bandes fondamentales, permet, beaucoup plus fréquemment que le visible ou l'ultraviolet, l'étude du phénomène de la dispersion anormale. Il offre ainsi un terrain aussi vaste qu'intéressant pour l'étude théorique et expérimentale des propriétés optiques des substances.

Bibliographie

1. J. Vincent-Geisse et J. Lecomte, J. phys. radium **21,** 794 (1960).
2. J. Vincent-Geisse et J. Lecomte, J. phys. radium **20,** 841 (1959).
3. G. Vagner-Dewulf, J. Vincent-Geisse, et Nguyen Tan Tai, Rev. optique **39,** 578 (1960).
4. G. Dewulf, Rev. optique **33,** 513 (1954).
5. J. Vincent-Geisse, C. R. Acad. Sci. **224,** 650 (1947).
6. J. Vincent-Geisse, J. phys. radium **9,** 175 (1948).
7. H. Arzeliès, Ann. phys. **2,** 181 (1947).
8. J. H. Jaffe, H. Goldring, et U. Oppenheim, J. Opt. Soc. Am. **49,** 1199 (1959).
9. J. Vincent-Geisse et J. Lecomte, C. R. Acad. Sci. **244,** 577 (1957).
10. J. Vincent-Geisse et J. Lecomte, Rev. optique **37,** 295 (1958).
11. J. Vincent-Geisse et J. Lecomte, C. R. Acad. Sci. **244,** 2152 (1957).
12. J. Dayet, Diplôme d'études supérieures, Paris 1961; C. R. Acad. Sci. **253,** 2905 (1962).
13. J. Vincent-Geisse, M. Queyrel, et J. Lecomte, C. R. Acad. Sci. **247,** 1330 (1958).
14. J. Vincent-Geisse, M. Queyrel, et J. Lecomte, Revue Universelle des Mines **15,** 507 (1959).
15. M. Cameo, C. R. Acad. Sci. **252,** 1434 (1961).
16. P. Cotton, Ann. phys. **2,** 209 (1947).
17. G. Dewulf et F. Gans, C. R. Acad. Sci. **243,** 1857 (1956).
18. M. Cameo et J. Vincent-Geisse, C. R. Acad. Sci. **252,** 1579 (1961).
19. J. Vincent-Geisse et J. A. Ladd, Spectrochimica Acta **17,** 627 (1961).

Applied Optics
Optical Activities in the Universities

reported by STANLEY S. BALLARD, Department of Physics, University of Florida, Gainesville, Florida. Professor Ballard hopes to receive news and comments for this column, which should be sent to him at the above address

One does not have to spend very many minutes looking through the present issue of *Applied Optics* before he realizes that there are two quite different types of applications of infrared radiation. The first and best known is to spectroscopy and spectrophotometry, in the study and analysis of atoms, molecules, and compounds. This is the academic side of the field which is taught in universities in either chemistry or physics courses, and, on the graduate level, provides the subject matter for many master's theses and doctoral dissertations. My column this month is devoted to the other facet of infrared physics and technology, namely the nonspectroscopic, radiometric type of applications often referred to, for want of a better term, as "field uses." The impetus here has come largely from military requirements, and there has been a tremendous surge of activity since World War II, when infrared devices were first used successfully in actual field operations. The nonmilitary aspects of infrared technology are also burgeoning, and may eventually outstrip the strictly military side if the present trend continues.

Relatively little is taught in college or university courses regarding the nonspectroscopic aspects of the utilization of infrared radiation. To be sure, the blackbody radiation laws are covered in modern-physics courses and perhaps in optics courses. The important subject of radiometry may be touched upon in one place or another but is seldom the subject of an entire course, except at the University of Rochester (as stated in my July column). I understand that Professor E. Scott Barr teaches a course at the University of Alabama which goes into radiometry and some applications of infrared instruments, but I am not aware that this sort of thing is done on many campuses—information on other such courses would be received with great interest. The book we still refer to here is *Measurement of Radiant Energy,* edited by W. E. Forsythe (McGraw-Hill, 1937).

The need for training along the lines being discussed has become so evident that special concentrated, short summer courses have been offered at at least three institutions: M I T offered such a course in the summer of 1954; U C L A has offered a two-week course for the last two years and is offering a somewhat altered course this summer; the University of Michigan is offering a one-week course in Fundamentals of Infrared Technology for the fourth year and will give it at two different times this summer, as well as offering an advanced course in special topics. The students who take these summer courses are largely drawn from industrial and government laboratories; their desire is to learn things they need to know in order to do their jobs better. I am not aware that regular university students take these courses to an appreciable extent.

Since so many people are having to learn on their own about infrared physics and technology these days, it is well to ask what instructional material is available for their use. Shortly after World War II, when a number of us realized that this field was going to grow rapidly, we were concerned about the lack of suitable books and other instructional material. Some of us wrote reports and booklets, which unfortunately often bore a security classification because much of the data on infrared detectors, radiation from missiles, detection ranges, etc., were then classified as Confidential or Secret by the military. Perhaps the best reference in those days was the German book, *Das Ultrarote Spektrum*, by Schaefer and Matossi (Julius Springer, Berlin, 1930). Unfortunately, this excellent book has never been translated into English, although a photolithoprint reproduction was brought out by Edwards Bros. of Ann Arbor, Michigan, in 1943. The article "Infra-Red Instrumentation and Techniques" by Van Zandt Williams, published in the *Review of Scientific Instruments* [**19**, 135–178 (1948)], was the first publication to bring together much of the new data on infrared materials and instruments. I could mention here the several excellent textbooks on spectroscopic instruments such as *Experimental Spectroscopy*, by R. A. Sawyer and *Practical Spectroscopy*, by Harrison, Lord, and Loofbourow, but these deal more with the spectroscopic use of infrared, which is not the primary subject of this column.

An excellent treatment of the physical basis for the field applications of infrared, and one that may not be known to many who require this information, is "Emission, Transmission, and Detection of the Infrared," by John A. Sanderson of the Naval Research Laboratory; it is the fifth chapter (pages 126 to 175) of *Guidance*, by Arthur S. Locke and collaborators (Van Nostrand, 1955), which is in the series "Principles of Guided Missile Design." In 1957 the Oxford University Press published *The Detection and Measurement of Infra-Red Radiation*, by R. A. Smith, F. E. Jones, and R. P. Chasmar. This book was the first readily available, detailed, theoretical, and factual treatment of what is now called infrared physics; its emphasis is largely on detectors of infrared radiation.

During the year 1958 it became apparent to many of the leading workers in the military applications of infrared that much of the basic information used by them and their associates was in fact unclassified—after all, it comprised simply physical, chemical, and engineering data. It was felt that considerable benefit would accrue if there could be an unclassified, widely distributed publication of as much of this information as possible. This hope was finally brought to fruition in the Special Issue on Infrared Physics and Technology of the *Proceedings of the Institute of Radio Engineers*, Vol. 47, No. 9, September 1959. There are 235 large-sized pages in double-column format which contain many articles on infrared physics, technology, systems, and applications. This volume represents the work of many authors; it was under my general supervision as guest editor of this special issue. On pages 1647–1649 is a short article by W. L. Wolfe of the University of Michigan, "A Selected Bibliography on Infrared Techniques and Applications," which includes 101 references in the infrared field. Incidentally, this number of the *Proc. IRE* was overprinted for single-copy sale, and I believe that copies can still be obtained by writing to the IRE at 1 East 79th Street, New York 21, N.Y.

The book *Infrared Radiation*, by Henry L. Hackforth (McGraw-Hill, 1960) gives an extensive review of the topics ordinarily included in infrared physics and technology. The treatment is necessarily somewhat superficial, but this book is recommended for a rapid review of the field and as a reminder of the many current applications of infrared radiation. *Infrared Methods, Principles, and Applications* by the English authors G. K. T. Conn and D. G. Avery (Academic Press, 1960) is an unusually detailed and authoritative treatment of the laboratory techniques used in dealing with sources of radiation, optical materials, detectors, amplifiers, and dispersive systems; there are some pages on applications to industrial gas analysis and radiation pyrometry. This is not a book for the beginner but is an excellent treatment for those who want to make actual use of infrared techniques in the laboratory and in the field—it should be regarded as required reading for such persons.

By the later 1950's it must have occurred both to book publishers and to prospective authors that a more detailed treatment of infrared physics was due, since several teams of authors started writing. The resulting books cover, in general, the five elements of a practical infrared system, namely the source of radiation, called the target in military parlance; the effect of atmospheric absorption over the path from the target to the detector; the optical system; the detector–preamplifier; and finally the readout, display, or other output of the system. The first book of a comprehensive nature to appear was *Elements of Infrared Technology*, by P. W. Kruse, L. D. McGlauchlin, and R. B. McQuistan, all of the Honeywell Research Center (Wiley, 1962). Their first volume, which was published in late January, deals with the generation, transmission, and detection of infrared energy; the second volume will deal with infrared systems and applications. *Fundamentals of Infrared Technology* by M. R. Holter, S. Nudelman, G. H. Suits, W. L. Wolfe, and G. J. Zissis, all of the University of Michigan, was published by Macmillan in June 1962. This is a one-volume treatment which covers in detail the five elements of infrared systems just listed. Germane to this column is Appendix C, "Sources of Information about Infrared Technology," which is especially recommended to the present readers. I understand that two more books on infrared are now in preparation for publication in early 1963. One is by John A. Jamieson of the Aerojet-General Corporation and his coauthors and gives more emphasis to statistical considerations. The other is written particularly for systems engineers who need to know more about the potentialities and limitations of infrared techniques; it is by Richard D. Hudson, Jr., of the Hughes Aircraft Company.

Thus we see that there is no dearth of descriptive and instructional material available in the field of infrared physics and technology. If more universities should recognize the need for instruction in this modern field of physics and engineering and should add such courses to their curricula, the instructors would be able to choose excellent texts and reference books.

Total Absorptance of Carbon Monoxide and Methane in the Infrared

Darrell E. Burch and Dudley Williams

The total absorptance $\int A(\nu)d\nu$ of the major infrared bands of carbon monoxide and methane has been measured as functions of absorber concentration w and equivalent pressure P_e over wide ranges of these variables. The experimental results are presented graphically, and empirical equations relating $\int A(\nu)d\nu$, w, and P_e are presented. By employing small values of w and large values of P_e, it has been possible to determine the band strengths or intensities $\int k(\nu)d\nu$ for the fundamental band of carbon monoxide and for ν_2, ν_3, and ν_4 fundamentals of methane; the values obtained are compared with results of other investigators.

The present paper is the second in a series of papers dealing with the total absorptance of gases found in planetary atmospheres. The laboratory techniques involved in the study of synthetic atmospheres consisting of pure samples of absorbing gases and samples consisting of absorbing gases mixed with nitrogen have been described in the first paper in the series.[1] The symbols and nomenclature employed in the present paper are those introduced in the first paper and in a still earlier article dealing with absorption line broadening in the infrared.[2] Total absorptance of carbon monoxide and methane will be discussed in the present paper.

Migeotte[3] first identified CO as a permanent atmospheric constituent on the basis of solar spectra obtained at Columbus, Ohio, and later verified his findings at the high-altitude laboratory located at the Jungfraujoch. Several investigators including Shaw[4] have subsequently made detailed spectroscopic studies of CO abundance and report a concentration of approximately 0.1 atm cm per air mass. Although it has long been known that CH_4 is present in large quantities in the atmospheres of the major outer planets of the solar system, not until Migeotte's Ohio work of 1948 was CH_4 shown to be a permanent constituent of the telluric atmosphere.[5] The average abundance of CH_4 in the earth's atmosphere has subsequently been found to be 1.6 parts per million by volume.

Although CO and CH_4 are relatively minor telluric atmospheric constituents and have relatively little influence on the earth's heat balance, their absorption bands in the infrared occur for the most part in "atmospheric windows" between the strong bands of carbon dioxide and water vapor. Therefore, CO and CH_4 bands are of considerable practical importance in limiting infrared transmission through the "windows" in which they occur.

Carbon Monoxide Absorptance

The fundamental band of CO is located at 2143 cm^{-1} near the ν_3 fundamental of N_2O. The major absorption by CO in this region is due to $C^{12}O^{16}$; however, there is some absorption due to less abundant isotopic species and to some difference bands, which are very weak at room temperature. For the purposes of the present study, all these overlapping absorption bands will be referred to as *the* 2143 cm^{-1} band. Approximately 180 records of spectral absorptance in this region were made with a double-beam spectrometer employing absorption cells of length 1.55, 6.35, and 400 cm. Different combinations of CO and N_2 were used to provide absorber concentrations w ranging from 9.6×10^{-4} to 45.6 atm cm and total pressures ranging from 3 to to 3000 mm Hg.

In Fig. 1 are shown several records of spectral absorptance in the vicinity of the CO fundamental; all records were obtained with the same spectrometer

---

The authors are of the Laboratory of Molecular Spectroscopy and Infrared Studies, Department of Physics and Astronomy, The Ohio State University. The present address of D. E. Burch is Aeronutronic Division, Ford Motor Company, Newport Beach, California. D. Williams is a National Science Foundation Senior Postdoctoral Fellow at the University of Liége.

Received 16 January 1962.

This work has been supported in part by Geophysics Research Directorate, Air Force Cambridge Research Laboratories.

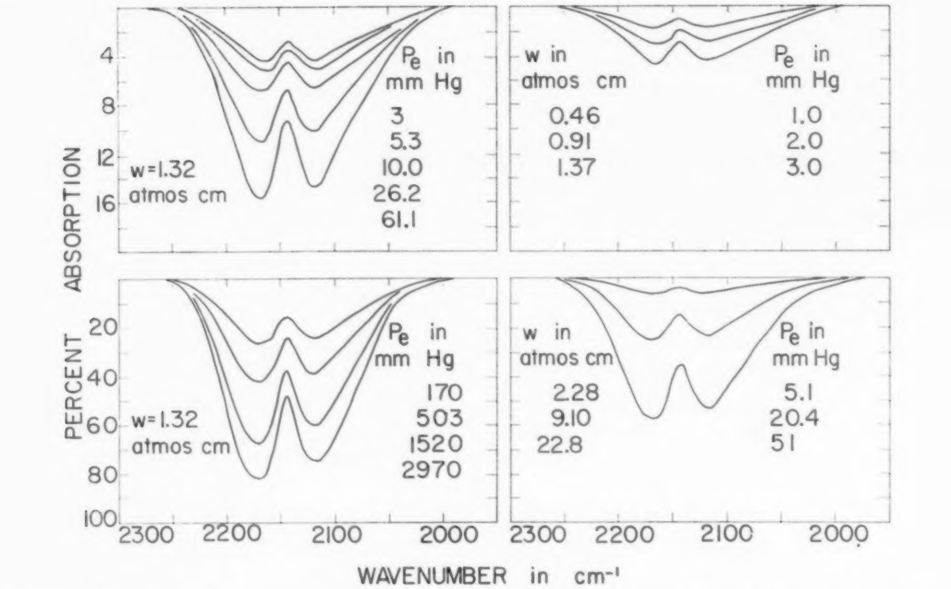

Fig. 1. Spectral absorptance $A(\nu)$, expressed as "Percent Absorption," in the vicinity of the CO fundamental at 2143 cm^{-1}.

slitwidths, which corresponded to approximately 25 cm^{-1}. The records in the left-hand panels of the figure were obtained with a single value of absorber concentration w and show the effect of increasing the total pressure P by the addition of N_2. The records in the right-hand panel show results obtained by simultaneous increase of w and P. Values of equivalent pressure P_e were obtained from the partial pressure p of CO and the total pressure P by the expression $P_e = P + 0.02p$, which is based on the self-broadening coefficient $B = 1.02$ determined for CO in earlier work.[2]

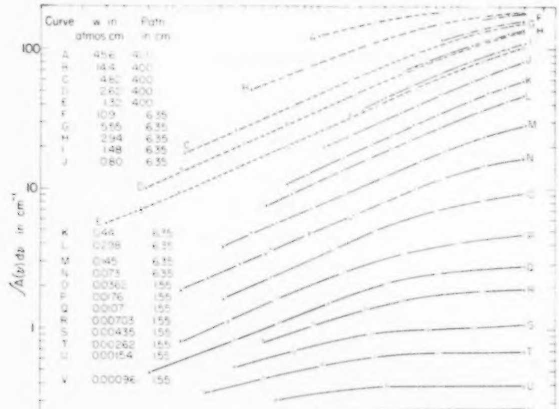

Fig. 2. Total absorptance $\int A(\nu)d\nu$ of the 2143 cm^{-1} band for various values of absorber concentration w as a function of equivalent pressure P_e.

Many of the experimental data are plotted in Fig. 2, which gives total absorptance $\int A(\nu)d\nu$ as a function of equivalent pressure P_e. Each curve shown in the figure corresponds to the fixed value of absorber concentration listed and shows the effect of increasing the equivalent pressure by the addition of N_2. Curves F, G, H, and I represent data obtained with the same range of absorber concentrations as the data represented by curves B, C, D, and E; in spite of the large differences in the absorption paths employed, the two sets of curves agree to ±3%.

The general features of the curves in Fig. 2 are similar to those discussed in some detail for the 2224 cm^{-1} N_2O band in the earlier article.[1] Some of the curves have portions that are nearly straight and parallel to one another; the slope of these curves is 0.44 and indicates that $\int A(\nu)d\nu \propto P_e^{0.44}$ for samples with P_e and w within the ranges covered by the linear portions of the curves. The value of the exponent 0.44 is greater than the corresponding value of 0.38 obtained from the nearby N_2O band but is somewhat less than the value of 0.5 to be expected on the basis of simple theory. It will be noted that there is a clustering of curves in the upper right-hand corner of Fig. 2 in the region of large w and large P_e due to the fact that $k(\nu)w \gg 1$ for most frequencies within the band. There is a gradual decrease in the slopes of the upper curves with increasing P_e but the "saturation effects" of the type noted for the 2224 cm^{-1} N_2O band[1] are not nearly so pronounced in the case of CO. This is presumably due to the smaller line half-width at a given pressure and to the greater separation of rotational lines in the spectrum of CO, resulting in the persistence of considerable rotational fine structure of the band even at $P_e = 3000$ mm Hg. On the basis of Shaw's work,[4] the half-widths of the lines would be expected to be equal to the line spacing for values of P_e equal to approximately 36,000 mm Hg; in this pressure range rotational fine structure would be nearly eliminated and curves such as those in Fig. 2 would converge and have near zero slope. The saturation effects for the lowest curves of Fig. 2 corresponding to low values of w are of the type to be expected for "completely broadened" spectral lines and for $k(\nu)w \ll 1$ for all frequencies in the band.

It should be noted that the curves in Fig. 2 are plotted for samples having constant absorber concentration. Related plots for samples of pure CO, in which w is proportional to P_e, give curves with linear portions having slopes of 0.98. Therefore, in these linear portions $\int A(\nu)d\nu \propto w^m P_e^n$, where $m + n = 0.98$. In view of the value 0.44 for the slope of the curves in Fig. 2, it would appear that $m = 0.54$ and $n = 0.44$. This stronger dependence of $\int A(\nu)d\nu$ on w than on P_e is similar to the results obtained for N_2O in the earlier study.[1]

Figure 3 shows curves of $\int A(\nu)d\nu$ as a function of w for various values of P_e. These curves are useful in making estimates of total absorptance for samples having any values of w and P_e within the entire range covered in the present investigation, since interpolations between the various curves can easily be made. The lower portion of the uppermost curve, which corresponds to $P_e = 3000$ mm Hg, is linear and has a slope of unity, indicating that $\int A(\nu)d\nu$ is directly proportional to w. From this portion of the curve it is possible to determine the value of band intensity $\int k(\nu)d\nu$ in terms of measured values of $\int A(\nu)d\nu$ and w. The value of band intensity of the CO fundamental is

$$\int k(\nu)d\nu = 260\ (\text{atm cm})^{-1}\ \text{cm}^{-1}. \tag{1}$$

This value, which is believed to be accurate to ±10%, can be compared with the value 237 reported by Penner and Weber,[6] who apparently did not reduce their value for w to STP. If the values of w in Fig. 3 had not been corrected to standard temperature, the value would have been 235, a result in nearly perfect agreement with the Penner-Weber value.

Although the curves in Fig. 3 tend to converge for large and small values of w, the five lower curves are linear and nearly parallel over a wide range of w near the centers of the curves. The slope of the parallel portions of these curves is approximately 0.55; thus, for the range of w involved, $\int A(\nu)d\nu \propto w^{0.55}$. This result is in excellent agreement with the relation $\int A(\nu)d\nu \propto w^{0.54}P_e^{0.44}$ proposed above. In view of this agreement, an attempt was made to obtain empirical equations relating $\int A(\nu)d\nu$ to $w^{0.55}P_e^{0.44} \approx (wP_e^{0.8})^{0.55}$ by plotting $\int A(\nu)d\nu$ versus $wP_e^{0.8}$. It was found that $\int A(\nu)d\nu$ can be expressed to an accuracy of ±5%

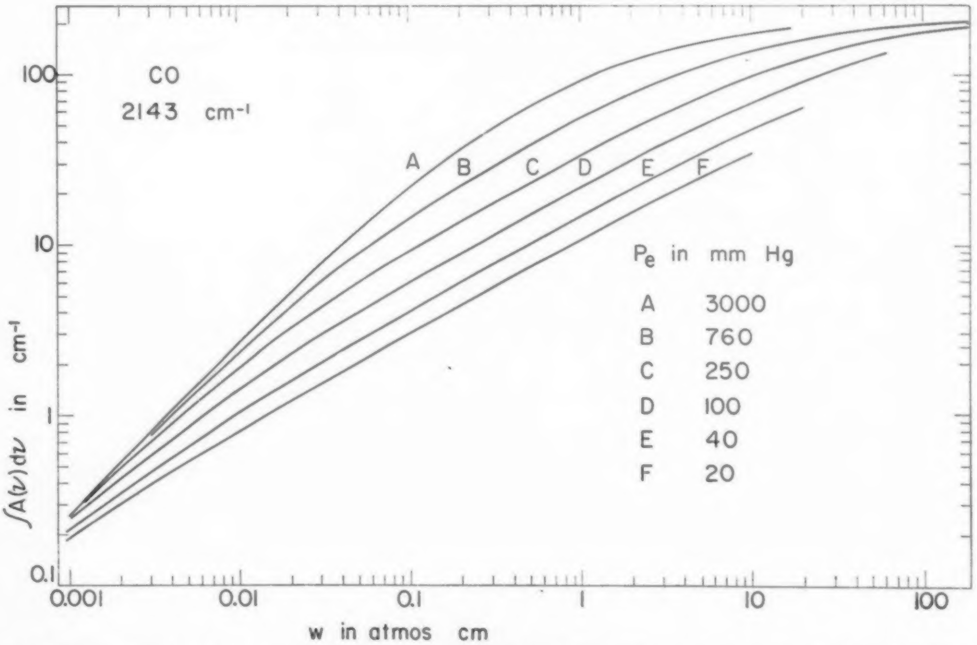

Fig. 3. Total absorptance of the 2143 cm^{-1} band for various values of equivalent pressure as a function of absorber concentration.

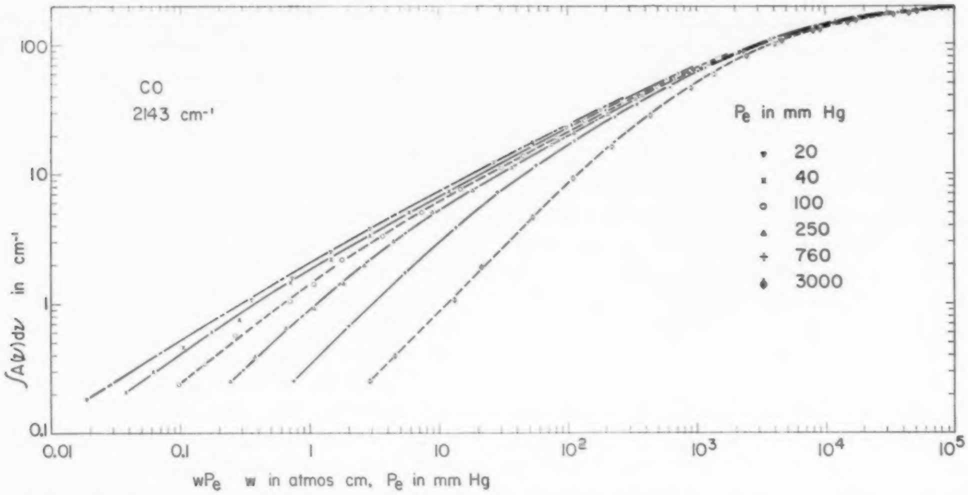

Fig. 4. Total absorptance of the 2143 cm⁻¹ band for various values of equivalent pressure as a function of the product of absorber concentration and equivalent pressure.

by the relation

$$\int A(\nu)d\nu = 2.75(wP_e^{0.8})^{.055} \qquad (2)$$

for $4 < \int A(\nu)d\nu < 40$ cm⁻¹ if $20 < P_e < 250$ mm Hg and for $10 < \int A(\nu)d\nu < 40$ cm⁻¹ if $20 < P_e < 760$ mm Hg. In (2) and in similar subsequent equations w is expressed in atm cm.

From the standpoint of existing theory, it is desirable to attempt to find relationships between $\int A(\nu)d\nu$ and wP_e. With this in view, the plots of $\int A(\nu)d\nu$ versus wP_e shown in Fig. 4 were prepared. Over the major portion of the figure, the curves corresponding to high values of P_e lie to the right of the curves for low values of P_e, as one might expect in view of (2). However, in the upper right-hand corner the curves tend to converge. Complete convergence would indicate the validity of the "strong-line approximation"[1]; on the basis of the experimental results plotted in Fig. 4, it can be concluded that the strong-line approximation is accurate to less than 5% error only for values of w so large that absorption within the band limits is nearly complete, and the variation of $\int A(\nu)d\nu$ with w and P_e is slight. However, for lower values of P_e the approximation introduces an error less than 20% over a rather wide range of variable wP_e. The range over which the approximation is valid to a given accuracy can be made larger by limiting its use to lower pressures.

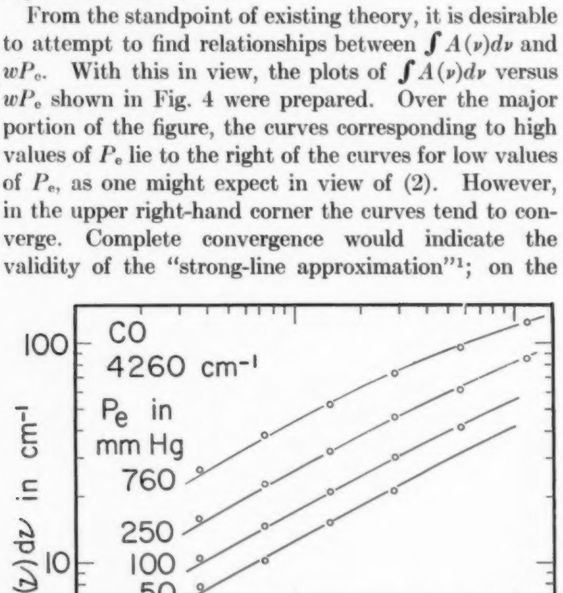

Fig. 5. Total absorptance of the 4260 cm⁻¹ overtone band of CO for various values of equivalent pressure as a function of absorber concentration.

On the basis of the plots in Fig. 4, the following emperical equations were developed:

$$\int A(\nu)d\nu = 3.20(wP_e)^{0.43} \qquad (3)$$

for $40 < \int A(\nu)d\nu < 120$ cm⁻¹ and $20 < P_e < 760$ mm Hg and

$$\int A(\nu)d\nu = -106 + 61 \log (wP_e) \qquad (4)$$

for $120 < \int A(\nu)d\nu < 200$ cm⁻¹ and $20 < P_e < 3000$ mm Hg. The empirical equations (3) and (4) are believed to be accurate to ±10%, except near the ends of their ranges of validity where errors as large as ±15% may be encountered. Extrapolations of (2), (3), and (4) should be avoided.

The CO overtone band at 4260 cm⁻¹ was investigated by means of a double-pass, single-beam Model 99 Perkin-Elmer instrument with spectral slit widths between 15 and 20 cm⁻¹. A multiple-traversal cell set to give absorption paths of 625, 1232, 2445, and 4875 cm was employed. On the basis of earlier studies of CO self-broadening in the overtone band, equivalent pressures were obtained from the expression $P_e = P + 0.08p$. This relation employs the value of $B = 1.08$ for the overtone, which is slightly larger than the value $B = 1.02$ for the fundamental; these measured values of self-broadening coefficients are believed to be accurate to ±6%.

In view of the fact that the overtone is much weaker than the fundamental, curves for the overtone corresponding to those in Fig. 2 for the fundamental show no saturation effects for the ranges of w between 37 and 1140 atm cm and P_e between 50 and 760 mm Hg covered in the present work. Plots of $\int A(\nu)d\nu$ versus w for various values of P_e are shown in Fig. 5. In comparing Fig. 5 with Fig. 3, which gives corresponding plots for the fundamental, it is interesting to note that, at a given value of P_e, $\int A(\nu)d\nu$ is the same for the two bands provided w for the overtone is 150 times that for the fundamental. In fact, the total absorption for the overtone can be determined from the curves in Fig. 3 by using the same value of P_e and a value of w that is 1/150 that actually used for the overtone; Eqs. (1), (2), (3), and (4) are probably applicable to the overtone provided $w/150$ is substituted for w in the equations.

Although the band intensity of the overtone was not determined directly in the present study, the results just cited would appear to be in close agreement with the earlier work of Penner and Weber,[6] who found that $\int k(\nu)d\nu$ for the fundamental was 145 times that of the overtone.

Methane Absorptance

The portion of the CH_4 spectrum investigated in the present study consists of the strong ν_3 fundamental at 3020 cm^{-1}, the strong ν_4 fundamental at 1306 cm^{-1}, and the much weaker ν_2 fundamental first definitely observed at 1534 cm^{-1} by Burgess, Bell, and Nielsen[7] and discussed more recently by Armstrong and Welsh.[8] The methane spectrum is more complicated than those of N_2O and CO, since each band has a Q-branch and a complex line structure.[9]

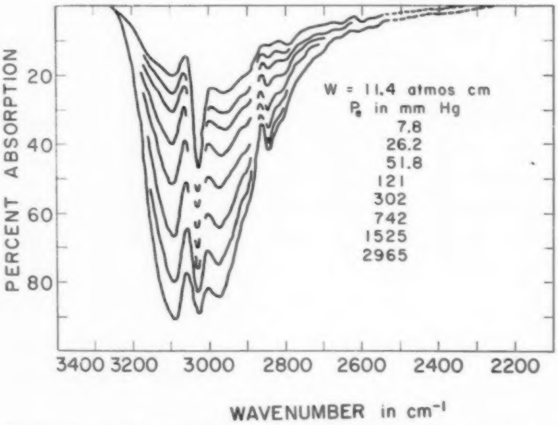

Fig. 6. Spectral absorptance of CH_4 in the vicinity of its fundamental ν_3 at 3020 cm^{-1}.

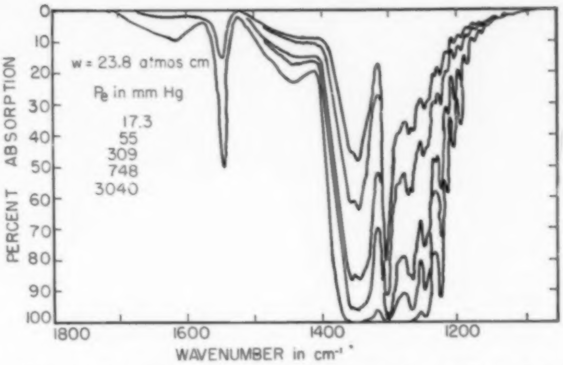

Fig. 7. Spectral absorptance of CH_4 in the vicinity of its strong ν_4 fundamental at 1306 cm^{-1} and its weak ν_2 fundamental near 1534 cm^{-1}.

Approximately 150 records of the spectral absorptance of CH_4 were made in the spectral region between 3400 and 700 cm^{-1}. Absorption path lengths of 6.35, 400, and 1600 cm were used to obtain data on samples having absorber concentrations in the range 0.015 to 188 atm cm and total pressures in the range 3 to 3000 mm Hg. Virtually all the observable absorption occurs in two spectral intervals, one between 3400 and 2200 cm^{-1} called *the* 3020 cm^{-1} band and the second between 1750 and 1100 cm^{-1}. Typical records of spectral absorptance in the 3020 cm^{-1} region are given in Fig. 6, which shows the effect of increasing the total pressure by adding N_2 to a cell in which the absorber concentration is kept constant; the spectral slit width was approximately 25 cm^{-1}. Figure 7 presents similar data for the second region of absorption obtained with an effective slit width of approximately 10 cm^{-1}. Some of the spectral absorptance curves shown in Figs. 6 and 7 have been corrected for spurious effects due to CO_2 and H_2O vapor present in the spectrograph and as slight impurities in the CH_4 samples.

It will be noted from Fig. 7 that the weak ν_2 fundamental overlaps the much stronger ν_4 fundamental. For the purposes of the present study, the 1750–1100 cm^{-1} region of absorption was arbitrarily divided at 1535 cm^{-1} into what is referred to as *the* 1306 cm^{-1} band and *the* 1550 cm^{-1} band; this procedure adds the weak absorption due to the P-branch of ν_2 to the much stronger overlapping ν_4 band.

Earlier studies[2] gave a value $B = 1.30$ for the self-broadening coefficient of CH_4 in the 3020 cm^{-1} band and $B = 1.38$ for the 1306 cm^{-1} band. Therefore, equivalent pressures were calculated from $P_e = P + 0.30p$ for the 3020 cm^{-1} band and from $P_e = P + 0.38p$ for the 1306 cm^{-1} band. The second expression was also used to obtain P_e for the neighboring 1550 cm^{-1} band, since no independent value could be obtained for this very weak band.

In the case of the 3020 cm^{-1} band, curves giving

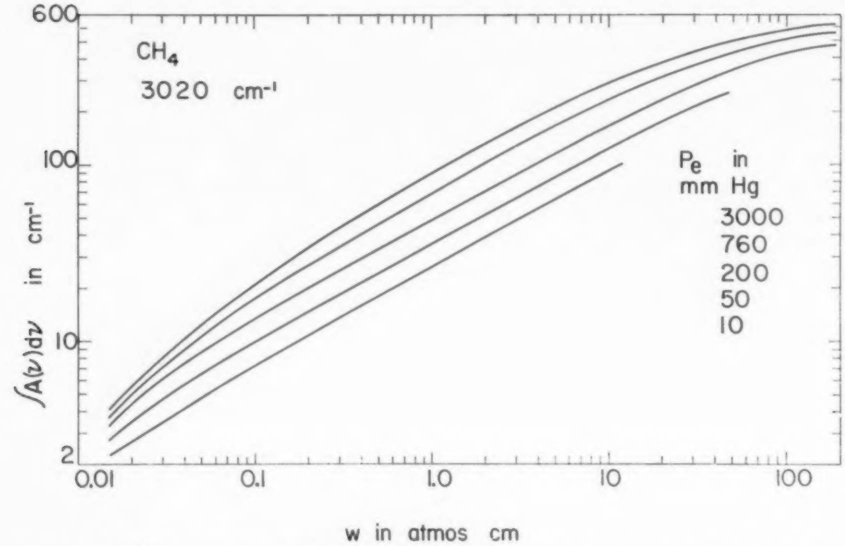

Fig. 8. Total absorptance of the 3020 cm^{-1} band of CH_4 for various values of equivalent pressure as a function of absorber concentration.

$\int A(\nu)d\nu$ for various values of w as a function of pressure on a logarithmic scale are nearly parallel and linear for intermediate values of P_e. The slopes of the linear portions of these curves have the value 0.22, which is considerably smaller than the corresponding slopes for N_2O and CO bands; this value indicates that $\int A(\nu)d\nu \propto P_e^{0.22}$ for intermediate values of pressure. There is little indication of "saturation" at high pressures for large values of absorber concentration. An unusual feature of these logarithmic plots for low pressures is that the slopes of some of the curves tend to *increase* with increasing pressure for values of P_e as high as 75 mm Hg, which is considerably greater than pressures at which Doppler broadening is important. This unusual dependence of $\int A(\nu)d\nu$ on P_e may result from the fact that the 3020 cm^{-1} band consists of strong lines clustered in widely separated groups and other much weaker lines occurring throughout the band. If the "clusters" of strong lines can be considered as single strong Elsasser lines,[1] their total absorptance might show a square-root dependence on pressure for low pressures at which the total absorptance due to the much weaker lines is nearly independent of pressure. With increasing pressure, the relative contribution of the pressure-dependent strong lines to the total band absorptance might increase; this phenomenon could account for the observed effects. This possible explanation could be checked by studies made with a spectrograph having high resolving power.

Plots of $\int A(\nu)d\nu$ versus absorber concentration w for various values of P_e are shown in Fig. 8, from which $\int A(\nu)d\nu$ can be obtained by interpolating between the curves for any value of w and P_e in the ranges covered in the investigation. The linear portions of the curves have slopes of 0.55, indicating that $\int A(\nu)d\nu \propto w^{0.55}$ for the ranges of w and P_e involved. It was found that total absorptance for the 3020 cm^{-1} band can be expressed by means of the following equations, in which w is given in atm cm:

$$\int A(\nu)d\nu = 15.5(wP_e^{0.4})^{0.55} \qquad (5)$$

for $15 < \int A(\nu)d\nu < 250$ cm^{-1} and $10 < P_e < 760$ mm Hg, and

$$\int A(\nu)d\nu = -375 + 272 \log (wP_e^{0.4}) \qquad (6)$$

for $250 < \int A(\nu)d\nu < 500$ cm^{-1} and $10 < P_e < 3000$ mm Hg. Values of $\int A(\nu)d\nu$ given by (5) and (6) are accurate to ±10%, except for values of $\int A(\nu)d\nu < 40$ cm^{-1}, for which errors as great as ±15% are encountered.

It will be noted from Fig. 8 that even for the smallest value of w and the highest value of P_e, the total absorptance increases with increasing P_e. Thus, the requirement that $k(\nu)w \ll 1$ is not fulfilled even for P_e = 3000 mm Hg and the smallest values of w; hence, a value of band intensity $\int k(\nu)d\nu$ cannot be obtained directly from the plot. However, by extrapolating the uppermost curve to smaller values of w with the requirement that its maximum slope be unity, an estimate of band intensity can be made. With w reduced to STP, the result is

$$\int A(\nu)d\nu = 320 \text{ (atm cm)}^{-1} \text{ cm}^{-1} \qquad (7)$$

for the 3020 cm^{-1} band. This value, which is believed to be valid to ±15%, is approximately 12% less than the value of 360 cm^{-1} reported by Welsh, Pashler, and Dunn[10] and 2.5% less than the value of 328 reported more recently by Armstrong and Welsh.[8]

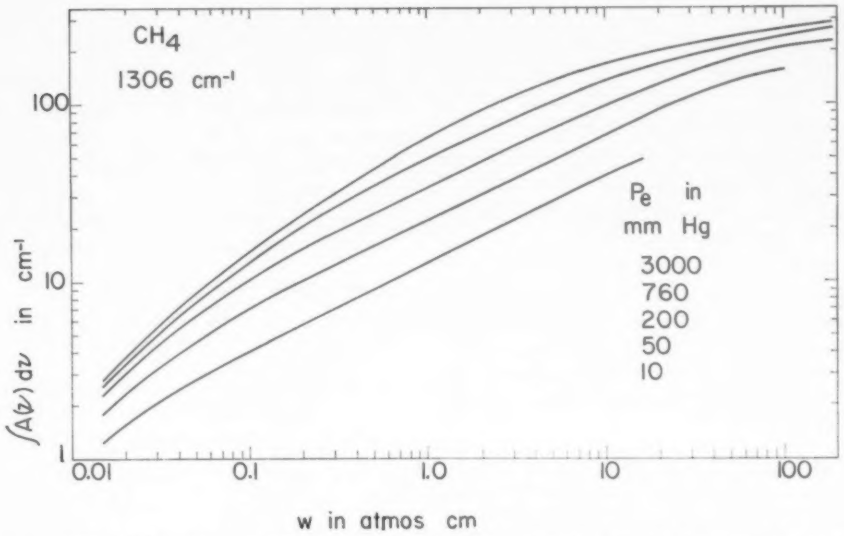

Fig. 9. Total absorptance of the 1306 cm^{-1} band of CH$_4$ for various values of equivalent pressure as a function of absorber concentration.

When values of $\int A(\nu)d\nu$ for the 1306 cm^{-1} band for various values of w are plotted as a function of P_e, some of the curves on the logarithmic plot have linear portions with a slope of 0.30 for intermediate values of P_e, indicating that $\int A(\nu)d\nu \propto P_e^{0.30}$; this pressure dependence is greater than that for the 3020 cm^{-1} band but is considerably less than the square-root dependence predicted by simple theory. At high pressures, there is some evidence of the onset of saturation for large values of w. At low pressures there is no evidence of the unusual features exhibited by the corresponding plots for the 3020 cm^{-1} band. High-resolution studies[9] indicate different structures for the two bands and hence it is not surprising that their pressure dependence is quite different.

Values of $\int A(\nu)d\nu$ for various values of P_e are plotted as a function of w in Fig. 9 for the 1306 cm^{-1} band. Considerable portions of some of the curves have a slope of 0.48, indicating that $\int A(\nu)d\nu$ varies essentially as the square root of the absorber concentration for the ranges of P_e and w involved. In view of the observed dependence of total absorptance on P_e and w, attempts were made to derive empirical equations in terms of $wP_e^{0.6}$ for intermediate values of $\int A(\nu)d\nu$. The following equation gives correct values of total absorptance to ±15% of the experimental values:

$$\int A(\nu)d\nu = 7.3(wP_e^{0.6})^{0.45} \qquad (8)$$

for $20 < \int A(\nu)d\nu < 130$ cm^{-1} and $10 < P_e < 760$ mm Hg and with w in atm cm at STP. For greater values of total absorptance, the following equation applies:

$$\int A(\nu)d\nu = -190 + 115 \log (wP_e^{0.6}) \qquad (9)$$

for $130 < \int A(\nu)d\nu < 300$ cm^{-1} and $10 < P_e < 760$ mm Hg. As usual, values of $\int A(\nu)d\nu$ for small values of wP_e cannot be easily expressed in terms of an equation, and direct use of Fig. 9 is necessary.

By extrapolating the curves of Fig. 9 to smaller values of w with the requirement of unity as the maximum slope for the top curve, the band intensity of the 1306 cm^{-1} CH$_4$ was estimated to be

$$\int k(\nu)d\nu = 185 \text{ (atm cm)}^{-1} \text{ cm}^{-1}. \qquad (10)$$

This value, which is believed to be in error by less than ±15%, is approximately 18% greater than the value of 157 reported by Welsh and Sandiford[11] and the value of 158 reported more recently by Armstrong and Welsh.[8]

Data for the 1550 cm^{-1} band are plotted in Fig. 10. This weak band is observable only for large values of

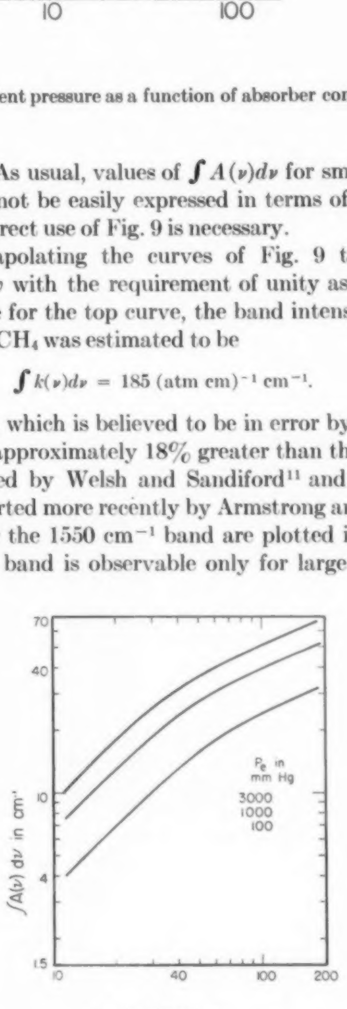

Fig. 10. Total absorptance of the 1550 cm^{-1} band of CH$_4$ for various values of equivalent pressure as a function of absorber concentration.

w, and the proximity of the strong 1306 cm^{-1} band together with the overlapping ν_2 band of atmospheric water vapor makes determination of $\int A(\nu)d\nu$ for the weak band rather difficult. Values of $\int A(\nu)d\nu$ plotted in Fig. 10 are probably accurate to $\pm 10\%$ for values greater than 30 or 40 cm^{-1} but may be in error by as much as $\pm 20\%$ for smaller samples. There would appear to be sufficient data to justify the relation $\int A(\nu)d\nu \propto P_e^{0.27}$ for certain ranges of w and P_e, but none of the curves in Fig. 10 has a slope of 0.5 as do corresponding plots for the other CH_4 bands. Apparently the values of w employed were not sufficiently large for the exhibition of any "strong-line properties" by this band. No attempt to establish empirical expressions for $\int A(\nu)d\nu$ for the 1550 cm^{-1} band seemed justified.

However, it was possible to obtain a rough estimate of band intensity for the ν_2 band of CH_4. On the basis of values obtained for *the* 1550 cm^{-1} band and on the assumption that the contribution of the P-branch, which in the present study was included in the stronger adjacent 1306 cm^{-1} band, is equal to the contribution of the R-branch to the total band intensity, it is estimated that $\int k(\nu)d\nu$ for the ν_2 band is between 2 and 3 (atm cm)$^{-1}$ cm^{-1}. To the knowledge of the authors, the only other published value is the value of 2.4 reported recently by Armstrong and Welsh.[8]

The authors wish to express their appreciation to Wilbur France and E. B. Singleton, who assisted in certain parts of the work. One of the authors, (D. W.) wishes to express his appreciation to P. Swings and M. Migeotte for the use of the library and other facilities of the Institut d'Astrophysique of the Universite de Liége during preparation of the paper.

References

1. D. E. Burch and D. Williams, Appl. Opt. **1,** 473 (1962).
2. D. E. Burch, E. B. Singleton, and D. Williams, Appl. Opt. **1,** 359 (1962).
3. M. V. Migeotte, Phys. Rev. **75,** 1108 (1949).
4. J. H. Shaw, Report 6, Contract AF 19(604)-1003, The Ohio State University Research Foundation (1957).
5. M. V. Migeotte, Phys. Rev. **73,** 519 (1948).
6. S. S. Penner and D. Weber, J. Chem. Phys. **19,** 807 (1951).
7. J. S. Burgess, E. E. Bell, and H. H. Nielsen, J. Opt. Soc. Am. **43,** 1058 (1953).
8. R. L. Armstrong and H. L. Welsh, Spectrochim. Acta **16,** 840 (1960).
9. A. H. Nielsen and H. H. Nielsen, Phys. Rev. **48,** 864 (1935).
10. H. L. Welsh, P. E. Pashler, and A. F. Dunn, J. Chem. Phys. **19,** 340 (1951).
11. H. L. Welsh and P. J. Sandiford, J. Chem. Phys. **20,** 1646 (1952).

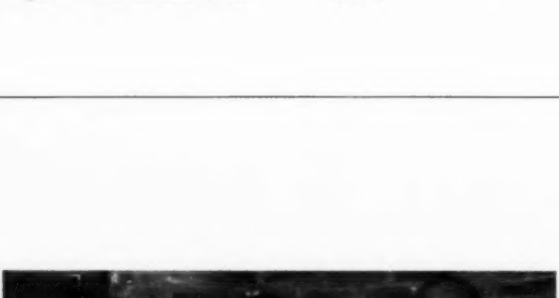

Three atmospheric infraredders: P. M. Goody *Director, Blue Hill Observatory of Harvard University*, K. Ya. Kondratiev *Dept. of Atmospheric Physics, Leningrad State University*, and J. N. Howard *AFCRL, Bedford, Mass.*

Emittance Measurements on Infrared Windows Exhibiting Wavelength Dependent Diffuse Transmittance

S. E. Hatch

The emittance of Irtran-1 windows of thickness 1.0, 3.8, and 7.6 mm has been measured at several temperatures over the range 300°C to 700°C. The emittance of 3.8 mm standard and short wavelength Irtran-2 windows has been measured at temperatures up to 500°C. The emittance of a 3.8 mm Irtran-3 window has been measured at temperatures in the range 300°C to 850°C. A method of matching sample and blackbody temperatures has been employed which avoids the necessity of making accurate absolute temperature measurements. The applicability and sensitivity of this method is discussed. An attempt has been made to establish the effect of scattering in the samples on the measurement results.

Introduction

Recently several new materials, referred to by the commercial name Irtran, have been developed which possess very interesting infrared optical properties. These materials consist of hot-pressed polycrystalline solids* of essentially theoretical density. In order to evaluate their potential as infrared transmitting domes, windows, lenses, etc., for use in high-temperature environments, it was necessary to measure their normal spectral emittance as a function of temperature.

A brief literature survey disclosed many papers concerned with the emittance of opaque materials, but only a limited number covering the case of transparent solids. An excellent discussion of the theory and experimental techniques applicable to transparent solids has been given by McMahon.[1,2] A method for use with translucent solids has been proposed by Weber.[3] The present work differs from the previous treatments in the method of heating used, the manner in which the contribution from scattering has been detected, and in the method of establishing sample and blackbody temperature equality.

The terminology concerning the relationship between emissivity-emittance, transmissivity-transmittance, etc., follows that proposed by Worthing,[4] in which the suffix *ivity* denotes a basic property of the material, and the suffix *tance* denotes a property of a particular body and is a function of its physical characteristics (e.g., thickness and surface quality).

Experimental

In the usual manner, the normal spectral emittance (E^*) of a particular body may be defined as the ratio of its normal spectral steradiancy to that of a blackbody at the same temperature. However, in the case of transparent or translucent materials, care must be taken to insure that the detection system records only that radiant energy which originates in the sample. Conventional methods of measuring emittance utilize a furnace surrounding the sample, with only small openings provided for viewing. Irtran-1 and Irtran-2 scatter appreciably at short wavelengths; hence, in the conventional methods of measuring emittance, errors are introduced when radiant energy originating at some hot surface outside the sample is scattered into the detection system by the sample. An attempt was made to minimize this error by reducing the "furnace" to the form of a stainless steel ring as shown in Fig. 1. The ring is heated by a 9600 cycle induction coil. This form of heating minimizes the heater surface seen by the sample, and energy emitted by the heater must be scattered by the sample at a large angle in order to enter the detection system. A further reduction in the effective hot surface seen by the sample was accomplished by electroplating gold over the entire surface of the stainless steel ring of Fig. 1. Several of the measurements of Irtran-1 and Irtran-2 made with the uncoated stainless steel ring were repeated after gold-coating in order to

---

The author is with Eastman Kodak Company, Apparatus and Optical Division, Rochester, New York.

Received 24 November 1961.

* The major chemical constituents are as follows: Irtran-1—magnesium fluoride, Irtran-2—zinc sulfide, Irtran-3—calcium fluoride.

evaluate the influence of scatter. The same samples were used for both sets of measurements on Irtran-1, but due to an experimental casualty it was necessary to use a different Irtran-2 sample for the repeated measurement. Repeat measurements were not made on Irtran-3 since this material is essentially scatter free.

A diagram of the measuring apparatus, which can be used for both emittance and transmittance measurements, is shown in Fig. 2. A movable plano mirror (E) and two spherical mirrors (C, D) allow the energy emitted by sample in its holder (F), and the energy emitted by the Barnes Model RS-88 blackbody (B) to be alternately focused on the entrance slit of a Perkin-Elmer Model 112 single beam monochromator (A). The emittance is directly computed from these two measurements. For the emittance measurements, the internal chopper of the monochromator was used. The system is checked for stray radiation by heating the sample holder with no sample in it. For transmittance measurements, the energy from a globar source (K) is chopped externally (J), then focused on the sample by means of the plano mirror (H) and spherical mirror (I). The energy transmitted by the sample is focused on the entrance slit of the monochromator by the same mirror system used for the emittance measurements. Energy emitted by the sample does not influence the measurements since the detection system is sensitive only to the chopped radiation. Measurement with and without the sample in its holder allows direct computation of the transmittance. High-temperature transmittance measurements were made subsequent to each of the emittance measurements reported herein. However, instability of the globar source introduced inaccuracies of sufficient magnitude in the data that their publication is unwarranted. More accurate measurements could be performed by providing a source monitoring and control system which would provide constant radiancy of the globar source.

The radiation temperature of the samples was established by varying the temperature of the stainless steel ring heater until the measured emittance of the sample, in the wavelength range where emittance is insensitive to temperature, equaled that derived from ambient transmittance and reflectance measurements. It is shown in the following paragraphs that the emittance at particular wavelengths will be essentially invariant with temperature, and hence can be derived from ambient measurements.

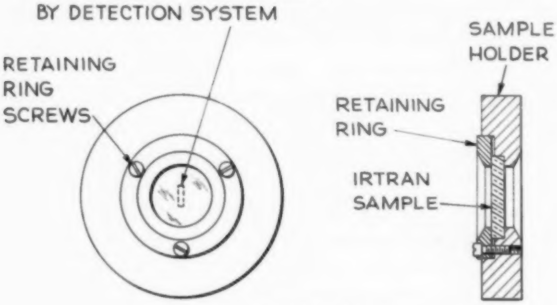

Fig. 1. Sample holder.

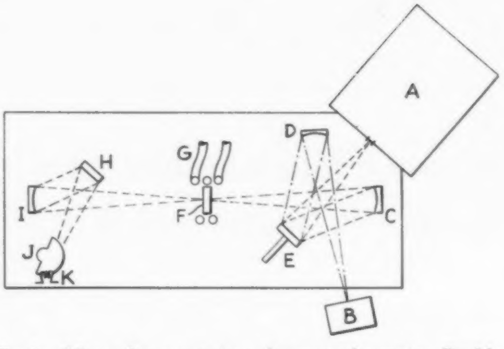

Fig. 2. Measuring apparatus: A—monochromator, B—blackbody, C, D, E, H, I—mirrors, F—sample holder, G—induction coil, J—external chopper, K—light source.

Under equilibrium conditions, thermodynamic analysis dictates that the emittance E^*, transmittance T^*, and reflectance R^* be related in the following manner†:

$$E^* + T^* + R^* = 1. \tag{1}$$

In a region where T^* is zero, Eq. (1) reduces to

$$E^* = 1 - R^*. \tag{2}$$

In the case of Irtran-1 in thicknesses of 1 mm or greater, measurements show T^* to be essentially zero from 10 to 15 μ; hence Eq. (2) is applicable in this region. Reflectance measurements performed on a Perkin-Elmer Model 221 spectrometer, equipped with a reflection attachment, show R^* to be less than one percent over the range 10 to 15 μ. This low value of R^* is not unreasonable in view of the known behavior of the refractive index over the range 1 to 8 μ, and the presumption that it must become even smaller with increasing wavelength as one approaches the restrahlen reflectivity peak at 20 μ.[5] With R^* established, it follows from Eq. (2) that E^* is 0.99 or greater over the range 10 to 15 μ. The quantities E^*, T^*, and R^* are all functions of wavelength and temperature, and when used in Eqs. (1) and (2) must, of course, be taken at identical wavelengths and temperatures. The values of T^* and R^* quoted above are ambient measurements; therefore the predicted E^* is valid only at ambient temperatures. However, with the following qualitative arguments this value can be extended to elevated temperatures.

---

† The transmittance of a body is defined as the ratio of the intensity of the radiation transmitted by the body to the intensity of the incident radiation. The reflectance of a body is defined as the ratio of the intensity of the radiation reflected by the body (including multiple internal reflections) to the intensity of the incident radiation. As used here and by McMahon,[1] these quantities refer to specular radiation at normal incidence and are, of course, functions of wavelength and temperature.

Previous measurements have shown the long wavelength cutoff to move toward shorter wavelengths as the temperature is increased. The argument that T^* is zero between 10 and 15 μ will then also apply at elevated temperatures. No high temperature measurements of R^* have been made, but a qualitative estimate of its variation can be made from other considerations. R^* is related to the reflectivity (frequently called the true reflectivity), and consequently to the refractive index n, in the following manner[1]:

$$R^* = R\left[1 + \frac{T^2(1 - R)^2}{1 - R^2T^2}\right], \tag{3}$$

where

R = reflectivity,† $R = [(n - 1)/(n + 1)]^2$,
T = transmissivity (or true transmissivity) and is by definition $e^{-\alpha x}$ with α being the absorption coefficient and x the sample thickness.

The transmittance T^* and transmissivity T are also related in a similar manner‡:

$$T^* = T\left[\frac{(1 - R)^2}{1 - R^2T^2}\right]. \tag{4}$$

It is apparent from (4) that, except for the trivial case of $R = 1$, T is zero when T^* is zero; hence in the region 10 to 15 μ Eq. (3) reduces to

$$R^* = R = \left(\frac{n - 1}{n + 1}\right)^2. \tag{5}$$

It follows that the variation of R^* with temperature, t, is given by

$$\frac{dR^*}{dt} = \frac{dR^*}{dn}\frac{dn}{dt} = \left[\frac{4(n - 1)}{(n + 1)^3}\right]\frac{dn}{dt}, \tag{6}$$

where dn/dt is the change in refractive index with temperature. The quantity in the bracket of Eq. (6) will be less than one regardless of the numerical value of n; hence dR^*/dt will be less than dn/dt. Values published for a single crystal magnesium fluoride[5] show dn/dt to be of the order of 10^{-5}°C^{-1}. Changes in R^* with temperature will then be of the order of 10^{-5}°C^{-1} or less which is insignificant for the purpose of these measurements. If inference may be drawn from the behavior[6] of SiO_2 and B_2O_3, in which very small changes are seen in the restrahlen reflectivity peak from −190°C to 2000°C, one would not expect any changes in the restrahlen peak of Irtran-1 with temperature to affect significantly the reflectivity over the 10 to 15 μ region. From these arguments it is concluded that the value of E^* greater than 0.99 between 10 and 15 μ is applicable for Irtran-1 at the temperatures used in this work.

The knowledge of E^* over a particular wavelength region offers a convenient method of matching sample and blackbody temperature. The sample is allowed to come to equilibrium at some particular value of power input to the heater. The radiation temperature of the sample is then determined by adjusting the blackbody source temperature to a value which results in a measured E^* of about 0.99 for the 10 to 15 μ wavelength range. When this emittance value is achieved the sample and blackbody are at the same temperature. The small temperature gradients which undoubtedly exist in the sample are conveniently averaged when the sample and blackbody are matched by the above method.

It was found that a change in blackbody temperature of less than 5°C produced a detectable difference in the value of E^* measured at 10 μ. From this it is concluded that the errors involved in matching blackbody and sample temperatures are within ±5°C. In view of the method of heating used and the resulting thermal gradients, it is doubtful that any improvement in the match could have been achieved by measuring the sample temperature with the most refined thermocouple techniques. Furthermore, the present method matches the blackbody temperature to that of the sample in the exact area viewed by the detection system, a condition which is particularly desirable in the presence of thermal gradients.

Ambient transmittance and reflectance measurements on Irtran-3 suggest an emittance of 0.98 to 0.99 over the range 11 to 13 μ. The argument justifying the use of this value at elevated temperatures is identical to that presented for Irtran-1. In the case of Irtran-2, which transmits to longer wavelengths and has a much higher refractive index, it was felt that a temperature measurement of the type used for Irtran-1 would not be sufficiently reliable. The same theory is applicable; however, the transmittance of Irtran-2 in a thickness of 3.8 mm does not approach zero until one has reached a wavelength of 14.7 μ. The blackbody energy at wavelengths greater than 14.7 μ is less sensitive to temperature change than at the shorter wavelengths used with Irtran-1. Furthermore, the low blackbody energy at the longer wavelengths necessitates greater electronic amplification, and the accompanying increase in noise reduces the accuracy with which the signal can be read. It was decided to attempt matching the sample and blackbody temperature by this method, and then later check the accuracy with thermocouple measurement. To do this, a hole was drilled in the sample at a point not viewed by the detection system and a monitoring thermocouple inserted in it. The sample and blackbody temperature were adjusted to give a measured emittance of 0.87 at about 15 μ, the value which was calculated from ambient measurements of reflectance. With this condition established, the emittance of the sample was measured over the 2 to 15 μ range, and the temperature of the monitoring thermocouple recorded. After completing these measurements, a small hole was drilled at the center of the area viewed by the detection system and a small calibrating thermocouple cemented in the hole. The sample was reheated until the monitoring thermocouple indicated the same temperature which had been recorded during the previous measurements; then the temperature of the calibrating thermocouple and the temperature of the blackbody, as found by adjusting it to give the calculated emittance, are shown in Table I. The temperature of the monitoring thermocouple is also listed for comparison.

---

† This form of the reflection formula is valid at these wavelengths since reflection measurements[5] indicate that the imaginary part of the refractive index does not make a significant contribution at wavelengths below 15 μ.

‡ Equations (3) through (6) are strictly applicable only to nonscattering materials; however, at wavelengths greater than 5 μ this condition is essentially satisfied for the Irtran materials used in this work.

Table I

Monitoring thermocouple	Blackbody temperature	Calibrating thermocouple
294°C	316°C	320°C
476°C	500°C	509°C

These results indicate that the method of determining the sample temperature by adjusting the blackbody temperature to achieve a calculated emittance is quite reliable, even when the matching must be done at long wavelengths. However, since the thermocouple techniques used are not infallible, it would seem unwise to claim an accuracy better than ±15°C. These results also point out the errors which can be incurred when improper thermocouple techniques are used. The calibrating thermocouple was located near the center of the sample, and the monitoring thermocouple about halfway between the center of the sample and the edge of the mounting ring. In peripheral heating, one would expect the thermal gradients to be such that the central area, where the calibrating thermocouple was located, would be at a lower temperature than the point midway to the mounting ring, where the monitoring thermocouple was located. The figures presented in Table I indicate that this is not the case. However, it is to be noted that the monitoring thermocouple was merely resting in a drilled hole in the sample, whereas the calibrating thermocouple was cemented in its hole, and hence in much better physical contact with the sample. Accurate matching of sample and blackbody temperature is extremely important in emittance work since the fourth power of the absolute temperature is involved in the radiation laws.

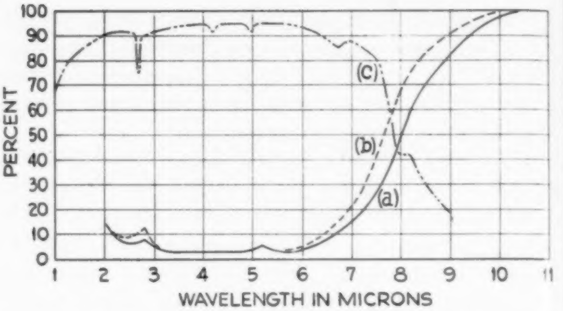

Fig. 3. Irtran-1, thickness 1 mm, stainless steel holder; curve (a) emittance at 374°C, curve (b) emittance at 592°C, curve (c) ambient transmittance.

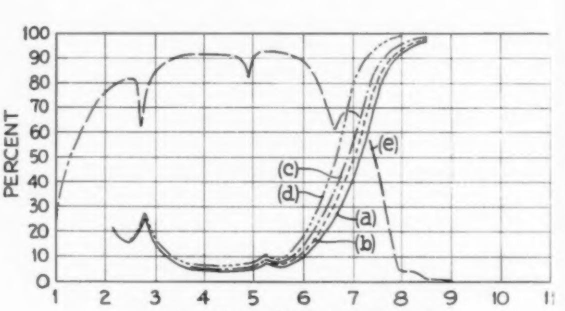

Fig. 4. Irtran-1, thickness 3.8 mm, stainless steel holder; curve (a) emittance at 316°C, curve (b) emittance at 374°C, curve (c) emittance at 592°C, curve (d) emittance at 697°C, curve (e) ambient transmittance.

Results

The normal spectral emittance of Irtran-1, -2, and -3, as measured using the uncoated stainless steel sample holder, is shown in Figs. 3 through 8. In each case the ambient specular transmittance has been included for reference. The results obtained from the measurements repeated after gold-plating the sample holder are shown in Figs. 9 through 11. The ambient specular transmittance is again included, and in Figs. 9 and 10 the emittance data found with the uncoated stainless steel holder are replotted for comparison. It should be pointed out that a major portion of the loss in the short wavelength specular transmittance of Irtran-1 and Irtran-2 is due to scatter. It should be noted also, in comparing the results on standard Irtran-2, that a different sample was used for the repeat measurement, and its short wavelength specular transmittance was somewhat lower than that of the sample used for the measurement with the uncoated stainless steel holder. In the case of Irtran-1, there are small absorption bands superimposed on the long wavelength cutoff (in the 6–10 μ region), and these bands appear, as expected, as small peaks in the emittance curve. Since the primary interest in this material is at wavelengths below the cutoff, these bands have been omitted in order to minimize the somewhat tedious job of data reduction and plotting.

Discussion

The variation in results before and after gold-plating the sample holder leads immediately to the conclusion that the presence of scattering in the samples has influenced the measurements, in spite of the very limited hot surface seen by the sample.

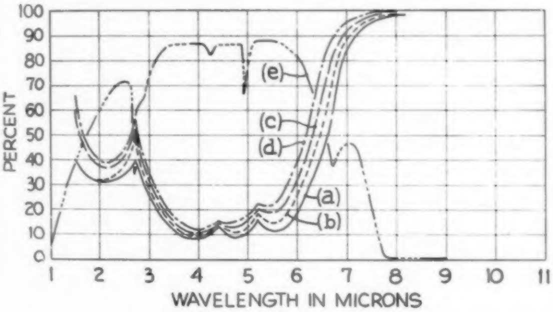

Fig. 5. Irtran-1, thickness 7.6 mm, stainless steel holder; curve (a) emittance at 321°C, curve (b) emittance at 374°C, curve (c) emittance at 592°C, curve (d) emittance at 697°C, curve (e) ambient transmittance.

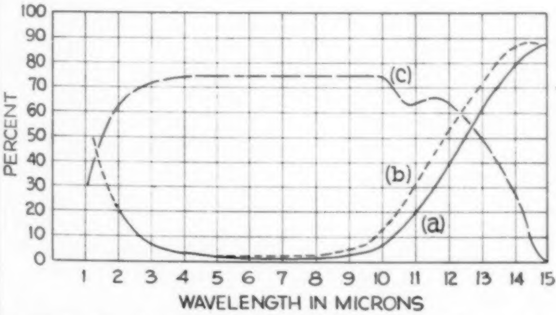

Fig. 6. Standard Irtran-2, thickness 3.8 mm, stainless steel holder; curve (a) emittance at 316°C, curve (b) emittance at 500°C, curve (c) ambient transmittance.

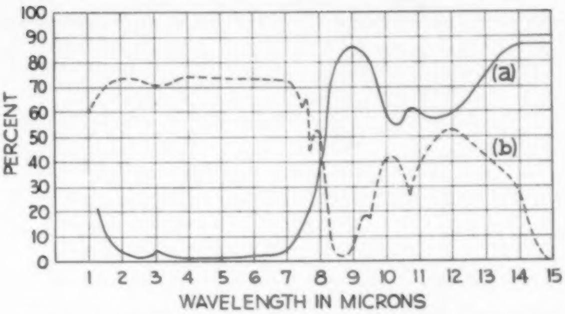

Fig. 7. Short wavelength Irtran-2, thickness 3.8 mm, stainless steel holder; curve (a) emittance at 500°C, curve (b) ambient transmittance.

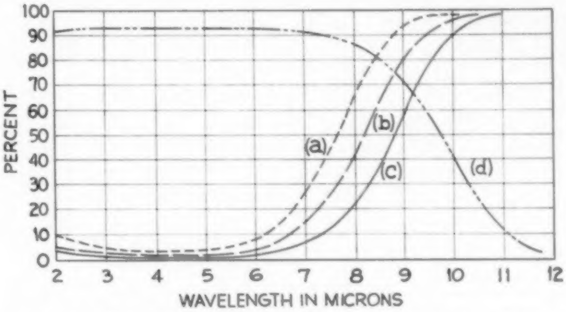

Fig. 8. Irtran-3, thickness 3.8 mm, stainless steel holder; curve (a) emittance at 850°C, curve (b) emittance at 592°C, curve (c) emittance at 316°C, curve (d) ambient transmittance.

It is difficult to evaluate accurately the extent to which the measurements are influenced by scattered light, but a qualitative estimate can be made through the following arguments. With the detection system focused on the sample, it records the sum of the energy emitted by the sample and that energy which originates elsewhere but is scattered into the detection system by the sample. If the energy emitted by the sample itself is designated by e_1, and the scattered energy entering the detection system by e_2, the measured emittance E_1^* will be:

$$E_1^* = \frac{e_1 + e_2}{e_b}, \tag{7}$$

where e_b is the energy recorded when the detection system is focused on a blackbody having the same temperature as the sample. Since e_2 must originate in the hot sample holder, it follows that a reduction in the emittance of the holder will result in a corresponding reduction in e_2. That is, if the emittance of the gold-plated holder is some fraction C of the emittance of the uncoated holder, the amount of energy scattered into the detection system is then Ce_2. The energy from the sample itself is still e_1 if the temperature is held constant; hence the emittance E_2^* measured with the gold-plated holder is:

$$E_2^* = \frac{e_1 + Ce_2}{e_b}. \tag{8}$$

The "true emittance" of the sample is e_1/e_b which can easily be found from Eqs. (7) and (8) to be:

$$\frac{e_1}{e_b} = \frac{E_2^* - CE_1^*}{(1 - C)}. \tag{9}$$

Table II. (**Temperature = 374°C**)

Wave-length (μ)	Sample thick-ness (mm)	"True emittance" as calculated by Eq. (9) (%)			Emittance as measured with the gold-plated sample holder (%)
		C = 1/5	C = 1/10	C = 1/15	
2	1	4.5	5.3	5.7	6.2
4	1	0.6	0.9	0.96	1.1
2	3.8	12.5	13.3	13.5	14
4	3.8	3.0	3.05	3.1	3.2

Table II shows the "true emittance" of the sample as calculated by Eq. (3) for values of $C = {}^1/_5, {}^1/_{10}, {}^1/_{15}$. The emittance as measured with the gold-plated holder is also listed for comparison.

This analysis is admittedly very qualitative, and based on gross assumptions. For example, it has been assumed that the temperature at which the sample holder must be held, in order to maintain a given temperature in the sample, is the same before and after gold-plating. If this were not true, the contribution from scattering would not be Ce_2 with the gold-plated holder. This assumption is not quantitatively accurate, but is probably a good approximation since the sample heating in both cases was mainly through physical contact with the heating ring, rather than by the radiative transfer of energy. The validity of this assumption was crudely verified by measurements with a thermocouple resting loosely in a hole near the periphery of the sample holder. In addition, it is necessary to assume a value of C. In view of the surface conditions of the stainless steel holder during the earlier runs, and the surface condition of the gold-plating, it would seem that $C = {}^1/_{10}$ is a reasonable estimate.

In the case of Irtran-2, an analysis of this nature is impossible since different samples were used before and after gold-plating the sample holder. It can be seen that the emittance of the sample measured with the gold-plated holder (Fig. 11) is virtually identical to that of the sample measured with the stainless steel holder (Fig. 6). It should, however, be noted that the sample used with the gold-plated holder has a somewhat lower specular transmittance at short wavelengths than the sample used with the stainless steel holder. Previous measurements have shown that the major portion of the differences seen in the short wavelength specular transmittance of Irtran-2 samples is related to differences in the scattering losses rather than differences in absorption. It can therefore be inferred that the influence of scattering on the emittance measurements of Irtran-2 was lowered by gold-plating the holder, as was the case with Irtran-1. It also follows that the "true emittance" of standard Irtran-2 is even lower than that shown in Fig. 11.

The total and diffuse transmittance, and the total and diffuse reflectance of Irtran-1 and Irtran-2 over the wavelength region 0.5 to 2.0 μ, have been measured on a Beckman Model DK2 equipped with an integrating sphere photometer. The results indicate that there is some absorption present which increases with decreasing wavelength. This would, of course, result in an increase in emittance with decreasing wavelength. It is possible to calculate the emittance which would be expected to result from this absorption if one assumes the absorption is invariant with temperature. This calculation has been made for Irtran-1, and the results are in reasonable agreement with the calculated "true emittance" at 2 μ, shown in Table II; however, the analysis is much too qualitative to warrant inclusion here. This is mentioned only to point out that one would expect an increase in the emittance of Irtran-1 and -2 with decreasing wavelength, and hence should not conclude that the increase shown in the accompanying figures is due entirely to scattering error.

It can be safely concluded that the results presented in Figs. 8 through 11 represent the maximum emittances

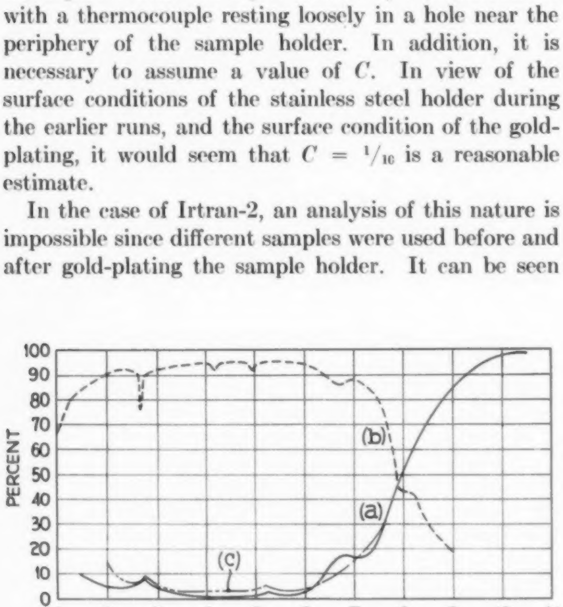

Fig. 9. Irtran-1, thickness 1 mm; curve (a) emittance in gold-plated holder at 374°C, curve (b) ambient transmittance, curve (c) emittance in stainless steel holder at 374°C (curve (a) of Fig. 3).

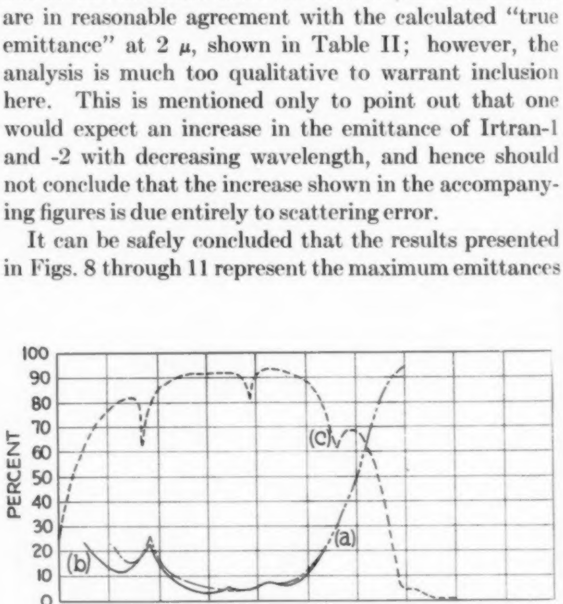

Fig. 10. Irtran-1, thickness 3.8 mm; curve (a) emittance in stainless steel holder at 374°C (curve (b) of Fig. 3), curve (b) emittance in gold-plated holder at 374°C, curve (c) ambient transmittance.

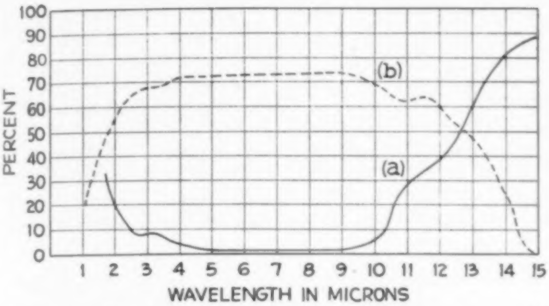

Fig. 11. Standard Irtran-2, thickness 3.8 mm; curve (a) emittance in gold-plated holder at 316°C, curve (b) ambient transmittance.

which could be found for these materials. The results presented in Table II suggest that the "true emittances" would not be significantly less than the values measured with the gold-plated sample holder.

Acknowledgments are due C. Salzberg and P. Mauer for many helpful suggestions and constructive criticisms. The technical assistance of W. M. Adams is also gratefully acknowledged.

References

1. H. O. McMahon, J. Opt. Soc. Am. **40,** 376 (1950).
2. H. O. McMahon, J. Am. Ceram. Soc. **34,** 91 (1951).
3. D. Weber, J. Opt. Soc. Am. **50,** 808 (1960).
4. A. G. Worthing, *Temperature: Its Measurement and Control in Science and Industry, Vol. I* (Reinhold, New York, 1941), pp. 1164–1187. A review and amplification of the associated terminology has been published by the Defense Metals Information Center, DMIC Memorandum 72, OTS PB 16122 (November 10, 1960).
5. A. Duncanson and R. W. H. Stevenson, Proc. Phys. Soc. (London) **72,** 1001 (1958).
6. E. P. Markin and N. N. Sobolev, Opt. i Spektr. **9,** 587 (1960), Optics and Spectroscopy **9,** 309 (1960).

Applied Optics
Of Optics and Opticists

This column is compiled partly from information sent by our Reporters in various centers of optics across the continent, but the Managing Editor welcomes news from any source

> These facts should all be noted down
> And ruminated on,
> By every boy in Oxford town
> Who wants to be a Don.
>
> *Hilaire Belloc*

As a result of approval shown by members of the **Infra-Red Discussion Group** of the United Kingdom at a meeting in the Fall of 1961 in favor of a central spectra library, plans have been made to start "in the near future" those parts of this which do not seem controversial, i.e., a library of infrared spectra indexed by the identity of their parent compounds. It is proposed to store spectra on film and to index in terms of an unambiguous nomenclature for which the Dyson code is being considered, but requests for data would not need to be in this code, and those relating to complex compounds would, indeed, best be made in terms of structural formulas. Of the doubts expressed about this **National Spectra Index,** the majority seem to concern the means of indexing in terms of the spectra themselves. Though it is felt that the photoelectric masking technique involving recognition of the shapes of spectra would be suitable for ultraviolet data (for which it was originally designed) and would be more able to distinguish other types of spectra than punching methods, it is believed that masking techniques more suitable for infrared (and probably also mass spectral) data which would overcome difficulties relating to varying background intensities, variation of band shape with concentration and some other difficulties, can now be devised. These could record each absorption and inflection at its exact wavelength (within perhaps 0.03 micron) and would be able to classify the strength of absorption into perhaps three levels. Coding of this type could be simple and rapid and would record sufficient data to ensure adequate discrimination in searching large collections (which punching methods do not). A machine-sorted index of this or similar type, combined with a machine-sortable structural indexing code, could be added to the existing spectra library as soon as suitable techniques and equipment were decided upon and available. When the above ideas have been fully studied, detailed proposals will be submitted to spectroscopists for their comments. Further information may be obtained from Dr. P. S. Davison, Scientific Documentation Centre, Halbeath, Dunfermline, Fife, Scotland, U.K.

The Mineral Products Division at the **National Bureau of Standards** has been renamed the Inorganic Solids Division. The names of two of its sections, Refractories and Constitution and Microstructure have been changed to Solid State Chemistry and Crystallography, respectively, to indicate better the division's present program and its expected trends. The new emphasis of the division is away from an industrial orientation and toward a more fundamental approach to inorganic solids . . . . The contract for the second construction phase of the NBS new laboratories in Gaithersburg, Md., has been awarded, and covers construction of the Radiation Physics Laboratory, Administration Building, Shops, Supply and Plant, and Service Building. This is another step in the ultimate relocation of the entire Washington facilities of NBS, which should be completed sometime in 1965.

Position changes of persons in the infrared and optics community include: **Raymond McFee** promoted to Research Director of Aerojet-General's Azusa Plant; **John Jamieson** named Research Director of Aerojet Avionics Division. Relocations include: **Harold Ritland** from Lockheed to Northrop Aircraft; **George Wagner** from Packard-Bell Electronics to Westinghouse; **Felix Cramer** from Boeing-Seattle to Lincoln Laboratory MIT; **Donald S. Cary** from Baird-Atomic to Xerox-Rochester; **Lowell Baskins,** from Lockheed to the vice presidency of Infrared Industries; **K. Knight** from Minneapolis-Honeywell to Aerospace; and **R. Stroupe** from

Hughes Aircraft to North American Aviation .... The Guggenheim Foundation of New York has given one of its international bursaries for 1962–63 to **Albéric Boivin,** professor of optics in the department of physics at Laval University. Dr. Boivin will spend his sabbatical leave in the USA where he will undertake research in electro-magnetic optics at the University of Rochester in collaboration with Emil Wolf .... Longtime OSA member **Robert O'B. Carpenter** has joined with another OSA member **H. Eugene Stubbs,** both formerly with Geophysics Corporation of America, to form the Mount Auburn Research Associates, Inc. Drs. Stubbs and Carpenter are President and Vice President respectively of this new company, located in Cambridge, Mass., which performs contract research in the physical sciences .... **Richard W. Rhyins,** formerly with Barnes Engineering, has joined Measurement Systems, Inc., as manager of Advanced Development Engineering .... **Leonard R. Heintré,** formerly an optical designer with the Kollmorgen Corporation, recently joined the Electro-Optical Division of Perkin-Elmer as an optical engineer .... **Harry McKinley,** formerly at Barnes Engineering, is now in the optical design section at Kollmorgen .... **Paul H. Keck** has joined the Corporate Research and Engineering staff of Texas Instruments Incorporated to direct programs in new technologies. His major responsibility will be to direct research and development in lasers. Dr. Keck pioneered the floating zone technique of materials purification and its application to silicon.

Congratulations to .... **John Strong,** head of the Laboratory of Astrophysics and Physical Meteorology at Johns Hopkins University, who has had the honorary degree of Doctor of Science conferred on him by Southwestern University .... **Herbert Friedman,** superintendent of the Naval Research Laboratory's Atmosphere and Astrophysics Division since 1958, who has been presented with the Navy Award for Distinguished Achievement in Science.

News from OSA Corporation Members includes .... **Kollsman Instrument Corporation** will build the optical subsystem including a space sextant, sunfinders, and navigation display equipment for the Apollo space project, working in support of MIT Instrumentation Laboratory, NASA's associate contractor charged with initial development of the Apollo navigation-guidance system, and the Space and Information Systems Division of North American Aviation. ... **Perkin-Elmer Corporation** will develop a series of long-range theodolite instruments which will be used to align the inertial guidance systems of Saturn space rockets prior to launching. P-E has developed and built similar type alignment equipment for the Titan, Atlas, Pershing, Mace, Thor, and Jupiter missile programs. ... **Bausch & Lomb** recently announced a reorganization of the company's research and engineering activities to provide more effective coordination of product development with the operations of the recently organized Ophthalmic and Scientific Instrument Divisions. Fred Jobe has assumed responsibility for ophthalmic product research and development, and Corwin Brumley will be in charge of all activities in scientific instrument research and engineering. Howard S. Coleman, vice president for research and engineering, has resigned.

The **Office of Aerospace Research** announced recently .... AFCRL scientists will conduct a series of high-altitude balloon astronomy experiments beginning later this year. Three separate programs—STAR GAZER, SKY TOP, and BALAST—each having different research objectives and each using different astronomical systems, are involved. The primary research aim is to obtain more complete and accurate information about space environments with emphasis on the Moon, Mars, and Venus .... recent contracts and grants including Stanford U., A. E. Siegman, W. W. Anderson, and O. Buneman *Optical and infrared masers, and coherent plasma phenomena* $60,000; MIT, P. Miles *Coherent light and radio optics* $50,000; Duke U., W. Gordy *Microwave and radiofrequency spectroscopy* $151,180; U. of Calif., W. A. Nierenberg and H. A. Shugart *Atomic and molecular beam research* $75,000; Mich. State U., P. M. Parker *Infrared and microwave spectra of asymmetric top molecules* $10,400; U. of Madrid, J. L. Amoros and M. L. Cnut *Thermal effects on crystal structure* $40,000; and U. of Saarbruecken, U. Wegner *Investigation of bending rectangular plates supported at four points for optical application* $7000.

Readers' attention is drawn to .... a new AEC Research Report AEC-tr-4471(Addendum) *Optics in equipment for the utilization of solar energy: Literature cited.* Feb. '62, 15 pp., $0.50; and *Infrared Band Handbook,* compiled by Herman A. Szymanski Canisius College and his students, which lists over 3000 compounds according to the position of their absorption bands. For any selected wavelength, compounds are listed when they have at least a medium intensity absorption band at that wavelength. The compounds are shown in the data sheets by structural formula. Information on sampling technique, instrument resolution, group vibration responsible for the band, and band intensity are also listed. The new infrared reference work is published by the Plenum Press; *A Portable Low Level Lightmeter,* A. Gebel, ARL, USAF, April 1961, 10 pp. AD 260 500, $0.50; *Measurement of the Infrared Reflecting Properties of Beaded Screens,* L. L. Collins and L. W. Nichols, NO Test Station, China Lake, Calif., April 1961, 54 pp. AD 266 306, $1.25 (the three reports mentioned are available from the Office of Technical Services, Washington 25, D.C.); .... to the ADOLPH LOMB OPTICAL LIBRARY at the University of Virginia. A catalog (U. of Va. Bibliographical Series Number 7) was published in 1947 with an introduction by James P. C. Southall, professor emeritus of physics of Columbia U., and lists Lomb's collection of scientific treatises and articles which is unique in its field .... the article "On Uniformity of International Usage" in the June issue of *Physics Today* (p. 19) discussing the proposals contained in the latest report of the Commission on Symbols, Units, and Nomenclature of IUPAP (SUN Commission). The AIP Publication Board urges consideration of these symbols but has not yet specifically adopted any of them .... a *Lasers Bibliography Dec. 1958–May 1962,* compiled by K. J. Spencer and issued in the Technical Information and Library Services Central Library (TIL 3) Bibliographical Series of the United Kingdom Ministry of Aviation Central Library.

In January 1961, a subcommittee of the National Academy of Sciences—National Research Council Committee on Geography and representatives from the Office of Naval Research, Geography Branch, met to discuss the need for applying techniques of remote sensing of environment to the earth sciences. As a result of this meeting, the Office of Naval Research, together with the Air Force Cambridge Research Laboratory, Geophysics Directorate, and the Army Research Office, contracted with the Institute of Science and Technology, University of Michigan, to investigate the subject. This project is now in progress. One of the major items under study is directed toward determination of the potential of existing remote sensing devices to provide earth scientists with a unique yet economical research capability. Special emphasis is being placed on instrumentation suitable for airborne and satellite use. Equipments of particular interest to this study are aerial cameras, infrared scanners and radiometers, microwave radiometers, radar and radio devices, airborne gravimeters, and airborne magnetometers. An indication of the degree to which these equipments might ultimately be exploited in future large scale interdisciplinary research programs will be a major outcome of the remote sensing of environment project.

Durable Narrow Absorption Band Infrared Filters Utilizing Powdered Mineral Materials on Polyethylene Substrates

Hugh R. Carlon

Infrared filters are normally fabricated using precise vacuum evaporation techniques or specialized coating procedures. The resulting filters demand careful handling. Narrow absorption band infrared filters were formed utilizing powdered mineral materials on polyethylene substrates. Various minerals caused specific infrared absorptions in the 9.0 to 11.8 μ region. These absorptions were chosen as desired for applications where narrow absorption band filters were required at specific wavelengths. Several minerals were investigated. Filters were achieved with nearly complete absorption at a specific wavelength, having spectral half-widths of as little as 0.3 μ. The filters were easily prepared, and very reliable.

I. Introduction

Since the inception of research dealing with military applications of the longer infrared wavelengths to the detection of atmospheric contaminants, a need has existed for infrared transmission filters having specific narrow-band absorptions in the 8 to 13 μ atmospheric window region. Such filters, when intended for use in instruments which must undergo severe punishment in field use, should be as durable and trouble-free as possible.

A method has been evolved for the production of very rugged, inexpensive, moisture-proof filters from materials having a desirable spectral characteristic. Such a spectral characteristic is exhibited by the mineral magnesium silicate, hydrated (talc). The problem was to devise a means of permanently attaching the talc to a suitable rigid or semirigid transmitting substrate, which would itself not undergo attack by moisture or atmospheric contaminants.

II. Experimental and Results

It was observed that fine talc particles were mechanically held to the surface of polyethylene sheeting in a bond that was extremely difficult to break. Investigations revealed that the polyethylene surface contained vast numbers of minute irregularities which were responsible for this ability to retain the talc particles, and that particles ranging from submicron to about three microns in diameter were readily retained. Once imbedded in the polyethylene surface, these particles could not be effectively removed through any amount of rubbing, washing or soaking in water for up to seven days, or deformation of the plastic surface. In addition, whereas previously used vacuum evaporation techniques for deposition of the talc particles on waxed sodium chloride, or other crystalline-salt, substrates required sizing of the talc particles to avoid scattering of incident radiation due to the larger particles, the polyethylene surface attained an "automatic" size separation of standard reagent grade talc. This was effected by the polyethylene surface imperfections, which accepted only the desired small particles from the reagent talc placed on the plastic surface, while permitting the larger particles to be carried away when the excess talc was wiped from the polyethylene surface during filter preparation. In this manner, very durable filters were obtained which achieved 80–85% absorption at 9.8 μ (the silicate band) with half-widths of less than 0.3 μ. Since the polyethylene films used in these experiments were 0.05 mm thick and possessed 15–20% neutral absorption, a net filter effect of 60–70% absorption at 9.8 μ was realized. Nearly complete 9.8 μ absorptions were achieved through stacking of similar filters. Half-widths of 0.3 μ were retained, but neutral attenutation was increased proportionately to the number of plastic films stacked. This effect was considerably offset through the use of 0.012 mm polyethylene, which gave similar talc absorption effects at considerably improved (reduced) neutral attenuations. However, in the application to which these filters were to be put, a certain precisely known neutral attenuation was required. This attenuation was achieved by

---

The author is in the U.S. Army Chemical Research and Development Laboratories, Army Chemical Center, Maryland.

Received 3 October 1961.

Table I. Mineral-Type Polyethylene Substrate Experimental Filters

Filter material	Major band(s) (μ)	Absorption Experimental peak (%)	 Spectral half-width (μ)
Silica gel	9.2	22	0.9
Magnesium silicate (talc)	9.8	63	0.3
Calcium carbonate	7.0	30	0.4
	11.4	8	0.3
Barium chromate	11.4	20	0.9
Potassium periodate (meta)	11.8	38	0.3
Aluminum silicate	9.7	36	0.5
The following materials give weak absorptions as indicated:			
Ammonium sulfate	9.0		
Lithium sulfate	9.0		
Nepheline	10.0		
Sodium chromate	11.0 to 12.0		

combining several thicknesses of talc-treated polyethylene to produce the desired filter, and further by treating either one or both surfaces of each of the plastic films with talc, thus also modifying the 9.8 μ absorption band.

Initial tests and experiments indicated that the filter formation mechanism was applicable not only to talc, but to any of a large group of water insoluble or semi-insoluble mineral (and other) type materials which were capable of being finely ground, the particle size itself being the most important factor. Still other materials showed promise for cases where use in humid atmospheres was not a prerequisite. However, experiments with several plastics as substrate materials revealed that, of those investigated, polyethylene alone was capable of forming acceptable filters of this type. Plastic materials tested included: polystyrene, teflon, mylar, polytrifluoromonochloroethylene, polypropylene, and cellophane. None of these possesses the desired surface porosity in combination with acceptable spectral characteristics for the application required. Accordingly, further work was undertaken to investigate the filter-forming properties of various minerals (and a few other materials) on polyethylene substrates only. Throughout these experiments, 0.05-mm polyethylene substrates were used, treated on both surfaces with the filter candidate material. Several of the materials chosen for evaulation were selected on the basis of spectra in the literature.[1,2] Each material was ground, pulverized thoroughly in a shaker mill, applied to the polyethylene substrate, and run in a Perkin-Elmer Model 21 Spectrometer* with a 0.05-mm polyethylene blank in the reference beam. Well-defined absorption bands were obtained for several of the materials tested. These are outlined in Table I. Experimental work was terminated before a very comprehensive listing of acceptable materials could be compiled. However, the existence of a very large number of potentially useful substances is indicated by the random sampling outlined in the table. Practically all materials tested gave some discernible result, but only those which appeared to be promising were tabulated.

In some applications, for instance, the quantitative measurement of 9.8 μ absorptions in the atmosphere using specialized military equipment utilizing optical "choppers" simulating the absorption bands to be monitored, it is desirable to fabricate filters with *small* but *uniform* talc absorptions over their entire surfaces. The one acceptable method for achieving this *small* but *uniform* absorption is the adulteration of the talc (which normally will produce a 40–50% absorption at 9.8 μ when applied to only one surface of a polyethylene sheet) with a large quantity of some material which has no specific absorption in the region of interest, and application of this mixture to the polyethylene surface. Rolling is not necessary to cause the randomly-dispersed talc particles to become attached in the surface of the plastic film. The material need only be distributed over the polyethylene surface, smoothed, and wiped away with a firm pressure. The resulting treated surface appears clean and transparent to the eye. Calcium silicate, a fluffy material, makes a good adulterant where such a small-absorption filter is desired.

As previously noted, filters may be formed on any thickness polyethylene substrate. However, thicknesses over 0.25 mm tend to cause an unacceptably large neutral attenuation. A thin substrate will give a sharper filter, with the 0.012 mm substrate approaching in its thickness a small multiple of the diameter of the largest imbedded mineral particles. In very thin films, unacceptably large particles would be "back-to-back." Hence, they are rejected by the surface, and only the very small particles remain at the surface. Thinner films enhance over-all transmission, but have little rigidity. A suitable mounting ring overcomes this difficulty. Table II summarizes polyethylene transmission as a function of wavelength and thickness.

Table II. Percent Transmission of Polyethylene Sheet in Various Thicknesses

Sheet thickness (mm)	Percent infrared transmission at: 8.0 μ	 9.8 μ	 12.0 μ
0.032	84	86	89
0.05	78	85	87
0.10	64	77	80
0.17	56	73	75
0.25	35	57	63

---

* Perkin-Elmer Corporation, Norwalk, Connecticut.

Polyethylene itself has two strong absorption bands in the vicinities of 7.0 and 14.0 μ, excluding the use of filter materials absorbing at these wavelengths except in optically nulled systems. However, at all other wavelengths from 3.0 μ to beyond 15.0 μ, acceptable filters may be produced provided that a material with an acceptable absorption at the desired wavelength may be found. Even materials shown in Table I as yielding low-efficiency filters may be expected to give considerably improved absorptions when properly sized. Talc should be considered the standard for filter-forming materials as regards its particle sizing and other physical characteristics.

III. Summary

Mineral-polyethylene filters may be readily prepared with a minimum of time and equipment. The resulting filters are very durable, resistant for indefinite periods of time to moisture and handling, retain their spectral characteristics, and are extremely economical.

References

1. J. M. Hunt, M. P. Wisherd, and L. C. Bonham, Anal. Chem. **22,** 1478 (1950).
2. F. A. Miller and C. H. Wilkins, Anal. Chem. **24,** 1253 (1952).

From the Editor

Three years ago this month the Institute of Radio Engineers devoted a fat feature issue of *Proc. IRE* to Infrared Physics and Technology. By all standards it was a handsome, comprehensive, 230-page look at the recent state of the art of infrared, and it is still considered a bible on the subject. Stanley Ballard, now President-Elect of the Optical Society, was Guest Editor for this feature, and at least two-thirds of the papers were written by OSA members. At the time this issue appeared the Optical Society did not publish *Applied Optics;* we had no such medium for spotlighting one area of optics research by devoting a special issue to the topic and specifically soliciting appropriate papers. In fact we can be grateful to *Proc. IRE* for their infrared issue because this helped persuade the Optical Society that a journal such as *Applied Optics* was indeed necessary.

Now we have also devoted a feature to the topic of infrared. Our feature on infrared differs in many ways from the *Proc. IRE* special issue. First of all, in reviewing the field we did not desire to retread the same ground, so we have attempted to review only the developments of the past three years, rather than the entire postwar effort (and some earlier) covered in *Proc. IRE*. A second difference is that we did not make any particular effort to solicit articles specifically for this infrared issue. We wrote a circular letter to many colleagues about a year ago announcing the feature, but we did not do much arm-twisting. As the time drew near to put this issue to bed we chose from our many contributed papers what appeared to be an interesting selection of papers; but several fine infrared papers have already appeared in previous issues of *Applied Optics*, and we are happy to say that we have many more that we shall print in future issues as soon as we can find room for them. A third difference is that the *Proc. IRE* issue was also stimulated by the military infrared community. A large part of the research in infrared physics and technology, at least in the United States, is supported or sponsored by the military or other government agencies. It is helpful for an army to be able to see in the dark, or to detect a distant target by its passive self-radiation. Some of this research is considered classified, as it involves military security, but a large part of it is open and unclassified and has just as much application to nonmilitary space studies, to spectroscopy, or to meteorology. Because of the military involvement, the IRIS (Infrared Information Symposia) organization was formed several years ago to permit these infrared researchers to exchange data and discuss results at classified meetings, free from the responsibility of deciding what is and what is not classified material. This organization and its history is discussed by Arthur Laufer in the Preface to the *Proc. IRE* Infrared Issue. IRIS even has its own journal, the *Proceedings of IRIS*. One of the problems that your Editor has to contend with is what to do when a statement in one of the papers of *Applied Optics* is documented by a reference to *Proc. IRIS*. This is not a good reference, as this journal is not available to those without access to the classified literature. On the other hand, it is not very helpful to anybody to reword these references as "private communication." The existence of classified literature is a fact, even though it may be scientifically regrettable. Our goal is to encourage these IRIS authors to separate their science from their military applications, and to publish wherever possible in the open literature. This issue of *Applied Optics* contains several articles written by IRIS workers, and besides *Applied Optics* there now exist two or three other journals also with the avowed aims of welcoming such papers back into the bright sunshine. A copy of this September issue is being sent to all IRIS people who do not already subscribe.

The results of military sponsorship are not all evil however. Most of the good infrared detectors that we have today were developed with military support. It seems to be another fact of life that, without the justification and the urgency of advanced technology for defense, the monies to support expensive research would simply not be forthcoming. One perhaps encouraging note in all this is that many government organizations are beginning to recognize that the requirements of space age technology are rapidly depleting our store of basic knowledge and that a larger share of our research effort must be devoted to basic and fundamental studies, not only of infrared radiation but of optics in general. Another encouraging aspect is the growing appreciation of infrared physics as a science, rather than as a military technique. Radiometers and infrared scanning devices that were considered useful only for military reconnaissance a few years ago are now being used to determine from satellites the heat budget of the earth for climatological studies, or its cloud cover, for weather prediction. By infrared space probes we shall know the molecular constituents and the thermal profile of the atmospheres of Mars and Venus long before any astronaut lands there. Some researchers think we shall even be able to determine the presence of life on these planets by such techniques. The military stimuli of the past have produced many useful results, but surely problems such as these present challenges to infrared scientists and engineers that are just as interesting and much more worthwhile.

John N. Howard

Papers to appear in subsequent issues

We have had so many papers submitted for publication since *Applied Optics* was announced last year that we have already built up a backlog which is as embarrassing for a new publication as it is a demonstration of the need for this journal. We are doing our best to publish papers as quickly as we can by bringing out bigger issues than had originally been intended this year, and becoming a monthly in 1963. The Editors wish to express their sincere appreciation to all contributors who have thus demonstrated their faith in *Applied Optics*.

An UV-Sensitive-Image Tube—*Skorinko*

A Ten-Meter Grating Spectrograph for the Vacuum UV—*Douglas and Potter*

Performance Prediction of Range-Finder Systems—*Patrick*

Three-Dimensional Wavefront Reconstruction—*Meyer-Arendt*

Proposed Pumping Scheme for Continuous Laser—*Kremen*

Nonlinear Optical Effects: An Optical Power Limiter—*Siegman*

Angular Measurements by Means of a Ronchi Ruling—*Meyer-Arendt and Miner*

Method of Inferring Single-Path Band Transmission Factors from Double-Path Measurements—*McKiernan and Wessely*

Silver Chloride Cavity Window for IR Liquid Cells—*Boetjer and Haendler*

Photomultiplier Cryostat—*Lipsett*

Luminescent Processes and Decay Laws in Crystalline Materials—*Pernick*

Thermal Radiation from a Hemispherical Source in Contact with an Infinite Plane—*Kester and Minardi*

Photoelectron Energy Distribution Measurements of 10 to 50 ev Photons with a Planar Analyzer and Electron Multiplier—*Heroux and Hinteregger*

Total Absorptance of CO_2 in the Infrared—*Burch et al.*

A Microwave Powered Hydrogen Lamp for Vacuum Ultraviolet—*Warneck*

Total Absorptance of Water Vapor in the Near Infrared—*Burch et al.*

Simulating the Solar Spectrum with a Filtered High-Pressure Xenon Lamp—*Boettner and Miedler*

Cloud Chamber for Optical Measurements of Aerosols—*Speyer*

Nine-Channel Polychromator for Observation of Time-Dependent Spectral-Line Profiles—*Spillman et al.*

Isocon Scan—A Low-Noise Wide-Dynamic-Range Camera-Tube Scanning Technique—*Cope and Borkan*

Polarization by Reflection and Some Optical Constants in the Extreme Ultraviolet—*Cole and Oppenheim*

Low Pressure Mercury Arc for Ultraviolet Calibration—*Childs*

Selected Ordinates for Solar Absorptivity Calculations—*Olson*

Design Theory for a Submersible Scattering Meter—*Tyler*

High-Speed Calculation of Diffusion Coefficients from Rayleigh Interference Fringes—*Hook et al.*

Comparison of AM and FM Reticle Systems—*Carpenter*

Effects of Telescopes on Astronomical Polarization Measurements—*Miller*

Modifications of a Beckman Spectrophotometer for Direct Measurements of Spectral Energy Distribution of Light Sources—*Grum*

Production and Use of Variable-Transmittance Sinusoidal Test Objects—*Lamberts*

Two Light Sources for Use in the Extreme Ultraviolet—*Newburgh et al.*

A Simple Voltage Amplifier for Photovoltaic Cells—*Paix*

Generation of Sinusoidal Light Intensity—*Julich*

An Automatic Rapid-Scanning Spectrophotometer to Study Thermoluminescence Spectra—*Ghosh*

Use of a Kaleidoscope to Obtain Uniform Flux over a Large Area in a Solar or Arc Imaging Furnace—*Chen et al.*

Photorefractometer-I. Extension of Sensitivity and Range: II. Measurement of N and K—*Kapany and Pontarelli*

On Diffraction Losses in Laser Interferometers—*Tang*

Faraday Rotation in FeNi Films—*Wieder and Collins*

Pumping Power Considerations in an Optical Maser—*Svelto*

Spectrally Selective Photodetectors for the Middle and Vacuum Ultraviolet—*Dunkelman, Fowler, and Hennes*

Photographic Emulsions as Computer Storage Media—*Levi*

Lighting Parameters and Generalized Characteristics of Xenon Lamps—*Marshak*

Design of Superachromatic Lenses—*Herzberger and McClure*

Reflection and Transmission of Infrared Materials—*McCarthy*

Absorption and Emission Frequencies in Lasers—*Condell and Mandelberg*

A Null Corrector for Paraboloidal Mirrors—*Offner*

Kinetic Absorption Spectra Recorded Edgewise across Flash-Heated Strips—*Nelson and Kuebler*

High Speed Photography Using a Ruby Optical Maser—*Yajima, Shimizu, and Shimoda*

Increase of Power of the Impulse Optical Quantum Generator on Ruby by Modulation of the Resonator Quality Factor—*Basov, Zuev, and Krjukov*

Information for Contributors

Scope: Papers are welcomed in the broad areas of applied optics, in disciplines related to optics and employing optical techniques. Papers should be sent to *The Editor, APPLIED OPTICS, 1155 Sixteenth St., N.W., Washington 6, D.C.* Manuscripts may be submitted in English, French, German, or Russian, and the presentation should be as succinct as comprehension will permit. In general, the metric system of units is preferred. One original and one carbon of the manuscript, with two sets of all illustrations, must be sent. Manuscripts should be typed double or triple spaced on one side of 22 × 28 cm ($8^1/_2$ × 11 in.) paper, leaving a 3.8 cm ($1^1/_2$ in.) margin all round.

An **abstract,** adequate as an index and summary, of not more than 100 words should appear at the beginning of the paper after the *title, author's name, affiliation, and address.* In the case of papers in a non-English language, they must be accompanied by an abstract in English as well as an abstract in the language of the paper.

Figures suitable for printer's use should be sent. Bear in mind that illustrations will normally be reduced to column width (8.4 cm—$3^5/_{16}$ in.—20 picas). *Halftones:* two sets of glossy prints are needed, which should be mailed flat, with any proportion or framing indicated on a working copy. *Line drawings* should be suitable for reproduction and be not larger than 22 × 28 cm ($8^1/_2$ × 11 in.). *Captions* should be listed on a separate sheet in addition to each caption appearing on each illustration.

Tables should be typed on separate sheets and the data therein be intelligible, by title, without reference to the text. Tables should include a minimum of vertical ruling.

References must be typed on a separate sheet, be numbered consecutively in the order of their appearance in the text, and follow this form:

1. F. C. Brown, Phys. Rev. **12,** 345 (1821).
2. J. Culpeper, *Space Optics* (Georgetown Institute of Technology Press, Washington, D.C., 1861), pp. 12, 345.

A list of abbreviations for the names of journals is published in the American Institute of Physics *Style Manual.* To make for uniformity of presentation generally, the *Style Manual,* second edition, should be used.

No **galley proofs** will be sent to authors; all proofreading will be done in the house. Therefore, an author will not see his paper from the time it is accepted and any alterations agreed between Editor and author, until it appears in print.

Letters to the Editor should follow the above suggestions, but no abstract is required.

Immersed Radiation Detectors

R. Clark Jones

This paper is concerned with the gain in performance that may be obtained by placing a detector element in optical contact with a lens having a high index of refraction. Three different kinds of "immersed" detectors are considered. The first is a highly impractical variety in which the detector element is spherical, and is placed inside a spherical shell of high index material. The second is a practical type in which the plane detector element is placed in optical contact with the plane surface of a hemisphere. The third involves a plane detector element in optical contact with the plane surface of an aplanatic hyperhemisphere. The evaluation is based on the detectivities usually denoted by D^* and D^{**}, and two mutually exclusive cases are considered: First, where the detectivity is determined by the internal noise of the detector, and second, where the detectivity is limited by the radiation noise of the ambient radiation. The immersion of the lens may change the effective area A of the detector (as seen from the outside), it may change the solid angle Ω from which the detector will accept radiation, or it may change both. The conclusions of the paper are summarized in two tables. Only the conclusions with respect to D^{**} may be summarized simply: For detectors limited by internal noise, immersing the lens increases D^{**} by the factor n, where n is the smallest index of refraction among the index of the lens, the index of the detector element, and the index of the cement (if any) used to fasten the detector to the lens; for detectors limited by radiation noise, immersion does not change D^{**}. The results are interpreted in terms of the optical invariant $A\Omega n^2$.

I. Introduction

During the last few years a number of different kinds of immersed radiation detectors have been introduced. Immersed radiation detectors are detectors whose responsive element is placed in optical contact with a lens that has a high index of refraction.

Immersed radiation detectors usually have a higher detecting ability than nonimmersed detectors. The gain in detecting performance is due to two independent effects: (1) There is a basic gain in detectivity due to the immersion. (2) There is also a gain in detectivity due to the use of a lens, which can be achieved without immersion. The first kind of gain is obtained without reducing the solid angle from which the detector accepts radiation. The second kind of gain is attained only at the cost of a reduced solid angle of acceptance.

It will be shown that the detectivity, usually denoted D^*, includes the effects of both kinds of gain. The detectivity D^{**} includes only the first gain. In more detail, we shall show that immersing a detector in a lens of index greater than unity yields no increase in the detectivity D^{**} if the detectivity is limited by radiation noise. On the other hand if the detectivity is limited by the internal noise of the detector, then the act of immersing the detector increases the detectivity D^{**} by the factor n_m, where n_m is the smallest of the indices of refraction of the lens, of the detector element, and of the cement (if any) between the lens and the detector element.

The detectivities D^* and D^{**} are sufficient for the purposes of this paper, but they do not, of course, tell the whole story about a detector. These parameters, for example, do not give the responsivity and the noise separately. The detectivities D^* and D^{**} depend on a number of physical parameters, including the wavelength and the modulation frequency of the radiation signal.

This paper is concerned with the properties of the detector considered by itself. The properties of optical systems that include immersed detectors have been considered by Wolfe and Duncan.[1]

II. The Area-Solid-Angle Product $A\Omega$

Consider the beam of radiation defined by the two apertures shown in Fig. 1. In many applications it is useful to consider the quantity that is the area of the first aperture, multiplied by the solid angle subtended by the second at the first. If A_1 and A_2 are the areas of apertures projected on a plane that is normal

---

The author is in the Research Laboratory of the Polaroid Corporation, Cambridge, Massachusetts.

Received 1 March 1962.

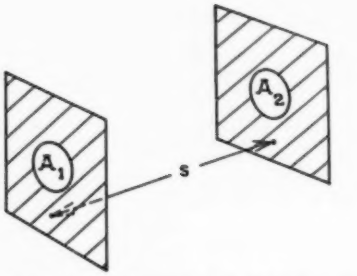

Fig. 1. Two apertures of areas A_1 and A_2 separated by the distance s define a beam with the area–solid-angle product $A\Omega$ equal to A_1A_2/s^2.

to the line connecting the centers of the apertures, this product may be written A_1A_2/s^2, a form that is symmetrical in the two apertures. In many applications, however, one of the apertures is at infinity, so that it is convenient to define one of the apertures by its area A and the other by its solid angle Ω.

Suppose that a source of uniform radiance N lies to the left of the apertures in Fig. 1. Then, provided that every ray that passes through the apertures intersects the source, the radiant power P of the beam that emerges from the right aperture is

$$P = A\Omega N. \qquad (2.1)$$

Provided that all of the images lie in air, the product $A\Omega$ is an invariant of an optical system. In order that this be an exact statement, however, one must define Ω more exactly. So long as the longest diameter of the aperture A_2 subtends no more than a few degrees at A_1, and vice versa, Ω is the solid angle as usually defined. But when some of the rays through A_1 and A_2 deviate more than a few degrees from the line through their centers, it is necessary to weight each element of solid angle $d\omega$ by the cosine of the angle θ between the ray and the line through the centers. The *projected* solid angle Ω is thus defined by[2]

$$\Omega \equiv \iint \cos\theta d\omega. \qquad (2.2)$$

In particular, if a solid angle is defined by all directions deviating from a given direction by not more than θ, the projected solid angle of this circular cone is

$$\Omega = \pi \sin^2\theta. \qquad (2.3)$$

Thus, the solid angle Ω of a hemisphere is π, not 2π. The numerical aperture of a microscope objective is defined as $NA = \sin\theta$, so that the solid angle of the light accepted by a microscope objective is

$$\Omega = \pi(NA)^2. \qquad (2.4)$$

For brevity the modifier *projected* is usually omitted, but should always be understood.

In order to illustrate what is meant by the statement that $A\Omega$ is an invariant, let us consider a radiation detector having an area of one square millimeter, which is placed at the focus of an $f/1$ lens with a 25 mm focal length. The effect of the lens is to focus a distant field of view on the plane occupied by the detector. At the lens, the field of view that is focused on the detector is square, with a side equal to 0.04 rad. The solid angle of the field of view is therefore $\Omega_1 = (0.04 \text{ rad})^2 = 0.0016$ sterad. The area A_1 that goes with this solid angle is the area of the lens, A_1 = area of a circle 25 mm in diameter = 4.91 cm². At the detector, the cone of radiation arriving from the lens has a numerical aperture of one-half (if the lens obeys the sine condition), whence by Eq. (2.4) the solid angle of the cone is $\Omega_2 = 0.785$ sterad. And, of course, the corresponding area is the area of the detector $A_2 = 0.01$ cm². One then finds $A_1\Omega_1 = 0.0785$ cm²-sterad, and $A_2\Omega_2 = 0.0785$ cm²-sterad. The equality of these two products exemplifies the fact that $A\Omega$ is an invariant of an optical system.

If, however, the index of refraction at the successive images is not the same, then it is not the product $A\Omega$ that is invariant, but rather the product $A\Omega n^2$, where n is the index of refraction. A well-known example of this is the oil-immersion microscope objective. A typical objective of this type is designed for an immersion index of 1.5, and is conventionally stated to have a numerical aperture of 1.25. This numerical aperture is not defined as $\sin\theta$, however, but as $n \sin\theta$, so that for the steepest ray within the oil, one has $\sin\theta = 1.25/1.5 = 5/6$. The solid angle Ω within the oil is therefore $\Omega = \pi(5/6)^2 = 2.18$ sterad. If, however, one naively substitutes $NA = 1.25$ in Eq. (2.4), one finds $\Omega' = 4.90$ sterad. This value is in fact n^2 times Ω, and is therefore the value of the solid angle one must employ if one wishes to use $A\Omega$ as the invariant, instead of $A\Omega n^2$.

III. The Detectivities D^* and D^{**}

The detecting ability of radiation detectors is usually expressed by stating the noise equivalent power P_N (the incident radiation power required to produce a signal output equal to the rms noise), or by stating its reciprocal, the detectivity D. Usually, the detectivity is stated for unit bandwidth of noise, and is then denoted by D_1.

Every detector has a receiving area A and a solid angle Ω of acceptance, such that the response is more or less equal if the radiation arrives from a direction within the solid angle, and reaches a point of the receiving area, and is small or zero if the radiation is otherwise directed. With most detectors, the receiving area A and the solid angle Ω of acceptance are sharply defined concepts. In the simple case where the detector is "naked" (not associated with any lenses or mirrors), the receiving area is equal to the area of the responsive element, and the solid angle of acceptance is π steradians, or perhaps somewhat less if the enclosure of the responsive element blocks off the more oblique rays.

There is both experimental[3,4] and theoretical[5] evidence for the statement that, other things being equal, the detectivity D_1 varies inversely as the square root of the responsive area A_d of the detector. This fact has been used to define the detectivity D^* by

$$D^* = D_1 A^{1/2}, \qquad (3.1)$$

where A is in general the receiving area. D^* is now widely used as a means of describing the performance of radiation detectors.

The detectivity D^{**} is defined by

$$D^{**} = D_1(A\Omega/\pi), \qquad (3.2)$$

where A is the receiving area of the detector, and where Ω is the solid angle from which the detector will receive radiation.

The detectivity D^{**} was introduced[2] for use in connection with cooled radiation detectors that employ cooled baffles to restrict the solid angle from which the detector will receive radiation. The detectivity D^{**} is useful, however, in any situation where one achieves a gain in the detectivity D^* by use of means that reduce the solid angle from which the detector will accept radiation.

In order to illustrate the difference between the detectivities D^* and D^{**}, we shall employ the detector–lens combination that was used in Section II to illustrate the invariance of the area–solid-angle product.

In the present illustration, we suppose that the detector has a detectivity D_1 equal to 10^{11} cps/watt, and that this detectivity does not depend on the solid angle from which the detector receives radiation. Then if the detector is used *without* any lens, the receiving area A is the area of the responsive element = 0.01 cm^2, and by Eq. (3.1) the detectivity D^* is equal to 10^{10} cm-cps$^{1/2}$/watt. The responsive element is able to receive radiation from every direction in the hemisphere, whence the solid angle of acceptance is $\Omega = \pi$. By Eq. (3.2), the detectivity D^{**} is also 10^{10} cm-cps$^{1/2}$/watt.

In contrast, we now consider the responsive element combined with the $f/1$ lens of Section II. The receiving area A of the lens–detector combination is 4.91 cm^2, whence the value of D^* for the lens–detector combination is $D^* = 2.2 \times 10^{11}$ cm-cps$^{1/2}$/watt. Using $A = 4.91$ cm^2 and $\Omega = 0.0015$ sterad, one finds $D^{**} = 0.5 \times 10^{10}$ cm-cps$^{1/2}$/watt.

In summary of this example, we see that the introduction of the lens has increased the detectivity D^* by the factor 22.1, whereas as it has decreased the detectivity D^{**} by the factor 0.5.

IV. Remarks on the Following Sections

In the following sections we calculate the effect of immersing the detector element on the detectivities D^* and D^{**}. This calculation is carried out for two mutually exclusive situations.

In the first, it is supposed that the detector has a detectivity limited by internally generated noise, whence it follows that the detectivity D_1 is independent of the optical configuration.

In the second situation, the detector is supposed to be limited by radiation noise, whence we may conclude that the detectivity D_1 varies inversely as the square root of the ambient power incident upon the detector element. To make the calculation explicit, it is supposed that the immersed detector is placed within an environment of uniform radiance, whence by Eq. (2.1) the detectivity D_1 varies inversely as the square root of the $A\Omega$ product.

V. The Spherical Immersed Detector

We consider first a kind of immersed detector that no one would consider constructing, but one that shows particularly clearly the modifications in performance produced by immersing a detector. The detector we consider has spherical symmetry. The detector element is a sphere of radius r, immersed in a concentric transparent spherical shell of radius R.

Unlike the more practical designs studied in the next two sections, the spherical detector has a solid angle of acceptance that is the same no matter what the indices of refraction are. Thus the spherical detector has the property that the gain in D^* produced by immersion is achieved without any cost in a reduced solid angle of acceptance.

We suppose first that the index n_s of the sphere is smaller than the index n_d of the detector. With respect to Fig. 2, parallel light is incident from the left. In particular, we consider the ray that strikes the sphere at Q at the distance y from the line through the

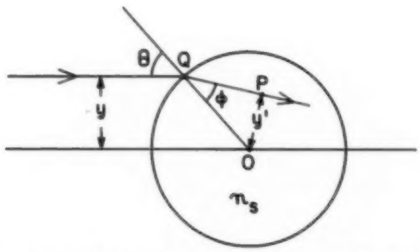

Fig. 2. The optical construction for the analysis of the spherical detector of Section V. The incident ray would pass a distance y from the center of the sphere if it were not refracted. The refraction at the point Q causes the ray to pass the center at the distance y'. The text shows that y and y' are related by $y = n_s y'$, where n_s is the index of refraction of the sphere.

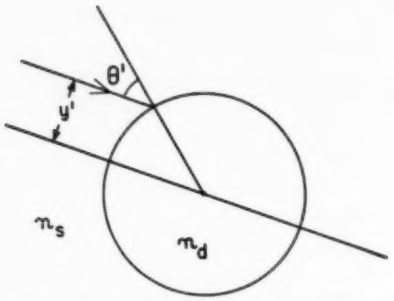

Fig. 3. The optical construction for the condition of total reflection at the spherical detector element. Total reflection occurs when $\sin\theta'$ is greater than n_s/n_d, where n_d is the index of the detector element.

center of the sphere. The sine of the angle of incidence θ is y/R, whence by Snell's law the sine of the refracted angle ϕ is y/n_sR. If now one examines the right triangle OPQ, one sees that the distance y' of closest approach of the refracted ray to the center of the sphere is

$$y' = R\sin\phi = y/n_s. \tag{5.1}$$

Accordingly, we conclude that all external rays with y not more than n_sr will intersect the detector. In particular, if r is not less than R/n_s, all rays intersecting the sphere reach the detector element.

Thus the effect of the immersion has been to increase the receiving area of the detector, as seen from outside the sphere, by the factor n_s^2. Because of the spherical symmetry, the external solid angle accepted by the system is the same before and after immersion. Thus, if we consider the detector element before and after immersion, the process of immersing the detector element has the effect:

$$\begin{array}{c} A \text{ multiplied by } n_s^2, \\ \Omega \text{ not changed.} \end{array} \tag{5.2}$$

It follows that the immersion of the detector element has served to increase the product $A\Omega$ by the factor n_s^2. The product $A\Omega n^2$ is not changed by the immersion, as would be predicted from the fact that this product is an optical invariant.

Second, we suppose that the index n_d of the detector is smaller than the index n_s of the sphere. In this case, not all of the rays that intersect the detector element are absorbed by the detector; with reference to Fig. 3, those that strike the detector sphere such that $\sin\theta' > n_d/n_s$ suffer total internal reflection. Thus, the largest value of y' that is not totally reflected is

$$y' = r\sin\theta' = rn_d/n_s = y/n_s, \tag{5.3}$$

whence

$$y = rn_d. \tag{5.4}$$

Thus, the receiving area of the detector is greater than the area of the responsive element by the factor n_d^2.

Finally, we consider the case where there is a layer of cement of index n_c between the immersing sphere and the detector element. If the index n_c is larger than the smaller of n_s and n_d, the cement has no effect on the considerations carried out so far. But if n_c is smaller than n_s and also smaller than n_d, and if the thickness of the layer is not less than about one wavelength of the radiation, then the controlling index for total internal reflection is n_c instead of n_d, and the apparent area of the detector is greater than its physical area by the factor n_c^2.

In summary of the above three cases, one finds that immersion has the effect:

$$\begin{array}{c} A \text{ multiplied by } n_m^2, \\ \Omega \text{ not changed,} \end{array} \tag{5.5}$$

where n_m is the smallest of the indices n_s, n_c, and n_d.

We now inquire how the immersion of the detector changes the detectivities D^* and D^{**}. Since the solid angle does not change upon immersion, the conclusions that hold for one also hold for the other. We choose to consider D^*.

Suppose first that the noise in the output of the detector is internal noise. Then the detectivity D_1 is not changed by immersing the detector. Immersing the detector, however, increases the effective area A by the factor n_m^2. We conclude from the definition (3.1) that the detectivity D^* is increased by the factor n_m by immersion.

We suppose, second, that the noise in the output of the detector is radiation noise, and we suppose that the environment of the detector has uniform radiance. Such a detector has the property that its detectivity D_1 is inversely proportional to the square root of the ambient power that is incident. Upon immersion, the amount of ambient power incident on the detector is increased by the factor n_m^2, so that D_1 is decreased by the factor n_m. The net result of the decrease in D_1 and the increase in A is that D^*, as defined by (3.1), is not changed by immersion.

The above two paragraphs confirm the theorem stated in the Introduction of this paper, since they hold for D^{**} as well as for D^*.

VI. The Detector in Optical Contact with a Hemisphere

The large majority of the immersed detectors that have been constructed are thermistor bolometers or photoconductive detector elements in optical contact with a hemisphere of high index,[6] as suggested by Fig. 4. Germanium, arsenic trisulfide glass, and strontium titanate have been used as the immersing medium.

In this and the next section, the increase in the receiving area A is calculated for a small area near the

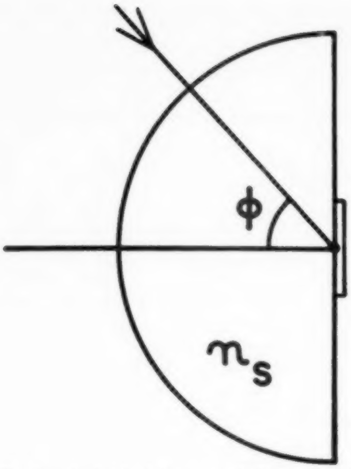

Fig. 4. The hemispherical immersed detector. The flat detector element is placed in optical contact with the plane surface of the hemisphere. The angle ϕ is the angle of incidence on the plane surface, both outside and within the hemisphere.

optic axis. The solid angle of the radiation accepted by the detector is calculated for the point on the optic axis. Thus, the results will be accurate for plane detector elements whose linear dimensions are sufficiently small compared with the radius of the sphere, but will be expected to become less accurate as the linear dimensions of the detector element are increased.

We consider first the situation where the index of the detector n_d is greater than the index of the sphere. Then all of the rays that strike the detector element are absorbed. The solid angle Ω of the detector, both externally and within the sphere, is π. Thus, immersion does not change the solid angle. The derivation in Section V of the lateral magnification holds here also; the effective area is increased by the factor n_s^2 by immersion. The effect of immersion is thus

$$\begin{array}{l} A \text{ multiplied by } n_s^2, \\ \Omega \text{ not changed.} \end{array} \tag{6.1}$$

The conclusion is that the product $A\Omega$ is increased by the factor n_s^2 by immersion.

Second, we consider the case where the index n_d of the detector is smaller than the index n_s of the sphere. In this case, all rays having in Fig. 4 a value of $\sin\phi$ greater than n_d/n_s will be totally reflected, with the result that the solid angle of the rays accepted by the immersed detector is

$$\Omega = \pi n_d^2/n_s^2. \tag{6.2}$$

The magnification is as before. The effect of immersion is thus

$$\begin{array}{l} A \text{ multiplied by } n_s^2, \\ \Omega \text{ multiplied by } n_d^2/n_s^2. \end{array} \tag{6.3}$$

The conclusion is that the product $A\Omega$ is increased by the factor n_d^2 by immersion.

Lastly, we consider the case where a layer of cement with index n_c lies between the lens and the detector. Analysis then yields the same result as in Section V: If and only if the index n_c is less than the index n_d, the index n_c should be substituted for n_d in the preceding paragraph.

We conclude from the analysis of these three cases that the effect of immersion is to increase the product $A\Omega$ by the factor n_m^2, where n_m is the smallest of the indices n_s, n_d, and n_c.

We now investigate how the detectivities D^* and D^{**} are changed by immersion, and we suppose first that the detectivity is limited by internal noise, so that the detectivity D_1 is not changed by immersion. By either (6.1) or (6.3), the area A is increased by the factor n_s^2, whence we conclude from (3.1) that the detectivity D^* is increased by the factor n_s by immersion. The product $A\Omega$ is increased by the factor n_m^2 by immersion, which permits us to conclude from (3.2) that the detectivity D^{**} is increased upon immersion by the factor n_m.

Second, we suppose that the detectivity is limited by radiation noise, and that the detector is placed in an environment of uniform radiance. By Eq. (2.1), the ambient power incident on the detector is proportional to $A\Omega$, and we have seen that this product is increased upon immersion by the factor n_m^2. Since the detectivity D_1 will vary inversely as the square root of the ambient power, one concludes that the detectivity D_1 is multiplied by $1/n_m$ upon immersion. The area is multiplied by n_s^2. From Eq. (3.1), one concludes that the detectivity D^* is increased by the factor n_s/n_m by immersion. Since the product $A\Omega$ is increased by the factor n_m^2, one concludes that the detectivity D^{**} is not changed upon immersion.

The conclusions about D^{**} in the two preceding paragraphs are in accord with the statement in the first paragraph of this paper.

The author's former colleague, David S. Grey (now at Lincoln Laboratory), has supplied the following information about the imaging system of Fig. 4. The lens is aplanatic—it has no spherical aberration and no coma. The lens has no longitudinal chromatic aberration, but it does have lateral chromatic aberration. The lens has astigmatism and curvature of field: the sagittal field is flat, and the tangential field has the radius of curvature $^1/_2 nR/(n-1)$, where R is the radius of the hemisphere, and n is its index.

VII. The Detector in Optical Contact with an Aplanatic Hypersphere

There is one other type of lens based on the sphere that is aplanatic. This is the aplanatic hyperhemi-

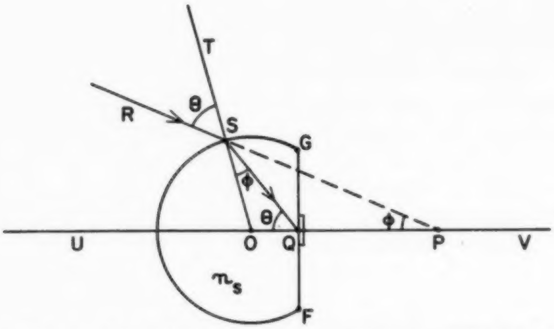

Fig. 5. The aplanatic hyperhemisphere is constructed by making a plane cut through a sphere at a distance from the center equal to the radius R divided by the index of refraction n_s. The point P is at a distance n_sR. A number of useful properties then follow from Snell's law of refraction. All rays directed toward P are refracted to Q. The line PG (not shown) is tangent to the sphere at G. The two angles marked θ are equal, as are the two angles marked ϕ. The detector is placed in optical contact with the sphere on the plane surface and is centered at the point Q.

sphere[7] shown in Fig. 5. This lens, which is drawn for an index of 2.0 in Fig. 5, is defined in general by the condition that the distance of the plane FQG from the center O is equal to the radius R divided by the index n_s of the sphere. The point P is located at the distance n_sR from the center of the sphere. The lens has the property that any ray, such as RS, that would strike the line UV at P is refracted at S so that it strikes the line at Q.

It then follows directly that the lateral linear magnification from Q to P is n_s^2.

The lens also has the property that the line GP is tangent to the sphere at G. The sine of the angle OPG is $1/n_s$, whence the solid angle of the rays in the external space that reaches the point Q is $\Omega = \pi/n_s^2$. This corresponds to the solid angle $\Omega = \pi$ of the rays within the sphere.

We now suppose that a detector of index n_d greater than n_s is placed in optical contact with the lens at the plane FQG, and consider the changes in the area and solid angle produced by immersion:

$$\begin{gathered} A \text{ multiplied by } n_s^4, \\ \Omega \text{ multiplied by } 1/n_s^2. \end{gathered} \tag{7.1}$$

We conclude that the product $A\Omega$ is increased by the factor n_s^2 by immersion, and that the product $A\Omega n^2$ is not changed by immersion. These conclusions are of course in accord with the general invariant principles discussed in Section II.

Second, we make the assumption that n_d is less than n_s. In order to analyze this situation, we need to use the additional geometrical facts in Fig. 5 that the angle OQS is equal to the angle RST (both marked θ) and that the angle OPS is equal to OSQ (both marked ϕ).

At the point Q, the rays will be totally reflected if $\sin\theta$ is greater than

$$\sin\theta = n_d/n_s \tag{7.2}$$

and thus by Snell's law the maximum angle ϕ at P is given by

$$\sin\phi = n_d/n_s^2. \tag{7.3}$$

The corresponding solid angle is

$$\Omega = \pi \sin^2\phi = \pi n_d^2/n_s^4. \tag{7.4}$$

Instead of (7.1), we now find that the effect of immersion is

$$\begin{gathered} A \text{ multiplied by } n_s^4, \\ \Omega \text{ multiplied by } n_d^2/n_s^4. \end{gathered} \tag{7.5}$$

We conclude that the effect of immersion is to increase the product $A\Omega$ by the factor n_d^2.

Finally, we consider the case where there is a layer of cement of index n_c between the lens and the responsive element. Then just as in Section V we see that if, and only if, n_c is less than n_d, the index n_d should be replaced by n_c in the preceding two paragraphs.

The three cases studied above permit us to conclude that the result of immersing a lens in an aplanatic hyperhemisphere is to increase the product $A\Omega$ by the factor n_m^2, where n_m is the smallest of the indices n_s, n_d, and n_c.

We now consider separately the effect of immersion on the detectivities D^* and D^{**} when the detectivity is limited by internal noise. The detectivity D_1 is not changed by the immersion. It then follows from (3.1) and either (7.1) or (7.5) that the detectivity D^* is increased by the factor n_s^2 by immersion. The detectivity D^{**} behaves differently. From the statement in the preceding paragraph, it follows that the detectivity D^{**} is increased by the factor n_m by the immersion.

Next, we suppose that the detectivity is limited by radiation noise, and we suppose that the environment of the detector has uniform radiance. The effect of immersion is to increase the ambient power incident on the detector by the factor n_m^2, whence D_1 is decreased by the factor n_m. Immersion increases the effective area by the factor n_s^4. The net result of these two factors is that D^* is increased by the factor n_s^2/n_m by immersion. Again, the detectivity D^{**} behaves differently. The product $A\Omega$ is increased by the factor n_m^2. From (3.2) it then follows that D^{**} is unchanged by immersion.

The conclusions of the two preceding paragraphs about D^{**} are in accord with the summary in the Introduction of this paper.

According to David S. Grey, the aplanatic hyperhemisphere is free of spherical aberration, coma, and astigmatism at the design wavelength. It does have chromatic aberration and curvature of field, with a radius equal to $\frac{1}{2}nR/(n-1)$.

Table I. The Factors by Which the Receiving Area A, the Acceptance Solid Angle Ω, and the Detectivities D^* and D^{**} Are Multiplied When the Detector Element Is Immersed in a Lens of Index n_s.[a]

Lens	A	Ω	D^* (internal noise)	D^{**} (internal noise)	D^* (radiation noise)	D^{**} (radiation noise)
Spherical shell	n_m^2	1.0	n_m	n_m	1.0	1.0
Hemisphere	n_s^2	n^2/n_s^2	n_s	n_m	n_s/n_m	1.0
Hyperhemisphere	n_s^4	n^2/n_s^4	n_s^2	n_m	n_s^2/n_m	1.0

[a] The index n_m is the smallest of the indices of the lens, the detector element, and the cement used to hold them together. The multiplying factors for D^* and D^{**} depend on whether the detectivity is limited by internal noise or by radiation noise.

Table II. The Numerical Aperture of the Cone of Rays Accepted by Each of the Types of Immersed Detectors

Lens	Numerical aperture
Spherical shell	1.0
Hemisphere	n_m/n_s
Hyperhemisphere	n_m/n_s^2

VIII. Discussion

The conclusions of this paper with respect to the detectivity D^{**} are very simply stated. If the detector has a detectivity limited by radiation noise, D^{**} is not changed by immersion; and if the detectivity is limited by internally generated noise, D^{**} is increased by the factor n_m, where n_m is the controlling index (the smallest of the indices of the sphere, of the cement, and of the responsive element).

The conclusions with respect to all of the parameters are summarized in Table I.

There is a number of advantages to be gained by immersing the detector element. The most fundamental is the gain by the factor n_m in the detectivity D^{**} when the limiting noise is internal noise. Also important is the substantial gain in the detectivity D^*, but it should be recognized that the gain in D^* (aside from a factor n_m with internal noise) is due to the gain in the speed of the optical system, and could be achieved by techniques other than immersion.

The disadvantages are more complex construction, and the fact that there is no gain in D^{**} when the detectivity is limited by radiation noise. In some cases the small solid angle of acceptance of the hyperhemisphere may increase the size of the rest of the optical system. For example, in an extreme case where the index n_s of the hypersphere is 4.0, and the controlling index n_m is 2.0, the numerical aperture of the accepted cone (see Table II) is only $2/4^2 = 0.125$, equivalent to $f/4$. This example suggests that it may be undesirable to employ a hyperhemisphere with an index markedly greater than the controlling index of refraction.

The usefulness of the hemispherical lens and the fact that it provides an increase in D^* by the factor n_s is described in a report[8] by R. DeWaard and Eric Wormser dated April 30, 1958. The use of the aplanatic hyperhemisphere for detector immersion was suggested by John Strong, and the fact that it provides an increase in D^* by the factor n_s^2 was discovered by Eric Wormser. According to Eric Wormser,[9] the idea of using immersion lenses with infrared detectors was first suggested by Stephen MacNeille and his associates at the Eastman Kodak Company about 1952.[10]

This work was supported by the Geophysics Research Directorate.

References

1. W. L. Wolfe and J. Duncan, Proc. IRIS **6,** 25 (1961).
2. R. Clark Jones, J. Opt. Soc. Am. **50,** 1058 (1960).
3. T. Limperis and W. Wolfe, Proc. IRIS **5,** 141 (1960).
4. R. Clark Jones, Proc. Inst. Radio Engrs. **47,** 1495–1502 (1959), esp. p. 1498.
5. R. Clark Jones, Rev. Sci. Instr. **24,** 1035–1040 (1953), esp. pp. 1039–1040.
6. R. W. Astheimer and E. M. Wormser, J. Opt. Soc. Am. **49,** 179 (1959).
7. A. C. Hardy and F. H. Perrin, *Principles of Optics* (McGraw-Hill, New York, 1932), pp. 96–98.
8. E. M. Wormser and R. DeWaard, "Thermistor infrared detectors, properties and development," Public Document PB-151767, Department of Commerce, Office of Technical Services.
9. Private communication, October 2, 1961.
10. D. S. Cary, U.S. Patent 2,964,636, filed June 5, 1956.

Erratum

Optics in France

Applied Optics May issue, page 262, right-hand column, penultimate paragraph, the last line should read:
"et la précision atteint 3/1000 de seconde de temps"
(instead of 3/100).

The Optical Society of America

Officers of the Society

President	David L. MacAdam, Research Laboratories, Eastman Kodak Company, Rochester 4, N.Y.
President-Elect	Stanley S. Ballard, Department of Physics, University of Florida, Gainesville, Fla.
Past President	Wallace R. Brode, 3900 Connecticut Avenue N.W., Washington 8, D.C.
Executive Secretary	Mary E. Warga, OSA, 1155 16th Street N.W., Washington 6, D.C.
Treasurer	Archie I. Mahan, Applied Physics Laboratory, 8621 Georgia Avenue, Silver Spring, Md.
Editor of the Journal of the Optical Society of America	Deane B. Judd, National Bureau of Standards, Washington 25, D.C.
Editor of Applied Optics	John N. Howard, Geophysics Research Directorate, AFCRL, Bedford, Mass.

Directors-at-Large

** Term expires December 31 of the indicated year.*

Bruce Billings (62)* Baird Atomic, 33 University Rd., Cambridge, Mass.
John A. Sanderson (62)* Naval Research Laboratory, Washington 25, D.C.
Van Zandt Williams (62)* Perkin-Elmer Corporation, Norwalk, Conn.
Rudolf Kingslake (63)* Eastman Kodak Company, Rochester 4, N.Y.
Earle K. Plyler (63)* National Bureau of Standards, Washington 25, D.C.
David Richardson (63)* Bausch & Lomb, Inc., Rochester 2, N.Y.
Georg H. Hass (64)* ERDL, Fort Belvoir, Va.
R. Clark Jones (64)* Polaroid Corp., Cambridge, Mass.
E. D. McAlister (64)* Scripps Institution of Oceanography, La Jolla, Calif.

Local Sections

Rochester	John L. Tupper, *President* Joseph L. Rood, *President-Elect* Sheldon Phillips, *Secretary* Eastman Kodak Co., Rochester 4, N.Y. Manuel Kiner, *Treasurer*
Detroit	Richard Majkowski, *President* Carl Leistner, *President-Elect* Daniel L. Harmon, *Secretary* 16152 Parkside, Detroit 21, Mich. Samuel Cohen, *Treasurer*
Niagara Frontier	E. Schustik, *President* Thomas Frost, *President-Elect* Calvin W. Young, *Secretary* Carborundum Metals Co., Box 32, Akron, N.Y. Ray Annino, *Treasurer*
New England	David S. Gray, *President* Charles Koester, *Vice-President* Geoffrey Harvey, *Secretary* Itek Corporation, 10 Maguire Rd., Lexington, Mass. William J. Davis, *Treasurer*
Texas	Charles S. Williams, *President* P. O'B. Montgomery, *Vice-President* Harry J. Auvermann, *Secretary-Treasurer* LTV Research Center P.O. Box 5003, Dallas 22, Tex.
Chicago	Paul F. Fenlon, *President* Harold F. Bennett, *Vice-President* C. Robert Anderson, *Secretary* 2421 North Luna Avenue, Chicago 39, Ill. Johann F. Mohler, *Treasurer*
Southwestern Connecticut	Leonard Eisner, *President* Robert C. Gore, *Vice-President* Martin Rome, *Secretary* Machlett Laboratories, Inc. 1063 Hope Street Springdale, Connecticut Edward Speyer, *Treasurer*
Southern California	R. Henry Frels, *President* Ernest Davidson, *Vice-President* Clifford O. Thomas, *Secretary* 10 Miramonte Drive, Fullerton, Calif. W. S. Gallaway, *Treasurer*
Northern California	Sumner P. Davis, *President* Robert E. Lewis, *Vice-President* Eldred F. Tubbs, *Secretary-Treasurer* General Telephone and Electronics Laboratories, Inc., 1015 Corporation Way, Palo Alto, Calif.
National Capital	Richard Tousey, *President* Frederick W. Paul, *First Vice-President* Harry K. Hammond, III, *Secretary* National Bureau of Standards Washington 25, D.C. Richard S. Hunter, *Treasurer*

The Optical Society of America was organized in 1916 "*to increase and diffuse the knowledge of optics in all its branches, pure and applied, to promote the mutual interests of investigators of optical problems, of designers, manufacturers and users of optical instruments and apparatus of all kinds and to encourage cooperation among them.*" The Society invites to membership all who are interested in any branch of optics, either in research, in instruction, in optical or illuminating engineering, in the manufacture and distribution of optical goods of all kinds, or in physiological and medical optics. Further information may be obtained from the Executive Secretary of the Society. **Annual Dues:** Regular members and Fellows, $17.00; Associate members, $13.00; Corporate members, $125.00. These dues include subscription to the Society's official journal, the *Journal of the Optical Society of America*, but not to its other publications.

Wedge-Immersed Thermistor Bolometer

Marc G. Dreyfus

A germanium-immersed thermistor bolometer infrared detector is described which utilizes cone-channel condenser techniques to supplement in one meridian the optical gain afforded by conventional immersion lens techniques in the presence of asymmetrical pupils such as the rectangular exit slit of a spectrometer. Data are presented describing its construction, properties, and installation at the spectral focal plane of an experimental spectrometer.

Introduction

Thermistor bolometers[1-3] convert infrared radiation into an electrical signal by means of a semiconductive flake with a high temperature coefficient of electrical resistance. Impinging radiation heats the flake, and the resultant change in flake resistance is a measure of the incident electromagnetic flux. The detectivity[4] of a bolometric detector varies inversely as the square root of detector area. Therefore, the sensitivity of an infrared instrument is maximized by minimizing the required detector area. As a result, infrared systems generally use detectors with an active area of no more than a few square millimeters; a batch of extremely small bolometers recently delivered had flakes only 30 μ square.

Immersed Thermistor Bolometers

Detector sensitivity can be improved by immersing[5] the thermistor flake, i.e., by placing it in optical contact with the surface of a condensing lens designed to focus the incoming flux onto a smaller area flake.

If the flake is immersed on the flat side of a hemispherical immersion lens of refractive index n as shown in Fig. 1(B), then this lens will reduce the linear dimensions of the image it intercepts by a factor of n in accordance with Lagrange's law.[6] Hence the area of the immersed flake may be reduced by a factor of n^2 as compared with its unimmersed size, yielding a factor of n gain in detectivity.

If the axial thickness t of a plano-convex immersion lens is made larger than its radius of surface curvature r as shown in Fig. 1(C), then the lens surface generates progressively more gain as t increases, passing through n^4 area reduction and a detectivity gain of n^2 at the aplanatic[7] focal condition when $t = r + r/n$.

Thus the immersion lens reduces the effective *f*-number of the over-all optical system without imposing the burden of a low *f*-number design on the entire system. For example, a thermistor flake immersed on a hemispherical germanium[8] lens ($n = 4.0$) with selenium cement ($n = 2.5$) will accept convergent energy from an attainable *f*/0.8 primary optical system and will produce the impressive equivalent optical speed of *f*/0.2 for the over-all system.

The gain realizable in immersed detectors is limited by the onset of total internal reflection[9] at the immersion interface. For 5 to 15 μ radiation a germanium immersion lens with selenium cement has a critical angle of 38.2° at the immersion interface, and the flake "sees" only that external radiation which enters through a cone with an included angle of ±38.2°. This critical angle limitation can be used to good advantage as a supplementary stop to help limit the detector's external field of view.

Asymmetrical Stops

When a thermistor detector is installed behind circularly symmetrical optical stops,[10] then the critical angle limitation noted above imposes a circularly symmetrical constraint on immersion gain and the spherical immersion lens types described above yield maximum gain in detectivity. However when asymmetrical optical stops (such as ovals or slits) are present in an optical system, then the critical angle limit established by the long axis of the stop system imposes a more stringent constraint on immersion gain than the critical angle limit established by the short axis of the stop system. For example, if a plano-convex immersion lens is de-

---

The author is with the Barnes Engineering Company, 30 Commerce Road, Stamford, Connecticut.

Received 5 March 1962.

This paper was presented at the 46th annual meeting of the Optical Society of America in October 1961.

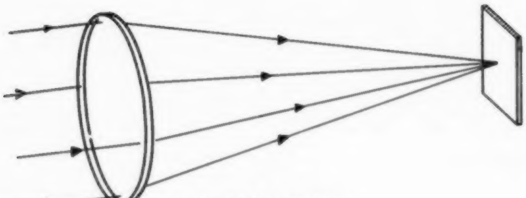

A-SPACE IMAGE

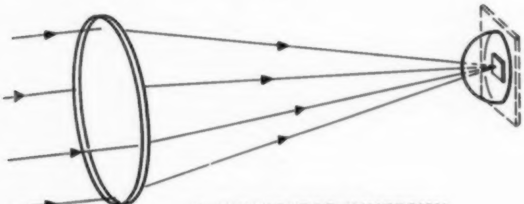

B-HEMISPHERE IMMERSION

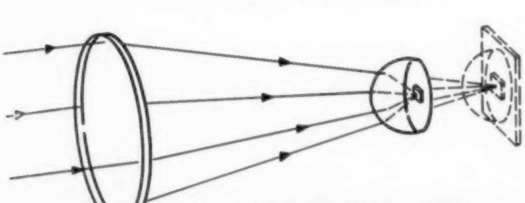

C-HYPERHEMISPHERE IMMERSION

Fig. 1. Germanium optical immersion.

signed for installation behind the oblong exit slit of an infrared spectrometer, then the immersion lens gain is limited by the angular subtense of the slit length, since rays converging on the thermistor flake from the slit ends will approach critical incidence angle while rays from the slit edges are still far from critical.

Lagrange's law shows that the convergence of a flux bundle determines the resulting image size; it should therefore be possible in the presence of asymmetric stops to reduce the size of the immersed flake preferentially in one direction by introducing additional convergent lens power in that meridian. The additional convergence could in principle be generated by adding supplementary aspheric lenses (such as cylinders and toroids) to the plano-convex immersion lens. However aspherics are difficult to manufacture and the resulting detectors would be burdened with extra losses due to surface reflection and internal absorption within the extra lens elements.

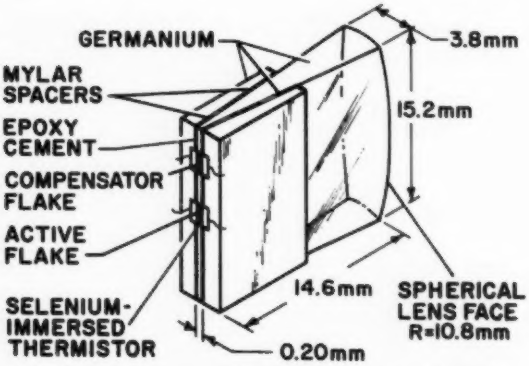

Fig. 2. Wedge-immersed thermistor detector schematic.

Wedge-Immersed Thermistor Bolometer

We have introduced additional single-meridian convergence and have achieved the desired flake size reduction by combining a wedge-shaped optical funnel[11] with the plano-convex immersion lens in the wedge-immersed detector shown diagrammatically in Fig. 2. The immersion lens shown consists of a solid wedge of germanium with flat polished sides, a spherical large end, and a flat small end. This lens is made by cutting down the edges of a plano-convex germanium lens until all that is left of the plano face is a 0.20 mm wide polished plateau. The resulting germanium wedge looks like a miniature blunt ax head. Flux incident on the large end of the wedge is refracted by the spherical lens face and then funneled by the wedged sides to a thermistor flake precisely aligned over the narrow end of the wedge.

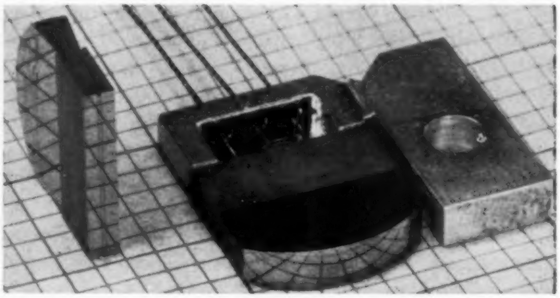

Fig. 3. Wedge-immersed thermistor detector. The small squares represent 2.5 mm (0.1 inch).

The compensator flake shown in Fig. 2 is shielded from external radiation; it is used in a bridge circuit to help measure the change in active flake resistance due to external radiation heating. The two germanium side-wedges shown support electrical leads to the flakes.

Barnes Engineering Company has made a number of the wedge-immersed thermistor detectors shown in Fig. 3 for use in an experimental spectrometer[12] shown schematically in Fig. 4. In that spectrometer each wedge detector is mounted immediately behind a 3.6 × 13.8 mm exit slit (not shown) which defines the spectral passband in the spectral focal plane. The convex surface of the wedge assembly is located about 64 cm away from a 13 cm square stop generated by the clear aperture of the diffraction grating and images this stop as an 0.8 mm square in the flake plane. The funnel portion of the wedge assembly reduces the image width from 0.8 to 0.2 mm, thus doubling the bolometric detectivity. The compact side-by-side packaging possible, using detectors of the type shown in Fig. 3, made it feasible to meet an additional design goal of this satellite spectrometer which required simultaneous measurement in several almost contiguous spectral intervals.

Test Data

The responsivity of these wedge detectors has been measured with a 13-mm aperture Barnes No. 11-110 blackbody on a lens bench. The blackbody was mounted 64 cm from the wedge detector on a carriage movable in two directions orthogonal to the wedge's optical axis, so that the blackbody could be used as a point source to map the detector's field of view.

Figure 5 shows a responsivity contour taken with the blackbody moving parallel to the long axis of the detector face. The shape of this contour is determined solely by the action of the spherical face of the immersion lens.

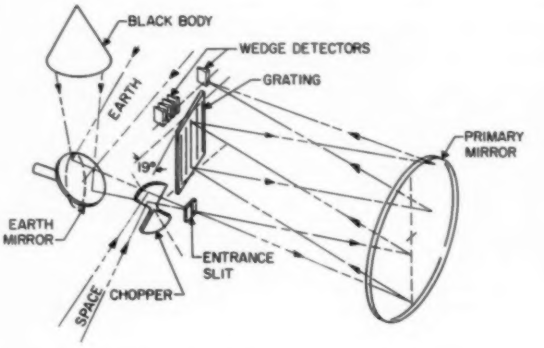

Fig. 4. Simplified optical diagram of satellite spectrometer.

Figure 6 shows a responsivity contour taken with the blackbody moving perpendicular to the long axis of the detector face. The actual flake width is optically enlarged about four times by the funnel effect of the wedge, and a detectivity gain approaching a factor of two due to the smaller flake is indeed realized.

Notice the curious dips in this sensitivity contour. We are unable to explain them. They seem to be related to the detector construction rather than to some peculiarity of the test bench setup since the dips change sides when the detector is tested upside down. However they do not seem to be a vignette effect at the edges of the convex lens surface since they are not changed by using only the central 5% of this surface. Nor do they seem to be an interference or diffraction effect since they are not changed by optically filtering the 600°C blackbody test radiation with an 8 μ longpass interference filter. We have found that their location with respect to the peak of responsivity changes as much as 2.5 cm from batch to batch.

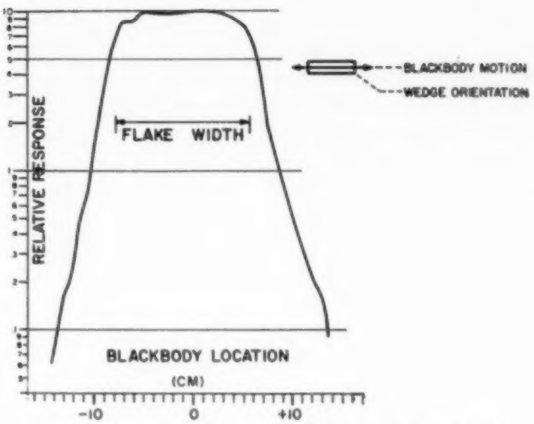

Fig. 5. Detector responsivity contour parallel to slit axis.

Design Considerations

As in most precision optics, the proportioning of constructional tolerances is important in this detector, and the cumulative effect of various tolerances takes its toll in detector speed and field of view.

The funnel effect increases the radiation's convergence angle as it reduces the required flake width; funnel gain is therefore limited by the 38.2° critical angle noted above. The corners of the convex detector surface are of limited efficiency because the convergences generated by the lens surface and by the funnel add vectorially and may (as in the case of any lens with an oblong aperture stop) exceed the critical angle at the flake for some of the flux through these corners.

The choice of cement joining the side wedges to the funnel is a question of some substance. Its refractive index, expansion coefficient, corrosiveness, and spectral absorption are all material considerations in this detector design.

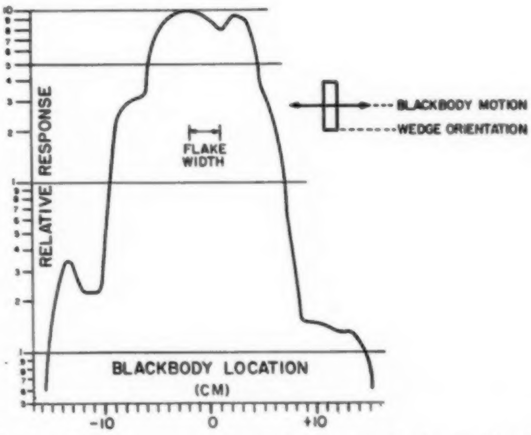

Fig. 6. Detector responsivity contour perpendicular to slit axis.

Its refractive index must be low enough to yield total internal reflection for all rays incident on the wedged side walls. This is a relatively easy requirement to satisfy with high-index infrared-transmitting lens materials since most organic polymer cements have indices of less than 2 and rays with a sizable incidence angle can be reflected by relatively small index differences. For example, the minimum ray incidence angle on the wedge surfaces of the satellite infrared spectrometer[12] detectors is 66°, so that any cement index less than $4 \sin 66° = 3.6$ will produce total internal reflection within the germanium wedge. We actually use epoxy cement with $n = 1.5$, yielding a critical angle of only $\sin^{-1}(1.5/4.0) = 22°$.

The cement's expansion coefficient should match the expansion coefficient of the immersion lens material to avoid straining or tearing the flake and its electrical leads during temperature cycling. The cement used in making the wedge detectors has an expansion coefficient of $6 \times 10^{-6}/°\mathrm{C}$, matching germanium. Chemical effects should not be overlooked; we have found that some cements attack selenium and can detach the active flake area from its leads in a few weeks. If the cement layer is too thin, then frustrated total internal reflection occurs and flux leaks into the side wedges; if it is too thick, it degrades the quality of the optical polish at the immersion interface.

Spectral absorption bands in the cement can reduce the efficiency of the internal reflections on the polished sides of the wedge, since even for incidence angles well beyond the critical angle, the radiation penetrates appreciably into the rarer medium.[13,14] The half-electric-field-intensity depth of penetration $X_{1/2}$ of electromagnetic radiation into a low-index nonabsorbing dielectric medium is given[15] by:

$$X_{1/2} = \frac{\lambda_1 \log_e 2}{2\pi (\sin^2 \theta - n_{21}{}^2)^{1/2}},$$

where

λ_1 = radiation wavelength in the denser medium,
θ = angle of incidence,
n_{21} = relative index of refraction = $n_2/n_1 < 1$.

All of the spectrometer rays are incident on the wedge's germanium-epoxy interface at far beyond its 22° critical angle, and hence penetrate relatively little into the epoxy cement. The deepest penetration into the satellite spectrometer wedge's epoxy cement occurs for the rays of 15 μ wavelength incident at 66° on the germanium–epoxy interface. For these rays $X_{1/2} = 0.5\ \mu$.

The epoxy cement selected for the wedge detectors exhibits a transmittance of over 90% for 0.5 μ thickness in the entire spectral interval from 2 to 16 μ. The Mylar[16] spacer material used to control the cement layer thickness exhibits transmittance of under 85% in 0.5 μ thickness from 7.7 μ to 8.2 μ and from 8.8 to 9.2 μ; however, the Mylar spacers were cemented against the polished wedge sides in locations that are outside the useful reflecting areas.

The above discussion of penetration depths suggests that two surfaces may in general be considered in "optical contact" when their separation is small compared to $\lambda_1 \log_e 2/2\pi = 0.1\lambda_1$, provided that the residual intervening material does not exhibit significant absorption bands in the spectral region of interest. In closing we would like to point out that the measurement of attenuated total internal reflection under controlled angles of incidence offers a promising new tool[17] for conveniently measuring the absorption spectra of controlled surface depths of a wide variety of materials without requiring elaborate preparation of thinned samples.

The author would like to acknowledge the contributions of John Strong, Robert Astheimer, and Russell DeWaard whose stimulating comments and advice materially aided in the development of the detector described above; the diligent assistance of James Moorhead in working out the design details and getting them built; the skilled services of Morton Lipkin's Precision Lapping Company in making the germanium lens parts, and the sponsorship of the United States Weather Bureau and the National Aeronautics and Space Administration.

References

1. R. DeWaard and E. M. Wormser, Thermistor Infrared Detectors, NAVORD Report 5495 (1958); available as Commerce Dept. OTS Rept. PB 151767.
2. R. DeWaard and E. M. Wormser, Proc. Inst. Radio Engrs. **47,** 1508 (1959).
3. F. A. Smith, F. E. Jones, and R. P. Chasmar, *The Detection and Measurement of Infra-Red Radiation* (Oxford University Press, New York, 1957), p. 111.
4. R. C. Jones, Appl. Opt. **1,** 607 (1962).
5. Cf. reference 1, Chap. 5.
6. A. C. Hardy and F. H. Perrin, *The Principles of Optics* (McGraw-Hill Book Company, New York, 1932), pp. 43 and 93.
7. H. H. Hopkins, *Wave Theory of Aberrations* (Oxford University Press, New York, 1950), pp. 120–121 and 127–132.
8. S. S. Ballard, K. A. McCarthy, and W. L. Wolfe, "Optical Materials for Infrared Instrumentation," University of Michigan, IRIA Report 2389-11-S (1959).
9. J. Strong, *Concepts of Classical Optics* (W. H. Freeman & Co., San Francisco, 1958), cf. Chap. 6.
10. Cf. reference 6, Chap. 5.
11. D. E. Williamson, J. Opt. Soc. Am. **42,** 712 (1952).
12. M. G. Dreyfus and D. T. Hilleary, Aerospace Engineering **21,** 42 (1962).
13. J. Fahrenfort, Spectrochemica Acta, **17,** 698 (1961).
14. N. J. Harrick, Phys. Rev. Letters **4,** 224 (1960).
15. B. Rossi, *Optics* (Addison-Wesley, Reading, Mass., 1957), p. 382.
16. R. E. Kagarise and L. A. Weinberger, "Infrared Spectra of Plastics and Resins," NRL Report 4369 (1954); available

as Commerce Dept. OTS Report PB111438; p. 23, Fig. 11(b).

17. Science **135,** 474 (1962), describing Attenuated Total Reflectance Attachment No. ATR-1 made by Connecticut Instrument Company.

Applied Optics BOOKS

Books for review should be submitted to the Managing Editor, APPLIED OPTICS, 1155 16th St., N.W., Washington 6, D.C.

Infrared Absorption of Inorganic Substances. By Katheryn E. Lawson. Reinhold, New York, 1961. 200 pp. $6.75.

Structural inorganic chemistry is currently in resurgence, and vibrational infrared and Raman spectra have been of much help to the modern inorganic chemist in solving structural problems. It is therefore a bit surprising that no book has yet appeared which covers the inorganic field in the manner of L. J. Bellamy's now classical work on the infrared spectra of complex organic molecules. Mrs. Lawson's "Infrared Absorption of Inorganic Substances" is a brief step in this direction. It is mainly a bibliography, however, and according to its preface is intended "to serve as a source book of spectral information for persons engaged in this phase of spectroscopy."

The book consists of three parts: an introduction of 14 pages dealing cursorily with techniques, a section of 70 pages called "Spectra-Structure Correlations," which reviews some of the recent literature on the spectra of inorganic compounds and contains a glossary of some fifty terms used in the preceding text, and finally a "Bibliography of Unclassified References" with about 1200 entries for the period 1950–1959, together with an index to the bibliography by elements, some compound names, and inorganic groups.

The first and second sections are too brief to be useful, and the publisher may be charged with exaggeration in placing on the dust cover the words "compiles and reviews all currently available information." The glossary apparently has not been checked against similar lists to make sure its definitions are authoritative; for example, the term *absorptivity* is not in general used to mean "the fraction of the incident radiation absorbed by a substance."

The bibliography is stated to have been constructed largely from the index to *Chemical Abstracts* for the period January 1952–December 1958. This arbitrary limitation is unfortunate because there are no comprehensive bibliographies on the subject in book form for the years up to 1952. The year 1959 is added in a supplementary list of references, and there is one 1960 reference (to the February issue of the *Journal of the Optical Society of America*). This latter entry hardly justifies the publisher's statement on the inner flap of the dust cover that the bibliography extends through April 1960. The index to the bibliography seems reasonably satisfactory.

This volume may be summed up as a bibliography for a limited period and a brief uncritical commentary on those aspects of the subject which are covered by some of the bibliographical entries. It is in no sense a treatise, and the "inorganic companion to Bellamy" is still to be published.

Richard C. Lord

Information Processing. Proceedings of the International Conference on Information Processing, Washington, June 15–20, 1959. Butterworth, Washington, 1960. 520 pp. $25.00.

The seven chapters of this book are entitled: Methods of Digital Computing; Common Symbolic Language for Computers; Automatic Translation of Languages; Pattern Recognition and Machine Learning; Logical Design of Computers; Special Session on Computer Techniques of the Future; and Miscellaneous Topics.

It is of interest to readers of *Applied Optics* for several reasons. One is new developments in the art of computation per se. There are no specific references or examples to computations in optics, but papers by P. Henrier and J. H. Wilkinson on round-off errors are of interest in the high precision required in ray-tracing.

A general topic of interest in optics is the question of being able to use a computer without having to be immersed in the intricacies of programming. Chapter II is a fairly revealing exposition of the philosophy of languages which bridge the gap between conventional scientific expression and machine language for execution. Anyone who expects to have his calculations carried out by a machine should appreciate this philosophy and keep it in mind in laying out his problem. The introduction by S. Gorn and papers on Algol by F. L. Bauer and K. Samuelson express the difficulties in finding a satisfactory language. The paper by J. W. Backus is not attractive to the physicist who merely wants computing done, because it is too far on the side of programming and proposes symbolism and language which accommodate the computer more than the problem exposition.

Chapter V can give the reader some picture of the capabilities of current computers, which has bearing on how optics may be advanced by computational facilities. The paper by A. L. Leiner *et al.* gives the philosophy of generating more powerful computers. Chapter VI looks to the potential improvements from advancements in technology and machine organization.

The material closest to optics is on pattern recognition, of which the most important current problem is the recognition of printed letters and numbers. Basically, this is optics, but the formulation of the problem from the point of view of optics is missing in this book as in much other literature. The papers by Wada and Sherman *et al.* digitize the characters into black or white "cells," which is quite disturbing in the light of all the recent understanding gained from transform theory and optical transmission functions. Sherman's discussion on the "topology" of the patterns, although elementary, is of interest in other optical methods of recognition.

H. Kazmierczak describes a flying-spot scan of the characters, the signal being clipped and stored as voltages generated in a two-dimensional array. These voltages are applied to a two-dimensional array of resistors. Each pattern results in a peculiar flow of current from the voltage-resistor arrays. Although this again is a digitizing of a continuous image, the flow of current smooths out the sampling. More elaborate equipment would in principle make a continuous analysis, and the concept of the potential field of an image transformed in this way is of some general interest in optics.

Gilbert W. King

Careers in Physics. By ALPHEUS W. SMITH AND WINSTON L. HOLE. Long's College Book Company, Columbus, Ohio, 1960. 310 pp. $5.95.

Careers in Physics is an up-to-date revision of the senior author's 1951 edition. It presents, in a carefully planned and clearly written style, the information needed by students contemplating physics as their professional field. The book should be studied by them and by their advisers so that intelligent career decisions may be made. The wealth of professional information contained in this book makes it profitable reading for all physicists.

The concept of physics as a powerful, dynamic, scientific endeavor which is advanced by physicists as human beings is stressed throughout its pages. The first chapter—a concise historical account of the development of the several major branches of physics and of the scientists making the major discoveries—blends this interplay of men and science. It introduces discussion of the personal and intellectual characteristics of individuals which appear essential to a successful career in physics.

The reader is next informed of the academic path which the student must follow in his preparation and of the particular hurdles which he will encounter. This is followed by some fifty pages of text in which the vast scope of activity in this profession is set out. Scores of fields of specialization in pure, and in applied physics, and in the interdisciplinary fields, are presented. Each of these reminds the reader of past accomplishments and of their impact and service to mankind. In addition many exciting, unsolved problems demanding attention are fascinatingly presented. The book, a dignified and excellent sales plan, should attract interested young people into the profession.

Information is supplied to help the student answer the question—Do I want to plan my career to be in an academic institution, in a federal, public, or private research institute, or in an industrial research laboratory? The book discusses these, and other more specific areas such as the nuclear laboratories, in terms of type of work, demands, salary scales, other rewards, etc. A chapter is devoted to named "Special Purpose Laboratories" stating the type of problems which they now sponsor.

The final chapter deals appropriately with "Physicists and the Future," leading to the conclusion—"Trends of the past few decades give every indication that opportunities for satisfying participation in the physical science programs of education, industry, and government will continue indefinitely in rapid and challenging expansion."

The book *Careers in Physics* should be available in the physics library of every college physics department. Students in both college and secondary schools who indicate interest and/or show ability in this field should be encouraged to read it. Their advisers would be remiss not to possess a copy.

C. J. OVERBECK

Introduction to Practical Infra-red Spectroscopy. By A. D. CROSS. Butterworths, London, 1960. 80 pp. $3.50.

This book is precisely what the title proclaims it to be: a brief account of the theory and techniques of infrared spectroscopy useful to the practicing chemist. In the short discussion of sampling techniques, operating procedures, and spectrum analysis the author has provided very sound guidelines for the novice spectroscopist. This book probably will find its largest audience among undergraduates who are majoring in chemistry.

M. KENT WILSON

Advances in Quantum Electronics. Edited by J. R. SINGER. Columbia Univ. Press, New York, 1962. xi + 641 pp. $15.00.

This book is a compendium of papers presented at the Second International Conference on Quantum Electronics, held in Berkeley, Calif., on March 23–25, 1961. The papers are divided into eight sections entitled: I. Optical Masers, II. Optical Pumping: Transitions in Gases and Solids, III. Interaction of Molecules with Photons in Resonant Structures, IV. Phonon and Paramagnetic Resonance Phenomena, V. New Investigations of Semiconductors, VI. Information Theory and Noise Studies, VII. Microwave Transitions, and VIII. Some New Ideas and Accomplishments.

It seems to me that, with regard to a book of this nature, a potential reader would ask for an evaluation of the importance and interest of the categories selected (and of the topics omitted!) as well as of the quality of the individual papers. Since the great majority of papers were written by leading experts for the benefit of their colleagues, the book is directed at workers in a rapidly advancing field. Thus it is of interest to know whether the papers have retained their aspect of novelty a year after presentation. Lacking novelty, are they of such fundamental importance that the reader is glad to have them assembled in one volume?

I shall try to cover these points for the various sections, emphasizing aspects likely to be of particular concern to optics people, and touching more briefly on others.

Since optical masers are of great interest in optics, Section I could have been very valuable. However, while the papers were representative of the state of the art at the time the Conference was held, most of that material has since appeared extensively elsewhere. I believe that a brief summary, such as given by Maiman, combined with references (including those to subsequent work by the authors) and with discussions, would have been a desirable replacement for the full text of all the papers in the group except the one by Townes, which I should have liked to see used as an introduction to the whole book. The present introduction certainly does not tend to stimulate a potential reader's eagerness to proceed.

The interest picks up sharply with Section II, the longest in the book, which starts out with two good papers on optical pumping by Brossel and Cohen-Tannoudji, respectively. Very exact measurements of optical properties of certain classes of materials are given by Low in "Optical Spectra of Paramagnetic Solids" and by Dieke in "Spectroscopic Observations of Maser Materials." Success in the maser field is predicated upon such data. The group of papers on apparatus should either have been expanded into a complete section or skipped altogether. As it is, the papers just skim the subject at random. While detection is of vital importance in practice, Forrester touches only briefly on photodetection and photomixing. Amplitude and frequency modulated detection are hardly touched on in the book, although Pershan and Bloembergen give some interesting thoughts on modulation. Other interesting papers are by Gamo on the correlation between intensity fluctuations started by the experiments of Brown and Twiss, and by Bloom and Bell, who describe an optical experiment dealing with applications of modulated light to optical pumping.

Section III contains a number of papers of fundamental interest on the characteristics of resonant structures at optical frequencies. It is the only section of the book devoted to precision optics analogous to lens design, as, for example, in the paper on "Resonant Modes in a Maser Interferometer" by Fox and Li. While some of the material here has appeared elsewhere, it is of sufficient value to warrant inclusion of the full

continued on page 626

Performance of the Beckman IR-7 Infrared Spectrophotometer
2. Frequency Reproducibility and Accuracy (200–800 cm^{-1})

Peter J. Krueger

A Beckman IR-7 prism/grating infrared spectrophotometer, modified with a fiducial frequency marking system, has been calibrated with an estimated absolute accuracy of up to ± 0.05 cm^{-1} in certain parts of the CsI foreprism range 200–800 cm^{-1}. This represents an approximate tenfold improvement over the manufacturer's specifications. The frequency reproducibility of the modified instrument and the linearity of the frequency (wave-number) presentation have been critically examined. A calibration scheme for this region is presented.

Introduction

The application of infrared spectroscopy in the near infrared (0.5–2.5 μ) and conventional rock salt region (2.5–16 μ) is now a very common technique in almost all phases of pure and applied chemistry. The rock salt region will probably continue to be the most widely used portion of the infrared for most applications, largely due to the availability and excellent characteristics of sodium chloride optics. Most of the functional group correlations used by chemists have also been well established in this region.

Recent instrumental advances have made the 15–50 μ-region available to chemical spectroscopists, where spectra can now be obtained with the same ease as in the rock salt region. There is no doubt that the molecular structural information gained from this region will complement that already available. In many cases this region will provide information not attainable by any other physicochemical method.

Measurements on the low-frequency vibrations are needed to complete the vibrational assignments of molecules. They are also essential for the calculation of thermodynamic properties from spectroscopic data. Torsional oscillations of molecules lie in this region, and these will provide new data on conformational mobility. Functional group analysis on molecules using vibrations involving very heavy atoms will become feasible. In general, it appears that the low-frequency skeletal vibrations of the molecule are very sensitive to changes in structure.[1] The vibrations arising from very weakly bound complexes also lie in this region, providing direct information on interaction effects between molecules. Far infrared spectra are very sensitive to crystal structure, leading to characteristic lattice vibrations. From a strictly analytical viewpoint, compounds which have very similar spectra in the rock salt region may differ more in the far infrared, and quantitative absorption measurements may be easier because of less overlapping of bands.[2] Characteristic absorption bands for inorganic ions in the far infrared have also been reported.[3]

Since information on chemical systems is still relatively scarce beyond 16 μ (the NaCl absorption cutoff), and almost nonexistent beyond 25 μ (the KBr absorption cutoff), it is essential that such spectra which are now obtained be largely free from absolute frequency errors, and from intensity errors due to stray radiation.

The Beckman IR-7 double-beam prism/grating infrared spectrophotometer installed in this department in 1960 has now been equipped with a commercial removable long-wavelength interchange operating out to 50 μ,[4] and it is the purpose of this report to describe its performance under very stringent test conditions. This optical interchange unit employs a 60 × 75 mm, 48° CsI foreprism and a 30 lines/mm, 64 × 64 mm grating blazed at 30 μ, together with a CsI thermocouple. By means of a scattering mirror, stray radiation is reduced to less than 0.1% at 699 cm^{-1}, and to less than 1.0% at 330 cm^{-1} according to the manufacturer's specifications.[5] The wave-number range of 220–700

The author is in the Department of Chemistry, University of Alberta, Calgary, Alberta, Canada.

Received 6 April 1962.

Presented in part at the Thirteenth Pittsburgh Conference on Analytical Chemistry and Applied Spectroscopy, March 5–9, 1962.

cm^{-1} (200–700 cm^{-1} on single-beam operation) is automatically covered in two grating orders which overlap by 50 cm^{-1}, and the linear frequency cams are actually calibrated up to 800 cm^{-1}.* Thus this interchange provides sufficient overlap with the standard NaCl foreprism/grating unit which covers 650–4000 cm^{-1}. The manufacturer's reproducibility specification is given as ±0.030 in. (chart paper) at any point.[5] With a maximum chart expansion of 2.50 cm^{-1}/in., this corresponds to ±0.075 cm^{-1}. A resolution of better than 1.0 cm^{-1} is readily achieved throughout most of its range, and a resolution of 0.3 cm^{-1} has been demonstrated at 292 cm^{-1}.[6]

The basic instrument had previously been modified to provide a fiducial marking system locked in with the cam system.[7] With this arrangement and an exhaustive calibration procedure, a reproducibility of the order of ±0.02 cm^{-1} and an absolute frequency accuracy of the order of ±0.05 cm^{-1} were obtained in the first grating order with the NaCl interchange.[8] The fiducial marking system is attached to the instrument base and the main monochromator drive shaft, which engages unequivocally with the cams of the optical interchange unit by means of a spring loaded pin caught in a slot in the clutch plate. This clutch plate has two slots at 180° to each other, and the same slot is used to engage both the NaCl and CsI foreprism/grating assemblies which are mounted, together with the associated wave-number cams, on duplicate cast mountings which are positioned kinematically to retain precise alignment.† The interchange not in use at any time is kept in a thermostated storage box to minimize temperature equilibrium time.

At no time were calibration drifts observed with the CsI or NaCl interchange, which could be caused by temperature changes depending on the length of time the Nernst glower has been on. Such drifts have been reported for some other types of modified commercial spectrophotometers.[9] In the IR-7 the glower is normally left in the "stand-by" state when not in use, conducting about 0.2 amp. The principal solution to this problem may lie in temperature stabilization at about 40°C, well above the ambient temperature.

Calibration Scheme

The vibration-rotation and pure rotation lines of simple gases at relatively low pressures were used, following established calibration procedures. Although our instrument has been modified to permit scanning in both directions,[10] the present measurements were made by scanning only in the direction of increasing frequency. The spectrum of each calibrant gas was independently obtained three times over a period of about one month, and the average position of each line on the arbitrary fiducial scale obtained, as well as the maximum deviation from the mean. The "tracking error" of the instrument was considered to be negligible at the scanning speed of 0.4 cm^{-1}/min used. Amplifier gain settings were around 25% of the maximum, and a pen response (filter period) of 32 sec was used to maintain a proper signal-to-noise ratio.

Double-beam operation was used throughout, except for measurements on atmospheric water vapor and carbon dioxide bands. Single-beam and double-beam measurements were found to be identical within the reproducibility limits established. For double-beam measurements the entire optical path was purged with dry air, also partially freed from carbon dioxide. Slit widths were programmed for constant energy using a regular "Select" setting that would give the resolution required and maintain a high signal-to-noise ratio. The approximate spectral slit widths used are given in Table I, together with the other relevant calibration data. Figure 1 shows some typical examples of resolution obtained.

The spectra were measured up and calibration curves and tables for use in high-resolution gas phase work constructed as previously described.[8] Since the wave-

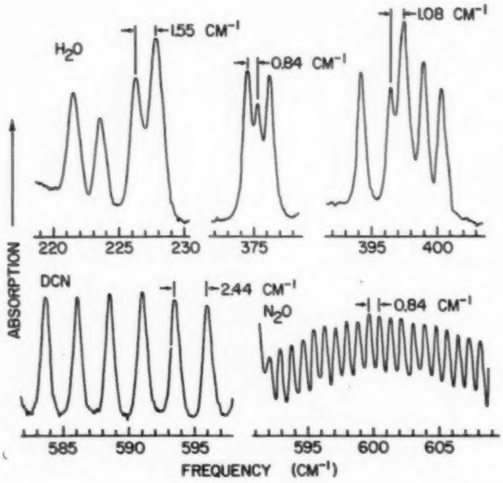

Fig. 1. Examples of resolution readily achieved with the IR-7 CsI prism/grating interchange unit. Water vapor spectra obtained in the first order; DCN and N_2O spectra in the second order of the grating.

---

* Continuous operation past the 700 cm^{-1} mark requires that the microswitch circuit which stops the scan at that point be made inoperative. This is conveniently done by installing a switch on the outside of the instrument so that the operator can select to scan to 800 cm^{-1} without disturbing the temperature equilibrium of the optical system. Electrical connections were made to that part of the circuit common to both interchanges, to avoid interfering with the rapid change-over of optics.

† This is conveniently achieved by rotating the cams until the CsI interchange is set at about 355 cm^{-1} and the NaCl interchange at about 700 cm^{-1} before either is removed from the monochromator.

Table I. Calibration Scheme (200–800 cm^{-1})

					Calibration lines		
Grating order	Calibrant	Region (cm^{-1})	Pressure (mm) in 10-cm cell[a]	Slit width[b] (cm^{-1})	Number used	Estimated absolute accuracy (cm^{-1})	Average max. deviation from the mean[c] (cm^{-1})
I	Water vapor,[d] rotational lines	200–500	*e*	0.7–0.9(200–220 cm^{-1}) 0.9–0.5(220–250 cm^{-1}) 0.5–0.7(250–500 cm^{-1})	72	±0.02[f]	0.02_2
II	Water vapor,[d] rotational lines	440–555	*g*	0.3–0.5	24	±0.02	0.02_5
	Deuterium cyanide,[h] ν_2 fund.	500–635	60	0.6–0.4	45	±0.03	0.02_1
	Ammonia[i]	500–700	250	0.6–0.4	31	±0.03	0.02_2
	Nitrous oxide,[j] ν_2 fund.	550–630	300	0.5–0.4	84	±0.02	0.02_2
	Carbon dioxide,[d] ν_2 fund.	630–700	*g*	0.4	40	±0.03	0.02_2
	Hydrogen cyanide,[k] ν_2 fund.	635–790	30	0.4	46	±0.01	0.02_3
	Acetylene,[l] ν_5 fund.	690–790	15	0.3–0.4	37	$\leqslant$ ±0.1	0.02_7
	Ammonia,[i] ν_2 fund.	730–770	75	0.3–0.4	13	$\leqslant$ ±0.1	0.02_2
		770–800	50	0.4	—		
				Total =	392		

[a] With KBr or CsBr windows.

[b] Approximate values (programmed slit used).

[c] Based on three independent experimental measurements of each line.

[d] Single-beam spectrum.

[e] Optical path purged with dry air.

[f] Except for lines with frequencies below 271 cm^{-1}; see text.

[g] Optical path length of 569.7 cm at about 30% relative humidity, 27°C.

[h] Prepared from D_2O, P_2O_5, and KCN.

[i] Matheson, anhydrous, 99.99% min.

[j] Matheson, 98.0% min.

[k] Prepared by action of dilute H_2SO_4 on KCN.

[l] Welder's grade.

number expansion of the CsI interchange is identical to that for the first two orders of the NaCl interchange, reference marks were obtained at intervals of 1.0 cm^{-1}.

The IUPAC Commission on Molecular Structure and Spectroscopy has recently issued a comprehensive comparative report giving recommended absorption lines for calibration in the 600–4000 cm^{-1} region,[11] but its recommendations for the far infrared region have not yet been published. The ammonia, acetylene, carbon dioxide, hydrogen cyanide, and nitrous oxide bands recommended were used for the 600–800 cm^{-1} region. Further values for N_2O lines below 600 cm^{-1} were obtained from Lakshmi, Rao, and Nielsen.[12] For deuterium cyanide the measurements of Checkland and Thompson[13] were used. Using 250 mm of pressure in a 10-cm cell, the strongest ammonia lines in the 500–700 cm^{-1} region could be measured, the reference data for these being obtained from Garing, Nielsen, and Rao.[14] Atmospheric water vapor is an ideal calibrant throughout this region because of the complex nature of its spectrum. The best values for the pure rotational lines in the 270–550 cm^{-1} region are those of Rao and co-workers,[15] believed to be accurate to ±0.02 cm^{-1}. Below 270 cm^{-1} recourse was made to the 1937 measurements of Randall *et al.*,[16] since these appear to be the latest results in the literature. These authors estimated their accuracy to be about ±0.05 cm^{-1}, but for lines above 270 cm^{-1} their measurements appear to be consistently higher than those of Rao[15] by about 0.19 cm^{-1} (average discrepancy). This amount was accordingly subtracted from the measurements of Randall *et al.*[16] in the 200–270 cm^{-1} region. Table I gives the estimated absolute accuracies of these secondary standard lines, as obtained from the references cited.

Frequency Reproducibility

Since all of the 392 calibration lines were independently recorded and measured three times over a period of about one month, the average maximum deviation from the mean value for all the lines in a given region should be a good measure of the frequency reproducibility. The last column in Table I shows that a reproducibility of 0.02 to 0.03 cm^{-1} was obtained throughout. This is as good as that found previously for the first two orders of the NaCl interchange.[8] Since no special temperature or humidity control was employed in the instrument room, this long-term stability speaks highly for the thermostatic temperature control of the instrument.

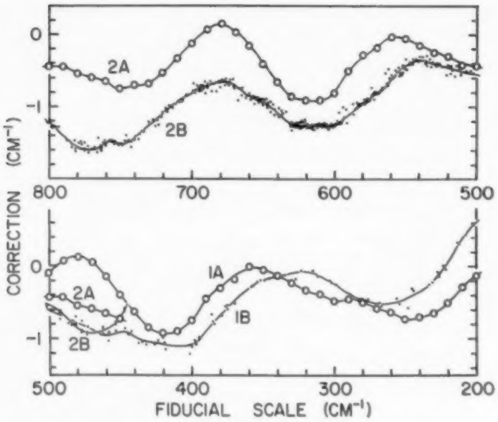

Fig. 2. Correction to be applied to dial wave-number read-out (B-A) and fiducial scale values (B) to give absolute frequency (cm^{-1}) for the range 200–800 cm^{-1}.

Frequency Linearity

The fiducial marking system incorporated into this instrument lends itself ideally to the examination of the linearity of the cam frequency drive system. To examine this aspect all of the 392 gas phase calibrant lines were plotted so that the absolute frequencies could be obtained at any point by applying a correction to the fiducial scale value. Examination of the "B" curve in Fig. 2 reveals the exact nature of the cam linearity, since the fiducial scale is linear by its very nature.

The precise relationship of the wave-number read-out dial relative to the uniform rotation of the main monochromator shaft (i.e., relative to the fiducial scale) was also established at 10 cm^{-1} intervals. These data are shown in the "A" curve in Fig. 2. Nonlinearity here must be ascribed to one or more periodic errors in the wave-number dial mechanism itself. No obvious periodicity related directly to the rotation of any one mechanical part could be found. Since the difference between the fiducial scale and the dial wave-number scale is within 1 cm^{-1} throughout, the vertical distance between the "A" and "B" curves at any given fiducial scale value corresponds very nearly to the correction to be applied to the dial wave-number value at that point. The absolute frequency discrepancies observed compare very favorably with ±0.5 cm^{-1} allowed in the manufacturer's specifications.[5]

Condensed Phase Measurements

The absorption bands observed in the spectra of pure liquids and solutions are usually very broad relative to line widths in gas phase spectra, and this severely limits the precision and accuracy of frequency measurements. Pure liquid indene, with camphor and cyclohexanone as additives, has recently been proposed as a suitable liquid calibrant for low-resolution spectrophotometers in the 600–4000 cm^{-1} region.[17] Jones, Faure, and Zaharias[18] have also indicated that this may be a useful calibrant below 600 cm^{-1}.

The reproducibility limit of manual indexing of the wave-number dial to the chart paper grid was investigated as a first step in the study of absolute accuracy that could be obtained without the use of the fiducial system. For ten independent spectra begun at each of the points 220 cm^{-1} in the first order and 500 cm^{-1} in the second order, the fiducial system showed a precision of ±0.03 cm^{-1} (maximum deviation from the mean) in the initial setting. This order of precision, which can readily be obtained if backlash is carefully eliminated in both monochromator and recorder mechanisms, is better by at least an order of magnitude than the precision that can be obtained in locating the maximum of an average condensed phase absorption band, and is thus not a limiting factor. The chart paper feed was found to be very regular relative to the monochromator drive, and repositioning errors of the recorder pen in the second order after an automatic order change too small to be significant in condensed phase spectra.

The double-beam indene–camphor–cyclohexanone (1:1:1 by weight) spectrum was obtained without the

Table II. Absorption Maxima in the Infrared Spectrum of Indene–Camphor–Cyclohexanone Suitable for Calibration of Low-Resolution Spectrophotometers (200–800 cm^{-1}).[a] Nominal Path Length 0.05 mm, CsBr cell. "Standard" Slit Schedule.[b]

Band no.	Frequency (cm^{-1}) Present measurements	Jones, *et al.*[18]
1	(221)	...
2	(248)	...
3[c]	301.6	302.0 ± 2
4	382.4	381.5 ± 1
5	393.3	393.5 ± 1
6	421.2	420.0 ± 1
7[d]	491.8	489.0 ± 1
8[c]	522.2	521.0 ± 1
9	552.4	551.5 ± 1
10[c]	572.0	571.0 ± 2
11	592.6	591.0 ± 1
12[d]	610.9	609.5 ± 1
13[c]	648.6	647.5 ± 1
14	694.0	692.8 ± 0.7
15	719.1	718.2 ± 0.3
16	730.4	730.1 ± 0.2
17	766.0	765.5 ± 0.5

[a] Three components 1:1:1 by weight; due to overlapping of bands some of these maxima may be concentration dependent.

[b] This constant energy double-beam slit schedule leads to calculated slit widths of $1.0–0.6_5$ cm^{-1} in the first order (200–500 cm^{-1}) and $0.5–0.7_5$ in the second order (450–800 cm^{-1}).

[c] Band due to camphor.

[d] Band due to cyclohexanone.

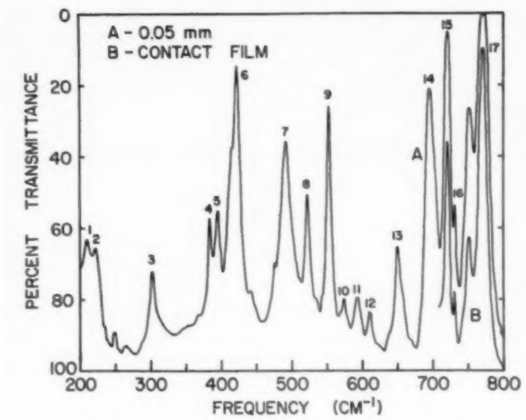

Fig. 3. Far infrared spectrum of indene–camphor–cyclohexanone solution suitable as a secondary calibrant.

fiducial marking system at a scanning speed of 8 cm^{-1}/min, an amplifier gain of 5%, a filter period of 8 sec, and abscissa expansion of 20 cm^{-1}/in. The recorder pen and wave-number dial were carefully indexed at 200 cm^{-1}, and measurements based on the inch-calibrated chart paper grid corrected according to Fig. 2. The frequencies obtained are tabulated in Table II, and good agreement was found with the values of Jones, Faure, and Zaharias.[18] The reference spectrum is given in Fig. 3.

Summary

This investigation has demonstrated:

(a) the high-frequency reproducibility inherent in the design of the Beckman IR-7 infrared spectrophotometer when operating with a CsI prism/grating interchange in the far infrared region,

(b) the operation of a fiducial marking system previously designed for the NaCl region, when used to overcome the difficulty of accurately reading out frequencies in the far infrared region,

(c) that an infrared spectrophotometer nominally linear in frequency, and using a cam system, is capable of accurate frequency measurements by conventional calibration methods,

(d) that correction curves obtained for the wave-number dial readings with the fiducial system produce satisfactory results for the less exacting measurements on relatively broad bands,

(e) that the design of the fiducial marking system used does not interfere with the rapid interchangeability of the NaCl and CsI optics, and

(f) that the optical interchanges maintain their calibration on removal.

The author thanks K. N. Rao and Mrs. Sinnett for making available their unpublished data for the pure rotational lines of water vapor in the far infrared. R. N. Jones kindly supplied the indene sample used.

References

1. J. E. Stewart, "Far Infrared Spectroscopy with Cesium Bromide Prisms," Beckman Application Data Sheet IR-94-MI.
2. F. W. Behnke, "Application in the Infrared Region from 800–400 cm^{-1}," paper presented at the Pittsburgh Conference on Analytical Chemistry and Applied Spectroscopy, Feb. 29–March 4, 1960.
3. F. A. Miller, G. L. Carlson, F. F. Bentley, and W. H. Jones, Spectrochimica Acta **16**, 135 (1960).
4. Bulletin 7000-20, "Beckman IR-7 Long Wavelength Interchange," Beckman Instruments, Inc. (1960).
5. "Cesium Iodide Long Wavelength Interchange Instruction Manual," Beckman Instruments, Inc. (1961).
6. Specification published in Anal. Chem. **33**, 61A (1961).
7. P. J. Krueger and G. H. Schulze, submitted for publication.
8. P. J. Krueger, Appl. Opt. **1**, 443 (1962).
9. R. N. Jones, K. S. Seshadri, and J. W. Hopkins, Can. J. Chem. **40**, 334 (1962); see also ref. 17.
10. P. J. Krueger and G. H. Schulze, submitted for publication.
11. IUPAC Commission on Molecular Structure and Spectroscopy, *Tables of Wavenumbers for the Calibration of Infrared Spectrophotometers* (Butterworths, London, 1961). Reprinted from Pure and Appl. Chem. **1**, 537–699 (1961).
12. K. Lakshmi, K. N. Rao, and H. H. Nielsen, J. Chem. Phys. **24**, 811 (1956).
13. P. B. Checkland and H. W. Thompson, Trans. Faraday Soc. **51**, 1 (1955).
14. J. S. Garing, H. H. Nielsen, and K. N. Rao, J. Mol. Spectroscopy **3**, 496 (1959).
15. K. N. Rao, Ohio State University, unpublished results.
16. H. M. Randall, D. M. Dennison, N. Ginsburg, and L. R. Weber, Phys. Rev. **52**, 160 (1937).
17. R. N. Jones, N. B. W. Jonathan, M. A. MacKenzie, and A. Nadeau, Spectrochimica Acta **17**, 77 (1961).
18. R. N. Jones, P. K. Faure, and W. Zaharias, Revue Universelle des Mines **15**, 417 (1959).

Books Received

An Ultraviolet Multiplet Table, National Bureau of Standards Publication #488, Sections 3, 4, and 5, by C. M. Sitterley, 1962.

Absorption Spectroscopy, by R. P. Bauman, Wiley, New York, 1962.

Proceedings of the Fifth International Congress on High-Speed Photography, ed. J. S. Courtney-Pratt. Society of Motion Picture and Television Engineers, 1962.

Direct Observations of Imperfections in Crystals, ed. J. B. Newkirk and J. H. Wernick. Wiley-Interscience, New York, 1962.

Fundamentals of Infrared Technology, by M. R. Holter, S. Nudelman, W. L. Wolfe, and G. J. Zissis. Macmillan, New York, 1962.

Icarus: International Journal of the Solar System, eds. Z. Kopal and A. G. Wilson. Vol. 1, #1, May 1962.

Books

continued from page 620

text in this book. Physical optics in the sense of instrumentation, such as measurement of amplitude and phase, are unfortunately missing. Equally unfortunate is Lamb's failure to amplify his very brief summary on "Angular Distribution of Stimulated Emission."

Section IV is worthwhile chiefly because of the contributions of Van Vleck, Bloembergen and Pershan, and Gill and Elliott on spin-lattice relaxation. Schlömann's article on spin-wave spectroscopy is very interesting, but only touches on the subject. The applications of the theories represent chiefly gadgets.

In a book where so much attention is devoted to semiconductors, it is unexpected to have three papers singled out as representing New Investigations of Semiconductors. Though limited in scope, this section is interesting, and the papers are of high caliber.

While the section on Information Theory and Noise Studies is rather abbreviated considering the importance of the subject for optical communications, I am glad to see this type of material included.

I feel that the concluding section dealing with such controversial subjects as Weber's Quantum Electronics and Gravitation might have been supplemented, for example, by a discussion of the experiments suggested by Schiff, which would have made the presentation less one-sided. An extremely interesting paper by Coleman on the "Cerenkov Approach to the Submillimeter Wave Problem" is one example of the vast potential inherent in the subject of the emission of coherent radiation and allied topics.

In spite of a few flaws in choice and editing, the book is an admirable one. When reviewing an ordinary text, a reviewer can hope that his suggestions will be incorporated in future editions. Since changes are unlikely in a work involving so many authors, the suggestions as to editorial presentation are obviously directed at reports of future conferences.

JENNY E. ROSENTHAL

Spectra and Analysis. By A. A. KHARKEVICH. Consultants Bureau Enterprises, Inc., New York, 1960. 222 pp. $8.75.

This excellent monograph is a translation of the revised third edition of the Russian text published in Moscow in 1957. It is devoted to spectral concepts and analysis as they apply to oscillations in electronic engineering. However, the author points out that this approach has wide applicability since "the analysis of any physical process consisting of the time variation of some physical quantity or other can be reduced to the analysis of an electrical process." And indeed this monograph is extremely pertinent to research being done in interferometric spectroscopy, sometimes referred to as spectroscopy by the Fourier method.

Chapter 1 begins with an elementary treatment of fundamental relations and definitions of Fourier expansion and the classification of spectra. Spectral theorems (which are used in later sections) are derived and discussed; a clear and well-written discussion of running and instantaneous spectra is presented. Spectra of well-known functions and of modulated functions are calculated in detail. One section is devoted to the relation between the duration Δt of a pulse and its frequency bandwidth Δf. There are many typographical errors in this section, but these are easy to detect and should not disturb the reader; and it should not disturb him to discover that Schwartz's inequality is Bunyakovskii's inequality. What should immediately strike the reader's attention is the following minimum value for the product $(\Delta f \Delta t)$ derived using variational methods:

$$(\Delta f \Delta t)_{\min} = \frac{1}{\sqrt{3}} \cdot \frac{1}{4\pi},$$

a value which is lower by almost a factor of two than the one this reviewer had considered to be the minimum when Δf and Δt are defined in terms of radii of gyration. However the factor $1/\sqrt{3}$ is a consequence (of which the reader should be made aware) of integrating only over positive frequencies in the definition of Δf. In Section XIV the sampling theorem for functions of bounded spectra (which the author indicates was first established from a communication-engineering point of view in 1933 by Kotel'nikov) is derived in a clear and intuitive manner. To summarize, in this chapter the author succeeds in giving a concise exposition, not mathematically overweight, of the basic ideas of the theory of spectra.

The second chapter entitled Analysis, which is defined as the operation of determining a spectrum, deals exclusively with the analysis of physical processes rather than of functions. A comparison between simultaneous and consecutive analysis using resonators (or filters) is made, and the relation between resolving power and analysis duration is arrived at. The reader should be warned that in some sections the term "resolving power" is used to mean sometimes Δf and at other times $f/\Delta f$, which leads to apparently contradictory statements. On page 111 one finds the statement "the greater the resolving power of the analyzer the greater will be the time necessary for analysis," and on page 113, "for a given system the time necessary for analysis is inversely proportional to the resolving power." Section 24 contains an excellent treatment of transient effects on the dynamic resolving power of resonators. There are excellent illustrations clearly depicting the evolution of the dynamic resolving power of a resonator from the time $t = 0$ (the time at which the input is fed into the resonator) till a time when the transients of the system have died down and the (static) resolving power depends only on resonator parameters. Section 25 presents a complete and detailed analysis of the effects on (a) peak amplitude, (b) peak position, (c) half-width of the resonator spread function when performing a consecutive analysis, i.e., the case when the resonator frequency is varied for the purpose of analysis. Again this section gives a clear and direct general approach to the problems, arriving at formulas of practical application. The last section in this chapter deals with the behavior of resonators for pulse analysis, and again the presentation is direct and thorough.

Chapter 3 is an extension of spectral ideas to random processes. Spectra of some stationary ergodic processes are calculated in detail and some examples of nonstationary processes are worked out. The problems involved in performing spectral analysis on random processes are discussed and the chapter ends with a consideration of various information preserving techniques of spectrum compression.

The last twenty or so pages are devoted to 7 appendices in which specialized calculations are carried out as an extension of topics already encountered in the text. The bibliography lists thirty-two references dating from 1917 to 1956. There are no student problems. This reviewer is unreservedly enthusiastic about this monograph. It is written in a fluid, easily readable style and enjoyable in every respect. Nowhere do mathematical formulas overshadow the clearness of the train of thought.

GEORGE A. VANASSE

The Detectivity of Infrared Photodetectors

S. Nudelman

This article presents a review and an analysis of the factors involved in determining the capability of semiconducting photodetectors to detect radiation. The photoconductive detector is used as the vehicle for this analysis. Signal and noise generation are examined individually for their contribution to noise equivalent power (NEP), the Jones classifications of detectors, and detectivity-star (D^*). Equations for NEP are derived that permit direct examination of the influence of parameters such as bandwidth, area, and time constant in detector performance.

I. Introduction

The purpose of this article is to present a review and an analysis of the factors involved in determining the capability of semiconducting photodetectors to detect radiation.

By 1953, considerable information on thermal detectors, photoemissive devices, and photographic film was available, to the extent that Jones[1] was able to present a detailed accounting of the "state of the art." In addition, he was able to ascertain consistent patterns of detector behavior, to formulate a system of detector classification, and to propose figures of merit. Semiconducting photodetectors were in the early stages of their development, and it was possible to include only some of the preliminary information on lead-compound detectors in the report. Since that time, considerable effort has been expended toward the development of background-noise-limited infrared detectors, and to the understanding of the basic physical mechanisms responsible for their performance. G-R (generation-recombination) noise was uncovered as a limiting fundamental process, while the role of shot noise in *p-n* junction detectors was ascertained. Excess ($1/f$) noise received intensive study, and significant reduction of this noise was achieved in the development of most photodetectors. However, its properties still remain to be organized and explained theoretically. The concept of detectivity-star (D^*) was introduced by Jones[2] to provide a numerical rating for a detector. This concept has proven useful, and on the basis of recent measurements appears to be fully applicable to semiconducting photodetectors. With the accumulation of this wealth of new information, it is now fruitful to present a re-examination of the mechanisms involved in photodetection and to derive expressions for noise equivalent power (NEP) for the various noise-limited conditions. An analysis of the meaning of D^* is also in order. The photoconductive detector is used as the vehicle for this analysis.[3]

II. The Photoconductive Detector

The solid-state quantum detector absorbs electromagnetic radiation (or photons) and generates from this absorption additional free charge carriers. The mechanisms of this process require that the quantum of energy associated with the photons ($E_{\mathrm{ph}} = hc/\lambda$) be greater than some critical energy corresponding to allowed transitions between the conduction band, the valence band, and/or a discrete energy level in the energy-gap region of the semiconducting detector. This process is carried out without any significant temperature change. The additional carriers that are generated appear in a form suitable for measurement as a voltage or a current.

A. Signal Generation

The photoconductive detector, which is the only device that will be discussed here, is generally operated with the simple circuitry of Fig. 1. The voltage drop V_c across the detector is given by:

$$V_c = \frac{V}{r_L + r_c} \cdot r_c, \qquad (1)$$

This paper was written while the author was at the Institute of Science and Technology, The University of Michigan, Ann Arbor, Michigan. His present address is: Armour Research Foundation, Chicago 16, Illinois.

Received 4 April 1962.

This paper is reprinted from the Proceedings of the Infrared Information Symposia, Vol. 6, No. 4, October 1961.

This work was supported in part by the Office of Naval Research and in part by the Aeronautical Systems Division, U.S. Air Force.

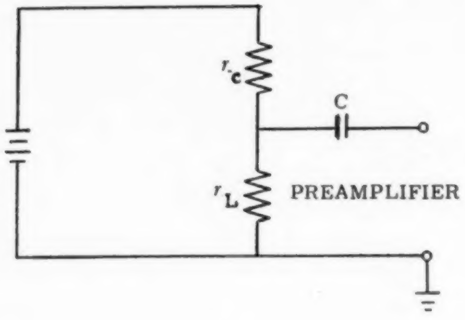

Fig. 1.

where

V = bias battery voltage,
r_L = load resistor,
r_c = resistance of the photoconductive detector.

The signal voltage is the variation in the voltage drop caused by the change in r_c, when the detector is exposed to signal radiation. Therefore:

$$\Delta V_c = I \cdot \Delta r_c + \Delta I \cdot r_c = I \cdot \Delta r_c, \tag{2}$$

where

I = bias current = $V/(r_L + r_c)$,
$\Delta I = 0$,

which is applicable when photoconductive detectors are operated under constant-current conditions.

The change in resistance is due to the change in the number of carriers created by the absorption of signal photons. For the simplest kind of analysis, consider here the case of the intrinsic photoconductor whose hole and electron mobilities are assumed equal. The general case of unequal mobilities, and including the impurity photoconductive detector, results in an analysis requiring significantly extra arithmetic, and for the purposes of this paper leads to the same conclusions. Let the detector shape be a parallelopiped, of length l, width w, and thickness d. The quantity lw represents the surface exposed to radiation and defines the detector area A, with the electrodes placed across the wd end faces. The cell resistance is given by:

$$r_c = \rho \frac{l}{wd} = \frac{l}{\sigma wd} = \frac{l}{2ne\mu wd}, \tag{3}$$

where

ρ = electric resistivity = $1/\sigma$,
σ = electric conductivity = $ne\mu_n + pe\mu_p = 2ne\mu$,
μ = mobility ($\mu_n = \mu_p$),
n = density of electrons,
p = density of holes.

When radiation is absorbed by the detector, it causes a change in the density of carriers Δn_s, and therefore a change in conductivity. The change in resistance is then given by:

$$\Delta r_c = \frac{dr_c}{dn} \cdot \Delta n = -\frac{\rho l}{wd} \cdot \frac{\Delta n_s}{n}. \tag{4}$$

The signal voltage is then

$$V_s = I \cdot \Delta r_c = \frac{V}{r_L + r_c} \cdot \frac{\rho l}{wd} \cdot \frac{\Delta n_s}{n} \tag{5}$$

or

$$V_s = \frac{V}{r_L + r_c} \cdot \frac{\rho l}{wd} \cdot \frac{\Delta N_s}{N} = Ir \frac{\Delta N_s}{N}, \tag{6}$$

where

ΔN_s = total number of additional electrons given by $\Delta n_s wld$, equal to $N(t) - N$,
N = number of electrons in the absence of signal,
$N(t)$ = instantaneous number of electrons.

The photodetector small signal properties are governed by[4]

$$\frac{d}{dt} \Delta N_s = A\eta_s J_s - \frac{\Delta N_s}{\tau}, \tag{7}$$

where

η_s = responsive quantum efficiency,
τ = electron-hole lifetime,
J_s = incident number of photons per unit area per second.

The solution of this equation for a sinusoidal signal of modulation frequency $f = \omega/2\pi$ is

$$|\Delta N_s(f)| = \frac{A\eta_s J_s \tau}{\sqrt{1 + (\omega\tau)^2}}. \tag{8}$$

The fractional change in conductivity is:

$$\frac{|\Delta N_s(f)|}{N} = \frac{\eta_s J_s \tau}{nd\sqrt{1 + (\omega\tau)^2}}. \tag{9}$$

The signal voltage is now

$$V_s = \frac{V}{r_L + r_c} \cdot \frac{\rho l}{wd} \cdot \frac{\eta_s J_s \tau}{nd\sqrt{1 + (\omega\tau)^2}}. \tag{10}$$

It is clear that signal response improves with longer lifetimes, improved quantum efficiencies, and decreasing equilibrium density of carriers.

B. Noise

There are five kinds of electrical noise that appear in the output of semiconducting photodetectors. They will be described below, briefly.

1. *Johnson Noise*

This type of noise is often referred to as Nyquist noise, since both Nyquist and Johnson treated this noise problem in 1928.[5,6] It can be expressed as:

$$\overline{v^2} = 4kTr\Delta f, \tag{11}$$

where

k = Boltzmann's constant,
T = absolute temperature,
Δf = electrical bandwidth,
r = resistance,
v = voltage, that is, $[v(t) - v_{av}]$.

2. *Generation-Recombination Noise*

This type of noise is inherent in the electronic system of semiconducting materials. All atoms in a lattice vibrate in an organized manner to the extent that their vibrations are quantized and can be described in particle terminology as "phonons." Valence-band electrons are continually jostled by the vibrations of the lattice atoms. Every so often, the nature and phasing of vibrations between atoms is such that an electron in their midst is able to gain enough energy to be freed from its bound (valence-band) state, and to move about in the conduction band. The electron is said to have suffered a phonon collision, and to have absorbed energy in the process.

When electrons leave the valence band for the conduction band, charge carriers (electrons and holes) become available for the purposes of current flow. The equilibrium number of carriers created increases with a crystal's temperature, and for any one temperature will be greater for diminishing forbidden energy gap. The thermal (phonon) excitation process is statistical in nature, and the rate at which electrons are excited to the conduction band fluctuates.

In addition to the statistical pulses of generation, we find that a similar situation exists for the recombination of carriers. The electrons and holes wander about the crystal lattice with some thermal motion, and, during a "lifetime" characteristic of the semiconductor material, get close enough together to recombine directly, or through a recombination center. The lifetime is a statistically fluctuating quantity, as is the instantaneous number of electrons and holes. Current carrier fluctuations are therefore inherent in any semiconductor. When a sample is placed in a constant-current electric circuit, one should expect, and in fact one does observe, conductivity fluctuations causing electrical noise completely described by the generation-recombination process.

Since this noise is a bulk property of the crystal, and is due to conductivity fluctuations caused by carrier density changes, it follows from Eq. (4) that

$$\Delta r = \frac{dr}{dn}\,\Delta n = \frac{\rho l}{wd}\cdot\frac{\Delta n}{n} = -\,\frac{\rho l}{wd}\cdot\frac{\Delta N}{N} \tag{12}$$

and

$$\overline{v^2} = I^2\cdot\overline{\Delta r^2}. \tag{13}$$

It can be shown that[7]:

$$\frac{\overline{(\Delta N)^2}}{N} = \frac{2\tau}{1 + (\omega\tau)^2}\cdot\Delta f. \tag{14}$$

Therefore,

$$\overline{v^2} = I^2\cdot r^2\cdot\frac{2\tau}{N[1 + (\omega\tau)^2]}\cdot\Delta f \tag{15}$$

or

$$\overline{i^2} = I^2\cdot\frac{2\tau}{N[1 + (\omega\tau)^2]}\cdot\Delta f \tag{16}$$

as shown by Van Vliet.[8]

3. *Current, 1/f, Modulation, and Excess Noise*

All of the names above have been used at various times as names for the same kind of noise. It is a noise that appears commonly in photodetectors in addition to the noise already discussed, and is generally found to have characteristics that can be described by the expression (see ref. 6):

$$\overline{i^2} = C\,\frac{I^2}{fAd}\cdot\Delta f, \tag{17}$$

where

I = total current through the sample,
f = frequency,
C = constant.

Actually, Eq. (17) is not universal in that cases have been cited where the current exponent has been found as small as 1.25 and as large as 4,[9] while the frequency exponent has ranged from 1 to 3.[10] However, these extreme exponential variations are not particularly common, and can usually be associated with a specific material, or to some unique treatment and physical condition of a material.[9]

The physical mechanism of this noise is the least understood of all the noise found to date. Petritz[11] introduced the name "modulation" noise to identify the mechanism as something quite different from simple carrier density fluctuations.

The modulation suggestion offered by Petritz, however, can still be only a part of the picture. Brophy and Rostoker,[12] Brophy,[13] and Bess[14] found with direct experimental evidence that the noise fluctuations in Hall voltage followed the same frequency dependence pattern as the noise from a conductivity measurement. It must be concluded, therefore, that, like conductivity, $1/f$ noise also follows the fluctuation in the density of the majority current carriers.

The location of a major source of $1/f$ noise (at least in the case of germanium filaments), has been found to be the surface of the crystal. Recent studies by MacRae[15] indicated that a surface inversion layer (a p-type surface on an n-type crystal or vice versa) is necessary to generate significant $1/f$ noise.

Although the surface provides $1/f$ noise, it is quite clear that this kind of noise can also be generated in the bulk material. Brophy[16] finds that, by plastic deformation, he can create noise sources and cause an increase of excess noise by orders of magnitude. These sources are uniformly distributed throughout the crystal, and also contribute an unusual I^4 dependence. Bess[17] assumed that the noise was due to edge dislocations with impurities diffusion along the edge. Such distributions throughout the bulk can provide noise spectra similar to that obtained by inversion surface layers.[18] Even when surfaces are treated so that their noise contribution is minimized, and bulk sources are removed, residual $(1/f)$ noise may still exist. This noise has been associated with nonohmic contact regions, probably due to minority carrier drift across the contacts. Thus the sources of $1/f$ noise can be found at the surface, in the bulk, and at the electrical contacts of a detector.

4. *Shot Noise*

This noise is usually associated with vacuum tubes; it is described as the electrical noise that appears in the output of a vacuum tube when the grid, if any, is held at a fixed potential. However, it is more precisely described in what is usually called the temperature-limited condition. By temperature limited, it is meant that the anode voltage on the tube is sufficient to collect all of the electrons emitted from the cathode. Consider a temperature-limited diode connected to a resistance r. Because of the discreteness of the electronic charge, the number of electrons emitted at equal time intervals will fluctuate around an average value. The fluctuating current causes a fluctuating voltage across r which can be amplified and measured. The mean square current fluctuation turns out to be constant up to frequencies of approximately the reciprocal of the transient time, and can be described by

$$\overline{I^2} = 2eI\Delta f, \tag{18}$$

where e is the electronic charge and I is the bias current.[19]

Semiconductor photovoltaic detectors and back-biased p-n junctions operating in a photoconductive circuit also exhibit shot noise. In a p-n junction diode, a space charge region is developed across the barrier and an associated electric field. Electrons or holes created by phonons or the absorption of background photons, diffusing into the barrier region, are swept from the n-type material to the p-type material, or vice versa. This results in current pulses appearing across the diode with the same characteristics that are observed for the vacuum tube.

Petritz (see ref. 7) has developed a theory applicable to the lead chalcogenide (PbS, PbSe, PbTe) photoconductive films, which is suitable for use here. These films are composed of a system of tiny crystallites separated by intercrystalline barriers, where space charge regions exist. The barrier regions contribute both Johnson and shot noise, while the crystallites generate the usual Johnson noise. For thin barriers, compared to the carrier diffusion length, the barrier contribution to shot noise is given by

$$\overline{v^2} = \frac{2er_c^2I}{n_l l}\cdot\Delta f, \tag{19}$$

where n_l is the number of crystallites per unit length, and r_c is the detector resistance.

5. *Background-Radiation Noise*

Background radiation can be thought of as a stream of photons originating from the detector environment. The cell walls surrounding the detector, its window, and the media viewed by the detector through the cell window all contribute to this radiation. The extent of the individual contributions is determined by their respective temperatures, emissivities, and geometry.

Photons originating from the background and impinging on the detector arrive and are absorbed in a statistically fluctuating manner. This results in a well-defined type of electrical noise. When this is the predominant noise, the photodetector is said to be "background radiation-noise limited." The generation of carriers by this process follows the same statistical law as the G-R noise. Thus the equilibrium density of carriers is given by $N_L = 2A\eta_L J_L \tau$, and the background-limited case is given by $N_B = 2A\eta_B J_B \tau$. The factor 2 arises from the generation of two carriers (an electron and a hole) for each photon, and

N_L, N_B are the equilibrium density of carriers generated by G-R, and background radiation, respectively;

η_L, η_B are the efficiency factors for the conversion of phonons and photons to carriers, respectively; and

J_L, J_B are the lattice flux and the radiation flux, respectively.

The complete expression that describes the fluctuation in carrier density, for the case of equilibrium where generation processes are equal to recombination processes, is given by Petritz[4,7] and Eq. (14) as:

$$\overline{\Delta N^2{}_{\text{noise}}} = \frac{4\tau^2\cdot\Delta f\cdot A(\eta_B J_B + \eta_l J_l)}{1 + (\omega\tau^2)}. \tag{20}$$

III. Noise Equivalent Power

Consider an infrared detector exposed to some incident radiation in a circuit which provides an electrical signal voltage proportional to the radiant power. Assume also that the dominant electrical noise in the circuit is generated by the detector, not the preamplifier. Let the rms radiant power P be expressed as $H\cdot A$, where H is the rms irradiance and A is the area of the detector. The absorption of power P by the detector results in a signal voltage V_S in the circuit. When the power source is removed or masked, and the detector allowed to see only the background, then a noise voltage V_N is obtained. The predominant mechanism causing this noise might be internal to the detector, such as from Johnson, shot, and/or lattice-governed G-R noise sources. In the case of the best detectors, this noise might well be governed by the fluctuations in photon flux irradiating the detector, that is, the background radiation-noise limited condition. A simple proportionality can be set up, relating these voltage readings and the power P:

$$\frac{\text{NEP}}{V_N} = \frac{H \cdot A}{V_S}. \tag{21}$$

Thus if Johnson noise is responsible for V_N, the NEP represents the amount of power that would have to fall onto the detector to generate a voltage equivalent to V_N. This relationship is more usually observed in the form:

$$\text{NEP} = \frac{H \cdot A}{V_S/V_N} \tag{22}$$

Clearly, NEP is also the power exposure required by the detector to obtain a signal-to-noise voltage ratio of unity.

A relatively simple analysis can be first attempted for the purpose of providing some insight to the area dependence of NEP. Assume first a simple detector in a circuit, from which is obtained a signal voltage V_S and a noise voltage V_N. The noise voltage is assumed due to a uniform distribution of noise sources throughout the bulk of the detector. Consider two of these detectors placed adjacent to one another (end to end) and connected electrically in series. The total signal voltage is simply $V_{S1} + V_{S2}$, since the signals are coherent. The noise voltages add as their mean squares, since they are incoherent. The noise voltage of each unit is the rms value of the voltage fluctuation, or $V_n = \sqrt{\overline{v^2}}$, where

$$v = v(t) - v_{av} \tag{23}$$

and $v(t)$ is the instantaneous value of the noise voltage and v_{av} is the average value. The signal-to-noise ratio from the combined units is:

$$\frac{V_{ST}}{V_{NT}} = \frac{V_{S1} + V_{S2}}{(V_{N1}^2 + V_{N2}^2)^{1/2}}. \tag{24}$$

If the two detectors are identical in area and thickness, $V_{S1} = V_{S2}$, and equal noise is generated by each of them. Then:

$$\frac{V_{ST}}{V_{NT}} = \frac{2V_{S1}}{\sqrt{2}\,V_{N1}} = \sqrt{2}\,\frac{V_{S1}}{V_{N1}}. \tag{25}$$

Suppose these two detectors are now placed side by side, and connected electrically in parallel. Since currents can be added in a straightforward manner when dealing with parallel circuits, consider the noise sources as current generators. The total noise becomes (similarly to the noise voltage analysis):

$$I_{NT}^2 = I_{N1}^2 + I_{N2}^2 \tag{26}$$

and for identical detectors:

$$I_{NT} = \sqrt{2I_{N1}^2}. \tag{27}$$

The signal current is now:

$$I_{ST} = I_{S1} + I_{S2} = 2I_{S1}. \tag{28}$$

The signal-to-noise current ratio becomes

$$\frac{I_{ST}}{I_{NT}} = \frac{2I_{S1}}{\sqrt{2}\,I_{N1}} = \sqrt{2}\,\frac{I_{S1}}{I_{N1}}. \tag{29}$$

The noise current can be expressed as a noise voltage by simply multiplying the total noise current by the effective resistance of the circuit. Therefore:

$$r_t = \frac{r_1 r_2}{r_1 + r_2} = \frac{r_1}{2} \tag{30}$$

for $r_1 = r_2$, and

$$V_{NT}^2 = I_{NT}^2 r_T^2 = \frac{I_{N1}^2 r_1^2}{2} \tag{31}$$

or

$$V_N = \frac{1}{\sqrt{2}} \cdot I_{N1} \cdot r_1.$$

The signal voltage is $V_{ST} = V_{S1} = V_{S2}$, since the circuit is now equivalent to two identical batteries placed in parallel. Then

$$\frac{V_{ST}}{V_{NT}} = \frac{I_{S1} \cdot r_1}{(1/\sqrt{2}) \cdot I_{N1} \cdot r_1} = \sqrt{2}\,\frac{V_{S1}}{V_{N1}}. \tag{32}$$

The analysis can readily be extended to three or more detector units. It is immediately apparent from the treatment with two units, however, that with either the series or parallel arrangement, the signal-to-noise ratio depends on the square root of the total detector area. This then indicates that the NEP of a detector should also depend on the square root of the area. The conclusions drawn are valid only for the special case of a uniform photoresponse and distribution of noise sources across the detector surface. It will also apply if the noise sources are uniformly distributed throughout the bulk of the detector. If a square-root areal dependence is not obtained for a particular detector type, then the generation of noise and/or signal is undoubtedly variable across the detector surface.

A detailed analysis of the dependence of NEP on area, for the various noise-limited cases, will be developed here starting with the definition of NEP, Eq. (22). The procedure followed will be to substitute appropriate expressions for the signal and noise voltages in this equation and to generate an equation which delineates the geometry, time constant, and bandwidth dependence of NEP. The factor for the incident power will be $H \cdot A$ where H is the irradiance, and the signal voltage is as given by Eqs. (2) and (10). Therefore:

$$\mathrm{NEP} = HA \frac{V_N}{I \cdot \frac{\rho l}{wd} \cdot \frac{\eta_s J_s \tau}{nd\sqrt{1 + (\omega\tau)^2}}}, \tag{33}$$

where V_N is the rms value of the noise fluctuation, that is, $V_N = \sqrt{\overline{v_N{}^2}}$.

A. NEP—Johnson-Noise Limited

Inserting Eq. (11) into Eq. (33), and using

$$\begin{aligned} \tau &= \rho l/wd, \\ I &= iwd, \\ i &= \sigma E, \\ E &= \text{electric field strength}, \\ \sigma &= 2ne\mu, \\ \mu &= D \cdot e/kT, \\ D &= L^2/\tau, \end{aligned}$$

gives

$$\mathrm{NEP} = K_1 \sqrt{\frac{A \cdot \Delta f \cdot (1 + \omega^2\tau^2)}{\tau}} \tag{34}$$

and

$$K_1 = \frac{kT\sqrt{2nd}}{e\eta_s J_s EL} \cdot H. \tag{35}$$

Thus the relationship between NEP, area, time constant, and bandwidth is clearly spelled out for the Johnson-noise limited case by:

$$\mathrm{NEP} \; \alpha \sqrt{\frac{A \cdot \Delta f}{\tau}}. \tag{36}$$

B. NEP—G-R and Background Noise Limited

In this particular case, it is informative to rewrite Eq. (33), using Eq. (6), to obtain:

$$\mathrm{NEP} = HA \cdot \frac{V_N}{V_S} = HA \frac{I\tau\sqrt{\overline{\Delta N^2{}_{\text{noise}}}/N}}{I\tau(\Delta N_{\text{sig}}/N)}, \tag{37}$$

$$\mathrm{NEP} = HA \frac{\sqrt{\overline{\Delta N^2{}_{\text{noise}}}}}{\Delta N_{\text{sig}}}. \tag{38}$$

Substituting Eq. (20) and Eq. (8) in Eq. (38) gives:

$$\mathrm{NEP} = K_2 \sqrt{A \cdot \Delta f}, \tag{39}$$

$$K_2 = 2H \frac{\sqrt{\eta_B J_B + \eta_l J_l}}{\eta_s J_s}. \tag{40}$$

In this instance, the signal and noise voltages are identically dependent on bias current flow, so that NEP is independent of this factor. Here the square-root areal dependence of NEP arises from the averaging process required in arriving at the value for the mean-square fluctuation in carriers generated at random by the background photons and lattice phonons. Notice that NEP in this case does not depend upon the time constant. This is due to the behavior of the detector now being controlled by the same processes for signal and noise. Both the quantities ΔN_{sig} and $\sqrt{\overline{\Delta N^2{}_{\text{noise}}}}$ are linearly dependent on τ. Their ratio being independent of τ means that the detector will respond equally well in frequency to background photons and signal photons.

C. NEP—Excess 1/*f*-Noise Limited

Inserting Eq. (17) into Eq. (33) provides:

$$\mathrm{NEP} = \frac{K_3}{\tau} \cdot \sqrt{\frac{A\Delta f(1 + \omega^2\tau^2)}{f}} \tag{41}$$

and

$$K_3 = \frac{nH\sqrt{C}d}{\eta_s J_s}. \tag{42}$$

In this instance, both the signal and noise are associated with bias currents. However, even though a complete understanding of the source of $1/f$ noise is not yet available, it is clear that, for a uniform generation of noise throughout the bulk and/or surface of the detector, the NEP will depend upon the square root of the detector area. In addition, NEP will vary as $f^{-1/2}$.

D. NEP—Shot-Noise Limited

Substituting Eq. (19) into Eq. (33) and using

$$I = \sigma Ewd = 2ne\mu^* Ewd,$$

$$\mu^* = \frac{L^2}{kT} \frac{e}{\tau},$$

where u^* is an average reduced mobility for carriers in the detector film, and L is the carrier diffusion length, it follows that:

$$\mathrm{NEP} = K_4 \sqrt{\frac{A\Delta f(1 + \omega^2\tau^2)}{\tau}} \tag{43}$$

and

$$K_4 = \frac{H}{\eta_s J_s L} \sqrt{\frac{dnkT}{eEn_l}}. \tag{44}$$

E. Summation

In all noise-limited conditions examined here, NEP is clearly dependent on the square root of the area (as expected from the geometrical arguments above) and on the square root of the bandwidth. The time constant and frequency dependencies of shot-noise-limited and Johnson-noise-limited detectors are identical.

This should be expected since both noise spectra are essentially flat. The factor in the NEP expression denoting this identical condition is

$$\sqrt{\frac{1 + (\omega\tau)^2}{\tau}}.$$

The case of $1/f$ noise provides a factor given by

$$\sqrt{\frac{1 + (\omega\tau)^2}{f}} \cdot \frac{1}{\tau},$$

while G-R noise leads to an expression independent of frequency and time constant. Finally, the background-noise-limited NEP does not contain any factors associated with a detector mechanism of operation. This should be expected since a detector measuring background noise is limited by that external noise, and thereby loses its identity. In other words, any number of different detectors operating with the same spectral characteristics could not be distinguished from one another in terms of NEP, if they were all limited by background noise. If the detectors are G-R phonon noise limited, then $J_L \gg J_B$. This condition can be identified by changing the detector's temperature and observing corresponding changes in noise. If the detector is background limited, then $J_B \gg J_L$, and changes in the background temperature would cause observable changes in the detector noise.

IV. Jones System of Classification

Jones[20] has contributed a substantial effort to the understanding and categorizing of infrared detectors. He suggested that the reciprocal of NEP, denoted as "detectivity," was a more suitable quantity for rating detectors. It represents primarily a psychological asset, in that larger detectivities, rather than smaller NEP's represent better detectors. Jones considers "detectivity" particularly desirable because it also avoids usage of the word "sensitivity," which has a variety of meanings in technical language. For the sake of completeness, a summary of the parts of Jones' paper (see ref. 1) pertinent to discussions here will be included below.

Jones observed that when data taken from thermal and photodetectors were examined, they could be distinguished or classified by the way in which their detectivity is related to time constant and frequency response. He noted that their behavior in one case is like the detectivity obtained for an ideal thermal detector, while in another, to an estimated best obtainable thermal detector. Accordingly, two classes of detectors were set up, the first based on the detectivity obtained for the ideal detector (capable of seeing background thermal or photon noise), while the second was based on the best obtainable heat detector from Havens' limit (see ref. 20).

In establishing this system of classification, a reference or detective time constant and a bandwidth are defined, such that $\Delta f = 1/4t$. These reference conditions are to provide a measurement of the detectivity for the important special case where the bandwidth of the noise is the same as the bandwidth of the detector. Thus if a detector has a response out to some upper limit of frequency f, the bandwidth of the noise extends out to the same frequency. For the purposes of the ensuing discussion of the various noise-limited cases, it will also be assumed that the detector is limited only by the type of noise singled out for analysis in any one particular case, throughout the responsive bandwidth of the detector. The classifications established by Jones are:

Class I: $$D = k_1 \frac{\sqrt{\tau}}{\sqrt{A}}, \qquad (45)$$

Class II: $$D = k_2 \frac{\tau}{\sqrt{A}} \qquad (46)$$

Detectors limited by a flat noise spectrum such as Johnson noise have a detectivity in a unit bandwidth classified as:

Class Ia: $$D_1(f) = \frac{k_1}{2\sqrt{A}\,\sqrt{1 + (\omega\tau)^2}}, \qquad (47)$$

Class IIa: $$D_1(f) = \frac{k_2\sqrt{\tau}}{2\sqrt{A}\,\sqrt{1 + (\omega\tau)^2}} \qquad (48)$$

In the case of the $1/f$-noise-limited detector, Jones finds it necessary to redefine the reference time constant, and in so doing the detectivities take the form:

Class Ib: $$D_1(f) = \frac{2k_1\sqrt{\pi}\,\sqrt{f\tau}}{\sqrt{A}\,\sqrt{1 + 16(\omega\tau)^2}}, \qquad (49)$$

Class IIb: $$D_1\, f) = \frac{2k_2\sqrt{\pi}\,\sqrt{f\cdot\tau}}{\sqrt{A}\,\sqrt{1 + 16(\omega\tau)^2}}. \qquad (50)$$

In Section III, analytical expressions were derived for NEP in the various noise-limited conditions. They can now be used to develop Jones' system of classification. Furthermore, it will suffice to use here the detector's responsive time, rather than Jones' reference time constant.

A. Detectivity—Johnson-Noise Limited

This detectivity is derived from Eq. (34). Thus

$$D = \frac{1}{\text{NEP}} = \frac{1}{K_1}\frac{\sqrt{\tau}}{\sqrt{A\cdot\Delta f}}\cdot\frac{1}{\sqrt{1+(\omega\tau)^2}} \qquad (51)$$

and, in a unit bandwidth, becomes

$$D_1 = k_1 \frac{\sqrt{\tau}}{\sqrt{A}\,\sqrt{1 + (\omega\tau)^2}} \qquad (52)$$

which is defined as a class IIa detector. In the bandwidth $\Delta f = 1/(4\tau)$, for $\omega\tau \ll 1$, the detectivity becomes

$$D = k_1' \frac{\tau}{\sqrt{A}} \qquad (53)$$

which is the form of the class II detector.

B. Detectivity—G-R-Noise Limited

In this case, both signal and noise depend on the frequency in the same manner. Thus the expression for NEP was found to be independent of the factor $\sqrt{1 + (\omega\tau)^2}$, and the detectivity is derived from Eq. (39) to be

$$D = \frac{1}{K_2} \cdot \frac{1}{\sqrt{A \cdot \Delta f}} \cdot \tag{54}$$

The detectivity in the reference bandwidth takes the form

$$D = k_2' \sqrt{\frac{\tau}{A}} \tag{55}$$

which is a class I detector.

C. Detectivity—Excess, 1/*f*-Noise Limited

This detectivity is derived from Eq. (41).

$$D = \frac{1}{\text{NEP}} = \frac{1}{K_3} \frac{\tau_p}{\sqrt{1 + (\omega\tau_p)^2}} \cdot \sqrt{\frac{f}{A \cdot \Delta f}} \tag{56}$$

and, for a unit bandwidth,

$$D_1 = \frac{1}{K_3} \frac{\tau_p}{\sqrt{1 + (\omega\tau_p)^2}} \sqrt{\frac{f}{A}} \cdot \tag{57}$$

The constant τ_p is the detector responsive time constant. Jones defines a reference time constant $\tau = \tau_p/4$. Using this time constant, it follows that:

$$D_1 = k_3 \cdot \frac{\tau\sqrt{f}}{\sqrt{1 + 16(\omega\tau)^2}} \cdot \frac{1}{\sqrt{A}} \tag{58}$$

which is the form of the class IIb detector.

D. Detectivity—Shot-Noise Limited

This detectivity is derived from Eq. (43).

$$D = \frac{1}{K_4} \frac{\sqrt{\tau}}{\sqrt{1 + (\omega\tau)^2}} \frac{1}{\sqrt{A \cdot \Delta f}} \cdot \tag{59}$$

Shot noise has a flat frequency spectrum, and provides a detectivity in a unit bandwidth similar to Johnson noise:

$$D_1 = \frac{k_4(\tau/A)^{1/2}}{\sqrt{1 + (\omega\tau)^2}} \tag{60}$$

and, in the responsive bandwidth,

$$D = \frac{k_4'}{\sqrt{1 + (\omega\tau)^2}} \frac{\tau}{\sqrt{A}} \tag{61}$$

and

$$D = k_4' \cdot \frac{\tau}{\sqrt{A}} \tag{62}$$

for $\omega\tau \ll 1$, which is the form of a class II detector.

E. Figures of Merit

By taking the ratio of the detectivity of class I detectors to that of the perfect thermal detector (limited by photon noise), Jones derives a figure of merit called M_1 (see ref. 1), expressed as:

$$M_1 = 2.76 \times 10^{-11} \times \frac{D\sqrt{A}}{\sqrt{\tau}} \cdot \tag{63}$$

A figure of merit for the class II detector was derived using Havens' limit as the reference detector.[21] Havens arrived at his estimate by treating such thermal detectors as heat engines, considering their operation from a theoretical analysis of the efficiency of such engines, and arriving at an ultimate limit of performance capability by including considerations of limiting noise, available materials, and techniques. On this basis, the class II figure of merit becomes:

$$M_2 = 3 \times 10^{-11} \times \frac{D\sqrt{A}}{\tau}. \tag{64}$$

F. *D*-Star (*D**)

The expressions for detectivity, for the different limiting-noise types, always contain the factor $1/\sqrt{A \cdot \Delta f}$. Therefore, they are a function of detector size and the electrical bandwidth of operation. A more useful number is one that establishes the performance of the detector independent of these quantities. Jones suggested that the quantity D^*, defined as

$$D^* = \frac{\sqrt{A\Delta f}}{\text{NEP}} = D\sqrt{A \cdot \Delta f}, \tag{65}$$

serves to characterize the detector in terms of the intrinsic properties of the material of which it is made (see ref. 2).

V. Discussion

The discussions carried out in Sections II to IV indicate that a considerable gain in understanding the noise properties of semiconducting photodetectors has been made since the Jones paper of 1953. The resultant analysis carried out in these sections indicates the following:

A. General

1. Class I detectors are limited by background and G-R noise.

2. Class II detectors are limited by all other sources of noise.

3. A class II detector can become a class I detector if its performance is improved to the point that background or G-R noise predominates over any other noise source. This can often be done by cooling a good detector. It appears that, when a detector becomes background limited, it loses its identity. The NEP

is descriptive of the rms fluctuation in background photons striking the detector. Thus the performance of the detectors is completely described by the condition of the background. If a number of different detectors, all having the same spectral response characteristics, were background limited, they could not be identified individually on the basis of NEP, D, D^*, or a class I designation. This would be so even though they might be made of different materials and/or have different time constants.

4. The significance of the figures of merit M_1 and M_2 is not clear, particularly in reference to Havens' limit. Since a detector can go from class II to class I, the reference might well be to the background-limited condition in both cases.

5. In a recent statistical analysis of the NEP's reported on lead-compound film detectors, Limperis and Wolfe[22] reported that these excess-noise-limited detectors follow an $(A)^{1/2}$ in accordance with the treatment of Section 3. Until about 1956, data did not clearly indicate a consistent geometry dependence for NEP. There were two factors which prevented obtaining consistent data:

(a) In bulk and film detectors, limiting-noise sources were not uniformly distributed through the detector. That is, most of the noise was generated at the electrodes around the detector periphery, localized regions on the crystal's surface, and similarly within the bulk.

(b) The photoresponse was generally nonuniform across a detector surface. The film detectors are particularly difficult to deal with in this regard.

It appears that detector technology has improved to the point where noise generation and signal response is sufficiently uniform to indicate a square-root areal dependence of NEP.

B. Units

The units of D^* have received considerable attention, and at one time were a matter of controversy. Jones' original definition of D^* appeared in the form

$$D^* = \sqrt{\frac{A}{1\ \text{cm}^2} \cdot \frac{\Delta f}{1\ \text{cps}}} \cdot \frac{1}{\text{NEP}}. \tag{66}$$

Thus it appeared that the definition normalized D^* to a unit area and bandwidth, and that the unit of D^* was reciprocal watts. This unit seemed appropriate since D^* was an intrinsic measure of a material's ability to detect radiation power. However, considerable opposition arose to the normalization procedure suggested by Jones, and the units ultimately accepted were those that appear in a straightforward examination of dimensions, namely cm·(cps)$^{1/2}$·watts^{-1}. These units might appear somewhat peculiar in that D^* is supposed to provide a measure of the intrinsic ability of a detector material to respond to radiation power and yet contains the dimensions of size and frequency. However, a recent analysis of a substantial amount of data indicates that D^* appears to do its job. An explanation of this seeming contradiction comes from an examination of the equations derived earlier for NEP in the various noise-limiting cases.

Consider the background-noise-limited case where, from Eq. (39),

$$\text{NEP} = \frac{\sqrt{J_b \eta_b}}{\eta_s J_s} \cdot 2H \cdot \sqrt{A \cdot \Delta f}. \tag{67}$$

The factor $\sqrt{A \cdot \Delta f}$ cancels out in the computation of D^*, so that the remaining factors provide the units. The quantities η_b and η_s are efficiency factors. Therefore, the dimensional analysis is simplified to:

$$D^* = \frac{J_s}{\sqrt{J_b}} \cdot \frac{1}{H} = \frac{\text{No. photons}_s/\text{cm}^2\ \text{sec}}{\sqrt{\text{No. photons}_b/\text{cm}^2\ \text{sec}}} \cdot \frac{\text{cm}^2}{\text{watt}}$$
$$= \frac{\text{cm}}{\sqrt{\text{sec}}} \cdot \frac{1}{\text{watts}} = \frac{\text{cm}\sqrt{\text{cps}}}{\text{watts}} \tag{68}$$

since the numbers of photons are dimensionless, and the reciprocal of time is equivalent here to a frequency. The derived units of D^* becomes cm(cps)$^{1/2}$ watts^{-1}, consistent with accepted usage.

An interpretation of the meaning of the units of D^* can now readily be put forth. In the measurement of NEP, radiation power from a blackbody illuminates a detector to generate a signal voltage V_S. A noise voltage V_N is obtained when the detector views an ambient black background. V_N may result from background fluctuations or noise sources internal to the detector. In the background-limited case, it was shown above that D^* is dependent only on the factors J_s, J_b, and H, while being explicitly independent of area and bandwidth. These are all factors in the measurement procedure, and the units of D^* can be attributed to J_s, J_b, and H. Since these quantities represent the numbers of photons and watts per unit area, it is clear that the measurement is inherently normalized. Thus if one wishes to perform a series of measurements in which the bandwidth and/or the area were variables, the experiment would be carried on at constant J_s, J_b, and H. The evaluation of D^* in this situation is truly independent of detector area. It appears, therefore, that Jones' judgment or the significance of D^* was correct.

It is fruitful to examine the units of D^* in the Johnson and shot-noise-limited cases. The appropriate expressions can be obtained by inserting Eqs. (34) and (43) into Eq. (65) respectively. They are: for D^* limited by Johnson noise:

$$D^* = \frac{\eta_s J_s e E L}{\sqrt{2nd\,kTH}} \cdot \sqrt{\frac{\tau}{1 + (\omega\tau)^2}}, \tag{69}$$

for D^* limited by shot noise:

$$D^* = \sqrt{\frac{L^2 eEn_l}{ndkt}} \cdot \frac{\eta_w J_s}{H} \cdot \sqrt{\frac{\tau}{1 + (\omega\tau)^2}}. \tag{70}$$

In the Johnson-noise case, the quantities eEL and kT represent electrical and thermal energies, and have the same basic units. Separating out these factors for the dimensional analysis, and omitting all numerical factors, results in

$$D^* = \frac{eEL}{kT} \cdot \frac{1}{\sqrt{nd}} \cdot \frac{J_S}{H} \cdot \sqrt{\tau}. \tag{71}$$

Substituting units provides:

$$D^* = \frac{\text{Energy}_{\text{(elect)}}}{\text{Energy}_{\text{(therm)}}} \cdot \frac{1}{\sqrt{1/\text{cm}^2}} \cdot \frac{\text{No. photons/area} \cdot \text{time}}{\text{watts/area}} \cdot \sqrt{\text{time}}$$

$$= \frac{\text{Energy}_{\text{(elect)}}}{\text{Energy}_{\text{(therm)}}} \cdot \frac{\text{cm}}{\text{watts}} \cdot \frac{1}{\sqrt{\text{time}}}, \tag{72}$$

$$D^* = \frac{\text{cm}\sqrt{\text{cps}}}{\text{watts}}. \tag{73}$$

In the case of shot noise, the quantity $n_l \cdot L$ is unitless, eEL is an electrical energy, and D^* can be expressed dimensionally as:

$$D^* = \sqrt{\frac{\text{Energy}_{\text{(elect)}}}{\text{Energy}_{\text{(therm)}}}} \cdot \text{cm}\ \frac{\text{No. photons/area} \cdot \text{time}}{\text{No. watts/area}} \cdot \sqrt{\text{time}}.$$

On simplifying:

$$D^* = \sqrt{\frac{\text{Energy}_{\text{(elect)}}}{\text{Energy}_{\text{(therm)}}}} \cdot \frac{\text{cm}}{\text{watts}} \cdot \frac{1}{\sqrt{\text{time}}}, \tag{74}$$

$$D^* = \frac{\text{cm}\sqrt{\text{cps}}}{\text{watts}} \tag{75}$$

It is clear that units are consistently maintained for D^* in the different noise-limited cases. An interesting feature of this examination reveals that the ratio of an electrical energy to a thermal energy appears as a factor for the Johnson-noise-limited case, and the square root of this quantity appears in the shot-noise case. This is consistent with different noise mechanisms responsible for the two cases. In both cases, an increasing bias voltage and a decreasing temperature should result in increasing D^*. The density of carriers n is also dependent on T, and decreases with reduced temperature. However, reduced T can also effect the magnitude of the energy gap, change the cutoff wavelength, and also affect the time constant τ. These apparently are the factors that are adjustable. In particular, when seeking the optimum bias for a photoconductive detector, it may well be a manner of raising the bias until an increased temperature from Joule heating results. Further biasing could cause adverse temperature effects, and therefore a reduced D^*.

The author wishes to thank T. Limperis and G. H. Suits for their helpful suggestions in reviewing the manuscript.

References

1. R. C. Jones, *Advances in Electronics* (Academic Press Inc., New York, 1953).
2. R. C. Jones, J. Opt. Soc. Am. **50,** 1058 (1960).
3. The photoconductive detector has also been treated in considerable detail by D. H. Roberts and B. L. H. Wilson, Brit. J. Appl. Phys. **9,** 291 (1958).
4. R. L. Petritz, Proc. IRE **47,** 1458 (1959).
5. J. B. Johnson, Phys. Rev. **32,** 97 (1928).
6. H. Nyquist, Phys. Rev. **33,** 110 (1928).
7. R. L. Petritz, Phys. Rev. **104,** 1508 (1956). See also ref. 4.
8. K. M. Van Vliet, Proc. IRE **46,** 1004 (1958).
9. J. J. Brophy, J. Appl. Phys. **27,** 1383 (1957).
10. T. G. Maple, L. Bess, and H. A. Gebbie, J. Appl. Phys. **26,** 490 (1955).
11. R. L. Petritz, Proc. IRE **40,** 1440 (1952).
12. J. J. Brophy and N. Rostoker, Phys. Rev. **100,** 754 (1955).
13. J. J. Brophy, Phys. Rev. **106,** 675 (1957).
14. L. Bess, J. Appl. Phys. **26,** 1377 (1955).
15. A. U. MacRae and H. Levinstein, Phys. Rev. **119,** 62 (1960).
16. J. J. Brophy, J. Appl. Phys. **27,** 1383 (1956).
17. L. Bess, Phys. Rev. **103,** 72 (1956).
18. J. R. Morrison, Phys. Rev. **104,** 619 (1956).
19. A. Van der Ziel, Proc. IRE **46,** 1019 (1958).
20. R. C. Jones, Proc. IRE **47,** 1495 (1958). See also ref. 1.
21. R. J. Havens, J. Opt. Soc. Am. **36,** 355(A) (1946).
22. T. Limperis and W. Wolfe, J. Opt. Soc. Am. **51,** 482 (1961).

ANNUAL SUBSCRIPTIONS

Per volume of six issues per year

OSA members	$ 6.00
Other AIP societies' members	$ 8.00
Non-members and libraries	$10.00
Single copies	$ 2.00

Subscriptions should be addressed to APPLIED OPTICS Subscription Handling, American Institute of Physics, 335 East 45th Street, New York, New York.

A Study of the Angular Response of Lead Sulfide Photoconductors

Gustave J. Schaefer

The response of lead sulfide photoconductors to a uniform field of monochromatic radiation, which was varied in wavelength from 0.4 to 3.0 μ and in angle of incidence from 0° to 80°, has been experimentally investigated and compared with derived response curves. Deviations from the ideal cosine response of up to 20% at 70° incidence were effected mainly by reflection losses from the detecting surface and by characteristics of the substrate. The results suggest that the grain size of the polycrystalline lead sulfide may considerably influence the reflection losses. Methods of correcting the observed deviations are discussed.

Introduction

A survey of the literature has revealed a paucity of papers dealing with the angular response of radiation detectors as a function of wavelength. While in spectroscopy this information is not needed because the detector is customarily mounted normal to the radiation, there are now applications, for example reflectometers and military sensors, where the detector must view a nearly hemispherical radiation field.

At discrete wavelengths through the range 0.4 to 3.0 μ lead sulfide photoconductive films were rotated in the beam of a monochromator to obtain their responses from 0° to 80° angle of incidence. The physical characteristics of the detectors were varied in an attempt to define individual causes for deviations from derived response curves based on the electromagnetic theory and published optical constants for lead sulfide.

Since a perfectly nondirectional detector in a uniform, unidirectional radiation field would have a response always directly proportional to the cosine of the incidence angle, both the observed and derived response curves are normalized with respect to a cosine response.

Derived Response

The normalized response of an actual detector can be expressed as

$$F(\theta) = \frac{S_\theta}{S_0 \cos\theta}, \tag{1}$$

where S is the response while θ and 0 refer to oblique and normal incidence, respectively. A theoretical approximation to Eq. (1) is[1]

$$F(\theta) = \frac{(1 - r_\theta - t_\theta) g_\theta y_\theta H_\theta}{(1 - r_0 - t_0) g_0 y_0 H_0 \cos\theta}, \tag{2}$$

where H is the incident flux in photons per second; t is the fraction transmitted; r is the fraction reflected; g is the number of excitations per absorbed quantum; and y is the photoconductive yield, or the number of electronic charges passed in the external circuit per charge carrier excited. It will be assumed that

$$\begin{aligned} g_\theta &= g_0, \\ y_\theta &= y_0, \\ H_\theta &= H_0 \cos\theta, \end{aligned}$$

and since by Bouguer's exponential law of absorption

$$t = (1 - r)e^{-Kx},$$

Eq. (2) can now be written as

$$F(\theta) = \frac{(1 - r_\theta)(1 - e^{-Kx})}{(1 - r_0)(1 - e^{-Kd})}, \tag{3}$$

where K is the absorption coefficient, x is the path length through the lead sulfide film, and d is the film thickness. Lead sulfide's high absorption coefficient[2] and large index of refraction,[3] which result in x being only slightly larger than d even for large angles of incidence, give transmission losses a negligible role in the expression for $F(\theta)$. For a lead sulfide film thickness of 0.75 μ, neglect of transmission losses causes errors which vary from less than 0.01% at 0.4 μ wavelength and 70° to 2% at 3.0 μ and 70°. Thus, a good approximation to Eq. (3) is

---

The author is in the Light Military Electronics Department, General Electric Company, Utica, N. Y.

Received 28 February 1962.

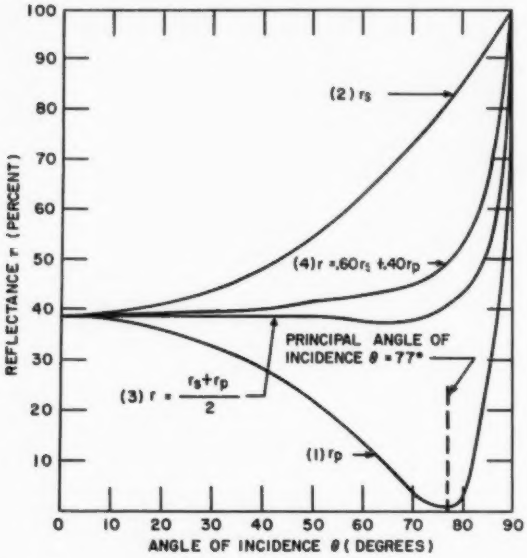

Fig. 1. Calculated reflectance curves for crystalline PbS when the incident radiation at 0.8 μ is: (1) plane polarized parallel to the plane of incidence, (2) plane polarized perpendicular to the plane of incidence, (3) unpolarized, (4) polarized as that measured in the P.E. 13U spectrophotometer beam at 0.8 μ.

$$F(\theta) = \frac{1 - r_\theta}{1 - r_0}. \tag{4}$$

If the index of refraction, the absorption coefficient, and the polarization of the incident radiation are known as a function of wavelength, the reflection coefficients can be calculated for various angles of incidence and wavelengths by use of the electromagnetic theory.[4,5] Convenient approximate expressions are given[4] as

$$r_s = \frac{n^2(1 + k^2) - 2n\cos\theta + \cos^2\theta}{n^2(1 + k^2) + 2n\cos\theta + \cos^2\theta}, \tag{5}$$

$$r_p = \frac{n^2(1 + k^2)\cos^2\theta - 2n\cos\theta + 1}{n^2(1 + k^2)\cos^2\theta + 2n\cos\theta + 1}, \tag{6}$$

where

r_s = reflectance of the incident component that is perpendicular to the plane of incidence,
r_p = reflectance of the parallel component,
n = index of refraction of the reflecting medium,
k = $K\lambda/4\pi n$ = absorption index of the reflecting medium,
θ = angle of incidence.

Equations 5 and 6 were used to calculate the reflectance of lead sulfide as a function of the angle of incidence at a wavelength of 0.8 μ. The resulting curves are shown in Fig. 1. The average of the ordinates for the r_s and r_p curves at each angle gives the reflectance of unpolarized radiation. The calculated reflectance curve for the polarization found in the spectrophotometer beam at 0.8 μ, which was near the maximum as shown in Fig. 2, is also plotted in Fig. 1. The values for Fig. 1 were found by using the relation

$$r = sr_s + pr_p, \tag{7}$$

where s is the fraction of beam intensity polarized normal to the plane of incidence and p is the fraction of beam intensity polarized parallel to the plane of incidence.

The combination of Eqs. (4) and (7) gives

$$F(\theta) = \frac{1 - s(r_s)_\theta - p(r_p)_\theta}{1 - s(r_s)_0 - p(r_p)_0}. \tag{8}$$

The derived angular response of a lead sulfide detector to radiation polarized as shown in Fig. 2 can be obtained from Eq. (8) and compared to the observed angular responses.

Experimental Apparatus and Procedure

A Perkin-Elmer 13U spectrophotometer together with external mirrors furnished a collimated, monochromatic beam in which the detectors were rotated. Beam uniformity was measured by scanning the cross section with a 1-mm² detector. The detector mount was then located such that beam variations would produce a minimum error. This error was calculated to be no greater than 3% of $F(\theta)$. Beam polarization was checked with a Glan-Thompson prism and an integrating sphere reflectometer. The radiation source was a tungsten ribbon-filament lamp.

Kodak Ektron detectors were used. These had the very thin layer of polycrystalline lead sulfide deposited upon a rectangular glass blank 0.75 mm thick. The manufacturer applies a thin coat of polystyrene over the lead sulfide film surface and substrate edges for protection against humidity and contamination.

Response data were taken of detectors with physical characteristics as follows:

1. Detector No. 1 was a standard commercial detector with a sensitive area 1.0 cm long by 1.0 cm wide.
2. Detector No. 1a was detector No. 1 after the

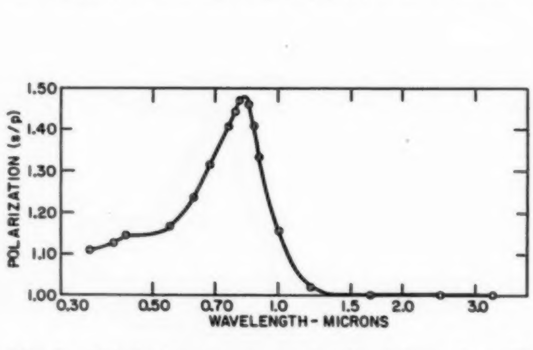

Fig. 2. Polarization versus wavelength of beam from P.E. 13U spectrophotometer and detector optics. Polarization is given as the quotient s/p of the fractions polarized perpendicular (s) and parallel (p) to the plane of incidence (horizontal plane).

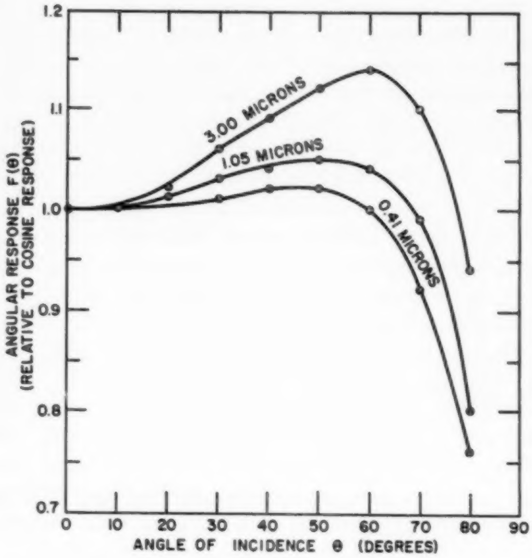

Fig. 3. Response of Detector No. 1, vs angle of incidence, to the P.E. 13U spectrophotometer beam having the polarization shown in Fig. 2. The angular response is shown for several wavelengths.

polystyrene coating had been dissolved in acetone, and the substrate edges and back surface had been coated with Sillers 32P28 flat black enamel. The spectral reflectance of this paint, measured with an integrating sphere reflectometer, was found to be consistently 3% relative to magnesium oxide through 0.41 to 2.6 μ wavelength.

3. Detector No. 2 had a sensitive area 1.0 cm long by 0.5 cm wide. The polystyrene was removed, but the substrate edges and back were left bare.

4. Detector No. 2a was detector No. 2 with the substrate sides and back screened with flat black paint.

The highly absorbing paint mentioned above was applied to all exposed surfaces of the detector mount to reduce stray radiation to a minimum.

Discussion of Results

The angular response $F(\theta)$ of the standard detector (No. 1) is plotted in Fig. 3 against angle of incidence at three wavelengths. It can be seen that the deviations from a cosine response increase as the angle of incidence increases until a maximum positive deviation is attained between 45° and 60°, then $F(\theta)$ falls off to a maximum negative deviation as θ approaches 90° or grazing incidence.

The variation of $F(\theta)$ with wavelength at a fixed angle of incidence is shown in Fig. 4 with plots of $F(70°)$ from the observed responses of the four detectors and the derived response, Eq. (8). Several distinct effects are apparent:

1. Detector No. 1 shows a rapid decline in $F(70°)$ with decreasing wavelength starting at 0.5 μ. Since the other curves are nearly flat in this region, this effect is probably caused by the increased reflectance and absorption of polystyrene at these short wavelengths. The departure from a cosine response is approximately 6% at 0.4 μ.

2. The two detectors with unpainted edges, No. 1 and No. 2, have $F(70°)$ from 15 to 25% greater than the other detectors. The exposed edges of the substrate evidently pass radiation directly from the monochromator and also after reflection from the detector mount even though all of the mount surfaces were painted with a matte black paint. This radiation can then be refracted and reflected within the substrate and passed into the lead sulfide film at the film-substrate interface. To substantiate this possibility, the response of detector No. 2 to radiation incident on its back surface was measured relative to the response of the front surface. The response was found to vary from 69% at 0.4 μ to approximately 100% at wavelengths longer than 1.8 μ. At large angles of incidence the amount of radiant energy incident on the substrate edge facing toward the source becomes significant compared to the energy incident on the front surface of the lead sulfide film.

3. As a result of beam polarization, the calculated response shows a pronounced dip of approximately 7% centered at 0.8 μ. Only the detector with a polystyrene coating, detector No. 1, has a similar dip.

4. All of the experimental curves show a 10% to 20% rise in $F(70°)$ at 3.0 μ over $F(70°)$ at 1.0 μ. Since no experimental variable was found which would significantly alter this effect, it is difficult to identify the cause or causes. However, the relation of the physical structure of the PbS film surface to this observed behavior can be profitably considered.

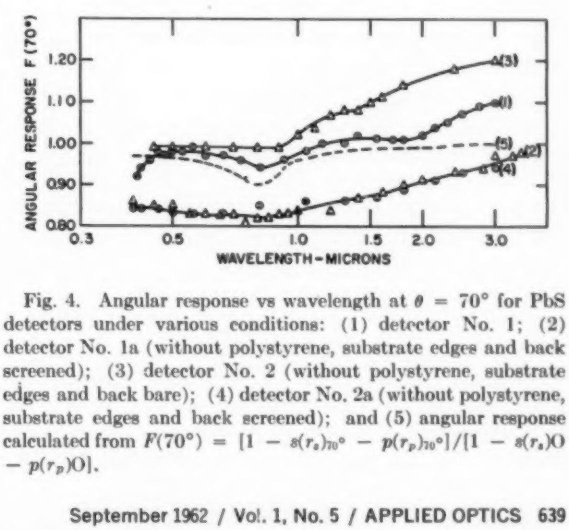

Fig. 4. Angular response vs wavelength at $\theta = 70°$ for PbS detectors under various conditions: (1) detector No. 1; (2) detector No. 1a (without polystyrene, substrate edges and back screened); (3) detector No. 2 (without polystyrene, substrate edges and back bare); (4) detector No. 2a (without polystyrene, substrate edges and back screened); and (5) angular response calculated from $F(70°) = [1 - s(r_s)_{70°} - p(r_p)_{70°}]/[1 - s(r_s)O - p(r_p)O]$.

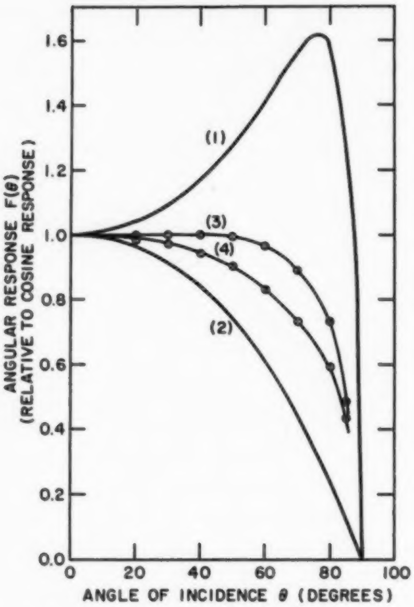

Fig. 5. Calculated (1 and 2) and observed (3 and 4) angular response of PbS detector 2a for polarized radiation parallel to (1 and 3) and perpendicular to (2 and 4) the plane of incidence at 0.7 μ wavelength. The observed polarization was approximately 90% complete. The polarization for the calculated responses was taken to be 100% complete.

According to Fig. 1, if a plane surface is assumed, the reflectance of unpolarized radiation is constant at 38.5% from normal incidence to 70°, and according to Fig. 2 the incident beam was unpolarized for wavelengths longer than 1.5 μ. In agreement with this result, Fig. 4 shows that the calculated response at wavelengths longer than 1.5 μ has an $F(70°)$ of approximately unity. The additional consideration of transmission losses gives an increase of 2% in $F(70°)$ at 3 μ, but this is far less than the change in the observed response.

If, on the other hand, the film surface is not plane because of a random orientation of the PbS crystal surfaces, and if the grain dimensions are approximately equal to or greater than the radiation wavelength, then the incident radiation would be reflected more strongly at large angles of incidence than at normal incidence. Electron micrographs of Kodak lead sulfide layers show that the cubical and tetrahedral grains have random surface orientation and that their dimensions are approximately one micron.[6] At 70° incidence to the mean crystal surface, which would probably be parallel to the substrate–film interface, some grains will cause reflection at angles less than 70°, but other grains will reflect at larger angles. Since at angles greater than 70° the reflectance increases rapidly, the average reflectance will increase. Thus, if the lead sulfide grain dimensions fall within the detector's response spectrum, one would expect the reflectance at a constant θ to change gradually as the wavelength of the incident radiation is varied from less than to greater than the typical grain size. As the wavelength becomes considerably greater than the grain size, the film surface becomes, in effect, a plane surface.

Transmission losses are likely to be only slightly affected by the random crystal orientation. A grain surface inclined toward the radiation source lengthens the path through the film, but a grain surface inclined away from the source shortens the path.

The polystyrene coating is nearly a plane surface for all wavelengths of the response spectrum. By refracting the incident radiation, the coating alters but does not mask the effects of the lead sulfide granular structure beneath. The expected dip in the response curves due to beam polarization appears only for the detector with a polystyrene coat because it is the only detector with a plane surface at 0.8 μ wavelength.

The angular response of detector No. 2a to 90% plane polarized radiation at 0.7 μ wavelength is compared in Fig. 5 to response curves calculated from Eq. (8). The degree of polarization was taken to be 100%, and r_p and r_s were taken from Fig. 1. The markedly slight deviation of the experimental curves from the cosine response and from each other can also be attributed to the granular structure of the lead sulfide film and the consequent random orientation.

Another possible cause of the variation from cosine response is the quarter-wavelength interference encountered with stratified media. Born and Wolf[5] treat the case of a conducting film on a dielectric substrate. For a film thickness d of 0.75 μ, absorption index k of 0.03, and refraction index n of 4.1, reflection maxima occur at the wavelengths 0.9, 1.1, 1.3, 1.7, and 2.4 μ. The slight waviness indicated by the data points in Fig. 4 may be partly due to this effect.

Conclusion

For most applications the ideal detector would have an angular response proportional to the cosine of the angle of incidence. The observed responses of the actual detectors exhibited deviations which arise from three principal causes. These deviations are quantitatively described below as being positive or negative in relation to the ideal cosine response.

1. The protective coating of polystyrene over the lead sulfide film (as on standard Kodak detectors) increased the reflection and/or absorption of short wavelength radiation at large angles of incidence. This produced a negative deviation which began at 0.5 μ and increased toward the shorter wavelengths. At 0.41 μ the deviation was −6% for an angle of incidence θ of 70° and −10% at 80°.

2. The unscreened edges of the detector's glass substrate passed increasing amounts of the incident radiation as the angle of incidence increased. Reflection of this radiation into the underside of the photoconductive film produced a large positive deviation over the entire spectral range of 0.4 to 3.0 μ. The deviation varied from $+14\%$ at 0.4 μ to $+25\%$ at 3.0 μ when θ equaled 70°. This effect can be modified by a number of factors such as the detector geometry, the substrate transmissivity, and the reflectance of the detector mount.

3. It is hypothesized that the reflection losses vary as the wavelength of the incident radiation varies from less than to greater than the typical grain size of the lead sulfide film (1 μ). At θ equal to 70°, the negative deviation is approximately constant at -16% for wavelengths up to 0.9 μ. From 0.9 μ to 3.0 μ the deviation decreases to approximately -4%. Thus, as the wavelength increases beyond 1 μ, the film surface becomes more like a plane surface, and the deviation due to reflection losses approaches zero for angles of incidence up to 70°.

The work described in this paper was performed at the University of California at Los Angeles as a project for a master's thesis. The author is indebted to D. K. Edwards of the University of California at Los Angeles for his guidance and technical assistance, and to David Dutton of the Institute of Optics, University of Rochester, for much of the basic information on lead sulfide detectors.

References

1. A. Smith and D. Dutton, J. Opt. Soc. Am. **48**, 1007 (1958).
2. W. W. Scanlon, Phys. Rev. **109**, 47 (1958).
3. D. G. Avery, Proc. Phys. Soc. (London) **66B**, 134 (1953).
4. R. W. Ditchburn, *Light* (Interscience, New York, 1955).
5. M. Born and E. Wolf, *Principles of Optics* (Pergamon Press, New York, 1959).
6. D. Dutton, private communication to G. Schaefer dated December 28, 1960.

Meeting Reports

13th Mid-America Spectroscopy Symposium, Chicago, April 30–May 3, 1962

Reported by Forrest F. Cleveland, Illinois Institute of Technology

The thirteenth annual Mid-America Spectroscopy Symposium was organized by the Chicago Section of the Society for Applied Spectroscopy, in cooperation with the SAS Cleveland, Detroit, Indianapolis, Milwaukee, Niagara Frontier, and St. Louis Sections, and in conjunction with the Gas Chromatography Discussion Group of Chicago. The number of registrants (586) was forty percent higher than last year's total. The General Coordinator of the symposium was John R. Ferraro, Argonne National Laboratory, and the Program Coordinator was Joseph S. Ziomek, De Paul University.

Fifteen technical sessions presented the largest number of papers on gas chromatography (15); tied for second place with 10 papers in each category were x-ray absorption, x-ray emission, and emission spectra. Other subjects covered include Raman, infrared, and far-ultraviolet spectra, infrared and Raman instrumentation, structure determinations by molecular spectra, data retrieval and global communication of spectroscopic information, nuclear magnetic resonance, flame photometry, and time-resolved spectroscopy. Summaries of the papers are included in the program, a copy of which can be obtained from Dr. Ferraro; the program also included sessions for general discussions of infrared, molecular, and optical emission spectra, nuclear magnetic resonance, and flame photometry. Selected papers will be published in book form.

Concurrent with the technical sessions, there were 22 exhibits of spectroscopic instruments. Thirty-minute intermissions in the morning and afternoon sessions, during which refreshments were served by various companies, provided time for informal discussions.

Plans for next year's symposium are already underway. The location of Chicago and its accessibility by air make it especially suitable for a symposium of this type.

Second Winter Institute of Quantum Chemistry and Solid State Physics, Florida, December 4, 1961–January 13, 1962

Reported by Gordon E. Gross, Midwest Research Institute

Conducted under the direction of Per-Olov Löwdin of the Universities of Uppsala and Florida, the Institute was supported by the National Science Foundation, with the cooperation of the two universities. The participants represented twenty-two nations.

The first portion of the Institute, held at the University of Florida in Gainesville, contained about 220 hours of lectures, exercises, and group discussions. Especially useful was the preparatory week intended for those desiring a warming-up period. Even for those who were well abreast of the usual graduate-school level of quantum theory, this time was of great assistance in preparing for the material to be presented during the following weeks. It was even more useful for the experimentalist who simply does not have time to maintain agility with theory. The remaining three weeks at Gainesville were devoted to the Introductory Course which contained a thorough introduction to projection operator formalism, many-body quantum mechanics, perturbation theory, and approximation methods. If one can judge from comments heard, the four weeks at Gainesville were a revelation and an awakening, and provided both theorists and experimentalists with renewed appreciation of the phenomenal development in this field during the past ten years. Many problems which were dismissed as tempting but too difficult to solve a decade ago are now solved to yield excellent agreement with experimental results. Outstanding examples of such problems are direct calculation of bond energies and reaction constants in large organic molecules and calculation of the energy bands in metals. It is to be recognized that some of these problems could be handled earlier but the present schemes are often far more elegant.

The advanced course, held on Sanibel Island, was more in the form of a two-week series of seminars covering new research. Most of the seminars were four or six hours long and gave excellent accounts of subjects ranging from quantum biochemistry to antiferromagnetism. The freshness of the work presented is best indicated by the fact that during this portion of the Institute, two of the participants (P.-O. Löwdin and Frank Harris) worked out a generalized solution to one of the integrals found in Paunez' treatment of alternant hydrocarbons.

Although the pace of the Institute can only be described as frantic, the constant exposure to the theory, with other thoughts crowded out by intense activity, must result in many persons returning to classrooms and laboratories with insight and enthusiasm beyond their most optimistic estimates. The improved quality of the research and teaching which they will perform in the coming years will more than compensate for the efforts of the organizers and the participants and for the cost of the program.

American Physical Society Spring Meeting, April 23–27, 1962

Reported by W. S. Rodney, NSF

The spring meeting of the Physical Society in Washington was characterized, with regard to optics' interest, by a large number of papers on spectroscopy oriented toward the search for energy levels which might be useful for light amplification. Another facet was the study of line broadening and line narrowing, which is related to questions of coherence. Attention was also given to fluorescence in the spectrum emitted by various fluorescent materials such as MgO, containing V^{++} ions. Optical analogs to AM and FM detectors were discussed, and there were some papers wherein the question of the generation of harmonics resulting from nonlinearities of the dielectric medium were described. The optical aspects of plasma physics such as the emission and absorption coefficients for fully ionized plasmas, the infrared invisible spectra of optical thick plasmas, radiometric and spectrometric temperature measurements, line shapes, oscillator strengths, and broadening effects of cesium lines as well as depolarization of radiation scattered from plasmas were discussed. A number of papers were given on relativistic aspects of electrodynamics. A large-aperture, fast-opening shutter for high-speed photography was described, which consists of buckling a magnetic foil placed in front of the camera lens. A 3-in^2 aperture may be opened in 45 μsec.

13th National Science Fair, May 2, 1962, and Seattle World's Fair

Reported by Richard K. McDonald, Boeing

Some 380 teenagers and their high-school teachers traveled to Seattle's World Fair on May 2nd for the 13th National Science Fair, two of whose awards were sponsored by the Optical Society of America. With about thirty of the projects related to optics, the judges had ample material to evaluate. The first OSA award of $100 (for materials, books, etc.) went to Richard Lee Falwell, 17, Walter Johnson H.S., Rockville, Md., for *Spot Cycles of Jupiter and Saturn*. His observations on the rotation and evolution of the planetary features had been accomplished over several years with a homemade 20.3-cm (8-in.) telescope. Judges were particularly impressed by his meticulous notebooks which included many colored sketches. The second prize (of $75) was awarded to Elizabeth Ferree Stilwell, 18, Vermillion H.S., Vermillion, S. Dak. for *Induced Color Halos Seen by Fifteen Color-Blind Persons and Fifteen Controls Tested with Monocular Vertically Bisected Bicolor Stimuli*. This was an exploratory-type investigation on an illusive subject. Miss Stilwell's exhibit included her test color samples and the subjective measurements of what colors were seen. Edward F. Turco, 17, of Cranston R.I., particularly impressed the OSA judges (Kenneth Clark and David F. Eggers of the University of Washington and Tom Rona of the Boeing Company) with a catadioptric telescope of his own design and manufacture. This incorporated one lens and three mirrors, and was unique enough to be patented.

While the World's Fair theme is science, the world of optics appears only occasionally. Perhaps the most impressive manifestations to the layman are the striking projection effects used in the Colliseum, the House of Science (Federal Science Exhibit), and the United States-Boeing Spacearium. The latter, which incorporates a hemispherical screen and a 180° projection lens, loses some of its effectiveness in portraying a trip to the stars because of poor technical execution. The stars appear as blurs, and white film streaks are common. On the other hand, the movie in the House of Science projected through seven synchronized units is a masterpiece technically and artistically. In the science building demonstrations of optical illusions and explanations of the nature of light appear. The most sophisticated exhibit is a closed circuit television camera connected to a microscope. Living organisms can be seen on a 53.3-cm (21-in.) screen. The supplier, Elgeet Optical Co. of Rochester, N.Y., believes this to be the first public demonstration of the technique.

Of the foreign exhibitors, Canada was alone in having an exhibit disconnected from commercial promotion. Several infrared instruments, built by the Canadian Armament Research & Development Establishment (CARDE) showed how thermal imaging could be employed to detect skin cancer and how objects could be detected by their passive emission. Spectators were allowed to trigger an audio alarm by placing their hands before an infrared radiometer. Other countries, such as Japan and Sweden, included cameras, microscopes, and even a planetarium projector (The Goto Co. of Japan) in their national displays.

It is natural that the American Telephone and Telegraph Co. should include a model of the laser in their show. Nevertheless their exhibit showing an application to space communication was too crude to do them justice. What was purported to be voice communication on a beam of light was immediately proved a fake by the fact that everybody put his hand in front of the mirrors without stopping the sound.

1962 Annual Conference of the Society of Photographic Scientists and Engineers, May 7–11, 1962

Reported by Edward K. Kaprelian, Army Signal R & D Lab

Over 400 registrants attended the SPSE Conference at Boston's Somerset Hotel; cosponsor with the Society was the Air Force Cambridge Research Laboratories. The conference program included nine paper sessions, a choice of several field trips, and an extensive group of exhibits by 44 manufacturers and distributors. Sixty-three papers by 90 authors were presented covering the areas of cameras and photoinstrumentation, satellite photography, aerial reconnaissance, exposure theory, processing equipments, materials and technology, image theory and measurement, photosensitive systems and theory, densitometry and sensitometry, and processing chemistry. Industry was the source of 47 papers, while government agencies and universities were responsible for 13 papers and 4 papers, respectively; of the total there were three from Germany, one from Japan, and one from England.

The annual banquet was again the occasion for awarding honors. Chester F. Carlson, pioneer in the development of electrophotography, was awarded Honorary Membership, the Society's highest honor, by SPSE president Steven Levinos. Fellowships were awarded to Burt Carroll, Rudolf Kingslake, and John Leermakers, while Herbert Meyer and Frank Smith were awarded Senior Memberships. The banquet speaker,

continued on page 677

Interference Filters and Fabry-Perot Interferometers for the Far Infrared

K. F. Renk and L. Genzel

This paper describes measurements on transmission interference filters for the far infrared (100–800 μ region). The reflection layers of these filters are metallic mesh. The measured coefficients of finesse, ten to sixty, are comparable with the values which can be obtained for interference filters in other spectral regions. Peak-transmission values up to 0.9 were reached. From these measurements the absorptivity of the single grids has been determined. Measurements on a variable spacing interference filter showed that the finesse is proportional to the square of the wavelength in accordance with theoretical predictions for interference filters constructed with reflection layers of one-dimensional wire gratings.

I. Introduction

Today there are available interference filters and Fabry-Perot interferometers in the ultraviolet, the visible, the near infrared up to 20 μ wavelength, and in the microwave region for wavelengths longer than 6 mm. In all these spectral regions it is possible to use dielectric multilayers as reflectors for the interference filters. In the visible region homogeneous metal layers also have been used with success, and in the microwave region metal gratings have been used. The purpose of this paper is to show that it is possible to make satisfactory transmission interference filters (IF's) or, in high order, Fabry-Perot interferometers for the far infrared by using metal grids. We have not considered dielectric multilayer IF's because of their restricted spectral range.

The ability to construct satisfactory IF's in a given spectral region depends upon the availability of good reflection layers. The demand on the optical properties of these layers follows from the Airy formula for the transmission τ through an IF: under the assumption of a symmetric IF we have

$$\tau = \frac{1}{[1 + (A/T)]^2} \frac{1}{1 + [4R/(1 - R)^2] \sin^2 \delta/2}, \qquad (1)$$

where R, T, and A are the spectral reflectivity, transmissivity, and absorptivity, respectively, of the single reflection layer of the IF, and where

$$\delta = (2\pi/\lambda)2nd + 2\Phi \qquad (2)$$

is the resultant phase difference of two successive beams in the multiple beam interference. In (2) it is assumed that the incident parallel beam of radiation is passing perpendicularly through the IF of spacing d. n is the refractive index of the medium between the reflection layers, λ is the vacuum wavelength, and Φ is the phase-shift for the reflection on one layer.

The resolving power (or Q-value) of the IF for a given interference order $k = \delta/2\pi$ can be put into the form

$$Q = \lambda/\Delta\lambda = kF_1, \qquad (3)$$

where λ is the wavelength of the peak transmission in kth order, $\Delta\lambda$ is the half-width of this line, and

$$F = \frac{\pi}{2 \arcsin [(1 - R)/2\sqrt{R}]} \qquad (4)$$

is the finesse (effective number of beams). For R greater than 0.6

$$F = \frac{\pi\sqrt{R}}{1 - R}. \qquad (4a)$$

F is a function of R only and increases rapidly as R approaches unity.

An IF has a peak transmission for $\delta = k \cdot 2\pi$ with the value

$$\tau_{\max} = \frac{1}{(1 + A/T)^2} \qquad (5)$$

which shows, together with (4), that the reflection layers of an IF should have a high reflectivity R and a small value of A/T in order to obtain high F and high $\tau_{\max}$.

From these conditions one can show that homogeneous metal layers are not suitable for IF's in the far infrared because of their optical properties.[1–4] There-

---

The authors are at Physikalisches Institut der Universität Freiburg im Breisgau, Germany.

Received 26 May 1962.

fore, we used metal grids as reflection layers. These have already been used for this purpose in the microwave region ($\lambda = 1.25$ cm) by Lewis and Casey,[5] and these authors attained F and $\tau_{\max}$ values of 50 and 0.6, respectively. More recently Culshaw[6,7] successfully used metal plates, which had regular spaced circular holes, as reflectors for a 6-mm Fabry-Perot interferometer. With respect to their electromagnetic properties these plates are similar to those of metal grids. This promising success in the microwave region aroused the hope that a similar arrangement would work in the submillimeter wave range also.

II. Theoretical Considerations

A. The Metal Grating and Grid

The electromagnetic behavior of metal gratings—both wire gratings and strip gratings—has been studied theoretically[8-14] and experimentally.[11,15,16] Such gratings are transparent to radiation of wavelengths greater than the grating constant, polarized with the electric vector perpendicular to the wires. The parallel polarized radiation does have a wavelength dependence and becomes strongly reflected at long wavelengths. It is this parallel polarized situation therefore that is of importance in the production of an IF.

Casey and Lewis[13] give a formula for the reflectivity of a wire grating for $\lambda > 2g$ and $a << \lambda$ (g is the grating constant, a the wire radius) and for the case where a is large compared to the skin depth. For a grating with good conductivity, the reflectivity is given by[13]:

$$R = \frac{1}{1 + [G(g/a, \lambda, \sigma) - \tan \Phi]^2} \tag{6}$$

where $G(g/a, \lambda, \sigma) = 0.157\ (g/a)(c/\sigma\lambda)^{1/2}$ shows the dependence upon the finite electrical conductivity σ of the wires and therefore accounts for the ohmic losses, and $\tan \Phi$ is a function of the geometry of the grating. It is

$$\tan \Phi = -\frac{2g}{\lambda}\left[\ln \frac{-g}{2\pi a} + H\left(\frac{\lambda}{g}\right)\right] \tag{7}$$

with

$$H\left(\frac{\lambda}{g}\right) = \sum_{m=1}^{\infty}\left\{\left[\frac{1}{m^2 - (g/\lambda)^2}\right]^{1/2} - \frac{1}{m}\right\}.$$

Φ is the phase of the reflected wave; compare Eq. (2). Casey and Lewis[13] also give for the absorption in a wire grating:

$$A = 0.314\,\frac{g}{a}\,R\left(\frac{c}{\sigma\lambda}\right)^{1/2}. \tag{8}$$

In the limiting case of $\lambda/g \gg 1$, with the restriction $G \ll (2g/\lambda)\ln(g/2\pi a)$, we obtain from (6), (7), and (8) the approximate equations for wire gratings

$$\left.\begin{aligned} &\tan \Phi = 0 \text{ or } \Phi = 0, \pi; \\ &R = 1 - \tan^2 \Phi = 1 - \left(\frac{2g}{\lambda} \ln \frac{g}{2\pi a}\right)^2, \\ &A = 2G = 0.314\,\frac{g}{a}\left(\frac{c}{G\lambda}\right)^{1/2} \ll T, \\ &T = 1 - R = \tan^2 \Phi = \left(\frac{2g}{\lambda} \ln \frac{g}{2\pi a}\right)^2. \end{aligned}\right\} \tag{9}$$

For gratings made up of thin strips rather than wires, Lamb's theory[8] gives the transmission for $\lambda \gg g$ as

$$T = \left(\frac{2g}{\lambda} \ln \sin \frac{\pi a}{g}\right)^2, \tag{10}$$

where a is here the half-breadth of the strips.

In contrast to the above-mentioned gratings no theory exists for two-dimensional gratings (grids). It is reasonable to assume that such a grid has approximately the same behavior for unpolarized radiation as the one-dimensional grating for the parallel polarized radiation. We make this assumption in order to compare our experimental results with the theoretical predictions.

B. Theory of the Metal Grating Interference Filter

Let us consider an IF built up with two identical wire or strip gratings. If the radiation falling perpendicularly on the IF is polarized with its electrical vector parallel to the conductors, then we have from (4), (9), and (10) for $\lambda >> g$

$$\left.\begin{aligned} F &= \pi\left[2g \ln \frac{g}{2\pi a}\right]^{-2} \cdot \lambda^2 \quad \text{for wire gratings,} \\ F &= \pi\left[2g \ln \sin \frac{\pi a}{g}\right]^{-2} \cdot \lambda^2 \quad \text{for thin strip gratings,} \end{aligned}\right\} \tag{11}$$

$$\left.\begin{aligned} \frac{A}{T} &= 0.314\,\frac{g}{a}\left(\frac{c}{\sigma}\right)^{1/2}\left[2g \ln \frac{g}{2\pi a}\right]^{-2} \cdot \lambda^{3/2} \\ &\qquad \text{for wire gratings,} \\ \frac{A}{T} &= 0.314\,\frac{g}{a}\left(\frac{c}{\sigma}\right)^{1/2}\left[2g \ln \sin \frac{\pi a}{g}\right]^{-2} \cdot \lambda^{3/2} \\ &\qquad \text{for thin strip gratings,} \end{aligned}\right\} \tag{12}$$

where a is the wire radius or the half-breadth of the strips and g is the grating constant. It is assumed here that the absorptivity of the strip grating is similar to that predicted for the wire gratings. No careful study has been made to verify this assumption.

In (11) and (12) we have made the assumption that the electromagnetic behavior of each of the two gratings in the IF is not influenced by the other. Casey and Lewis[13] showed that this is the more correct, the higher the electrical conductivity of the wires. In our case of copper and nickel grids the influence of the grids on one another is negligible.

The equations (11) and (12) show that the finesse increases proportional to λ^2 and that the A/T value increases with $\lambda^{3/2}$. This A/T value determines, according to (5), the peak transmission $\tau_{\max}$, and we see that $\tau_{\max}$ decreases with increasing λ.

One can see from the formulas that thin strip gratings are better than wire gratings in IF's for use over a wide wavelength range.

III. Experiments

A. Measurements on a Single Grid

All the spectral measurements were made on our vacuum-grating-spectrometer for the far infrared.[17–19]

We studied first the optical properties of the single grid which was used as a reflector in the IF. The grid had a grating constant of $g = 50\ \mu$, a strip breadth of $2a \approx 12\ \mu$, and a strip thickness of about 6 μ. We measured both a copper and a nickel grid of this same geometry without a supporting substrate. No essential difference in the behavior of the copper and nickel grids was observed. Figure 1 shows the result of transmission measurements with unpolarized radiation on these grids between 40 μ and 280 μ wavelength, which corresponds in the λ/g-scale to values between 0.8 and 5.5. For comparison, Fig. 1 also shows measurements of Pursley[16] on one-dimensional gratings with parallel polarized microwave radiation. It is interesting to see that the general optical behavior of our grid is similar to, but not the same as, the behavior of one-dimensional gratings in the parallel polarization case. Especially surprising is the shift of the maximum transmissivity from $\lambda/g = 1$ to λ/g of about 1.15, which we have not been able to explain up to now. The maximum transmissivity is around 0.97. For $\lambda > 2g$, we obtain $T \approx 0.49 \times 10^4\,\lambda^{-2}$ (λ in microns).

From the measured transmission of a single grid we can determine the finesse F of an IF made of two parallel grids. Under the assumption of negligible absorption in a grid we obtain from (4) the finesse $F \approx 6.4 \times 10^{-4}\lambda^2$, where λ is measured in microns (compare Fig. 3). If we assume, furthermore, that the absorption in a strip grid is similar to that of a strip grating, then we can calculate A from (9) and this, together with the experimental value of T, gives for nickel mesh $A/T \approx 2.5 \times 10^{-5}\,\lambda^{3/2}$ (λ in microns). From this we can calculate, according to (5), the expected peak-transmission $\tau_{\max}$ (compare Fig. 4).

B. Measurements on Metal Grid Interference Filters

With the mesh described we have made IF's with a usable area of diameter greater than 6 cm.

In order to hold the grids flat they were cemented with thinned collodion onto plane plates of crystal quartz. With an adjustable holder similar to the variable thickness cells used in infrared spectroscopy,[20,21] the distance between the two grids could be regulated from zero to several millimeters with an accuracy of about one or two microns without disturbing the parallelism of the quartz plates.

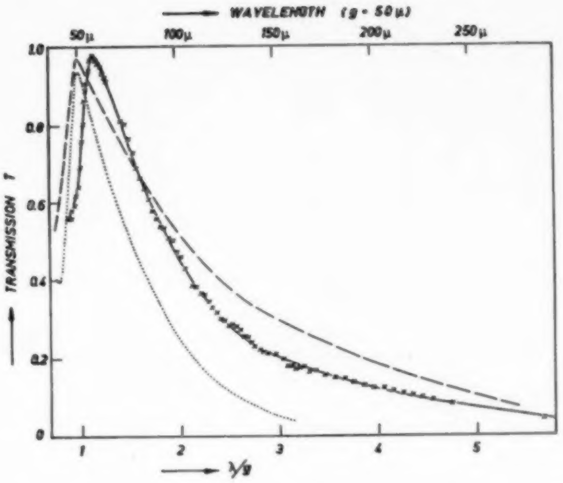

Fig. 1. Measured transmission of metal gratings with grating constant to strip half-breadth ratio of 8. . . . . ., one-dimensional grid, thick strips (Pursley,[16] microwave measurements). - - -, one-dimensional grid, thin strips (Pursley,[16] microwave measurements). ×, two-dimensional grid (infrared measurements).

For a mesh distance of $d = 300\ \mu$, Fig. 2 shows the IF transmission in the 100–600 μ wavelength region. The figure shows a harmonic relationship of the reciprocals of the wavelengths of the peak-transmission values and therefore it follows from Eq. (2) that the phase-shift Φ has the value 0 or π. Furthermore, one can see that the finesse increases with increasing wavelength.

For such a variable IF we have determined experimentally the wavelength dependence of the finesse and the peak transmission by carefully measuring the first IF order lying in the wavelength range from 100 to 800 μ. The results for the wavelength range 100–350 μ are shown in Figs. 3 and 4. For this IF the finesse (Fig. 3) is proportional to the square of the wavelength in accordance with the theoretical expectations. The experimental coefficients of finesse, however, are smaller than expected. This may be caused by an insufficient flatness of the grids on the plates. The values for the peak transmission (Fig. 4) are large, considering the fact that the measurements include losses by reflection from the two quartz plates. The curve $\tau_{\max}$ of the IF is nearly the same as the transmissivity of the two quartz plates without grids and at large separation.

Measurements in the 400–800 μ wavelength region were made with a spectrometer resolution comparable with the IF resolution. Therefore we had to correct the measured curves to a zero value of spectrometer slit-width. In this spectral region the finesse is large

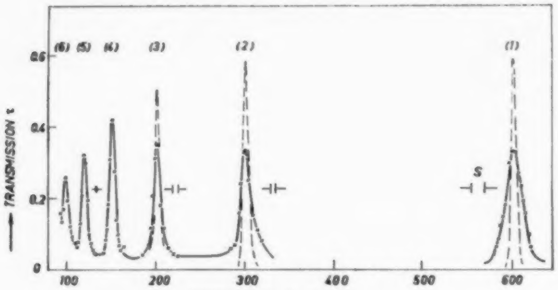

Fig. 2. Measured characteristic of an interference filter (grids on crystal quartz plates, each 5 mm thick). ×, measured - - -, corrected to zero spectrometer slit-width and parallel beams. *S* is the equivalent spectrometer slit-width. The orders of interference are given in parentheses.

enough to require correcting the measurements for the fact that the IF was measured in a convergent, rather than parallel, beam. For these corrections we used methods described by Koppelmann and Krebs.[22,23] Within the experimental errors the values for finesse and peak transmission meet on the discussed curves. For instance we found that at 600 μ wavelength $F \approx 60$ and $\tau_{\max} \approx 0.6$.

The grids do not have any polarization characteristics and the rotation of one grid relative to the other in the IF had no effect.

The simplest method of obtaining two parallel grids is to place them on the surfaces of a thin transparent film. We cemented the grids with collodion onto a polyethylene film. The peak-transmission values are obtained from (2) for $\lambda = 2nd, 2nd/2, \ldots,$ where n is the refractive index and d is the thickness of the film. For some first-order IF's the results are shown in Figs. 3 and 4. Because of the unevenness of the films it was not possible to reach the maximum expected values for finesse and peak transmission.

The best IF's were made with parallel mesh without substrate. The holder of one mesh is shown in Fig. 5. The grid is cemented on a frame. Some screws press the ring against the mesh, stretching the mesh tightly into the plane of the ring surface. The evenness of the grid depends only on the flatness of the surface of the inner ring. The coefficients of finesse for such IF's reach nearly the values expected from transmission measurements on single grids (see Fig. 3). The peak-transmission values are approximately those expected from the theoretical values of absorptivity of a single grating, together with the transmission values measured on the single grid (see Fig. 4).

The measurements on IF's from unsupported grids and on the variable IF show that, for $\lambda > g$, the phase-shift for the reflected amplitude of a grid is zero or π. This is not in agreement with the theoretical approximation given in Eq. (7) when $\lambda \approx 2g$.

IV. Some Applications of Metal Grid Interference Filters in the Far Infrared

A. Properties of Metal Grids

It is possible to determine the properties of metal grids from the properties of the IF's: The finesse gives from Eq. (4), the reflectivity, and the peak transmission of an IF and the known transmission of a single grid give, from (5), the absorptivity of a single grid. From the measurements on unsupported grids we found good agreement between the experimental and theoretical values of absorptivity. In the 100–250 μ region the absorptivity is about one percent.

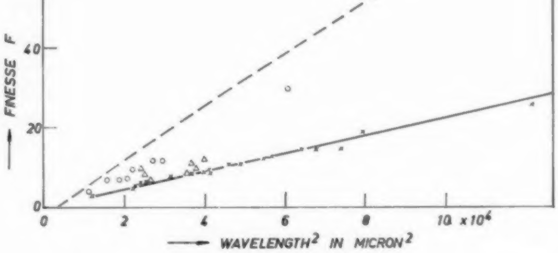

Fig. 3. Finesse of metal grid interference filters. - - -, expected from transmission meaurements on single grids (copper or nickel). ×, metal grids of copper on crystal quartz plates, each 5 mm thick. △, metal grids on polyethylene film. ○, metal grids of nickel unsupported.

B. Narrow Band-Pass Filter

Using grids with suitable dimensions it is possible to make IF's with high finesse. For a variable IF used at one wavelength the finesse is fixed, but, by changing the spacing, the order of interference can be changed and the resolving power is proportional to the order of this interference. Figure 6 shows the measured filter transmission lines for the wavelength range 150–300 μ of an IF which has the peak transmission in fourth order at 200 μ. By combination with an IF whose first-order peak transmission lies at 200 μ, it is possible to eliminate neighboring peaks (Fig. 6, lower curve).

A special application of a metal grid IF is the separation of the harmonics which are obtained in the harmonic generation[24,25] of millimeter or submillimeter waves.

C. Interference Filter Spectrometer

With the aid of a variable IF it is possible to build a simple spectrometer. Using the grid type described, the resolution of an IF in first order is comparable with the useful resolution of other far-infrared spectrometers for $\lambda \geqslant 300\ \mu$.

D. Fabry-Perot Interferometer

With regard to the low resolving power of the far-infrared spectrometers, our measurements were made in low IF orders. It is easy, however, to use the IF's in high orders by increasing the distance d between the reflecting grids in order to obtain high resolving power Q. With the grid we have measured it would be possible, for example, to construct a Fabry-Perot interferometer for 1 mm wavelength having $F \approx 600$ and with $d = 10$ cm, having a Q-value of 120,000 and $\tau_{\max} \approx 0.6$.

E. Measurements of Refractive Index

The IF's together with a grating spectrometer can be used, as in other spectral regions, for the determination of the refractive index of the medium between the plates. The use of these grids on the parallel surfaces of a plane sample would sharpen the channel spectrum peaks[26,27] and therefore aid in the measurement of indices of refraction and their wavelength dependences.

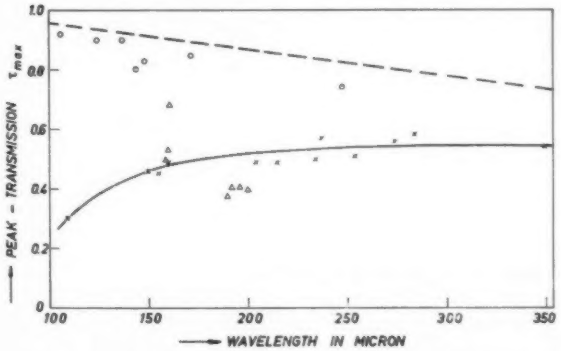

Fig. 4. Peak transmission of metal grid interference filters. - - -, calculated from experimental transmissivity together with theoretical absorptivity of a single grid (nickel). ×, metal grids of copper on crystal quartz plates, each 5 mm thick. △, metal grids on polyethylene film. ○, metal grids of nickel unsupported.

F. Examination of Radiation Purity

A metal grid IF allows a simple quantitative proof of the presence of short wavelength radiation, especially in a grating monochromator. If one wishes to test whether radiation of 600 μ contains, for instance, radiation of 300 μ, then one may use an IF with the first-order peak transmission set at 300 μ. Because the metal grid IF is opaque to radiation of wavelengths greater than the first-order wavelength, the 600-μ wavelength will not pass through the IF. If radiation of wavelengths shorter than 300 μ has been eliminated, and if there is radiation passed by the IF, then this transmitted radiation must have a wavelength of 300 μ. Thus it is possible in this case to check quantitatively for the fraction of short wavelength radiation in grating spectrometers.

G. Elimination of $\lambda/2$

An IF, or combination of IF's, has peak transmissions not only for a desired wavelength λ but also for $\lambda/2$, $\lambda/3, \ldots$. In the far infrared it is often difficult to eliminate the radiation of wavelength $\lambda/2$. This elimination should be possible, however, by reflecting the radiation on a single metal grid whose maximum transmission $T \approx 1$ (Fig. 1) lies at $\lambda/2$, or by reflecting on a metal grid IF with the first-order peak transmission at $\lambda/2$. With metal grids of suitable dimensions it should be possible to reduce the $\lambda/2$ radiation without diminishing appreciably the intensity at λ. A further possibility is to combine an IF whose peak-transmission values lie harmonically with an IF whose peak-transmission values lie anharmonically. The anharmonic situation may be produced by placing between the reflection layers a material which has a wavelength dependent refractive index. In the far infrared, however, it is difficult to find a nonabsorbing material with sufficient dispersion.

This work was done in the Departments of Physics of the Universities of Freiburg and Frankfurt (Main), Germany. We wish to thank Prof. Dr. M. Czerny for permission to work in his Institute in Frankfurt. We also wish to express our thanks to Prof. E. E. Bell, The Ohio State University, and to Ir. R. Geick for many helpful discussions. We are very grateful to the Deutsche Forschungsgemeinschaft for supporting this work.

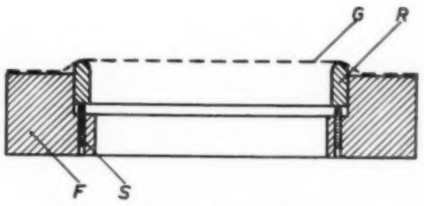

Fig. 5. Cross section of the holder for unsupported grids. F—frame, R—ring, S—screws, G—metal grid.

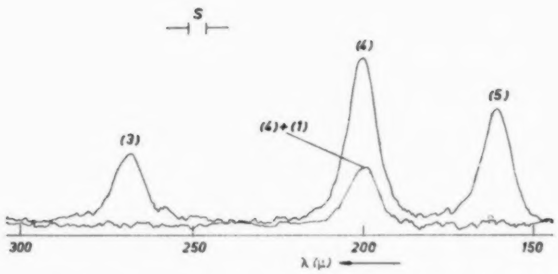

Fig. 6. Recording of the transmission lines of a combination of two interference filters. Upper curve: interference filter with the fourth-order peak transmission at 200 μ. Lower curve: interference filter with first-order peak transmission at 200 μ in addition to the fourth-order 200-μ interference filter. *S* is the equivalent spectrometer slit-width. The orders of interference are given in parentheses.

References

1. L. N. Hadley and D. M. Dennison, J. Opt. Soc. Am. **37**, 451 (1947).
2. H. H. Theissing and J. McGue, Rev. Sci. Instr. **26**, 1203 (1955).
3. U. Oppenheim, J. Opt. Soc. Am. **46**, 628 (1956).
4. H. Schröder in M. Auwärter, *Ergebnisse der Hochvakuumtechnik und der Physik dünner Schichten* (Stuttgart, Germany, 1957), p. 225.
5. E. A. Lewis and J. P. Casey, J. Opt. Soc. Am. **41**, 360 (1951).
6. W. Culshaw, IRE Trans. on Microwave Theory Tech. **MTT-7**, 221 (1959).
7. W. Culshaw, IRE Trans. on Microwave Theory Tech. **MTT-8**, 182 (1960).
8. H. Lamb, Proc. Math. Soc. (London) XIX, 523 (1897/98).
9. W v. Ignatowsky, Ann. Physik **44**, 369 (1914).
10. W. Wessel, Hochfrequ. u. El.-ak. 53/54, 62 (1939).
11. R. Honerjäger, Ann. Physik **4**, 25 (1948).
12. E. A. Lewis and J. P. Casey, J. Appl. Phys. **23**, 605 (1952).
13. J. P. Casey and E. A. Lewis, J. Opt. Soc. Am. **42**, 971 (1952).
14. R. Müller, Z. Naturforsch. **8A**, 56 (1953).
15. A. Esau, E. Ahrens, and W. Kebbel, Hochfrequ. u. El.-ak. 53/54, 113 (1939).
16. W. K. Pursley, Techn. Rep. 2351-1-T, The University of Michigan.
17. L. Genzel and W. Eckhardt, Z. Physik **139**, 578 (1954).
18. L. Genzel, Z. Physik **144**, 311 (1956).
19. R. Geick, Z. Physik **163**, 499 (1961).
20. V. J. Coates, Rev. Sci. Instr. **22**, 853 (1951).
21. A. V. Stuart, J. Opt. Soc. Am. **43**, 212 (1953).
22. G. Koppelmann and K. Krebs, Z. Physik **157**, 592 (1960).
23. G. Koppelmann and K. Krebs, Z. Physik **158**, 172 (1960).
24. W. C. King and W. Gordy, Phys. Rev. **93**, 407 (1957).
25. L. Genzel, H. Happ, and R. Weber, Z. Physik **154**, 1 (1959).
26. R. E. Kagarise, J. Opt. Soc. Am. **51**, 830 (1961).
27. R. Geick, Z. Physik **161**, 116 (1961).

Future Issues

Each issue will specially feature one area of applied optics in addition to the usual contributed papers, shop and technical notes, reports of meetings, Letters to the Editor, book reviews, Meetings Calendar, and special columns. The feature subject of each issue is the responsibility of the named editor.

1962	November	**Ultraviolet**	—
1963	January	**Astronomy**	James G. Baker
	February	**Information Theory**	F. Dow Smith
	March	**Instrumentation**	W. L. Hyde
	April	to be announced	
	May	**Interferometry**	R. A. Woodson
	June	to be announced	
	July	**Spectroscopy**	Mary E. Warga
	August	to be announced	
	September	**Lens Design and Computers**	D. P. Feder
	October	**Bubble Chamber Optics**	S. Rosin
	November	to be announced	
	December	**Chemical Optics**	M. Kent Wilson

Applied Optics Reporters

These reporters submit information from which are compiled in part the news columns of *APPLIED OPTICS*. They have a rather thankless and seldom properly recognized task, and the *APPLIED OPTICS* editors are very grateful to them.

L. H. Chasson, *San Francisco*
T. K. McCubbin, *Pennsylvania*
Stanley S. Ballard, *Florida*
E. Scott Barr, *South East*
J. L. Rood, *Rochester*
E. M. Wormser, *Connecticut*
R. A. Oetjen, *Japan*
L. E. Bergstein, *New York City*
D. J. Lovell, *Michigan*
R. Kraushaar, *New Jersey*
Mary E. Warga, *D.C. and Baltimore*
R. K. McDonald, *North West*
M. Kent Wilson, *Boston*
David M. Gates, *Denver*
K. M. Baird, *Canada*
C. S. Williams, *Texas*
A. J. Cussen, *Los Angeles*
H. McAllister, *Hawaii*
A. Smith, *Chicago*
A. Walsh, *Australia*

An Analytical Infrared Radiation Model of the Earth

R. A. McGee

The spectral distribution and total intensity of the earth's radiation to space is of interest in the design of instrumentation systems for satellites and in the computation of radiant heat transfer to a satellite. In the absence of sufficient experimental data, an analytical model has been derived covering several types of atmospheric conditions. The necessary equations and relationships are derived, and some results (based on a 1959 ARDC model atmosphere) are presented for several different cloud conditions. An estimate of the appearance of the earth's infrared horizon is also presented.

Introduction

Instrumentation systems which must detect infrared radiation from the earth have traditionally been designed to take advantage of the atmospheric window between 8 and 12 μ. The earth has generally been assumed to be a blackbody radiator at a temperature of approximately 280°K. Maximum spectral radiance occurs at about 10 μ, which is also the point of maximum atmospheric transmission. A large share of the earth's radiant energy can be collected in this spectral region, and the gradient between earth and space should be a maximum.

Recent observations of Tiros' records and other data, however, have raised questions about the effect of clouds and other atmospheric conditions. Large changes in apparent earth temperature have been noted, and in many cases these appeared to be related to the presence of large storms or cloud formations. To determine how best to handle these variations, it was necessary to verify the cause. A study was, therefore, undertaken to determine the infrared characteristics of the earth as viewed from space for several atmospheric temperature profiles under varying conditions of cloud cover.

Obviously, the best approach to this problem would be to collect experimental data and use them to construct a model. The data might be obtained from a low-resolution scanning spectrometer in an earth satellite. This approach is extremely complicated and expensive, since no such instrumentation exists. The best available data are those from Tiros II and III, which are equipped with scanning radiometers which have channels encompassing the 8–12-μ and 8–30-μ spectral regions. Some of these data were studied in an attempt to determine whether the effect of clouds could be deduced. A comparison of some of the data with Weather Bureau data indicated that there were large drops in energy in some areas where there were cold cloud formations. The energy loss was much greater in the 8–12-μ channel than in the 8–30-μ channel. While this appeared to verify the conclusion that clouds might affect the operation of horizon-sensor systems, it was far from conclusive evidence. Therefore, it has been necessary to develop an analytical model and, in the absence of sufficient experimental data, to attempt to draw conclusions from it.

Description of Model

Previous attempts have been made to deduce the infrared radiation characteristics of the earth. One of the first was the analysis by Goldman and Singer.[1] In this analysis, the earth and its atmosphere is represented as two concentric spheres. The inner sphere is assumed to be a blackbody radiator at a temperature of 267°K. The outer sphere corresponds to the atmosphere at a blackbody temperature of 213°K. It is further assumed that the atmosphere absorbs all of the earth's radiation except that between 8 and 13 μ. The result is an estimate of the expected radiation to space in the 8–13-μ region, and an assumption that, at longer wavelengths, the earth looks like a blackbody at the temperature of the tropopause.

A slightly more detailed analysis was performed by L. Good.[2] The atmosphere was split into four layers as shown in Fig. 1, and each layer was assigned the temperature indicated. An ARDC model atmosphere (temperature and pressure profile) was assumed, and the radiation from the earth and each layer, and the amount absorbed in each layer, was calculated to give

---

The author is in the Light Military Electronics Department, General Electric Company, Utica, N.Y.

Received 28 February 1962.

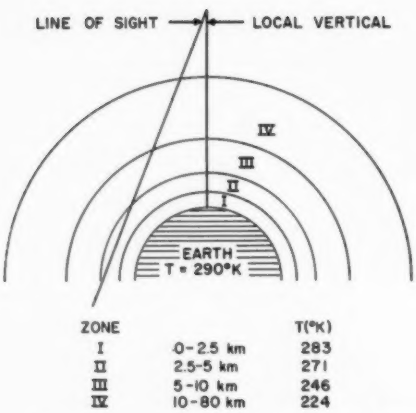

Fig. 1. Four-layer model (L. Good).

an estimate of the expected radiation levels. This model also ignores the effect of clouds, but gives an idea of the gradient from space to earth. The present model is an attempt to obtain a better estimate of radiation levels and the gradient at the horizon, and also to estimate the effect of clouds. The approach used in the derivation of this model is also the work of L. Good.

The atmosphere has been stratified into nine layers, as shown in Fig. 2. Each layer was assigned a temperature, which is the average temperature for that altitude. Five different temperature profiles were used in the study. These profiles are given in Table I, along with the altitude of the tropopause for each model. Clouds were assumed to exist at 2, 6, 10, and 12.5 km, and the temperatures shown in Table II were assigned to the clouds. It was necessary to assume that a cloud will transmit no radiation, so that the cloud itself becomes the lowest source of radiation.

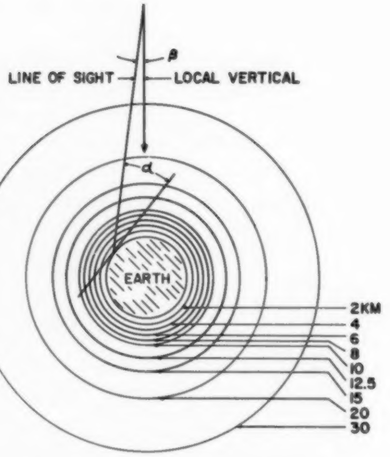

Fig. 2. Earth-model geometry.

Irradiance Due to Atmosphere

The scheme for determining the irradiance due to an element of atmosphere is illustrated in Fig. 3. The spectral irradiance at the detector is given by

$$\Delta H_\lambda = \omega N_\lambda t_\lambda \epsilon_\lambda, \tag{1}$$

where

ΔH_λ = spectral irradiance due to Δh,
ω = solid angle of optical system,
N_λ = spectral radiance of a blackbody,
t_λ = fractional transmission of medium between Δh and detector,
ϵ_λ = emissivity of Δh at wavelength λ.

Table I. Atmospheric Temperature Profiles (Temperatures are in °K)

Altitude (km)	ARDC	Hot	Tropical	Arctic	Cold
Earth	288	314	305	253	222
0–2	282	307	299	250	234
2–4	269	293	286	248	244
4–6	256	279	272	237	234
6–8	242	266	259	225	221
8–10	224	252	245	216	210
10–12.5	218	236	230	216	207
12.5–15	216	231	214	215	205
15–20	216	234	200	214	187
20–30	219	241	221	213	198
Altitude of tropopause (km)	11	12	17	8	9

This equation assumes that the element whose thickness is given by Δh occupies the entire field of view. The transmission of the optical system is not considered, and may be taken as unity at this point. Lambert's absorption law states that the fractional transmission of a substance is given by

$$t_\lambda = e^{-k_\lambda h}, \tag{2}$$

where k_λ is the fractional absorption coefficient and h is the optical thickness of the medium. If the medium has zero reflectivity, the fractional absorption is

$$a_\lambda = 1 - t_\lambda.$$

If the emissivity of the atmospheric element is assumed to be the same as its absorption, we can say

$$\epsilon_\lambda = 1 - t_\lambda.$$

Therefore,

$$\epsilon_\lambda = 1 - e^{-k_\lambda \Delta h}$$

for the atmospheric element. For very small x,

$$1 - e^{-x} \approx x$$

so that the above relation becomes

$$\epsilon_\lambda \approx k_\lambda\, \Delta h. \tag{3}$$

Substituting (3) and (2) in (1),

$$\Delta H_\lambda = \omega N_\lambda e^{-k_\lambda h}\,\Delta h. \tag{4}$$

Now if the spectral radiance N_λ is considered constant over the region from h_1 to h_2, then as $\Delta h \rightarrow 0$,

$$\begin{aligned} H_\lambda &= \omega N_\lambda \int_{h_1}^{h_2} k_\lambda\, e^{-k_\lambda h}\, dh \\ &= \omega N_\lambda [e^{-k_\lambda h_1} - e^{-k_\lambda h_2}]. \end{aligned}$$

For many sections, then, where N_λ is different in each section,

$$H = \omega \sum_{i=1}^{n} N_\lambda(i)[t_\lambda(h_{i-1}) - t_\lambda(h_1)]. \tag{5}$$

These results are based upon Eq. (2), which is true only for monochromatic radiation. Since radiation over a wide spectral band is to be considered, t_λ must be obtained for broadened spectral absorption lines. Elsasser's approximation[3] has been used for all component gases except water vapor. This results in an error-function absorption law,

Table II. Cloud Altitudes and Temperatures (Temperatures are in °K)

Altitude (km)	ARDC	Hot	Tropical	Arctic	Cold
2	275	300	293	251	246
6	249	272	266	231	228
10	223	245	238	216	208
12.5	...	230	222	...	...

$$t_\lambda = 1 - \text{erf}\,[(\lambda l a d)^{1/2}/\delta], \tag{6}$$

where

δ = separation of absorption lines,
d = absorption line half-width,
l = optical thickness of gas,

and a is the mean exponential-law absorption coefficient, defined as

$$a = \frac{1}{\Delta\lambda}\int_{\lambda}^{\lambda+\Delta\lambda} a_\lambda d\lambda.$$

The error function is defined by

$$\text{erf}\,(x) = \frac{2}{\pi^{1/2}}\int_0^x e^{-t^2}\,dt.$$

If we define

$$L_\lambda = (\lambda\, ad)^{1/2}/\delta$$

then (6) may be written

$$t_\lambda = 1 - \text{erf}\,(L_\lambda l^{1/2}). \tag{7}$$

For water vapor, Goody's results[4,5] have been used.

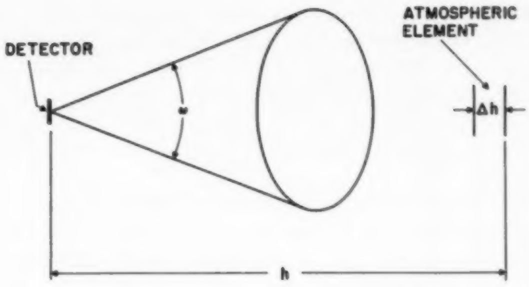

Fig. 3. Scheme for determining ΔH_λ.

$$t_\lambda = e^{-L_\lambda w^{1/2}}, \tag{8}$$

where w is the optical path of precipitable water vapor, and L_λ is defined as before. The total transmission is taken to be

$$t_\lambda(\text{total}) = t_\lambda(\text{H}_2\text{O})\cdot t_\lambda(\text{CO}_2)\cdot t_\lambda(\text{O}_3)\cdot t_\lambda(\text{N}_2\text{O}).$$

The L_λ for the various constituents have been obtained from Larmore,[6] Altshuler,[7,9] and from the absorption tube experiments of Howard, Burch, and Williams.[8]

Temperature and Pressure Corrections

The optical thicknesses of the constituents have been determined by the procedure developed by Altshuler.[9] These values are valid, however, only for the ARDC model atmosphere. For other models, corrections must be made for temperature and pressure. The pressure profiles used are shown in Table III. For water vapor, the corrections are given by

$$w = w'\left[1 + \frac{P - P'}{P}\right] C_T\,(\text{H}_2\text{O})\; k\,(\text{H}_2\text{O}).$$

Table III. Atmospheric Pressure Profiles (Pressures are in mm Hg)

Altitude (km)	ARDC	Hot Tropical	Cold Arctic
0	760	760	760
1	674	675	671
2	595	598	591
3	525	529	520
4	462	467	456
5	405	411	399
6	353	360	348
7	308	315	302
8	267	274	261
9	230	238	224
10	198	205	192
11	169	176	164
12	145	151	140
13	124	130	120
14	106	111	102
15	90	95	87
20	41	44	40

The primed quantities are those associated with the ARDC model atmosphere. The $k(H_2O)$ is a correction factor for tropopause altitude.[9] The temperature correction is given by[9]

$$C_T(H_2O) = \frac{P_v}{P'_v}\left(\frac{T'}{T}\right)^{1/2},$$

where P_v and P'_v are the saturation vapor pressures at the corresponding temperature. It is true that this correction is due to an absorption-band broadening effect, as are the others to be made, and should be made to the absorption coefficient. However, correcting the optical thickness produces the same numerical result.

For CO_2 and N_2O, corrections are made according to

$$l = l'\left[1 + \frac{2(P - P')}{P}\right]C_T.$$

The values of C_T have been taken from ref. 9. For ozone, the corrections used are

$$l(O_3) = l'(O_3)\left[1 + \frac{0.3\,(P - P')}{P}\right]\left[1 - \frac{0.15\,(T - T')}{T}\right].$$

Method of Solution

By this time, it has become apparent that solution of Eq. (5) would be, at best, a tedious process. This solution was left to the Burroughs 220 computer. It was assumed that N_λ is blackbody radiation and can be obtained from

$$N_\lambda = \frac{C_1}{\pi\lambda^5}\,\frac{1}{(e^{C_2/\lambda T} - 1)}$$

which is Planck's law for blackbody radiation. Equation (5) was then written out for the model described in Fig. 2:

$$\frac{H_\lambda}{\omega} = N_\lambda(20\text{–}30)\,[t_\lambda(30) - t_\lambda 20)] + N_\lambda(15\text{–}20)\,[t_\lambda(20) - t_\lambda(15)] + N_\lambda(12.5\text{–}15)\,[t_\lambda(15) - t_\lambda(12.5)] + N_\lambda(10\text{–}12.5)\,[t_\lambda(12.5) - t_\lambda(10)] + N_\lambda(8\text{–}10)\,[t_\lambda(10) - t_\lambda(8)] + N_\lambda(6\text{–}8)\,[t_\lambda(8) - t_\lambda(6)] + N_\lambda(4\text{–}6)\,[t_\lambda(6) - t_\lambda(4)] + N_\lambda(2\text{–}4)\,[t_\lambda(4) - t_\lambda(2)] + N_\lambda(0\text{–}2)\,[t_\lambda(2) - t_\lambda(0)] + N_\lambda(0)\,t_\lambda(0). \quad (9)$$

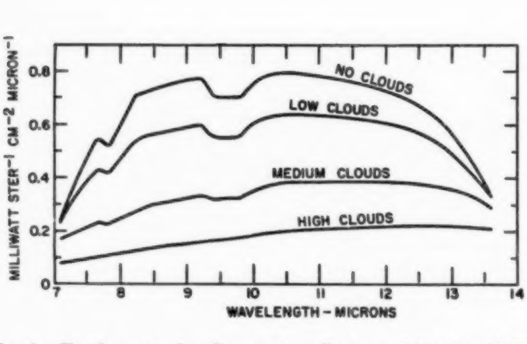

Fig. 4. Earth spectral radiance at nadir (α = 90°) (an ARDC atmosphere is assumed).

Referring to the geometry shown in Fig. 2, it can be seen that the optical paths, and therefore the t_λ, will vary with the angle α. The optical paths were computed for each altitude and α by Altshuler's procedure.[9] When clouds are present, the series (9) is truncated at the cloud altitude, and a term of the form $N_\lambda(C)t_\lambda(h_c)$ is added, where N_λ is computed for the cloud temperature, and t_λ is computed for the altitude of the top of the cloud.

Results

Results were obtained in increments of 0.1 μ from 2.7–5.3 μ; 0.5 μ from 5.6–7.1 μ; 0.2 μ from 7.6–11.0 μ; and 1.0 μ from 11.6–13.6 μ. These values were chosen primarily because of the optical transmission characteristics of a particular optical system. The values that are of interest to this portion of the study are those from 7.1–13.6 μ. This encompasses the atmospheric window, and is the region where clouds will have the greatest effect on the net radiation to space.

Some typical curves of the spectral radiance of the earth from 7.1–13.6 μ for an ARDC model atmosphere are shown in Figs. 4 and 5. Figure 4 assumes that the instrument looks straight down along the local vertical, and Fig. 5 assumes that it is looking at the horizon. Similar curves have been obtained for the other atmospheric models, and all indicate the severe effect of clouds in the spectral region. Curves have also been obtained for the case where the atmosphere, but not the earth, is in the field of view. A typical one is shown in Fig. 6. This shows the atmosphere to be a rather poor emitter in this wavelength interval, as is to be expected as a result of the assumption that emissivity is equal to absorptivity. When a cloud, which is a good emitter, appears the amount of energy escaping to space increases significantly.

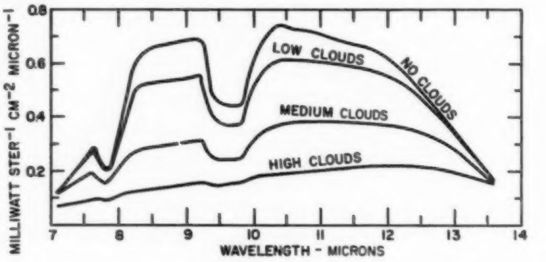

Fig. 5. Earth spectral radiance at the horizon (α = 0°) (an ARDC atmosphere is assumed).

To estimate the appearance of the infrared horizon, curves of the type of Figs. 4–6 were integrated, and a plot made of the resulting radiance as a function of look angle β. A typical set of results is shown in Fig. 7. It is evident that the location and nature of the infrared horizon is greatly dependent on cloud conditions. On the average, about 52% of the earth is covered by clouds.[10] This cloud cover varies with geographical location and season, and ranges from about 10% in the Sahara to regions of more than 80%. Thus, it is virtually inevitable that an instrument which detects sudden changes in IR radiant intensity and which operates in the 8–12-μ region will detect the presence of clouds.

If it is the purpose of the device to indicate the local vertical, the variations in the IR horizon will almost certainly produce errors. At high altitudes, however, these errors will be quite small. Reference to Fig. 7, which is drawn for an altitude of 148 km, indicates that appreciable error can occur at low altitudes.

So far, very little has been said about the nature of the radiation at shorter or longer wavelengths. At short wavelengths, the problem is that there is very little energy to detect, particularly in the presence of cold clouds. At wavelengths longer than 13.6 μ the carbon dioxide and water vapor in the atmosphere result in very low values of t_λ. The atmosphere will, therefore, absorb a large part of the radiation from the earth and the lower atmospheric layers. The emissivity of the top of the atmosphere, however, must be fairly high at these wavelengths in order to maintain thermal equilibrium. It can, therefore, be assumed that in the absence of clouds the earth will appear to be very nearly a blackbody radiator whose temperature is that of the air at the tropopause. When clouds are present at or above the tropopause altitude, the cloud will be the dominating radiator. As can be seen from Table I, the tropopause temperature will vary from approximately 200°K to 236°K, with the most probable temperatures around 215°K. High-altitude clouds will vary from 200°K to 240°K. Furthermore, a cloud is most likely to be at a temperature near that of its surroundings. Therefore, large thermal gradients are not likely to occur, and a system operating at longer wavelengths will not be able to detect the presence of clouds.

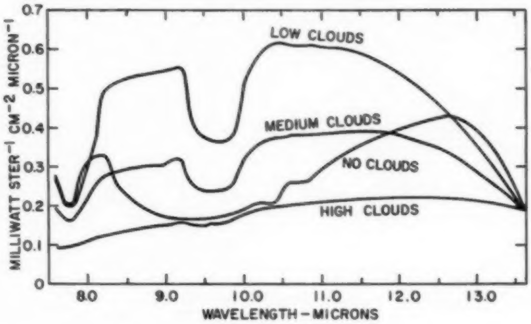

Fig. 6. Spectral radiance of the atmosphere.

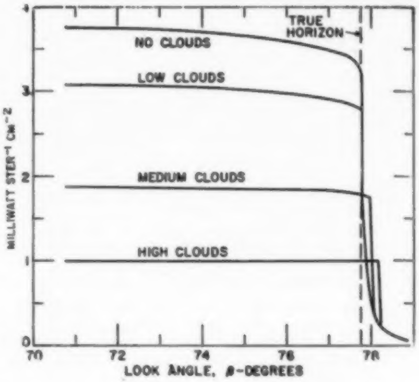

Fig. 7. Spectral radiance as a function of look angle β for various cloud conditions.

References

1. D. T. Goldman and S. F. Singer, Astronautica Acta **3**, 110 (1957).
2. L. Good, "Earth Background Radiation Analysis," General Electric Report No. R60ELC94 (Dec. 1960).
3. W. M. Elsasser, *Heat Transfer by Infrared Radiation in the Atmosphere*, Harvard Meteorological Studies 6 (Cambridge, Mass., 1942).
4. R. M. Goody, J. Roy. Meteor. Soc. **78**, 165 (1952).
5. H. Mayer, Los Alamos Report LA 647 (Oct. 31, 1947).
6. L. Larmore and S. Passman, Proc. IRIS **1** (1), 14 (1956); *ibid.* **1** (2), 15 (1956). These tables have also appeared in the *Handbook of Geophysics* (Macmillan, New York, 1959).
7. T. L. Altshuler, "A Procedure for Calculation of Atmospheric Transmission of Infrared," General Electric Report No. R57ELC15 (May 1957).
8. J. N. Howard, D. E. Burch, and D. Williams, "Near-Infrared Transmission through Synthetic Atmospheres," Geophysical Research Papers, No. 40, Ohio State University (1955).
9. T. L. Altshuler, "Infrared Transmission and Background Radiation by Clear Atmospheres," General Electric Report No. R61SD199 (Dec. 1961).
10. R. Duersch, "Conditions Affecting the Operation of Infrared Horizon Seekers," General Electric Report No. R60-EML67 (Sept. 1960).

Bibliography

H. L. Hackforth, *Infrared Radiation* (McGraw-Hill Book Company, Inc., New York, 1960).

M. Jakob and G. S. Hawkins, *Elements of Heat Transfer and Insulation* (John Wiley and Sons, Inc., New York, 1950), 2nd ed.

Proc. IRE **47**, 1413–1700 (1959). (Special Issue on Infrared Physics and Technology.)

T. L. Altshuler, "Methods for Determining the Optical Thicknesses of Various Atmospheric Gases and Vapors," General Electric Report No. CPO 1063 (1959).

Meetings Calendar

continued from page 558

September

— Internatl. Conf. on Information Theory, Sendai, Japan *G. L. Turin, U. of Calif., Berkeley, Calif.*

October

1-6 Internatl. Soc. of Photogrammetry, Commissions 1-4 Mtg., Milan *A. L. Nowicki, c/o Army Map Service, 6009 Mass. Ave., N.W., Washington, D.C.*

— Internatl. Conf. on the Science of Photography, Turin, Italy

— 4th Internatl. Color Conf., Budapest *M. K. Egyesülete, Szabadság-ter 17, Budapest 5, Hungary*

— IAU, 23rd Exec. Comm. Mtg., Erevan, Armenia, U.S.S.R. *D. H. Sadler, c/o Royal Greenwich Observatory, Herstmonceux Castle, Hailsham, Sussex, England*

1964

June

21–26 ASTM Ann. Mtg., Conrad Hilton Hotel, Chicago *ASTM, 1916 Race St., Philadelphia 3, Pa.*

FUTURE MEETINGS

OPTICAL SOCIETY OF AMERICA

1962 4–6 October
Rochester, N.Y.
Manger Hotel
Details to be announced
1963 24–28 March
Spring Meeting
Jacksonville, Fla.
1963 22–26 October
Fall Meeting
Chicago, Ill.
1964 Spring Meeting
Washington, D.C.
Fall Meeting
New York, N.Y.
1965 Spring Meeting
Dallas, Tex.

Executive Office
1155 16th Street, N.W. Washington 6, D.C.

Back Numbers of the Journal of the Optical Society of America

The OSA Executive Office is anxious to locate for its Library one copy each of the publications listed below. If any reader has a copy available, will he please contact the Assistant Secretary at the OSA Executive Office, 1155 Sixteenth Street, N.W., Washington 6, D.C.

Year	Volume	Number	Month
1920	IV	5	September
1921	V	1	Jan.-Feb.
1921	V	4	July-Aug.
1921	V	5	Sept.-Oct.
1921	V	6	Nov.-Dec.
1922	VI	3	March
1923	7	9	September

SCIENTWISTS

Reproduced by kind permission of the Editor of CHEMunications

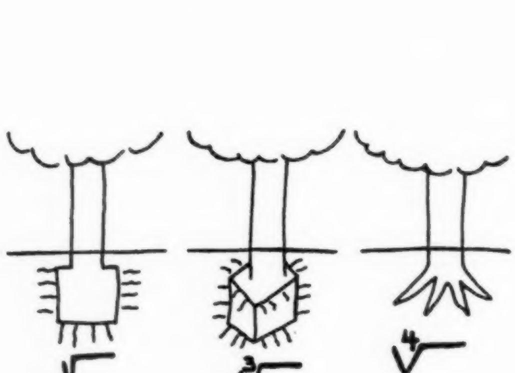

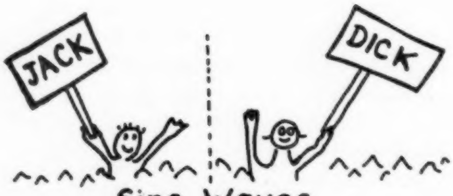

Sine Waves
(Convection Currents)

New Backscattering Computation and Tables for Dielectric and Metal Spheres

Simpson B. Adler and Robert S. Johnson

This paper presents the results of new computations of radar cross sections for dielectric and metal spheres. Tables resulting from digital computer solutions of the classical Mie scattering coefficients are given in increments of 0.01 circumference to wavelength ratio. The phase of the backscattered wave is also given. Recursion relations are used to transform the scattering coefficients for machine computation. The precision of the new computation is discussed.

Introduction

The availability of modern apparatus and techniques has renewed interest in the subject of electromagnetic scattering. This has been particularly true in the missile and satellite tracking field where increased demands on optical instruments and radar have resulted in their use for the measurement of target cross section. Large-scale digital computers also have made it possible to obtain numerical solutions of the classical Mie scattering coefficients, thus making available theoretical solutions for comparison with experimental data. This paper presents the results of such computations for teflon, lucite, bakelite, water, and aluminum spheres in the region $0.1 \leq 2\pi r/\lambda \leq 10$. These computations were used to compare with radar data on 5518, 5600, and 5800 Mc/sec (reported elsewhere).*

Background

The scattering of a plane wave by a sphere was first solved by Mie[1] in 1908. The solution of this boundary value problem for backscattering is given by[2]

$$\frac{\sigma}{\pi r^2} = \frac{1}{\rho^2}\left|\sum_{n=1}^{\infty}(-1)^n(2n+1)(a_n - b_n)\right|^2, \tag{1}$$

where the scattering coefficients are given by

$$a_n = -\frac{j_n(\rho)[N\rho j_n(N\rho)]' - j_n(N\rho)[\rho j_n(\rho)]'}{h_n^{(2)}(\rho)[N\rho j_n(N\rho)]' - j_n(N\rho)[\rho h_n^{(2)}(\rho)]'} \tag{2}$$

and

$$b_n = -\frac{N^2 j_n(N\rho)[\rho j_n(\rho)]' - j_n(\rho)[N\rho j_n(N\rho)]'}{N^2 j_n(N\rho)[\rho h_n^{(2)}(\rho)]' - h_n^{(2)}(\rho)[N\rho j_n(N\rho)]'}, \tag{3}$$

where

σ = radar cross section,
r = radius of the sphere,
n = integer,
$\rho = k_2 r = 2\pi r/\lambda$ (free space),
$N = k_1/k_2$ is the refractive index with k_1 and k_2 the respective propagation constants within the sphere and the surrounding medium,
λ = wavelength,
$j_n(\rho)$ and $h_n^{(2)}(\rho)$ are the spherical Bessel and Hankel functions and the prime denotes differentiation with respect to the argument.

A number of workers in this field have called attention to the difficulty in reducing the solution to numerical results. This is because of the lack of tables for the spherical functions of complex argument and because of the slow convergence of the series. In the present work, recursion relations were used to put the equations into a form that could be programmed on a digital computer.

Radar Cross Section of Metal Spheres

In the special case of metal spheres, whose conductivity is large relative to the surrounding medium, $N\rho >> 1$, the use of the asymptotic expressions for the Bessel functions results in a simplification of the scattering coefficients. Thus in this approximation[3] Eqs. (2) and (3) become

$$a_n = -\frac{j_n(\rho)}{h_n^{(2)}(\rho)}; \quad b_n = -\frac{[\rho j_n(\rho)]'}{[\rho h_n^{(2)}(\rho)]'}. \tag{4}$$

Using the recursion relation

The authors are with Radio Corporation of America, Moorestown, N.J.

Received 30 October 1961.

* This work is based on a thesis submitted to the Temple University Graduate Council in partial fulfillment of the requirements for the Ph.D. degree.

$$[\rho z_n(\rho)]' = \rho z_{n-1}(\rho) - n z_n(\rho), \tag{5}$$

$$z_n = j_n \text{ or } h_n^{(2)},$$

the scattering coefficients difference becomes

$$a_n - b_n = -\frac{j_n(\rho)}{h_n^{(2)}} + \frac{\rho j_{n-1}(\rho) - n j_n(\rho)}{\rho h_{n-1}^{(2)}(\rho) - n h_n^{(2)}(\rho)}, \tag{6}$$

which reduces to

$$a_n - b_n = \rho \frac{h_n^{(2)}(\rho) j_{n-1}(\rho) - j_n(\rho) h_{n-1}^{(1)}(\rho)}{h_n^{(2)}(\rho)[\rho h_{n-1}^{(2)}(\rho) - n h_n^{(2)}(\rho)]}, \tag{7}$$

Table I. Normalized Radar Cross Section and Phase for Conducting Spheres ($N = \infty$)

ρ	$\sigma/\pi r^2$	ψ (deg)	ρ	$\sigma/\pi r^2$	ψ (deg)
0.4000	0.2229	−1.4489	5.2000	0.8336	53.2326
0.5000	0.5296	−3.0260	5.3000	0.7361	68.6973
0.6000	1.0451	−5.5349	5.4000	0.7207	85.5386
0.7000	1.7707	−9.0909	5.5000	0.7877	101.5538
0.8000	2.5960	−13.5323	5.6000	0.9160	115.2063
0.9000	3.2939	−18.3288	5.7000	1.0691	126.3344
1.0000	3.6376	−22.7189	5.8000	1.2057	135.5616
1.1000	3.5477	−26.0263	5.9000	1.2903	143.6793
1.2000	3.1046	−27.8520	6.0000	1.3026	151.4219
1.3000	2.4543	−27.9681	6.1000	1.2424	159.4603
1.4000	1.7377	−25.9683	6.2000	1.1279	168.4415
1.5000	1.0756	−20.6233	6.3000	0.9909	178.9876
1.6000	0.5727	−8.4286	6.4000	0.8677	191.5557
1.7000	0.3115	18.0585	6.5000	0.7896	206.0796
1.8000	0.3290	54.8465	6.6000	0.7753	221.6136
1.9000	0.5936	78.1788	6.7000	0.8260	236.6284
2.0000	1.0081	89.0380	6.8000	0.9258	249.9611
2.1000	1.4445	94.5851	6.9000	1.0465	261.3434
2.2000	1.7862	98.0825	7.0000	1.1557	271.1429
2.3000	1.9569	100.9409	7.1000	1.2250	279.9554
2.4000	1.9286	103.9221	7.2000	1.2377	288.3976
2.5000	1.7200	107.6555	7.3000	1.1923	297.0587
2.6000	1.3895	112.9593	7.4000	1.1025	306.5023
2.7000	1.0227	121.1512	7.5000	0.9931	317.2377
2.8000	0.7126	134.2634	7.6000	0.8933	329.5951
2.9000	0.5336	154.0184	7.7000	0.8287	343.4708
3.0000	0.5208	177.6036	7.8000	0.8151	358.1353
3.1000	0.6627	197.7373	7.9000	0.8541	12.4605
3.2000	0.9093	211.6438	8.0000	0.9337	25.5378
3.3000	1.1892	221.0060	8.1000	1.0314	37.0690
3.4000	1.4284	227.8129	8.2000	1.1212	47.2664
3.5000	1.5676	233.4059	8.3000	1.1798	56.5839
3.6000	1.5751	238.7127	8.4000	1.1926	65.5434
3.7000	1.4543	244.5255	8.5000	1.1576	74.6631
3.8000	1.2419	251.6997	8.6000	1.0854	84.4362
3.9000	0.9974	261.2719	8.7000	0.9960	95.2879
4.0000	0.7853	274.3550	8.8000	0.9133	107.4663
4.1000	0.6580	291.3352	8.9000	0.8585	120.8659
4.2000	0.6422	310.3806	9.0000	0.8452	134.9145
4.3000	0.7351	327.9355	9.1000	0.8754	148.7460
4.4000	0.9063	341.9116	9.2000	0.9399	161.6234
4.5000	1.1074	352.5338	9.3000	1.0208	173.2474
4.6000	1.2844	0.8825	9.4000	1.0962	183.7337
4.7000	1.3914	8.0038	9.5000	1.1466	193.4349
4.8000	1.4031	14.7594	9.6000	1.1595	202.7932
4.9000	1.3204	21.9066	9.7000	1.1324	212.2646
5.0000	1.1688	30.1965	9.8000	1.0735	222.2812
5.1000	0.9909	40.4132	9.9000	0.9992	233.2037
			10.0000	0.9292	245.2319

Substituting in Eq. (1),

$$\frac{\sigma}{\pi r^2} = \frac{1}{\rho}\left|\sum_{n=1}^{\infty} (-1)^n (2n+1) \frac{h_n^{(2)}(\rho) j_{n-1}(\rho) - j_n(\rho) h_{n-1}^{(2)}(\rho)}{h_n^{(2)}(\rho)[\rho h_{n-1}^{(2)}(\rho) - n h_n^{(2)}(\rho)]}\right|. \tag{8}$$

This equation for the normalized radar cross section of metal spheres was programmed for the digital computer for critical size values $0.4 \leq \rho \leq 10$ in increments of 0.01. The machine computations were made using the recursion relation

$$z_{n-1} + z_{n+1} = \frac{2n+1}{\rho} z_n \tag{9}$$

and the auxiliary relations

$$j_0(\rho) = \frac{\sin\rho}{\rho}; \quad h_0^{(2)}(\rho) = \frac{\sin\rho + i\cos(\rho)}{\rho},$$

$$j_1(\rho) = \frac{\sin\rho - \rho\cos\rho}{\rho^2},$$

$$h_1^{(2)}(\rho) = \frac{\sin\rho - \rho\cos\rho + i(\cos\rho + \rho\sin\rho)}{\rho^2}. \tag{10}$$

The phase of the backscattered wave was also computed during the same operation. The angle ψ is defined as follows:

$$iS = |S_0| e^{i\psi}, \tag{11}$$

where

$$S = \sum_{n=1}^{\infty} (-1)^n (2n+1)(a_n - b_n). \tag{12}$$

Then (1) becomes

$$\frac{\sigma}{\pi r^2} = \frac{1}{\rho^2}|S|^2 = \frac{|S_0|^2}{\rho} e^{2i\psi}. \tag{13}$$

The computer solutions for metal spheres are given in graphs and tables to 4 decimal places with the last

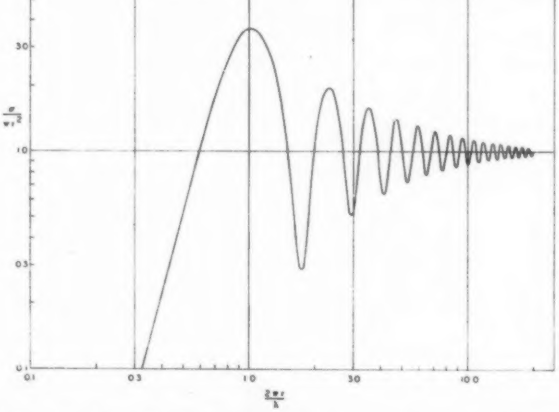

Fig. 1. Normalized cross section for conducting spheres.

Table II. Normalized Radar Cross Section and Phase for Teflon Spheres $N = 1.45957 - 0.01897i$

ρ	$\sigma/\pi r^2$	ψ (deg)		ρ	$\sigma/\pi r^2$	ψ (deg)	
0.2000	0.0005	−2.1358		2.6000	0.2286	43.5670	
0.3000	0.0023	−2.3572		2.7000	0.1451	14.3999	
0.4000	0.0071	−2.7872		2.8000	0.1102	−26.8545	
0.5000	0.0167	−3.5050		2.9000	0.1448	−68.0675	
0.6000	0.0326	−4.5978		3.0000	0.2391	83.2484	−540
0.7000	0.0559	−6.1601		3.1000	0.3661	63.4339	↓
0.8000	0.0863	−8.2921		3.2000	0.4935	47.4691	
0.9000	0.1216	−11.0980		3.3000	0.5849	32.3670	
1.0000	0.1570	−14.6875		3.4000	0.6022	16.3050	
1.1000	0.1856	−19.1866		3.5000	0.5259	−1.9088	
1.2000	0.1996	24.7691		3.6000	0.3855	−23.4329	
1.3000	0.1923	−31.7329		3.7000	0.2513	−50.4406	
1.4000	0.1619	−40.6793		3.8000	0.1827	−85.1872	
1.5000	0.1140	−53.0116		3.9000	0.2025	57.8681	−720
1.6000	0.0629	−72.6551		4.0000	0.3087	28.4344	↓
1.7000	0.0296	68.4667	−180	4.1000	0.4834	6.0734	
1.8000	0.0349	9.0318	↓	4.2000	0.6791	−13.3276	
1.9000	0.0874	−27.9194		4.3000	0.8079	−32.1432	
2.0000	0.1751	−48.6276		4.4000	0.7931	−50.9463	
2.1000	0.2711	−63.4930		4.5000	0.6502	−69.7785	
2.2000	0.3479	−76.0250		4.6000	0.4680	−89.6747	
2.3000	0.3864	−87.9883		4.7000	0.3240	66.5718	−900
2.4000	0.3764	79.1593	−360	4.8000	0.2592	35.9153	↓
2.5000	0.3181	63.7943	↓	4.9000	0.2988	1.0089	
				5.0000	0.4562	−30.7682	

place rounded off. The normalized radar cross section, Eq. (8), is given in Fig. 1 and Table I.[4] The phase of the backscattered wave is also given in Table I.

Radar Cross Section of Dielectric Spheres

The complete formal solution, Eq. (1), with coefficients, Eqs. (2) and (3), must be computed for the case of dielectric spheres. The equations for the coefficients were simplified for machine computation as follows.

From the recursion relation (5) the scattering coefficients become

$$a_n = \frac{j_n(N\rho)j_{n-1}(\rho) - Nj_n(\rho)j_{n-1}(N\rho)}{Nh_n^{(2)}(\rho)j_{n-1}(N\rho) - h_{n-1}^{(2)}(\rho)j_n(N\rho)},$$

$$b_n = \frac{N\rho j_n(\rho)j_{n-1}(N\rho) - N^2\rho j_n(N\rho)j_{n-1}(\rho) + n(N^2-1)j_n(N\rho)j_n(\rho)}{N^2\rho j_n(N\rho)h_{n-1}^{(2)}(\rho) - N\rho h_n^{(2)}(\rho)j_{n-1}(N\rho) - n(N^2-1)j_n(N\rho)h_n^{(2)}(\rho)}, \quad (14)$$

defined as follows:

$$N^2 = \left(\frac{k_1}{k_2}\right)^2 = \left(\frac{\epsilon}{\epsilon_0} - i\frac{\sigma_e}{\omega\epsilon_0}\right) = (\epsilon_1 - i\epsilon_2) = \epsilon_1(1 - i\tan\delta), \quad (15)$$

where

ϵ/ϵ_0 = dielectric constant or permittivity relative to vacuum,
$\tan\delta$ = dielectric loss tangent or dissipation factor,
σ_e = electrical conductivity,
ω = circular frequency.

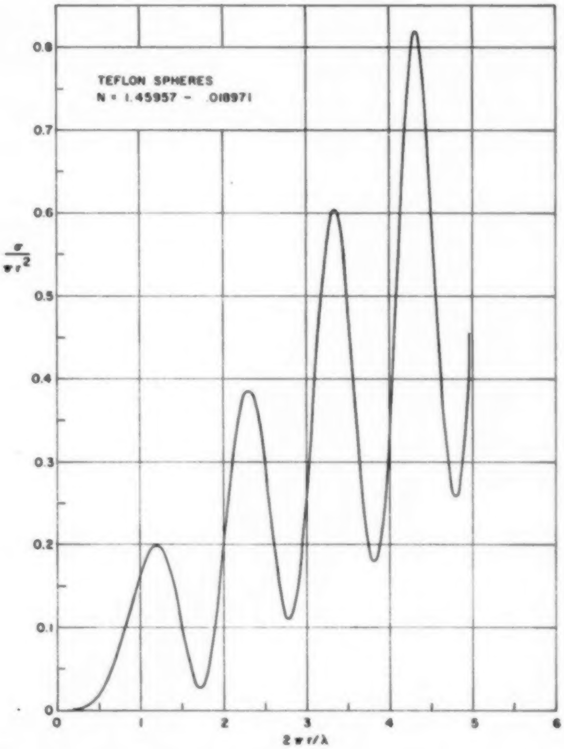

Fig. 2. Normalized cross section for teflon spheres.

Table III. Normalized Radar Cross Section for Lucite Spheres $N = 1.628 - 0.01953i$

ρ	$\sigma/\pi r^2$	ρ	$\sigma/\pi r^2$
0.2000	0.0008	2.7000	0.3617
0.3000	0.0040	2.8000	0.5650
0.4000	0.0122	2.9000	0.7783
0.5000	0.0287	3.0000	0.9862
0.6000	0.0566	3.1000	1.1381
0.7000	0.0979	3.2000	1.0962
0.8000	0.1520	3.3000	0.8312
0.9000	0.2143	3.4000	0.5843
1.0000	0.2741	3.5000	0.5381
1.1000	0.3158	3.6000	0.7017
1.2000	0.3220	3.7000	1.0625
1.3000	0.2812	3.8000	1.6547
1.4000	0.1974	3.9000	2.3912
1.5000	0.0994	4.0000	2.7083
1.6000	0.0413	4.1000	2.2910
1.7000	0.0759	4.2000	1.6517
1.8000	0.1986	4.3000	1.2125
1.9000	0.3444	4.4000	1.1044
2.0000	0.4568	4.5000	1.4243
2.1000	0.5181	4.6000	2.3759
2.2000	0.5197	4.7000	3.7111
2.3000	0.4461	4.8000	4.2674
2.4000	0.3080	4.9000	3.8841
2.5000	0.1951	5.0000	3.1578
2.6000	0.2143		

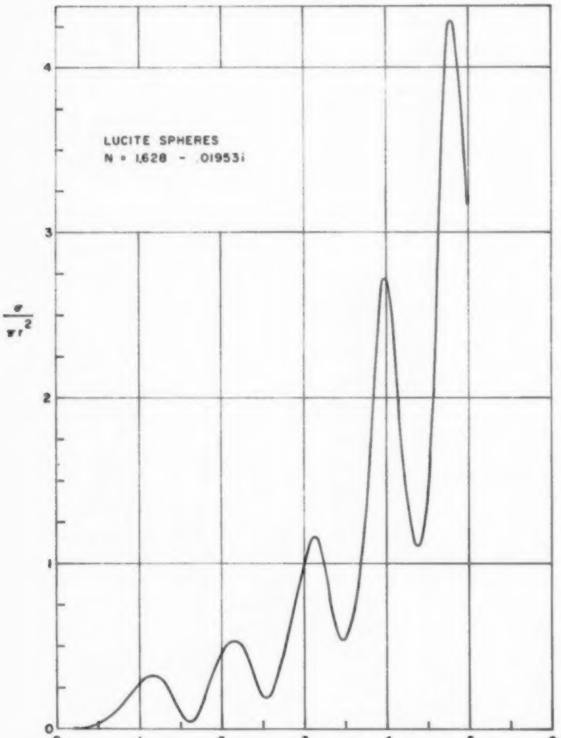

Fig. 3. Normalized cross section for lucite spheres.

The refractive indices of teflon, lucite, and bakelite were determined from the measured values of dielectric constant and loss tangent for these materials. The actual values used in the machine computation were: Teflon $N = 1.45957 - 0.01897i$, Lucite $N = 1.628 - 0.01953i$, Bakelite $N = 1.98511 - 0.02481i$, and Bakelite $N = 2.01284 - 0.03923i$.

The normalized radar cross section for these dielectric spheres was computed by solving Eq. (1) with coefficients given by Eq. (14) and the above values of refractive index. The solutions for values $0.2 \leq \rho \leq 5$ in increments of 0.01 are given in graphs and numerical tables to 4 decimal places with the last place rounded off. The normalized radar cross section for teflon is given in Fig. 2 and Table II.[4] The phase of the backscattered wave is also given in Table II. The normalized radar cross section for lucite is given in Fig. 3 and Table III,[4] and for two values of bakelite in Figs. 4 and 5 and Tables IV and V.[4]

Precision

In view of the moderate size of the numbers N and ρ under consideration, the only numerical difficulty to be expected was the usual one of losing accuracy in generating Bessel functions from the recurrence relation (9). Several different checks on the accuracy of our results were made, as described below.

1. The results for teflon were compared with experimental data, the agreement being good, as illustrated in Fig. 6.
2. Values of the Total Mie Scattering Coefficient, which were readily available from intermediate results, were compared with results given by Penndorf[5] for $N = 1.5$, $\rho = 2$, and $\rho = 9$, and were found to agree exactly with his to as many figures as he reports.
3. The normalized radar cross section $N = 8.18 - 1.96i$ is tabulated in Kerr[6] for a small range of values of ρ. This tabulation was made from values of a_n, b_n listed in "Tables of Scattering Functions for Spherical Particles" (National Bureau of Standards). The values of a_n, b_n are given there only to four digits, the last of which appears to have been truncated instead of rounded off. These may be compared with our results which are given in Table VI.[4] There is no reason to doubt that our results are the more accurate.
4. Both of the bakelite computations were repeated by using double-precision arithmetic, and never differed from the single-precision results by more than one part in ten thousand.

On the basis of these checks we are led to conclude that our results are accurate to the number of figures reported.

Programming

The equations were programmed for the IBM 709 in the Fortran II language. The current version of

Table IV. Normalized Radar Cross Section for Bakelite Spheres $N = 1.98511 - 0.02481i$

ρ	$\sigma/\pi r^2$	ρ	$\rho/\pi r^2$
0.2000	0.0016	2.6000	3.6047
0.3000	0.0078	2.7000	5.5696
0.4000	0.0242	2.8000	5.1723
0.5000	0.0577	2.9000	3.8064
0.6000	0.1151	3.0000	3.3068
0.7000	0.2007	3.1000	3.3088
0.8000	0.3113	3.2000	3.6863
0.9000	0.4289	3.3000	6.7074
1.0000	0.5145	3.4000	9.4308
1.1000	0.5106	3.5000	8.0491
1.2000	0.3668	3.6000	6.4456
1.3000	0.1187	3.7000	4.2459
1.4000	0.0294	3.8000	2.5464
1.5000	0.3319	3.9000	3.0459
1.6000	0.6325	4.0000	5.6918
1.7000	0.6947	4.1000	5.9825
1.8000	0.6587	4.2000	7.0778
1.9000	0.6668	4.3000	7.0125
2.0000	0.7867	4.4000	3.7286
2.1000	1.0682	4.5000	2.2518
2.2000	1.5839	4.6000	2.4128
2.3000	2.1516	4.7000	1.7282
2.4000	2.5493	4.8000	2.1928
2.5000	2.8235	4.9000	4.2308
		5.0000	3.7463

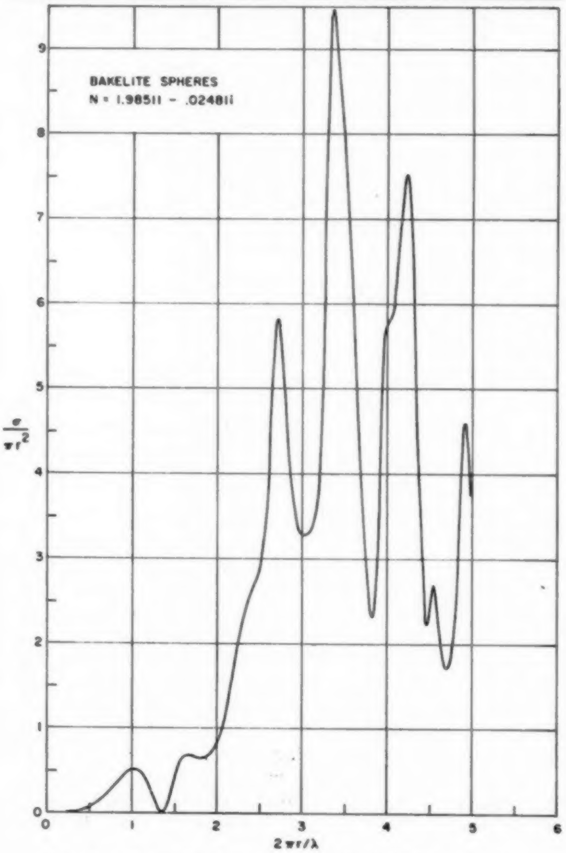

Fig. 4. Normalized cross section for bakelite spheres.

Table V. Normalized Radar Cross Section for Bakelite Spheres $N = 2.01284 - 0.03923i$

ρ	$\sigma/\pi r^2$	ρ	$\sigma/\pi r^2$
0.2000	0.0016	2.6000	3.7635
0.3000	0.0081	2.7000	4.8423
0.4000	0.0252	2.8000	3.8236
0.5000	0.0600	2.9000	2.9077
0.6000	0.1196	3.0000	2.6968
0.7000	0.2082	3.1000	2.8424
0.8000	0.3219	3.2000	3.6760
0.9000	0.4404	3.3000	6.5351
1.0000	0.5206	3.4000	6.9608
1.1000	0.5002	3.5000	5.8743
1.2000	0.3302	3.6000	4.2642
1.3000	0.0740	3.7000	2.4639
1.4000	0.0445	3.8000	1.7040
1.5000	0.3793	3.9000	2.8279
1.6000	0.6292	4.0000	3.7600
1.7000	0.6547	4.1000	4.4146
1.8000	0.6085	4.2000	5.1272
1.9000	0.6100	4.3000	3.7554
2.0000	0.7015	4.4000	1.8409
2.1000	0.9918	4.5000	1.3705
2.2000	1.5579	4.6000	0.8708
2.3000	2.1205	4.7000	0.8635
2.4000	2.4809	4.8000	1.5951
2.5000	2.7956	4.9000	2.3705
		5.0000	1.6867

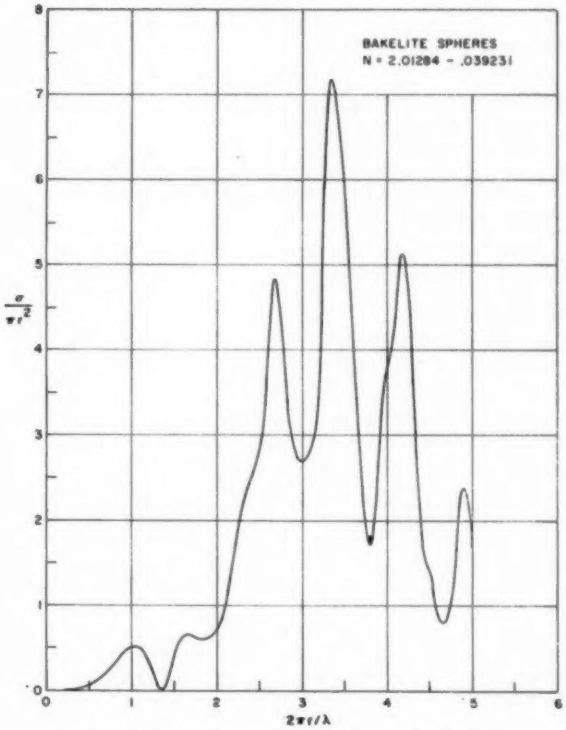

Fig. 5. Normalized cross section for bakelite spheres.

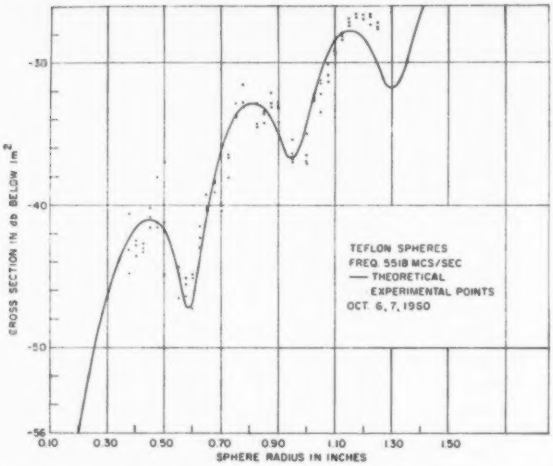

Fig. 6. Comparison of computed and experimental values of normalized cross section for teflon spheres.

the program also calculates the Total Mie Scattering Coefficient and the (normalized) Total Scattering Cross Section as defined by Kerr,[7] since these quantities can be obtained with very little additional labor.

Thanks are due J. L. Bohn for his advice and encouragement of this work and to J. H. Andrews who assisted with the programming. The authors also appreciate the cooperation of the U.S. Army Signal Corps.

Bakelite, teflon, and lucite are trademarks.

Table VI. Normalized Radar Cross Section for Water Spheres
$N = 8.18 - 1.96i$

ρ	$\sigma/\pi r^2$	ρ	$\sigma/\pi r^2$
0.1000	0.0004	2.3000	1.2719
0.2000	0.0050	2.4000	1.1619
0.3000	0.0251	2.5000	0.9542
0.4000	0.2062	2.6000	0.7081
0.5000	0.5131	2.7000	0.4891
0.6000	0.8415	2.8000	0.3487
0.7000	1.3832	2.9000	0.3186
0.8000	2.1040	3.0000	0.3980
0.9000	2.5087	3.1000	0.5488
1.0000	2.5236	3.2000	0.7262
1.1000	2.3419	3.3000	0.8909
1.2000	1.9657	3.4000	0.9897
1.3000	1.4520	3.5000	0.9887
1.4000	0.9331	3.6000	0.9142
1.5000	0.5089	3.7000	0.7932
1.6000	0.2370	3.8000	0.6289
1.7000	0.1584	3.9000	0.4815
1.8000	0.2756	4.0000	0.4160
1.9000	0.5296	4.1000	0.4071
2.0000	0.8302	4.2000	0.4430
2.1000	1.0918	4.3000	0.5655
2.2000	1.2496	4.4000	0.7076

References

1. G. Mie, Ann. Physik **25**, 377 (1908).
2. D. E. Kerr, ed., *Propagation of Short Radio Waves* (McGraw-Hill, New York, 1951), p. 451.
3. D. E. Kerr, see ref. 2, p. 452.
4. Tables for incremental values of $\rho = 0.01$ have been deposited as Document Number **S-289** with University Microfilms Inc., 313 N. 1st Street, Ann Arbor, Mich. A reprint or microfilm copy may be obtained at a nominal price.
5. R. B. Penndorf, J. Opt. Soc. Am. **47**, 1010 (1957).
6. D. E. Kerr, see ref. 2, p. 612.
7. D. E. Kerr, see ref. 2, p. 449.

REFEREES

The following people referee papers submitted to APPLIED OPTICS from time to time, and the Editors wish to acknowledge with gratitude this service:

H. H. Allen, Jr., G. F. Aroyan, J. G. Atwood, A. V. Baez, J. G. Baker, S. S. Ballard, R. Barakat, R. B. Barnes, E. Barr, E. S. Barr, A. M. Bass, J. R. Benford, L. E. Bergstein, B. H. Billings, L. S. Birks, H. H. Blau, W. S. Boyle, E. Burstein, F. F. Byrne, H. Cary, R. M. Chapman, L. H. Chasson, C. B. Childs, C. H. Church, K. C. Clark, G. W. Cleek, V. J. Coates, R. J. Collins, W. A. Craven, Jr., A. Danti, H. A. Daw, E. S. Dayhoff, J. A. Dobrowolski, K. Dressler, M. Dreyfus, W. G. Driscoll, S. Q. Duntley, D. Dutton, H. Edgerton, D. F. Eggers, Jr., R. S. Estey, E. Evtuhov, W. Fastie, D. P. Feder, P. A. Franken, J. S. Garing, N. Ginsburg, J. P. Gordon, G. E. Gross, F. F. Hall, Jr., G. B. Harrison, L. W. Herscher, M. Herzberger, I. C. Hisatsune, R. E. Hopkins, G. A. Hornbeck, E. O. Hulburt, R. S. Hunter, W. L. Hyde, J. A. Hynek, S. S. Impiombato, R. C. Jones, R. N. Jones, K. Innes, J. A. Jamieson, L. D. Kaplan, S. Katz, J. W. Kemp, K. G. Kessler, J. I. F. King, R. Kingslake, W. F. Koehler, N. Kriedl, E. W. Kutzscher, J. Lambe, E. Leith, E. V. Lowenstein, D. J. Lovell, C. F. Luck, T. K. McCubbin, R. K. McDonald, R. H. McFee, J. R. McNally, Jr., R. P. Madden, A. D. May, A. B. Meinel, P. E. Mengers, L. H. Meuser, D. F. Nelson, P. Nolan, R. A. Oetjen, J. Parsons, F. H. Perrin, G. N. Plass, E. K. Plyler, H. D. Polster, R. Potter, R. W. Powell, D. Richardson, D. W. Robinson, D. Z. Robinson, N. Rosenberg, J. A. Sanderson, J. B. Saunders, A. L. Schawlow, B. F. Scribner, J. H. Shaw, E. H. Siegler, W. Sinton, F. S. Smith, E. Snitzer, P. P. Sorokin, I. Spiro, V. J. Stakutis, O. N. Stavroudis, S. Sternberg, H. S. Stewart, B. Stoicheff, G. W. Stroke, R. E. Stroup, R. Tabeling, R. M. Talley, Y. Tanaka, R. W. Terhune, R. Tousey, A. F. Turner, G. A. Vanasse, M. E. Warga, J. U. White, B. W. Wild, P.G. Wilkinson, P. A. Wilks, Jr., V. Z. Williams, D. E. Williamson, M. K. Wilson, W. Wolfe, E. M. Wormser, N. Wright, H. W. Yates, M. Zelikoff, and G. J. Zissis.

Measurements of Second Harmonic Generation of the Ruby Laser Line in Piezoelectric Crystals

Albert Savage and Robert C. Miller

The relative efficiency of a number of materials which generate the second harmonic of the ruby laser line has been measured. Potassium dihydrogen phosphate (KDP) was the most efficient crystal measured. There seems to be no general correlation between the second harmonic intensities of the crystals investigated and their physical properties, e.g., crystal symmetry, and whether or not the crystal is ferroelectric. In all cases where a second harmonic output was expected it has been observed. Of particular interest is guanidine carbonate which did not exhibit second harmonic generation. This result is in agreement with recent theoretical considerations which predict that second-order polarization should not occur in crystals with point symmetry D_4 or D_6 even though these crystals may be piezoelectric.

Introduction

Several investigations on the generation of optical harmonics have recently been described in the literature. Franken *et al.*[1] were first to report second harmonic generation at 3467 Å of the pulsed ruby laser line at 6934 Å in crystalline quartz. In later investigations, second harmonic light was observed in triglycine sulfate[2] (TGS), potassium dihydrogen phosphate[3,4] (KDP), and in several other piezoelectric materials.[5] A comparison of the relative efficiencies for second harmonic generation of a wide range of materials has not been described in the literature.

The restrictions imposed on the generation of the second harmonic are that a material should have suitable nonlinear dielectric coefficients for second-order polarization and in addition be transparent to the fundamental optical frequency and to its second harmonic.[1] The point symmetry of the medium will yield a six by three matrix with 18 independent coefficients in the most general case. If this matrix, called the second-order polarization matrix, is then multiplied by the six-component column vector **E E**, directions in the crystal can be deduced for which the intense coherent incident beam will produce a light output at half the wavelength of the incident beam.

This paper describes experiments and presents quantitative data on the room temperature relative intensities of second harmonic light of the ruby laser line in a variety of crystals. Eight nonferroelectric piezoelectric materials reported on here are: potassium dihydrogen phosphate (KDP), ammonium dihydrogen phosphate (ADP), crystalline quartz, sodium chlorate, sodium bromate, Rochelle salt, tourmaline, and guanidine carbonate. In addition, seven materials which are ferroelectric at room temperature were measured; triglycine sulfate (TGS), barium titanate, potassium-doped sodium niobate, guanidine aluminum sulfate hexahydrate (GASH), and three of its isomorphs guanidine aluminum selenate hexahydrate (GASeH), guanidine gallium sulfate hexahydrate (GGSH), and guanidine gallium selenate hexahydrate (GGSeH).

Method

Multiplication of the second-order polarization matrix by the symmetric tensor **E E** indicates the more favorable crystal directions for second harmonic generation. Desired crystal cuts which could not be cleaved or which did not occur as suitable cuts in their grown state, were cut from the parent crystal and polished using conventional techniques. The thickness of the crystals was such that of the order of 90% or more of the light of second harmonic frequency would be transmitted.

The experimental apparatus used for measuring the output light intensity is shown in Fig. 1. The laser beam is focused in the material under investigation near the front surface with a 16-mm *f*/2 microscope objective, L_0. The crystal is mounted on the entrance

---

The authors are at Bell Telephone Laboratories, Murray Hill, New Jersey.

Received 24 April 1962.

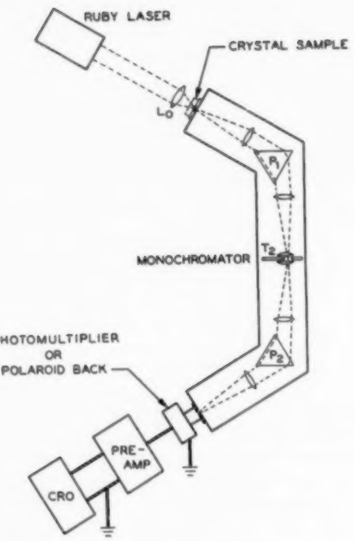

Fig. 1. Experimental arrangement for irradiating crystals with ruby laser light (6944 Å) and measuring the second harmonic blue light output (3472 Å). L_0 is a 16-mm focal length $f/2$ lens for focusing the laser beam in the samples. The path of the blue light through the $f/4.5$ double-prism monochromator is indicated. The blue light is incident on a photomultiplier tube, the resultant signal amplified, and displayed on a dual-beam oscilloscope. The photomultiplier tube may be replaced with a Polaroid camera back.

slit of the double-prism monochromator tuned to 3467 Å. To eliminate scattered red light that finds its way through the monochromator, filters (Corning 5874, 9863, and $NiSO_4$ aqueous solution) were inserted in the light path at a point in the system where the light is parallel, namely, before and after the second prism, P_2. For quantitative measurements the ultraviolet second harmonic was detected with a photomultiplier tube. The integrated output of the photomultiplier was fed through a wide-band amplifier, the output of which was viewed on a dual-beam oscilloscope. Part of the laser output reflected from the focusing objective was detected by a phototube and observed simultaneously along with the second harmonic output on the oscilloscope.

On occasion, the photomultiplier tube was replaced with a Polaroid back loaded with ASA 3000 film. In cases where the output second harmonic signal exceeded of the order of 10^5 photons, a spot on the Polaroid film was easy to see after one flash of the laser. With the photomultiplier as a detector, as few as about 10 second harmonic photons could be observed.

To determine whether or not the observed output was the second harmonic, wherever possible four tests were used. The first was to insert a filter (Corning 3850) in the light path within the monochromator which eliminated all wavelengths below 3600 Å. This, however, was not a conclusive test since "white light" may result from crystal damage by the extremely intense incident beam. The second test was to adjust the monochromator to pass some wavelength above or below 3467 Å and to observe the output. A sharp reduction in the detuned position indicates that the signal observed at the tuned position is not due to "white light." The third test was to introduce a calibrated neutral density filter in the incident laser light beam path. If then the light output being observed was indeed the second harmonic, its intensity should vary as the incident intensity to the second power.[1] The fourth test involved the polarization of the incident beam. Second harmonic generation in the KDP, ADP, Rochelle salt, $NaClO_3$, and $NaBrO_3$ samples measured (110), i.e., the laser beam normal to the (110) crystal face, should show a marked dependence on the polarization of the incident beam. If the incident beam were polarized in the z direction for the (110) orientation, for example, second harmonic generation should not occur. However, if the beam were polarized perpendicular to the z axis a second harmonic output can occur. Consideration of the results of the four tests described above will give a conclusive answer whether or not the second harmonic is being observed, rather than some spurious light or electrical noise.

Some of the crystals measured could be damaged by the focused laser beam which was about 200 W at the focusing objective aperture. It was therefore necessary in these cases to use calibrated neutral density filters in the path of the incident light beam and to correct the second harmonic output accordingly. The crystals for which the input light attenuation was necessary were $NaClO_3$, $NaBrO_3$, and K-doped $NaNbO_3$.

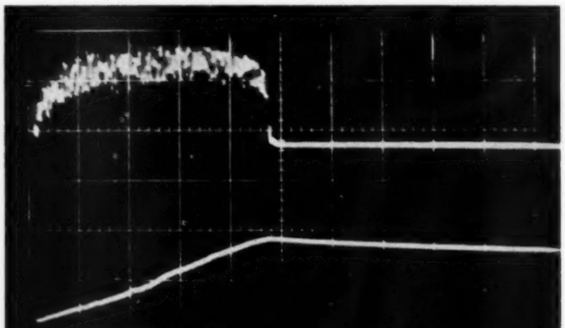

Fig. 2. Photograph of the oscilloscope trace of a typical output sequence. The upper and lower traces show the laser and the integrated second harmonic output, respectively, versus time.

Table I. Relative Values of Second Harmonic Output

Material	Crystals measured	Orientation[a]	Relative value
KDP	2	(110)	1000
ADP	2	(110)	720
K-doped NaNbO$_3$	2	(101)	230
Quartz	3	(001)	34.0
NaClO$_3$	2	(110)	11.0
NaClO$_3$	2	(111)	8.0
Tourmaline	1	(001)	10.0
TGS	2	(101)	3.2
TGS	2	(100)	1.3
TGS	2	(001)	1.0
Rochelle salt	3	(110)	1.2
NaBrO$_3$	2	(111)	0.54
GASeH	1	(001)	2.0
GGSH	1	(001)	0.82
GASH	3	(001)	0.39
GGSeH	1	(001)	0.21

[a] Crystal face normal to the laser beam.

Results and Discussion

Figure 2 shows a typical trace observed on the dual-beam oscilloscope. The upper wave form is the laser output and the lower wave form the integrated second harmonic output. The difference in output from one sample to another of the same material and orientation was generally less than 25%. Surface irregularities may account for this variation.

Table I gives the relative second harmonic outputs for all the crystals investigated. The relative values listed are averages of the results obtained for a given material and orientation. The value for KDP has been taken as 1000. The crystals which did not give a second harmonic output, BaTiO$_3$ and guanidine carbonate, have not been listed and will be discussed later.

It should be noted that the second harmonic output depends in part on the coherence volume[1,3,4] (the crystal volume over which the second-order polarization wave and the second harmonic light wave remain in phase) and the intensity of the optical electric field at the focus of the lens. Both of these quantities are determined by the detailed characteristics of the optical properties of the medium and will therefore vary from one material to another. Hence, the results given here simply indicate the over-all efficiency of second harmonic generation for samples of specified orientation placed at the focus of a fixed experimental arrangement and do not necessarily relate directly to the appropriate nonlinear coefficients of the materials investigated.

There does not seem to be any general correlation between the relative values. KDP, the most efficient second harmonic generator measured, and ADP are of the D_{2d} crystal class and do show a similarity in their relative harmonic intensities. However, tourmaline and GASH are of the crystal class C_3, and show a difference of about a factor of 25 in the relative harmonic output. Likewise, NaClO$_3$ and NaBrO$_3$ are of the same crystal class, T, and show an order of magnitude difference in output. In comparing the output intensities from the bromate and chlorate samples, it is interesting to note that the output intensity of the second harmonic is very sensitive to the halide ion in this structure. The ferroelectric crystals measured exhibit a wide range of efficiencies. The output of the (001) samples of GASH and TGS differ by little more than a factor of two. On the other hand the K-doped NaNbO$_3$ shows an output an order of magnitude larger than GASH or TGS. The isomorphs of GASH showed no consistent differences in their relative efficiencies. BaTiO$_3$ is an example of a material which does not fulfill the requirements of a second harmonic generator of the ruby line in that the crystals are opaque to wavelengths below 4000 Å.[7]

Of somewhat special interest is guanidine carbonate which, though it is piezoelectric and passes the fundamental and second harmonic wavelength, did not give any detectable second harmonic output. It has been suggested[6] that the coefficients d_{14}, d_{25}, and d_{36} in the second-order polarization matrix should all be equal. Hence, since $d_{36} = 0$ for guanidine carbonate,[8] second harmonic generation in this crystal should not occur. This prediction is in agreement with the present data. It should be emphasized that in all other cases where a second harmonic output is expected it has been observed.

The present results of the relative second harmonic intensities of TGS and quartz seem to disagree with the data of Bass *et al.*[2,9] The data presented here (obtained with an $f/2$ focusing lens and an $f/4.5$ monochromator) show that TGS is about one and a half orders of magnitude less efficient than quartz. Bass finds with his arrangement, $f/2$ focusing lens and an $f/22$ spectrograph,[9] that TGS appears to be more effective than quartz for the production of optical harmonics. In the present work, various cuts of TGS were measured so that all of the second-order polarization matrix elements were involved in at least one measurement. However, as shown in Table I none of the TGS crystals showed an output as large as that given by quartz. It may be in the case of TGS and quartz that the angular distribution of the second harmonic light is such that the relative measured intensities are a function of the f-number of the spectrograph.

The authors wish to thank D. A. Kleinman for several informative discussions and J. P. Remeika and E. M. Kelly for the excellent crystals used in these experiments.

References

1. P. A. Franken, A. E. Hill, C. W. Peters, and G. Weinreich, Phys. Rev. Letters **7**, 118 (1961).
2. M. Bass, P. A. Franken, A. E. Hill, C. W. Peters, and G. Weinreich, Phys. Rev. Letters **8**, 18 (1962).
3. J. A. Giordmaine, Phys. Rev. Letters **8**, 19 (1962).
4. P. D. Maker, R. W. Terhune, M. Nisenoff, and C. M. Savage, Phys. Rev. Letters **8**, 21 (1962).
5. B. Lax, J. G. Mavroides, and D. F. Edwards, Phys. Rev. Letters **8**, 166 (1962).
6. D. A. Kleinman, Bull. Am. Phys. Soc. Ser. II **7**, 195 (1962) and to be published.
7. T. Norie, K. Kawabe, and S. Sawada, J. Phys. Soc. Japan **9**, 323 (1954).
8. "IRE Standards on Piezoelectric Crystals," Proc. IRE **46**, 764 (1958).
9. P. A. Franken, private communication.

HAVE YOU SENT IN YOUR SUBSCRIPTION FOR 1962?

Contents of Optics and Spectroscopy

VOL. XII, JUNE 1962. *This issue will be published in complete translation by the Optical Society of America in* August.

Yu. I. Ostrovsky and N. P. Penkin. Measurement of the Absolute Values of Oscillator Strengths in Atomic Spectra. III

L. A. Korostyleva. Optical Hyperfine Structure and the Magnetic Moment of Plutonium 239

A. P. Dronov, A. G. Sviridov, and N. N. Sobolev. Continuous Luminescence Spectrum of Krypton and Xenon behind a Shockwave

E. E. Nikitin. On the Interaction of Electrons in Long Molecules with Conjugated Bonds

B. N. Snegirev. Vibrational Spectra of Aromatic Compounds. XIII

E. M. Popov and L. A. Gribov. Calculation of Electro-Optical Parameters of Some Polyatomic Molecules

L. N. Ovander. Temperature Dependence of Infrared Absorption Lines. II

G. G. Kirei and M. P. Lisitsa. Effect of Temperature on the Infrared Spectra of Organo-Silicon Compounds. III

L. N. Ovander. Combination Scattering in Piezoelectric Crystals

V. V. Obukhov-Denisov and V. P. Cheremisinov. Combination Scattering Spectrum and the Structure of Glass-like Polyphosphate

V. E. Kholmogorov and D. N. Glebovsky. On the Electron Paramagnetic Resonance Spectra in Organic Dyes

S. F. Kilin. Duration of the Photo and Radio-Luminescence of Organic Substances

N. A. Tolstoi and Liu Zun-foo. Luminescence Kinetics of Chromium Luminophors. I

A. N. Georgobiani. Effect of the Bond Type of Crystal Phosphors on Their Electroluminescent Ability

I. K. Vereshchagin. Electroluminescence of ZnS-Phosphors under the Excitation by Square Pulses of Different Duration

K. A. Valiev and L. D. Eskin. Rotational Diffusion of Molecules and Light Scattering in Liquids. I

M. A. Vorob'eva. Sensitivity of the Radiant Point Method. III

I. N. Shklyarevsky and N. A. Nosulenko. Experimental Verification of Drude Formulas

R. S. Sokolova and T. N. Krylova. Multilayer Dielectric Systems with Films of Unequal Optical Thickness

Yu. A. Anan'ev and A. A. Mak. Limiting Sensitivity of Methods for Recording Time-Resolved Emission Spectra

L. M. Kutsyna and E. T. Verkhovtseva. Effect of 1-Methylnaphthalene on the Optical Characteristics of Certain Substituted Oxazoles and Oxadiazoles

R. Ya. Damburg. Excitation of the $2s$ and $2p$ Levels of the Hydrogen Atom by Electron Impact

G. A. Almanov, L. Ya. Dzhavakhishvili, and G. D. Ketilade. Measurement of the EPR Spectrum of Teflon at Helium Temperatures

T. N. Popova and N. M. Sashchenko. Franck-Condon Factors for Some Vibrational Transitions in the Fourth Positive System of CO

Ladislav Dunaisky. On the Phase Shift for the p-Component of Reflected Light

I. N. Shklyarevsky and V. K. Miloslavsky. On the Magnitude and Sign of the Phase Difference $\Delta = \delta_p - \delta_s$.

E. E. Fradkin and M. P. Chaika. Continuous Radiation of a Three-Level Quantum Generator with Optical Pump

E. F. Yamshchikov. Dispersion Curves of n-Perfluoro—Heptane and Completely Fluorated Methylcyclohexane

E. F. Yamshchikov. Dispersion Curves of n-Pentane, Isopentane and n-Octodecane

A. I. Finkelstein. Relation between the Symmetric and Antisymmetric Vibrations of the XH_2-Type Groups

A. N. Georgobiani and N. P. Golubeva. Excitation of Electroluminescence in Alkali-Halide Compounds

A. N. Zaidel. On the Article "The Absorption Spectra of Neodimium Chloride in Aqueous Alcoholic Solutions at Low Temperatures"

Optics -

beyond job titles

Itek's basic and applied research programs in optics have created the need for a new breed of optics man.

One half of this position, while requiring a good general knowledge of optics, demands a superior intellect able to earn the confidence of senior optics research men; in addition to a sincere respect for their worth and the unique value of their work.

The second half of this position demands the best qualities of a business-minded administrator; one who considers the group more important than any single member — including himself.

While his own responsibilities will make considerations of profit mandatory, his knowledge and respect for research and researchers will allow him to judge a program's progress beyond its immediate profitability.

Specific duties will include managing several of our optical research projects, wherein several optical study programs must be coordinated in the study phases and carried to stages of applied research and hardware.

We think it improbable to find such a man, but we would welcome the opportunity to discuss your being such a man in the near future.

To arrange for a discussion direct your inquiry, including a brief history of your education and professional experience, to:

Mr. William C. O'Connell
Technical Placement Director

Itek

10 Maguire Road
Lexington, Mass.
VO 2-6200, Ext. 581

'An equal opportunity employer'

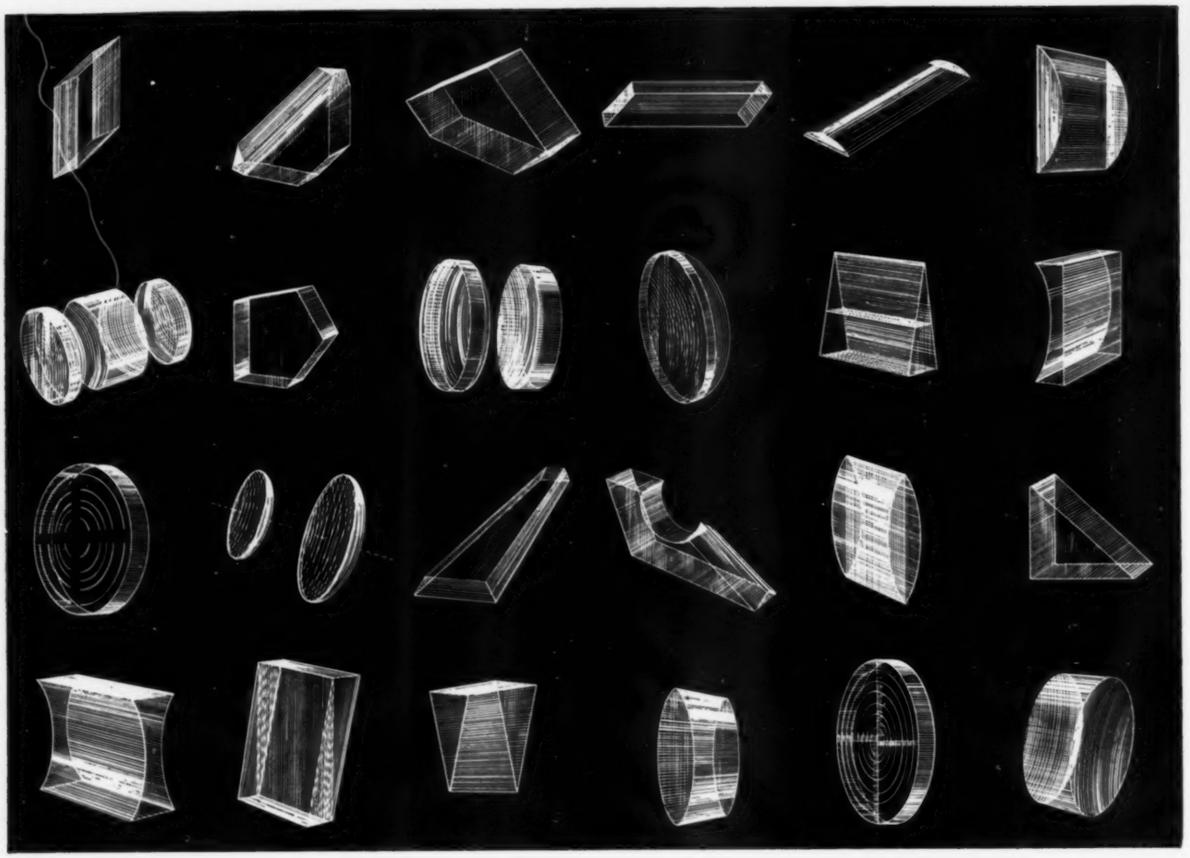

OPTICS FOR ELECTRONICS . . .

Components and systems for visible, ultraviolet, and infrared radiation. GEC's Astron-Optics Division specializes in design, development, and manufacturing of optical components and systems for the ultraviolet through infrared spectrum.

Here are a few of the optical components you can order from Astron-Optics: prisms, flats, spherical, aspherical and parabolic surfaces, reticles, information choppers, encoders, precision vacuum coating, and optically polished synthetic crystals.

Also available from Astron-Optics are infrared and optical-electronic systems.

For complete information regarding your precision optical requirements, write today to:

ASTRON OPTICS DIVISION
. . . precision optics at work

GENERAL ELECTRODYNAMICS CORPORATION
4430 FOREST LANE • GARLAND, TEXAS • BROADWAY 6-1161

Introducing...
B/A
ELECTRO-OPTIC
light modulator

The B/A Electro-Optic Light Modulator, a solid state device, provides a practical source of light pulses in the micro-second range and serves as a light beam modulator at frequencies from D.C. through the video region. Numerous applications have been found for these units in the fields of laser modulation, communications, polarimetry, densitometry, photography, photometry, interferometry and the measurement of semiconductor parameters.

B/A now has a series of standard models, each bridging a specific range of operations. For example, types are available for applications that require large linear aperature with no obstructions. These units are manufactured with transparent electrodes. A model is also made giving maximum contrast ratio with low driving voltage achieved through the use of double crystal construction.

If your application involves modulation at high frequencies, thick single crystal units are available from stock that can be operated continuously up to 5 megacycles.

Continuing research by Baird-Atomic scientists has demonstrated that the crystals used in these modulators can be operated at frequencies of 80 megacycles and pulse times of 20-30 nanoseconds. Others have operated similar crystal units at frequencies as high as 25 Kilomegacycles.

Baird-Atomic engineers invite you to submit your modulation specifications.

Write Adv. Dept. today for current brochure.

Engineers and scientists: *Investigate challenging opportunities with B/A. Write Industrial Relations Director. An equal opportunity employer.*

BAIRD-ATOMIC, INC.
33 University Road · Cambridge 38, Mass.

ADVANCED OPTICS AND ELECTRONICS...SERVING SCIENCE

Vacuum-Deposited Coatings for Glass, Metal or Plastic

In the field of optics, Liberty Mirror Division of Libbey•Owens•Ford Glass Company has worked extensively for 20 years with laboratory and production technicians here and abroad in the development and application of vacuum-deposited coatings for a wide range of optical and scientific purposes. Three types of these coatings are treated below.

Front-surface mirrors give perfect reflection without double images.

Recommended for optical, scientific and commercial uses where a single reflection of high perfection is desired. Back-surface mirrors reflect a second image from the front surface of the glass.

The opaque, reflective aluminum deposit is coated with hard quartz to increase durability. These mirrors can be made to withstand temperatures well in excess of 200° F. They resist moisture and salt atmosphere far better than chemically silvered mirrors. Can be readily cleaned by any normal, non-abrasive glass cleaning procedure.

Dichroic reflectors put light and heat to work, your way.

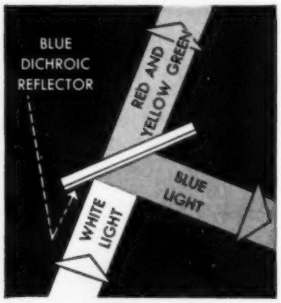

What do you want to do with a light beam? In millimicrons, what wave lengths do you want reflected? Where do you want spectrophotometric reflection to peak?

Liberty Mirror offers a standard line of dichroic coatings that reflect 90% or more of incident light in wave lengths from as low as 400 millimicrons up to 800 millimicrons. If a Hi-Efficiency dichroic coating hasn't already been pinpointed to meet your specifications, Liberty Mirror will go to work on one.

Multiple coatings deliver wave lengths, to order.

These coatings, applied in separate layers to glass or plastic, allow you to split light beams in many ways on a single application. Multilayer coatings can be applied to produce a specific beam-splitting result.

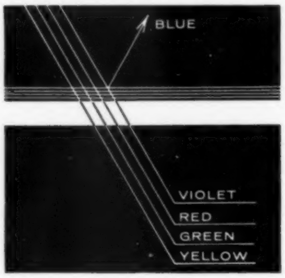

Liberty Mirror engineers can do all the design and development work on any potential use for this technique, or help solve application problems.

★ ★ ★

Among the coatings available from Liberty Mirror are aluminum, chrome and gold front-surface mirrors, neutral filters, transparent mirrors, high-efficiency beam splitters, beam-splitting dichroic mirrors and filters. Metallic and transparent electrically conducting coatings are available for resistance heating. Static-dissipating and high-frequency shielding coatings are also available.

Liberty Mirror can apply coatings to all types of glass, plastics, epoxy material and highly polished metals.

Vacuum-deposited coatings are used in such varied products as scientific and optical instruments, cameras, aircraft and missiles. Free data sheets are available on all coatings. Write L•O•F, Liberty Mirror Division, 5552 Libbey•Owens•Ford Building, Toledo 2, Ohio.

Relationship between the Near Field Characteristics of a Ruby Laser and Its Optical Quality

Michael Hercher

It is shown, theoretically and experimentally, that there is a correspondence between the near field distribution of light from a ruby laser and its interferogram. Specifically, it is shown that, in general, filaments occur in ruby lasers but that these are not present for good quality crystals. An interferometric method for assessing crystal quality is described. The results of preliminary investigations of the spatial distribution of coherence in the near field of a good laser are given, and it is shown that there is a high degree of coherence between points separated by as much as 3.2 mm on the face of a ruby laser.

Introduction

Considerable evidence has been reported leading to the conclusion that laser amplification in a ruby crystal is restricted to small filaments running the length of the crystal.[1,2] It has been suggested that this phenomenon might be due to variations in either the refractive index or the doping concentration within the crystal.[1] As a result of experiments performed at the Institute of Optics, it appears that the existence of these filaments is due primarily to variations in the optical path between the reflecting surfaces of the laser. By selecting a relatively homogeneous crystal it has been possible to demonstrate an absence of filaments. We have also found that, with a fairly good crystal, we are able to predict with fair accuracy where lasing will occur in the near field on the basis of an interferometric study of the crystal.

Theory

It is well known that a ruby laser with plane parallel reflecting surfaces achieves its high amplification and narrow line width through a high Q feedback mechanism.[3] The pump light serves to invert the chromium ion (Cr^{+++}) population in the R_1 and ground states in ruby and effectively produces a medium with a negative absorption coefficient. A spontaneous emission which occurs while the population is inverted will thus be amplified. The parallel reflecting surfaces constitute a resonant cavity, and amplification becomes very large for the proper modes. By considering an ideal laser as a Fabry-Perot interferometer containing an amplifying medium, the angular distribution of the emitted light may be shown to be[4]:

$$\frac{I}{I_0} = \left(G^{D/2d\theta} + 1\right) \frac{1}{1 + \dfrac{4G}{(G-1)^2} \sin^2\left(\dfrac{2\pi}{\lambda} nd \cos\theta\right)}, \qquad (1)$$

where:

I_0 = constant which is proportional to the transmission of the transmitting surface,
α = absorption coefficient of the medium (which is negative during lasing),
D = diameter of the reflecting surfaces,
d = length of the laser,
n = refractive index of the crystal,
λ = wavelength of the emitted light,
θ = internal angle of incidence of the light at the reflecting surfaces,
G = intensity gain per traversal of the laser: $G = Re^{-\alpha d}$,
R = geometric mean reflectivity of the end surfaces.

(The singularity for $\theta = 0$ in Eq. (1) disappears when scattering and diffraction losses and the finite time during which G exceeds unity are taken into account.) Although experiments confirm the existence of a large number of the off-axis modes given by Eq. (1), which appear as rings in the far field pattern of the laser, the axial mode is the dominant one. Fox and Li have shown that, for a perfectly homogeneous laser with plane, parallel, and circular reflecting surfaces, the intensity in the near field due to the axial mode (TEM_{00}) has a maximum value at the center of the aperture and falls off radially in a uniform manner due to diffraction effects.[5] If, however, the laser is either

---

The author is at the Institute of Optics, University of Rochester, Rochester, New York.

Received 11 May 1962.

This work was supported by the U.S. Army Research Office (Durham) and by the United Aircraft Corporation.

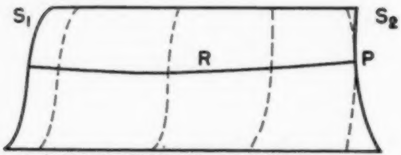

(a) INHOMOGENEOUS CRYSTAL

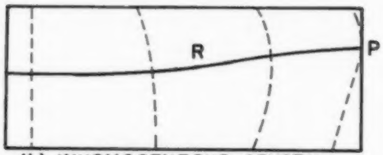

(b) INHOMOGENEOUS CRYSTAL

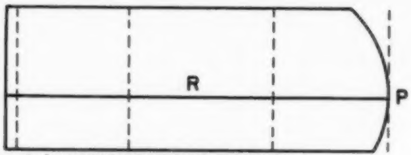

(c) HOMOGENEOUS CRYSTAL

Fig. 1. Eigenrays for different crystals. The dashed line represents successive positions of a wave front which starts in coincidence with the left-hand crystal face (S_1). The points P are the points of tangency between the wave front and the right-hand face (S_2). The solid lines labeled R are the eigenrays.

inhomogeneous or does not have plane parallel reflecting surfaces, then, in general, it no longer constitutes an ideal resonant cavity, and the degree of amplification is greatly reduced.

Consider an inhomogeneous crystal whose end surfaces are not necessarily plane and parallel. Of the infinite number of possible rays along which light may travel between the reflecting surfaces, there will generally be some which are incident normally at both ends. These rays, which we call eigenrays, will be reflected back along themselves and, for appropriate frequencies, they represent axial modes (or standing waves). Thus the amplification of light traveling along an eigenray will be a maximum with respect to nearby rays, and we would expect lasing to be concentrated along filaments in the neighborhood of the eigenrays. Since the eigenrays are normal to both ends of the crystal, they must all be associated with a wave front which starts out in coincidence with either end of the crystal. If such a wave front, starting in coincidence with one end of the crystal, traverses it to the other end, then the eigenrays are located in those parts of the wave front which are tangent to the second surface at the point of reflection. This situation is shown in Fig. 1(a). If both ends are plane and parallel, as in Fig. 1(b), then it is apparent that the eigenrays, being perpendicular to both surfaces, have optical paths which are relative extrema. In other words, if the laser has plane parallel reflecting surfaces, then we would expect high amplification to be concentrated along filaments whose optical paths are either relative maxima or minima. On the other hand, if the laser is homogeneous and has just one plane surface, then the eigenrays will intersect the uneven surface at those points where it is parallel to the flat surface. In this case [Fig. 1(c)] the eigenrays again have optical paths which are either maxima or minima.

It is interesting to point out that, if a laser crystal has one surface which is flat, it is theoretically possible to compensate for refractive inhomogeneities by figuring the other surface. For example, consider Fig. 1(b); if the surface S_2 were distorted to coincide with the tangent wave front, then all the rays in that wave front would be eigenrays and we would expect amplification to be uniform throughout the crystal (assuming uniform absorption of pump light). Should ruby prove too hard to polish locally (diamond dust must be used to polish ruby), a layer of softer material might be evaporated onto the ruby surface. This material, whose refractive index should be approximately the same as that of ruby, could then be figured using standard polishing materials.

Measurement of Crystal Quality

In assessing the quality of a polished laser crystal, it has been a standard practice to make independent measurements of the surface characteristics (flatness and parallelism), and the crystal properties (homogeneity and local variations in the direction of the optical axis). These measurements are made using standard interferometric methods and x-ray techniques, respectively.[2] In view of the conclusions of the previous section, however, it would appear advantageous

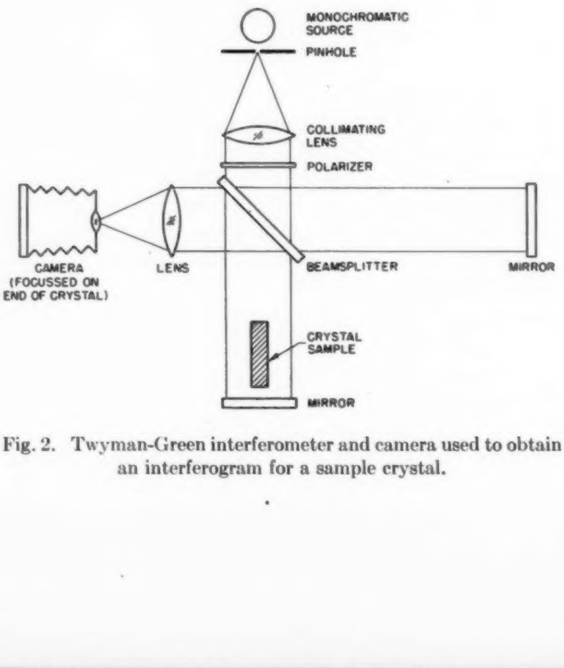

Fig. 2. Twyman-Green interferometer and camera used to obtain an interferogram for a sample crystal.

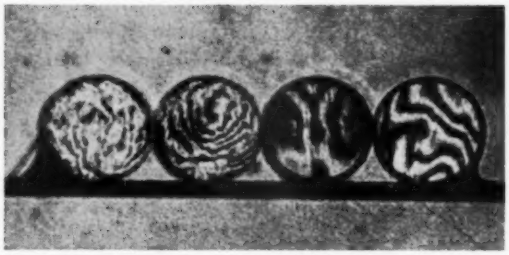

Fig. 3. Interferograms. The two left-hand rubies both are 0° cuts and the right-hand rubies are 90° cuts. The light was polarized in the same direction as that emitted by the 90° lasers.

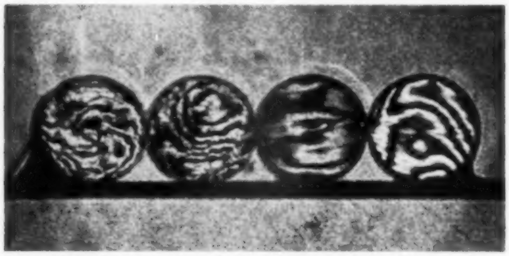

Fig. 4. Interferograms. The rubies are the same as those in Fig. 3, but the polarizer has been rotated 90°.

to make a direct measurement of the variations in optical path between the two reflecting surfaces. This may be done conveniently by means of a Twyman-Green interferometer. When a laser rod, without reflective coatings, is placed in one arm of the interferometer, the resultant interference pattern approximates a contour map of the optical thickness of the sample. The condition for a bright fringe in the interference pattern is given by:

$$2(n - 1)d = m\lambda, \tag{2}$$

where m is an integer, so that the separation between adjacent fringes corresponds to small variations Δn and Δd in the refractive index and length such that:

$$2(n - 1)\Delta d + 2d\Delta n = \lambda. \tag{3}$$

If the ends are flat and parallel ($\Delta d = 0$), then the change in optical path between fringes is $^1/_2\ \lambda$; if the crystal is homogeneous ($\Delta n = 0$), then the change in optical path between fringes is $n\lambda/2(n - 1)$, or about 1.2 λ. Thus, if we think of the fringes as contours of equal optical path, then they are generally separated by between 0.5 and 1.2 wavelengths, depending on whether the optical path variation is due primarily to poor surface quality or inhomogeneity.

Figure 2 shows the layout of the interferometer and camera used in photographing the interference patterns. Because the stimulated emission from a ruby laser is known to be polarized in a direction perpendicular to both the optical and longitudinal axes,[6] it is necessary to use similarly polarized light in the interferometer (since we are interested only in those refractive characteristics pertinent to the emitted light). The cut of a particular ruby rod is specified by the angle between its longitudinal and optic axes; for example, a 90° rod has its optic axis at right angles to the longitudinal axis. Figure 3 is a photograph of the interference patterns obtained from four different polished ruby rods. The two rods on the left are 0° rods and those on the right are 90° rods. Figure 4 shows the same rods, but with the polarizer rotated through 90°. Figures 3 and 4 both indicate that the 90° rods are of better homogeneity than the 0° rods.

Either a cadmium or hydrogen lamp may be used as a source of light for the interferometer. The photographs shown here were made using a selected hydrogen discharge tube (6563 Å) with a red filter. A parallel-sided glass plate, whose optical thickness was approximately the same as that of the ruby rods, was placed in the sample arm of the interferometer as a compensating plate to allow observation of the background fringes. Such a compensating plate would be unnecessary with a cadmium lamp.

Near Field Intensity Distribution

The integrated near field intensity distribution may be recorded by photographing one end of the ruby during lasing. By varying the energy delivered to the pump light, one may obtain near field patterns for different levels of laser power output. Figures 5 and 6 are photographs of the near field for increasing values of input energy with two different rubies. In the upper left of each figure, the interferogram of the ruby is shown for comparison purposes.

Near threshold, both rubies emit stimulated emission in those regions where the interferogram shows a definite extremum in optical path. In the case of the ruby in Fig. 5 the intensity spreads out more or less uniformly as the energy input is increased; we would expect this from the relatively slight variation in optical path across the face of the ruby (less than $1^1/_2$ wavelengths). In Fig. 6, however, the near field has a number of small bright areas which increase in size as the pump energy is increased, until they merge together. These bright areas are the ends of the filaments referred to earlier. Although the first such filament to appear is clearly at an extremum for the optical path, other filaments appear (at higher energy levels) which apparently are not at positions of relative extrema, although they are located where the optical path gradient is least. It is probable, however, that these filaments actually are at positions of relative extrema, but that the interference fringes (or optical path contours) are too widely spaced to resolve them as such. Figure 7 illustrates this point more clearly.

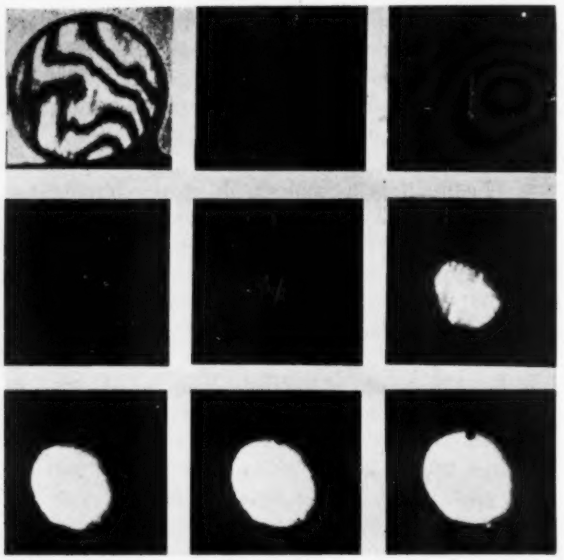

Fig. 5. Photographs of the end of a 90° ruby laser during lasing for increasing values of the input energy. At the upper left the interferogram is shown for comparison.

Coherence in the Near Field

In order to measure the degree of coherence between two points in the near field of a ruby laser, a mask with two small pinholes (125 μ diam) is placed adjacent to one end of the laser. If the stimulated emission is coherent at the two pinholes, then there will be an interference pattern where the beams from the two pinholes overlap. This interference pattern may be photographed in the focal plane of a lens, where fringes extend over a region corresponding to the Airy disk of one of the pinholes. It should be pointed out that it is preferable to place the two small apertures in *series* with the laser, rather than putting them directly in the reflecting film. This is because, in the latter case, the light from adjacent apertures acquires a considerable portion of its coherence through multiple diffractions at each aperture.

If I and I' are the separate intensities due to the two pinholes, then the modulus of the degree of coherence, $|\gamma_{12}(0)|$, may be determined from a measurement of the visibility of the interference fringes[7]:

$$|\gamma_{12}(0)| = V \frac{I + I'}{2(II')^{1/2}}, \tag{4}$$

where the visibility, V, is given by:

$$V = \frac{I_{\max} - I_{\min}}{I_{\max} + I_{\min}}.$$

Figure 8(a) is a photograph of the interference fringes obtained with a pinhole separation of 0.32 cm, and Fig. 8(b) is from a microdensitometer trace of the central part of the negative. The ruby laser used was that shown in Fig. 5 and the energy input to the pump light was approximately 10% above threshold. The degree of coherence is estimated to be 0.8, so that the area of coherence reported by Collins and Nelson[1] has been increased by a factor of nearly 2000. Preliminary investigations indicate that most of the surface of any reasonably good laser, such as that shown in Fig. 6, can be made coherent if the input energy is high enough, although this has not been conclusively demonstrated. The advantage in using a really good crystal is that it will emit a very nearly plane wave front, which is coherent across the near field aperture, at energy levels near threshold—where the laser output has only a few spectral components.* Further work in this area is presently being carried out.

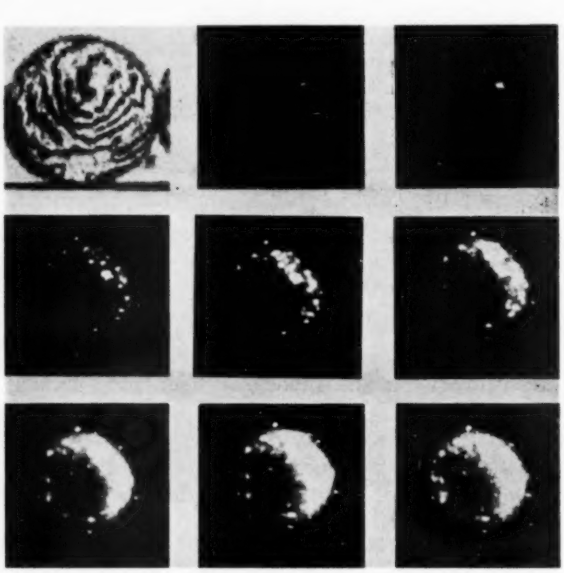

Fig. 6. Photographs of the end of a 0° ruby laser during lasing for increasing values of input energy, ranging from 1.0 to 2.5 × threshold energy. At the upper left the interferogram is shown for comparison.

Discussion

The correlation between the interferograms and near field intensity distributions, for the two lasers we have examined, attests to the usefulness of the Twyman-Green interferometer in assessing potential laser characteristics. It seems to be a general characteristic of the finished laser rods available from commercial manufacturers that the surfaces are flat to within a quarter wavelength, parallel within one or two wavelengths, and that the crystal has inhomogeneities which are equivalent to optical path variations of from one to ten wavelengths. Thus the errors in achieving parallelism and homogeneity are somewhat greater than most research workers would desire. The use of a Twyman-Green interferometer in quality control of polished crystal lasers is recommended. This could be accomplished most easily with disk boules of ruby[8]; two surfaces could be polished plane and parallel on the edge of the disk, and the crystal could then be examined interferometrically. One of the two surfaces could then be figured to improve the interference pattern, and the best portions of the boule then selected for use as lasers.

---

* The spectral output of a laser is characterized by a number of sharp lines lying within the fluorescent linewidth of the ruby and separated by $\Delta\lambda = \lambda^2/2nd$. The number of these components, corresponding to different axial modes, is determined by the input energy level and the fluorescent linewidth.

It should be pointed out that the observed width of the beam from a laser with plane parallel ends is due primarily to the width of the axial mode and *not* to diffraction effects. Due to the singularity for $\theta = 0$ in Eq. (1), it is not possible to give a simple expression for the angular spread in the axial mode, but it is clear that the axial mode width increases with increasing G or increasing D/L. Fox and Li, on the other hand, have shown that the *diffraction* effects are even less than predicted on the basis of a plane wave.[5] Thus the fairly widespread idea that a large angular beam width is due to diffraction, and is an indication of narrow filaments, is not necessarily correct. (By the same argument, the width of the central fringe in a conventional Fabry-Perot interferometer is not ordinarily due to diffraction, but to the spectral width of the incident light and to the finesse of the interferometer, as well as to any imperfection in the flatness and parallelism of the reflecting surfaces.)

Technical Data

All the ruby lasers referred to in this paper were purchased from Adolf Meller, Inc., Providence, R.I. The reflective coatings were of silver with an approximate reflectivity of 96.7%, and were protected by a layer of magnesium fluoride. The rods were 5.08 cm (2 in.) long and 6 mm (0.25 in.) in diameter. The experiments described were performed at room temperature. The source used for pumping consisted of four Edgerton, Germeshausen, and Grier FX-100 flash tubes, arranged adjacent to the ruby crystal and wired in series.[9] The energy discharged through the flash tubes could be varied from 0 to 1200 J. Aluminum foil was wrapped around the flashlamps and served as a trigger wire and reflector. The input energy required for

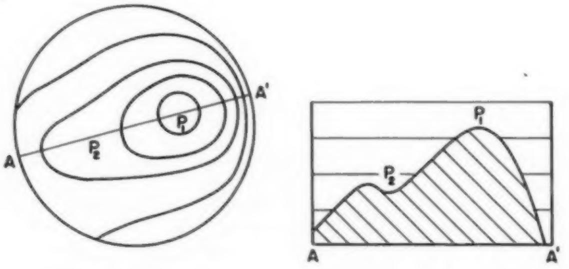

Fig. 7. On the left is a typical interferogram and on the right is a plot of optical path in the section AA′. P_1 and P_2 are extrema in optical path, but only P_1 is explicitly evident in the interferogram.

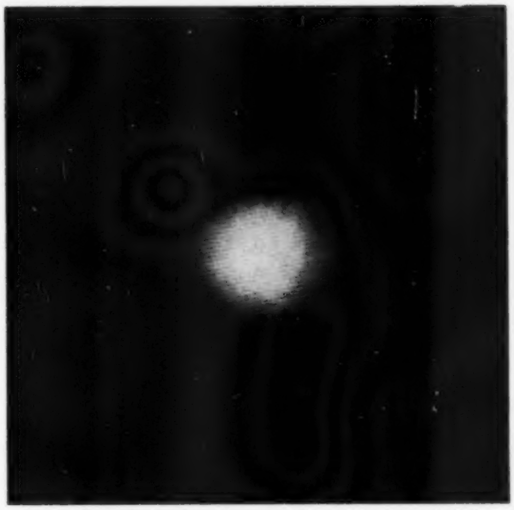

Fig. 8(a). Fraunhofer interference fringes for two pinholes separated by 3.2 mm in the near field of a ruby laser.

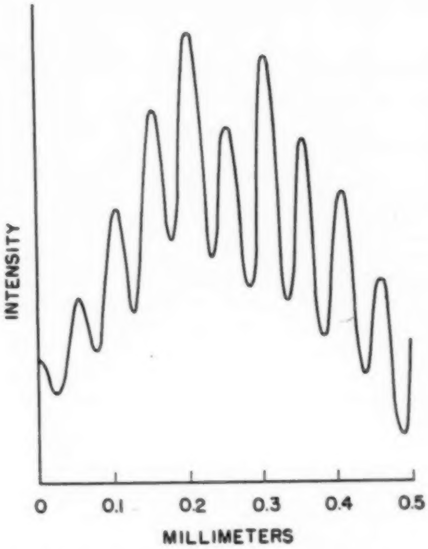

Fig. 8(b). Intensity distribution in the interference pattern shown in Fig. 8(a), taken from a microdensitometer trace of the central portion of the negative.

lasing (threshold) was in the neighborhood of 250 J with this geometry for a good crystal. The film used in taking photographs was Kodak Plus-X (35 mm) except for Fig. 8(a) in which Kodak High Speed Infrared (35 mm) was used.

The author is indebted to Carroll Alley of the Institute of Optics at the University of Rochester for his many enlightening discussions; to Mrs. G. Eyer and William Cook for their assistance in preparing the figures and photographs; and to Francis Turner of Bausch & Lomb, Inc., Rochester, New York, for kindly providing the reflecting coatings for the lasers.

References

1. D. F. Nelson and R. J. Collins, J. Appl. Phys. **4,** 739 (1961).
2. R. J. Collins *et al.*, Phys. Rev. Letters **5,** 303 (1960).
3. T. H. Maiman, Phys. Rev. **123,** 1145 (1961).
4. M. M. Hercher (to be published). A similar expression has been developed by S. J. Sage, Appl. Opt. **1,** 173 (1962).
5. A. G. Fox and Tingye Li, Bell System Tech. J. **40,** 453 (1961).
6. D. F. Nelson and R. J. Collins, *Advances in Quantum Electronics*, edited by J. R. Singer (Columbia Univ. Press, New York, 1961), p. 79.
7. M. Born and E. Wolf, *Principles of Optics* (Pergamon Press, New York, 1959), p. 503.
8. R. D. Olt, Appl. Opt. **1,** 25 (1962).
9. H. E. Edgerton and P. A. Miles, J. Appl. Phys. **32,** 740 (1961).

Applied Optics Letters to the Editor

Letters to the Editor should be addressed to the Editor, APPLIED OPTICS, 1155 16th St., N.W., Washington 6, D.C.

Mean Atmospheric Moisture Profiles to 31 km for Middle Latitudes

Murray Gutnick

Meteorological Development Laboratory, Air Force Cambridge Research Laboratories, Bedford, Massachusetts.

Received 1 June 1962.

Average yearly vertical profiles up to 31 km in middle latitudes of mixing ratio and dewpoint-frostpoint, derived independently, are presented in a table and a figure. Also, since the relation between mixing ratio and frostpoint is nonlinear, other moisture expressions were derived from each of the basic profiles, using Standard Atmosphere conditions. Up to 7 km the basic profiles were developed from conventional radiosonde humidity measurements; above that level they are based upon experimental humidity ascents, subjectively selected and weighted.

The annual mid-latitude mixing ratio profile decreases from 6150 ppm (mg/kg) at the surface to 9 ppm at 16 km, then increases slightly with height; the surface dewpoint is taken at 4°C, decreasing to −78°C at 18 km, then increasing 0.5 deg/km.

This letter is a brief summary of a comprehensive study[1] presenting preliminary models of the variation of atmospheric moisture with height. The concept is similar to that of other standard atmospheres. The paucity and ambiguity of upper-air moisture data make the models offered here quite crude. As observations increase, the models can be revised, refined, and extended evolving in the same way as other representations of atmospheric structure.

The tropospheric portion of the mixing ratio profile was derived by estimating, from recent maps, the mean annual precipitable water above each of four widely separated surfaces at 45°N. The corresponding mean mixing ratios were assumed to be those of two stations having the same precipitable water as the derived mean annual values. The stratospheric portion of the mixing ratio profile is a weighted average of the best soundings from each of half-a-dozen sets of experimental moisture ascents, and the means of all valid ascents of the two sets of routine stratospheric moisture measurements. In the figure, symbols represent:

BRL—Mean of 2 hygrometric ascents by Ballistic Research Laboratories;

NRL—Mean of 3 hygrometric ascents by U.S. Naval Research Laboratories;

U of D—One hygrometric and one spectroscopic ascent by University of Denver;

JMA—Means of the Japanese Meteorological Agency hygrometric ascents; 100 of which reached or exceeded 300 mb and two of which reached 10 mb;

MRF—Means of the British Meteorological Research Flight hygrometric ascents, 400 of which reached or exceeded 300 mb;

Vapor Trap—Mean of seven ascents of the United Kingdom Atomic Energy Authority's water vapor absorption device;

Molecular Sieve—A single ascent of the General Mills, Inc., water vapor absorption device.

The dewpoint profile was constructed by the same procedure. Stratospheric frostpoints were approximated when unavailable from the soundings.

Resulting mean annual vertical profiles to 31 km in middle latitudes (35 to 55°N) of mixing ratio and dewpoint-frostpoint, obtained as independent means from the same basic measurements of stratospheric moisture and routine tropospheric radiosonde observations, are presented in the accompanying table. Neither profile can be obtained from the other, since the nonlinear relation between mixing ratio and condensation temperature (dewpoint-frostpoint) insures that the means, separately obtained, will differ.

From each of the basic profiles, other expressions for the moisture content of the atmosphere have been derived, using Standard Atmosphere conditions where required. The two sets of values for absolute humidity (vapor density), vapor pressure, precipitable water, and relative humidity differ, of course. Preferred values are indicated by asterisk. Relative humidity up to 7 km was computed directly from radiosonde data.

The most reliable single element is the mixing ratio, because all the selected data were given in terms of mixing ratio and required no approximations, such as those used for the dewpoint-frost-

Mean Annual Mixing Ratio ($\bar{w}$) and Dewpoint-Frostpoint ($\bar{T}_d, \bar{T}_f$) in Middle Latitudes, to 31 km[a]

HT	Standard atmosphere						Typical moisture content from:											
	Basic			Derived			Mean mixing ratio						Mean frostpoint					
gp km	T (C)	P (mb)	ρ (g/m³)	e_s (μb)	ρ_s (mg/m³)	w_s (ppm)	$\bar{w}^*$ (ppm)	e_v (μb)	ρ_v (mg/m³)	U (%)	T_f (C)	W^* (μ)	$\bar{T}_f^*$ (C)	$e_v'^*$ (μb)	$\rho_v'^*$ (mg/m³)	U'^* (%)	w' (ppm)	W' (μ)
0	+15.0	1013	1225	17044	12830	10473	6150	10016	7534	59	+7	10410	+4	8129	6360	75	5192	8901
2	−2.0	795	1006	7055	5559	5526	3200	4090	3219	58	−5	4367	−9	3097	2541	62	2526	3450
4	−11.0	616	819	2644	2186	2669	1580	1565	1294	59	−17	1673	−22	1054	909	49	1110	1254
6	−24.0	472	660	883	768	1163	700	531	462	60	−29	568	−33	382	344	43	522	440
8	−37.0	356	525	257	236	449	270	154	142	60	−42	150	−46	99.6	95	39	181	106
10	−50.0	264	413	39.35	38.21	92	37	15.70	15.3	40	−57	22	−60	10.8	11	28	26	14
12	−56.5	193	311	17.22	17.25	55	17	5.27	5.3	31	−65	8	−69	3.03	3.22	18	10	6
14	−56.5	141	227	17.22	17.25	76	10	2.27	2.3	13	−71	4	−74	1.42	1.55	8	7	2
16	−56.5	103	165	17.22	17.25	104	9	1.49	1.5	9	−74	3	−77	0.89	0.98	5	6	2
18	−56.5	75.0	121	17.22	17.25	142	13	1.57	1.8	9	−73	3	−78	0.76	0.84	4	7	2
20	−56.5	54.7	88.0	17.22	17.25	196	18	1.58	1.6	9	−73	4	−77	0.89	0.98	5	11	2
22	−54.5	40.0	63.7	22.32	22.16	348	27	1.74	1.7	8	−73	4	−76	1.04	1.14	5	18	2
24	−52.5	29.3	46.3	28.80	28.32	616	38	1.79	1.8	6	−73	4	−75	1.22	1.33	4	29	3
26	−50.5	21.5	33.7	36.99	36.06	1070	58	2.01	2.0	5	−72	4	−74	1.43	1.55	4	46	3
28	−48.5	15.9	24.6	47.30	45.62	1854	86	2.19	2.1	5	−71	5	−73	1.66	1.80	4	73	4
30	−46.5	11.7	18.0	60.22	57.57	3198	128	2.41	2.3	4	−71	2	−72	1.94	2.08	3	116	4
31	−45.5	10.1	15.4	67.84	64.57	4193	150	2.43	2.3	4	−70	—	−71	2.25	2.41	3	157	—

[a] Based on available routine and experimental data considered reliable, with related quantities computed (where required) for conditions of Revised U.S. Standard Atmosphere, 1962.

Standard atmosphere: from U.S. Standard Atmosphere, 1962 ("USSA").

T, P, ρ: temperature (°C), pressure (mb), density of air (g/m³) (assumed dry).

Pressure of water vapor, in microbars: $1\ \mu\text{b} = 0.001\ \text{mb} = 1\ \text{dyn/cm}^2$.

e_s: if saturated at ambient USSA temperature; from SMT 94 and 96.

e_v: having mixing ratio $\bar{w}$ at ambient USSA pressure; $e_v = \bar{w}\,P/0.622$.

$e_v'^*$: having dewpoint $\bar{T}_d$ or frostpoint $\bar{T}_f$; from SMT 94 and 96.

Absolute humidity or vapor density or vapor concentration in mg/m³ ($1\ \text{mg/m}^3 = 0.001\ \text{g/m}^3$).

ρ_s: If saturated at ambient USSA temperature and density, from SMT 108 and 109.

ρ_v: having mixing ratio $\bar{w}$ at ambient USSA pressure and density; $\rho_v = \rho\bar{w}$.

$\rho_v'^*$: having dewpoint $\bar{T}_d$ or frostpoint $\bar{T}_f$; from SMT 108 and 109.

Mixing ratio, ratio of mass of water vapor to that of dry air in mixture, in mg/kg, or parts per million.

w_s: if saturated at ambient USSA temperature and density; $w_s = \rho_s/\rho$.

$\bar{w}^*$: estimated mean mid-latitude value, from available mixing ratio data considered reliable.

w': having dewpoint $\bar{T}_d$ or frostpoint $\bar{T}_f$ at USSA density; $w' = \rho_v'/\rho$.

Precipitable water, water vapor content of air in 2-km layer above indicated level, if condensed to liquid, in microns ($1\ \mu = 0.000\,1\ \text{cm} = 0.000\,1\ \text{g/cm}^2$).

W^*: $= \underline{(p_2 - p_1)\bar{w}/g}$; $\bar{w}$ is mean mixing ratio between pressures p_1 and p_2 2 km apart (USSA); $g = 980\ \text{cm/sec}^2$.

W': $\underline{\rho_v'h}$, where h is layer thickness in meters, $= \rho_v'(Z_1) + \rho_v'(Z_1 + 2\ \text{km})$.

Relative humidity, in percent.

U: ratio of pressures of water vapor at mixing ratio $\bar{w}$ and if saturated at USSA temperature; $U = e_v'/e_s$.

U'^*: up to 6 km, weighted average of observed relative humidities; above 6 km, $U' = e_v'/e_s$, for air having frostpoint $\bar{T}_f$ and USSA temperature.

Dewpoint and frostpoint temperature, in degrees Celsius.

T_d, T_f: from SMT 94 and 96, using e_w as derived from $\bar{w}$.

$\bar{T}_d^*$, $\bar{T}_f$: estimated mean mid-latitude values, from available data expressed as dewpoints and frostpoints.

Notes: * Indicates values recommended for general use; other values derived for comparison only. SMT = *Smithsonian Meteorological Tables*, sixth revised edition, prepared by R. J. List, Washington 1951. Saturation assumed with respect to plane surfaces of liquid water above −40°C, of ice below −40°C.

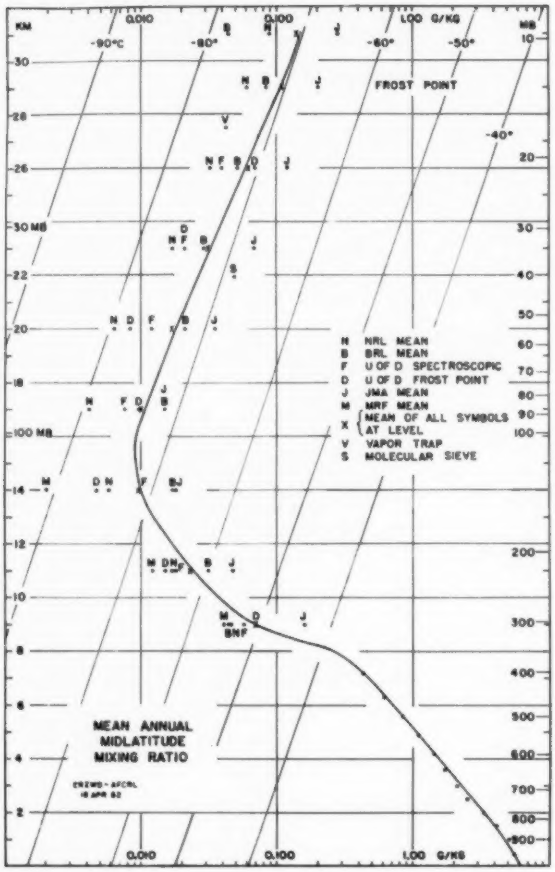

Fig. 1. Mean annual mid-latitude mixing ratio.

points. However, the values derived from the dewpoint-frost-point are more reliable than those based on the mixing ratio, because fewer Standard Atmosphere assumptions are used.

The tentative moisture profiles presented herein undoubtedly will be revised and extended as the state-of-the-art advances. The large amount of subjectivity used in deriving the stratospheric portion of the moisture profiles makes revision especially desirable. Despite their deficiencies, these models are suggested for general use as mid-latitude standards.

Reference

1. M. Gutnick, Air Force Survey in Geophysics 147, AFCRL, Bedford, Mass. (July 1962).

Editor's Note: The mean moisture profile of the atmosphere is not in itself an optics matter. However, almost every application of infrared studies involves the estimation of the transmission of infrared radiation through real atmospheres, and one of the great imponderables to date has been the question of how much water vapor there is in the stratosphere. Only a handful of individual measurements of this quantity exists, and the amount of data is not sufficient to draw conclusions concerning geographical, latitudinal, or seasonal variation. The present report by Gutnick represents his best estimate of the water vapor profile and the Editor feels this should be presented to the optics audience. A complete report describing the treatment of the data in detail will soon be available as Air Force Survey in Geophysics No. 147, July 1962 and can be obtained upon request from the author after September 15.

Spatial Distribution of Light Across the End of a Ruby Laser

David Weisman

Maser Optics, Inc., 89 Brighton Ave., Boston 34, Mass.

Received 2 March 1962.

In a recent article,[1] Kisliuk and Walsh claim that their observations imply that the spatial distribution of light across the end of the ruby laser is the same (within 0.01 of the ruby diameter) for each spike during one discharge of a flash tube. This contradicts the results reported by Dayhoff and Kessler[2] who report changes in the light patterns photographed from the ends of ruby crystals in successive microsecond exposures. Similar photographs by Clark *et al.*[3] suggest that in some cases the spatial pattern does remain the same.

Detailed analysis of the experimental arrangements shown in Figs. 1(a) and 1(b) of Kisliuk and Walsh shows that their diagram Fig. 6 and associated reasoning does not apply to either of their experimental arrangements, although for different reasons.

The apparent image of end B is not merely separated from the apparent image A, but also rotated with respect to it (see our Figs. 1(a) and 1(b). As a result the central interference maximum stays at the center line of the figure as long as the spatial distribution in both ends varies in the same way over a period of time

In experimental arrangement 1(a) of Kisliuk and Walsh, there is a left to right reversal; our Fig. 1a shows this in detail. This reversal causes the light from the upper part of the two object ends to appear as the outer part of the image ends. Therefore the center of the interference pattern will appear on the center of symmetry of the apparatus as long as the spatial distribution of light is instantaneously identical at the two ends (on a filament-by-filament basis).

Still referring to Fig. 1a, a change of the "center of gravity" of the light from one side of the rod "X" to the other side "Y" would change the apparent separation of the interfering sources and thus change the spacing of fringes a corresponding fraction. If this occurred during one photographic exposure, there would be a washout effect near the nth fringe, where n is approximately equal to $^1/_4$ the ratio of the separation distance of the images of the rod ends to the diameter of the rod.

Kisliuk and Walsh do not give the distance for the image separation. The number that they do give—the separation of the fringes (0.008 cm)—does enable us to calculate approximately the angle θ between the axes of the rod images at the film (approximately 0.009 rad). From this, a second calculation, using a Fraunhofer approximation, shows that if the rod image-to-film distance L satisfies the condition $L < 110\ nf\ (4r)$ (here r is the radius at the face of the rod and n is approximately the number of fringes (in a sequence) that show clearly without washout), then the center of gravity of the light emitted by the rod could not have moved more than a fraction f during the photographic exposure. It would appear from Kisliuk and Walsh's paper that n is approximately 40 and r is 0.5 cm. Therefore their statement that the center of gravity moved less than 0.01 of the diameter of the rod would be true if L, for their statement, were less than 88 cm (although not for the reason they gave).

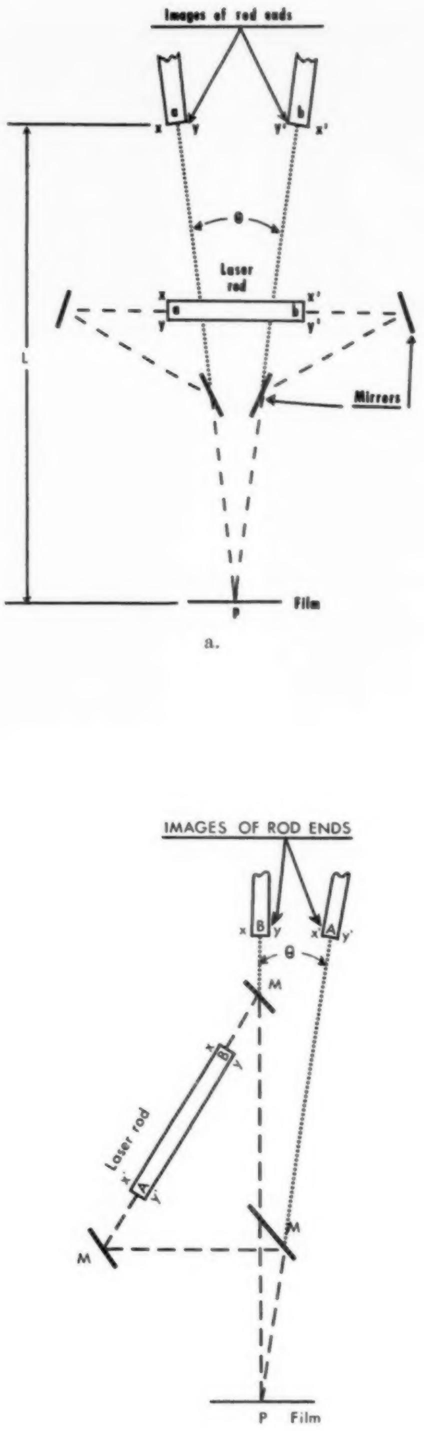

a.

b.

Fig. 1. Diagrams of experimental arrangements with images formed by mirrors indicated a) for Kisliuk and Walsh's Fig. 1(a); b) for Kisliuk and Walsh's Fig. 1(b).

Kisliuk and Walsh's Fig. 6 is inconsistent with their Fig. 1(b) because the images of the rod ends are separated and actually perpendicular to the corresponding lines joining the image rod central axis with the center of the diffraction pattern formed on the film by a uniformly emitting rod face (see Fig. 1b). Referring to Fig. 2, which illustrates our Fig. 1b more diagrammatically, if point P is such that there is zero phase difference between path OP and O′P there is also zero phase difference between PX and PX′; likewise between PY and PY′ (congruent triangles). Thus, P is the center of interference pattern for any spatial distribution on XOY provided the same distribution exists simultaneously on X′O′Y′.

To first order there is no washout effect applicable to their Fig. 1(b) since the separation distance XX′ is approximately equal to YY′.

It would thus appear that only their setup Fig. 1(a) can be useful in determining if the center of gravity of the light pattern remains substantially unchanged, and this, only with a proper choice of experimental dimensions. Even with such proper choice, other factors (motion of center of gravity parallel to fringes, peculiar variations of intensity or phase) might fortuitously fix the fringes while the basic pattern at the source was moving.

References

1. P. Kisliuk and D. J. Walsh, Appl. Opt. **1**, 45 (1962).
2. E. S. Dayhoff and B. Kessler, Bull. Am. Phys. Soc., Ser. 2, **7**, 15 (1962).
3. G. L. Clark, R. F. Wuerker, and C. M. York, Sp. Tech. Lab.. 9844-0036-NO-00 (November 1961).

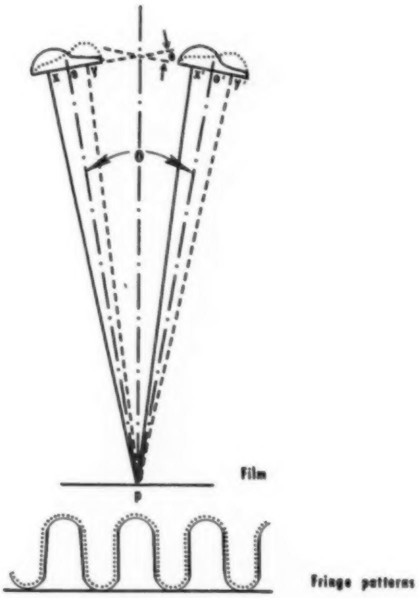

Fig. 2. Two possible intensity patterns for Fig. 1b and the resulting interference patterns.

Mode Selection and Enhancement with a Ruby Laser

John A. Baker and C. W. Peters

The University of Michigan, Ann Arbor, Michigan. J. A. Baker is in the Institute of Science and Technology and C. W. Peters is in the Department of Physics.

Received 7 June 1962.

The angular distribution of the laser output from a ruby rod is determined by the characteristics of the standing wave pattern inducing the emission. If the angular spread of the latter is limited by an aperture in an external optical system through which the standing wave must pass, the stimulated emission will be limited to the same angular spread. In addition, the intensity of the laser beam along the axis should be increased because of the suppression of the standing wave pattern in off-axis directions, since the stimulated emission, which normally would have gone into the off-axis modes, will be channeled into the axial modes.

The apparatus was arranged as indicated in Fig. 1. A 9.5-mm diameter, 7.6-cm long ruby rod, with 0.05 mole % chromium, was used at room temperature with a spiral xenon flash tube. The back face was silvered, and the front face was coated with MgF_2 to be antireflecting for red light. A limiting circular aperture was placed at the focal plane of the 20.3-cm focal length lenses. The flat was partially silvered to give about 80% reflectivity. The components were mounted on an optical bench and aligned to be coaxial, with the flat surfaces perpendicular to the axis. The angular distribution could be photographed at the focal plane of a 127-cm focal length lens. Intensity measurements were made with a photomultiplier placed behind a 3.18-mm diameter hole located on-axis in the focal plane of this lens.

Representative results are shown in Fig. 2. Threshold for laser action occurred with about a 2200 J discharge through the flash lamp. The data were taken with 2650 J discharges. No stimulated emission was observed with the optical flat obscured. The angular spread of 2.5×10^{-3} rad with a limiting aperture corresponded exactly to that calculated from the diameter of this aperture (1.02 mm). The angular distribution without the aperture depended upon the power input into the flash tube, but was always wider than 2.5×10^{-3} rad, as indicated by the spot size in Fig. 2. The intensity of the laser beam, measured by a photomultiplier placed behind the exit hole on the axis at P, was extremely sensitive to alignment when the aperture was in place, as would be expected for such an interferometer. The several traces shown in the lower half of Fig. 2 indicate an increase in intensity of about 50% due to the presence of the aperture stop, other conditions being maintained as constant as possible. The particular value of the intensity change is dependent upon the quality of the optical system as well as the original angular distribution of the laser beam. The method would appear to be effective down to the diffraction limit.

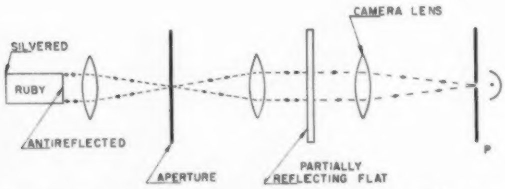

Fig. 1. Diagram of apparatus. A photographic film may be placed at the focal plane of the camera lens, P; or, as shown, a small opening with a photomultiplier behind it.

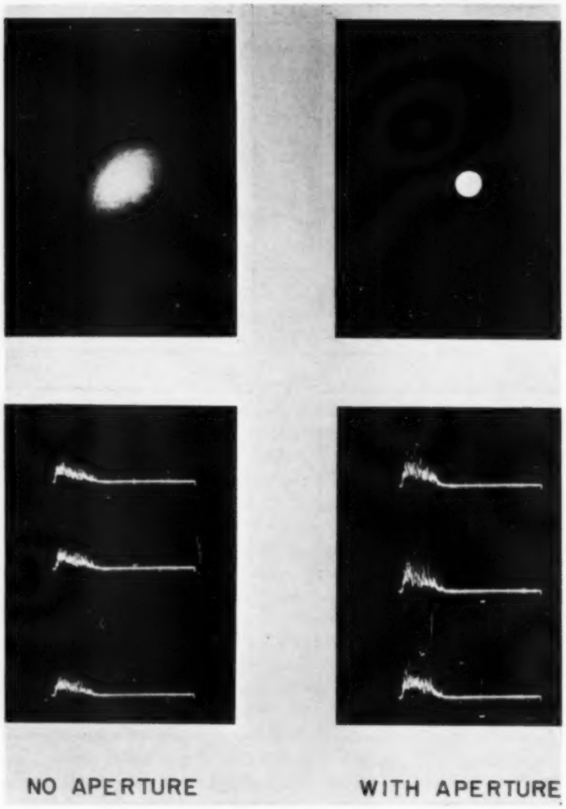

Fig. 2. Effect of limiting aperture on laser output. Top: angular distribution photographed at P. Bottom: 3 traces of photomultiplier output behind hole at P—conditions identical except for presence or absence of aperture.

This work was conducted by Project MICHIGAN under a Department of the Army Contract, administered by the U.S. Army Signal Corps.

An Image Reducer—Immersed Detector System for the Infrared

Robert G. Greenler

Research Division, Allis-Chalmers Mfg. Co., Milwaukee 1. Wisconsin.

Received 31 May 1962.

The reflection image reducer shown in Fig. 1 has been described[1] as a method of demagnifying an infrared image to match the small sensitive area of an infrared detector. If a magnification of $-1/M$ is desired, the relationship between the mirror radii and their separation is

$$R_1 = -2MD/(1 - 2M),$$

$$R_2 = 2D/(M - 2),$$

when the object and image are located in the mirror apertures. To the limits of the third-order approximation, spherical aberration is eliminated when the radii of the mirror are equal, giving a reduction in image diameter of 3.7.

A useful modification of this system is the solid optical system illustrated in Fig. 2. The spherical surfaces are produced on the bases of a truncated cone of a suitably transparent optical material. The external surfaces are aluminized, leaving an aperture in the center of each film for the transmission of radiation. The surface in the first aperture can be given an antireflection coating to reduce reflection loss, and a radiation detector can be placed in optical contact with the surface in the rear aperture. A photoconductive detector can be deposited directly on the surface of the solid material, or a thermocouple or bolometer detector can be cemented to the solid material with a cement of the proper index of refraction and thermal conductivity.

The formulas connecting the demagnification with the radii of the surfaces are the same in this case as in the air system of Fig. 1, and are independent of the index of refraction of the material. However, this system has the feature of accepting a lower *f* number beam to provide the same demagnification, with the same *f* number beam converging on the detector. The comparison is shown by the solid and dashed lines converging on the first surface in Fig. 2. Alternatively, greater demagnification can be obtained using this system for a beam of given *f* number converging on the detector. This greater ultimate demagnification is important when the increase in detectivity with the decrease of area of many infrared detectors is considered.[2] The advantage gained from this system will become greater for higher indices of refraction of the optical material. The one-piece construction of the system should make it a compact, rugged detector unit with high detectivity.

Some of the advantages obtained by placing a detector in optical contact with a lens of high index material (i.e., the immersed detector) are realized by a system, currently in use, of a bolometer detector in optical contact with the plane side of a hemispherical germanium lens. Such a system will give a demagnification factor equal to the index of refraction of the germanium, which is about 4 in the infrared. This would permit a reduction in detector area of 16 which would yield an increase in detectivity of about 4^2. The solid optical system shown in Fig. 2, designed to eliminate third-order spherical aberration, would give about the same image reduction. If it were made of germanium the *f* number of the beam converging on the detector would be the same in the two cases. However, when the image size and the *f* number are such that introducing a certain amount of spherical aberration will not significantly decrease the energy reaching the detector, then the system of Fig. 2 may be designed to give a greater demagnification with a corresponding increase in detectivity. For such applications the image reducer-immersed detector system described here should be particularly useful.

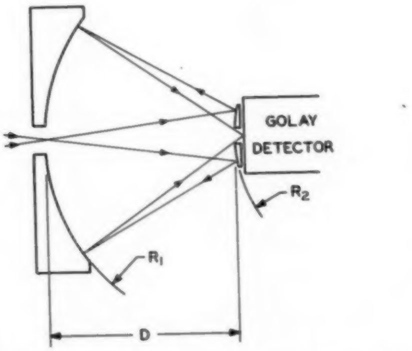

Fig. 1. Diagram of the two-mirror image reducer used with a Golay detector.

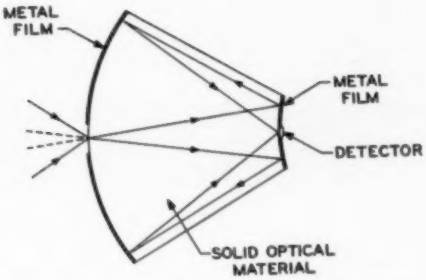

Fig. 2. Diagram of the solid image reducer-immersed detector system.

References

1. R. G. Greenler, J. Opt. Soc. Am. **46,** 433 (1956).
2. R. C. Jones, Advances in Electronics, **5,** 2–96 (1953).

Spectra Associated with High-Speed Projectiles in Rarefied Air Obtained with a Large-Aperture Slitless Spectrograph

I. D. Liu

Canadian Armament Research and Development Establishment, Valcartier, P.Q., Canada.

Received 7 April 1962.

Spectroscopic studies of the luminous trails produced by high-speed pellets in normal atmosphere have been carried out by White and his co-workers.[1] Similar studies are also performed at the Canadian Armament Research and Development Establishment in rarefied atmospheres in a high-altitude free-flight testing range. Briefly the range consists of a three-stage hypervelocity light gas gun, capable of launching 5 cm diameter scaled models at speeds up to 6 km/sec into an evacuated test section in the form of a 60 meter × 2 meter diameter steel tank.[2] In White's experiments, in order to achieve the desired resolution, a spectrograph slit was placed very close to the trajectory of the pellets, but it was not considered practical in our case. Arrangement was then made such that the image of the luminous trail, which was very much demagnified by means of a short-focal

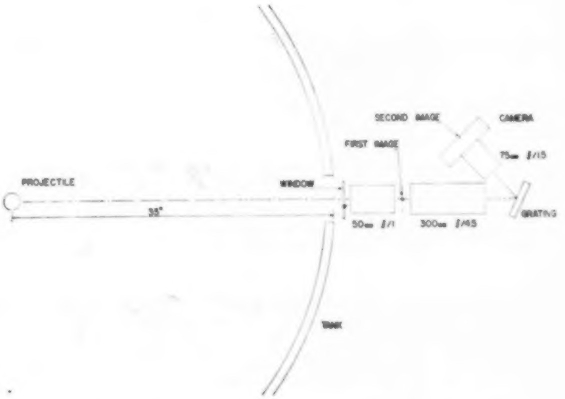

Fig. 1. Schematic layout of the spectrograph on the flight test range.

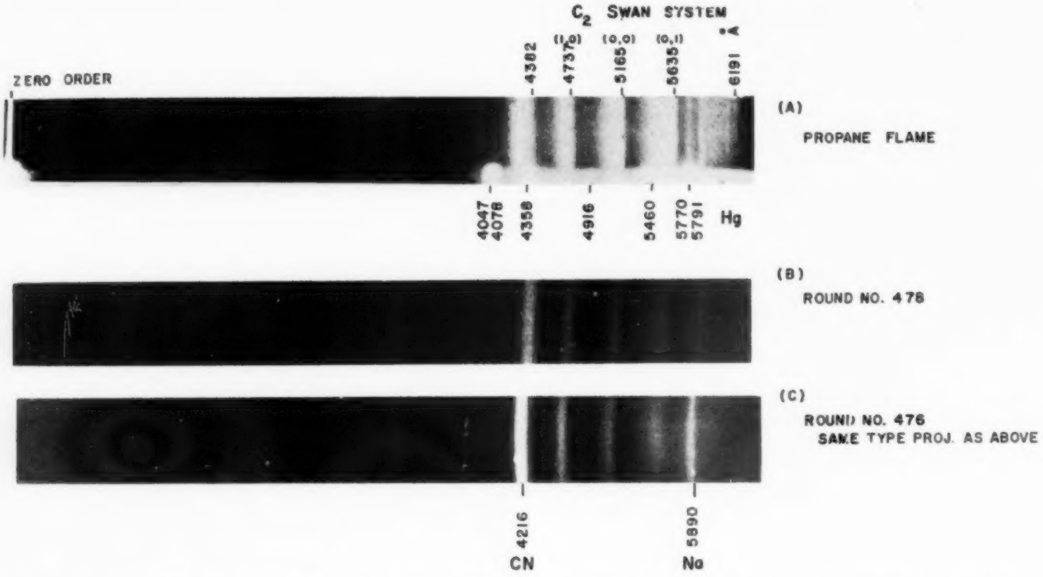

Fig. 2. Spectra of high-speed projectiles made of ethocel blue plastic. (Wavelengths in Ångstroms.) (B) 38-mm ethocel cup with Mg liner. $V = 5.46$ km/sec, $P = 0.5$ mm Hg. (C) $V = 5.36$ km/sec, $P = 0.5$ mm Hg.

large-aperture lens, could be used effectively as the slit of a spectrograph. The spectrograph used was a large-aperture grating instrument based on a design due to Bass and Kessler[3] utilizing commercially available photographic objectives. The collimating lens is a Carl Meyer 300-mm $f/4.5$ telephoto lens and a Carl Zeiss Biotar 75-mm $f/1.5$ lens is used as the camera lens. The replica plane grating has 600 grooves per mm on a 102 × 102 mm ruled area with a blaze angle of 13°. A Carl Meyer 50-mm $f/1$ lens was coupled to the collimating lens as shown in Fig. 1. The spectrograph was oriented in such a way that the grooves of the grating were parallel to the flight trajectory of the projectile which in turn intersected the optical axis of the collimating lens. The experimental layout is illustrated schematically in Fig. 1. The image of a 50 mm width streak is successively demagnified to 0.4 mm at the photographic plate. A linear reciprocal dispersion of 80 Å/mm in the first order is indicated, which was thought adequate in the preliminary work. Considerably improved dispersion can be obtained by a proper choice of the lenses. Some of the results under typical testing conditions are presented in Fig. 2 for ethocel-X blue plastic projectiles and in Fig. 3 for magnesium projectiles. Note the zeroth-order line in the spectra, which was used conveniently

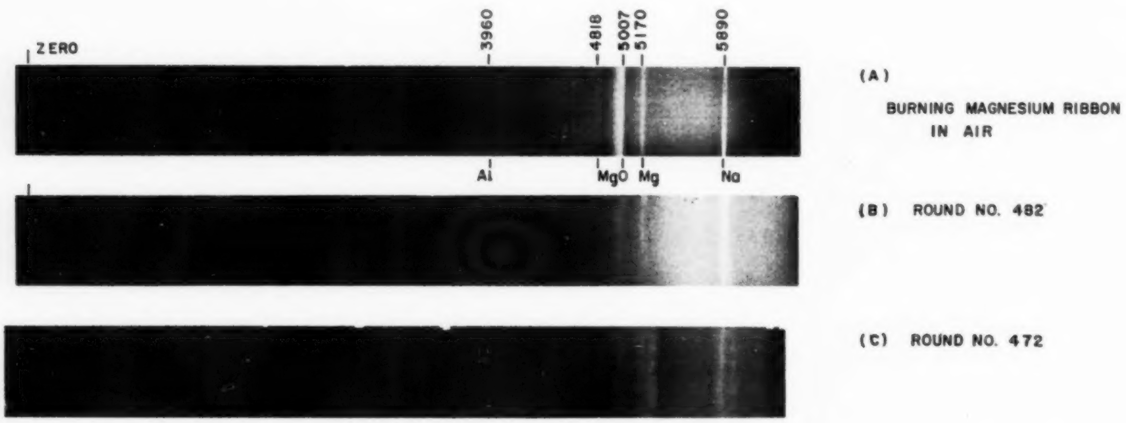

Fig. 3. Spectra of high-speed magnesium projectiles. (Wavelength in Ångstroms.) (B) 38-mm magnesium cup. $V = 4.07$ km/sec, $P = 3.5$ mm Hg. (C) 38-mm magnesium cylinder on ethocel base. $V = 4.70$ km/sec, $P = 3.5$ mm Hg.

as a reference for wavelength determination of the band systems. For ethocel-X blue plastic which is chemically an ethylcellulose, the bands resemble strongly those of the hydrocarbon-oxygen flames comprising the well-known C_2 Swan bands, CH, and possibly CN (0, 1) bands. The spectra for magnesium projectiles are similar to the spectra of magnesium ribbon burning in air, and the unresolved Mg triplet and the MgO bands are easily identified.

Work supported in part by ARGMA and paper presented at the Optical Society of America Pittsburgh Meeting, March 2–4, 1961.

Dr. Liu is now with Optics Technology, Inc., Belmont, California.

References

1. J. S. Rinehart, W. A. Allen, and W. C. White, J. Appl. Phys. **23,** 132 (1952); ibid. **23,** 198 (1952); ibid. **23,** 297 (1952).
2. G. V. Bull, Conference Anglo-American Aeronautical Institute of the Aeronautical Sciences (US) Paper 59-143, 1959.
3. A. M. Bass and K. G. Kessler, J. Opt. Soc. Am. **49,** 1223 (1959).

Meeting Reports

continued from page 642

Harold Edgerton, also an Honorary Member, covered the subject of stroboscopic lighting and showed films of underwater lighting equipment in use.

Four invited papers related to subjects of interest to readers of *Applied Optics*. R. M. Schaffert, IBM, San Jose, presented the results of investigations on the characteristics of the electrical fields associated with electrostatic images and the changes in field intensity and shape resulting from changes in the electrical environment of the image. Meyer Sugarman, APECO, assessed the various elements in electrophotographic document copier design—mechanical, electrical, and optical—from the viewpoint of optimum performance. T. T. Hill, 3M Company, reviewed comprehensively recent developments in the diffusion transfer reversal process and commented on its future trends both in camera usage and office-copy areas. E. R. Swanson, Air Force Aeronautical Chart and Information Center, described new specialized equipments for increasing the efficiency of the cartographer-compiler.

It is hoped that the invited papers as well as the many interesting contributed papers will appear in early issues of *Photographic Science and Engineering;* space limitations permit brief reporting on no more than a few of the contributed papers. J. Kaplan, Fairchild Camera and Instrument Corporation, described a means for automatic focusing of a high-acuity camera by photoelectric scanning of the film plane image and incremental stepping of the lens toward better focus. D. Rees and M. Lisic, Detroit Arsenal, presented the design of a 360° viewing system for combat vehicles employing a hyperboloid of revolution and a concave ellipsoid of revolution. The Minitrack Optical Tracking System was explained by D. Harris, J. Berbert, E. Habib, and B. McKendree of Goddard Space Flight Center, and S. Henriksen, U.S. Army Map Service, related the experiences in the design of cameras for photography of artificial satellites. N. Crabill, NASA, described the photoinstrumentation equipment used for the Echo II suborbital development test and showed the motion picture results of the first test. M. Rosenau, Jr., Perkin-Elmer, analyzed the effect of the atmosphere in modulating object brightness in aerial photography. A study by J. Goldhammer and F. Edwards of Chicago Aerial Industries concluded that tri-camera arrays with long focal length oblique lenses and an extreme wide-angle vertical angle possessed advantages over panoramic cameras. R. Heimer of the same company described the design and performance of a high-acuity 8-element $f/4$ photoreconnaissance objective of 122-cm (48-in.) focal length. R. Wolfe and S. Tuccio, Eastman Kodak, related picture definition in aerial photographs to the orientation of unsymmetrical spread functions with reference to the solar azimuth. C. West, Polaroid, in two papers, described and evaluated the step-scale system for photographic exposure quantities which, although utilizing ordinary ratio-numbers, is metrically adequate and consistent. R. Gundlach and C. Claus, Xerox, disclosed a novel xerographic method in which exposure of a plastic-overcoated photoconductor produces a charge pattern which causes selective wrinkling or frosting of the plastic, when the latter is heated, to form a light-scattering image. R. Mach and T. Gardner, IBM, described the automatic digital techniques employed for transforming Tiros I satellite photographs into mercator projection. M. Saffian, OPTOmechanisms, described a camera–processor–projector unit for acquiring display data in which exposure, development, fixing, and washing is achieved in six seconds. A controlled development processor for films from 35 mm to 241 mm in width was described by Capt. R. Burke, Wright-Patterson AFB. After brief initial development the film density is read by reflected infrared light, the data punched on tape, and the tape record used to control heat burst stations.

H. Frieser and K. Biedermann, Technische Hochschule, Munich, were authors of a report on image quality as related to the contrast transfer function and granularity of various negative materials. R. Shaw, Ilford Ltd., reported on the application of Fourier techniques and information theory in arriving at a figure of merit for information capacity of an emulsion. H. Zweig and J. Altman of Kodak showed how maximum information packing in emulsions, whether limited by granularity or spread function, is related to the number of density levels. Experiments on the visual sharpness of synthesized photographic edges with predetermined density distributions by J. Altman and R. Peden of Kodak showed the necessity of emphasizing the toe region of the curve. E. Haugh, Du Pont, Parlin, presented explicit equations for the optical density and amount of developed silver as functions of exposure to permit the experimental evaluation of significant parameters governing the H&D curve. R. Clark Jones, Polaroid, discussed the possibility of making improved films for aerial and astronomical photography in terms of the detective quantum efficiency rather than in terms of speed. Marilyn Levy, U.S. Army Signal R&D Laboratory, presented data to show that in many cases high-contrast development does not improve the contrast of microimages. R. Matejec, Agfa, Leverkusen, presented data on boundary-layer equilibria and diffusion of Frenkel defects in silver halide crystals. H. Meier, Staatliches Forschungsinstitut für Geochemie, Hamberg, described experiments on the electronic mechanism of the photoconductivity of sensitizing dyes. R. Lindquist and E. Ryskiewicz, IBM, San Jose, described the extension of wavelength sensitivity of photorefractive materials sensitized with a diazonium salt. W. Elbrecht and W. Seifert, Kalvar, presented several methods of gamma control in Kalvar film and their effect on other image characteristics. H. Medley and R. Kay of IBM, San Jose, described an ultraviolet sensitometer, a thermostatically heated roller, and a projection densitometer for the sensitometry of vesicular materials. R. Alfaya, Fairchild Camera and Instrument Corporation, discussed new diazo materials having ultra high resolution at unit gamma. A. Shepp, L. Corben, and I. Theodorou, Technical Operations, and R. Dunker, Wright-Patterson AFB, presented a method of preparing photographic emulsions by immersing a light-insensitive layer into a bath containing excess silver ions. Ira Current, Ansco, described the techniques for the sensitometric evaluation of high-speed direct-recording silver halide oscillograph papers. A high-quality automatic resolution testing sensitometer, built by Kodak, was described and data obtained through its use were presented by R. Summers and R. Dunker of Wright-Patterson AFB. L. Tregillus, Kodak, described a transfer process in which an exposed negative is placed in contact with a supporting web carrying a hydrophilic layer containing physical-development nuclei and processing solution. Y. Miura and Y. Hayakawa, Fuji Photo Film, described the development-accelerating effect of arginine on development with *p*-formaldehydehydroquinone developer. The effects of amines on the chemical sensitization of silver iodobromides and the mechanisms involved were presented by V. Chambers and A. Oberth, Du Pont, Parlin.

S. Kitrosser, Conference Chairman, H. Howell, Papers Chairman, and the members of the various conference committees are to be credited with the production of a successful and satisfying meeting.

Erratum The international aspects of this journal have introduced many editorial problems in orthography: the Greek and Cyrillic alphabets, accent marks in French, tildes and cedillas in Spanish, the umlauts of German, and all of the other jots, tittles, and diacritical marks that plague foreign languages. Your Editor had prided himself on his umlauts, but Pride goeth before a Fall, and we erred sadly in last month's Editorial. We were wrong both etymologically and orthographically, at least as far as the AIP *Style Manual* is concerned. We said "Angstrom becomes Ångstrom again." What we should have said was "angstrom becomes ångström again, and its symbol A becomes Å."

SUPPLEMENT ON OPTICAL PUMPING AND MASERS

An *Applied Optics* **Supplement** on Optical Pumping and Masers will be published in December 1962. This special edition will gather together all the papers in that area of activity published in *Applied Optics* during the first year of publication and include articles not previously published such as a survey of gas lasers by W. R. Bennett, Jr. In addition, a 15,000 word review will be written by O. S. Heavens, *Royal Holloway*, which will not only survey the present state of the art and give fundamental theories but will integrate all the papers published in the **Supplement.** This **Supplement** will be sold at not more than $5.00 a copy.

ORDER FORM

Optical Society of America
1155 16th Street, N.W.
Washington 6, D.C.

Please enter my/our order for the **APPLIED OPTICS FIRST SUPPLEMENT—OPTICAL MASERS,** to be published in December 1962 at a cost of not more than $5.00 a copy

Name..
Address...
....
....

TO APPLIED OPTICS ADVERTISERS:

Optics and Spectroscopy, an NSF-sponsored English translation of the leading Russian journal in this field is now accepting advertising from **Applied Optics** advertisers. **OiS** coverage includes, in addition to optics, articles in solid-state physics, atomic, molecular, and applied spectroscopy (including spectrochemistry) and apparatus and instrumentation. It has had free distribution for the past three years of some 7,000 copies per issue (1962 on is sold on subscription). Space in this journal may be purchased for $100.00 by any **Applied Optics** advertiser who wishes his **Applied Optics** ad to be picked up and run in the next issue of **Optics and Spectroscopy.**

The advertising deadline for the immediate future issues are:

July—published in English translation October
advertising closes **September 20.**

August—published in English translation November
advertising closes **October 20.**

September—published in English translation December
advertising closes **November 20.**

Persons interested in placing orders or desiring additional information should contact OiS Advertising Dept., Optical Society of America, 1155 Sixteenth Street, N.W., Washington 6, D.C. Tel.: DI 7-6177 (Area Code 202).

ADVERTISING

Advertising Agent | Alfred P. Oppenheim
Assistant | Ruth Steger

Advertising inquiries, orders, plates, and correspondence should be addressed to the Applied Optics Advertising Office, 55 West 16th Street, New York 11, New York. CHELSEA 2-1311

A FLY'S EYE—150X MAGNIFICATION

like to hire a new kind of private eye?

Looking for a new kind of eye? Impressed by the long distance vision of TIROS and NIMBUS? Those were ELGEET lens systems specifically engineered to prove that "pie-in-the-sky" could become actual "eye-in-the-sky" concepts. At ELGEET we have the optical know-how and the design imagination you may be seeking for your own project. We'll send our Design Section to meet with you in your office and take that optical problem off your desk. We feed it into experienced minds and high-speed computers to break-through to your possible solutions. Let ELGEET be your Private Eye. Take your choice of a deep look, a quick look, a dim look, a bright look, a wide look, a forward look, a top-side look or an underbelly look. But first: *write to* ELGEET OPTICAL COMPANY, *838 Smith Street, Rochester 6, New York for a fully illustrated information file on our optical capabilities and performance.*

CREATIVE OPTICS
Elgeet
FOR EARTH AND SPACE

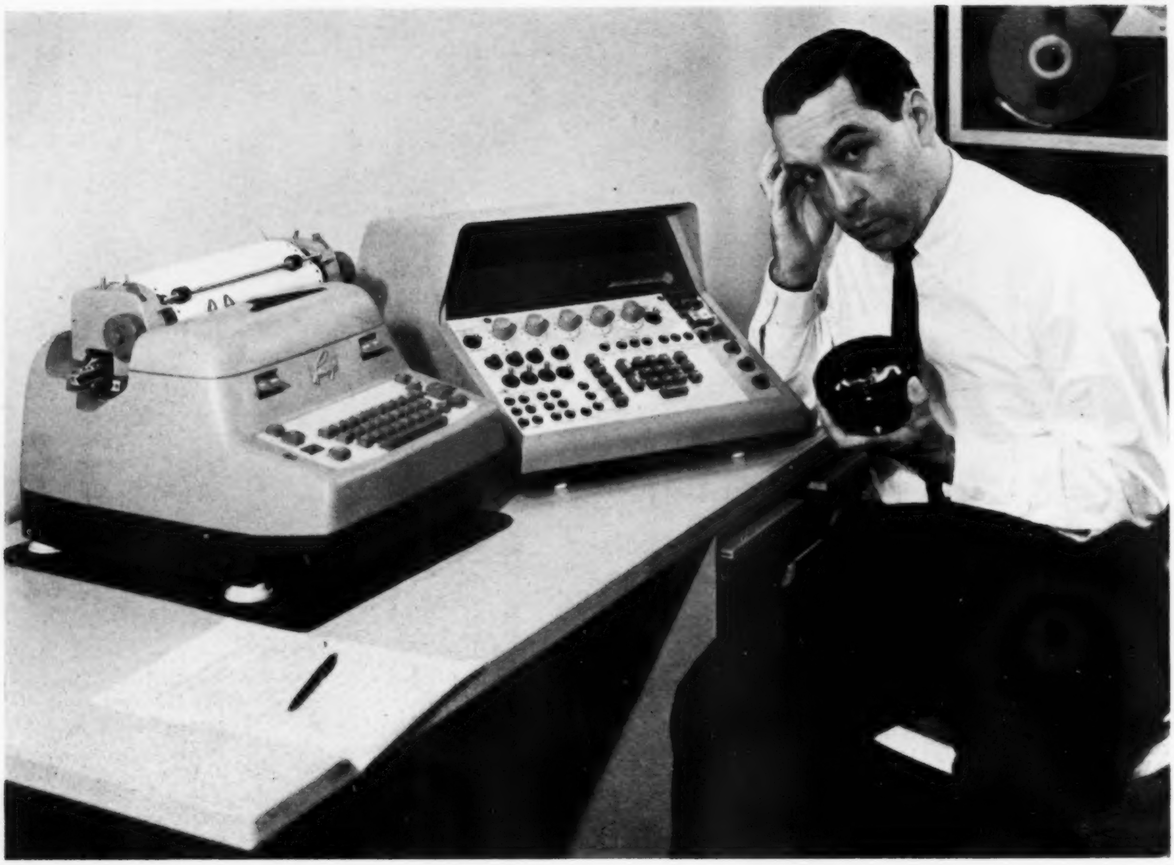

How to save 10% on optical glass and spend more on lens design changes

A fable specially designed for Design Engineers who think the lowest-priced optical glass is best

Once upon a time there was an optical engineer who loved his battery of computers better than anything else in the entire world. He spent all of his days and many of his nights while his computers clicked their relays and flashed their five watt bulbs just like a movie marquee.

Every so often he would feed his favorite computers with a mixture of formulas and problems and stand back to wait for the results he expected to be correct every time.

And correct they were! For the computer had a wonderful brain, and as fast as new lens designs were completed they were rushed into Production where talented craftsmen slowly worked the designs into optical perfection.

When all of the lenses were polished and finished everyone stood back and admired the work. Everyone, that is, except the customer. "The products are beautiful, the computers are brilliant, the craftsmen are skilled," he said, "but the lenses aren't uniform. They're worthless and must be re-worked, every one."

Glass not uniform? "It's that bonehead purchasing agent," thought the designer. But when he confronted the purchasing agent he found the P.A. had followed the specs to the tenth place and bought the lowest-priced glass—as the designer had suggested.

And that's the story of how quality optical glass, the kind Ohara produces, came to be the only glass allowed near the designer's favorite computers. The results have been rewarding. Glass now costs a bit more to start, but lens designs are guaranteed.

Moral: The best of computers and men are helpless when optical glass lacks uniformity through multiple melts.

Ohara Optical Glass not only provides .0008n_D on the first melt, but Ohara's ability to maintain melt uniformity guarantees the same high quality melt after melt.

If you require the very finest quality glass then specify Ohara.

For your copy of Ohara's reference catalog just write or call today.

OHARA OPTICAL GLASS

Exclusive distributors:

Pacific Optical Corporation

120 South Glasgow
Inglewood, California

WHAT'S NEW!

Our Optical Bench Catalog! And why not: The optical bench business is booming. For the past several months demand has kept ahead of mounting production. It is temerity indeed to further spur things on with a new catalog. Yet we've done it, we're glad, and we hope you'll not waste a minute writing for your free copy.

In addition to our seasoned favorites, the sturdy triangular "Zeiss" form and the magnificent Beck Precision Research Bench, three new benches of intermediate price have been added.

First is the 22–950, a 2 meter lathe bed bench of heavy cast iron, flat over its length to about 0.003–0.005 inch and priced at $395. *That* is real value.

Next comes a similar 2 meter lathe bed bench of better quality cast in stress-free Meehanite, and guaranteed flat to 0.0025 inch. This bench is the 22–965 priced at $990. How does that smack you?

The third is a real bombshell. Our newest Research Lathe Bed Optical Bench, the 22–990, is a massive 8 ft. Meehanite stress-free casting, machined to a guaranteed accuracy of at least 0.001 inch over its entire length—and it is priced at just $3,400.

If the truth be known, this bench is a close relative of the 23-000 Beck Precision Research Bench, differing (apart from price) only in the absence of side slide carriers and a slightly lower guarantee of precision on flatness, the Beck 23-000 being guaranteed flat to 0.0005 inch and costing an appropriate $6,350.

Needless to say, over 50 accessories including Nodal Slides are available and interchangeable for all benches except for the two Research Benches which share their magnificent goodies compatibly.

Should these few modest lines start a stampede of unforseen dimension, we'll take our chances with phlegmatic poise. Foresightedly we have placed large orders with the manufacturers. If you are seriously considering one of these new benches, give me a ring. It's Frank Ferguson, Sales Manager, at the number listed below. Let's talk about it. In the meantime send for the new catalog.

THE Ealing CORPORATION

33 University Road,
Cambridge 38, Massachusetts
Telephone : 617 — KI 7-5760
Cable : Ealing

"SQUARED" BAND INFRARED FILTERS DEVELOPED AT OCLI

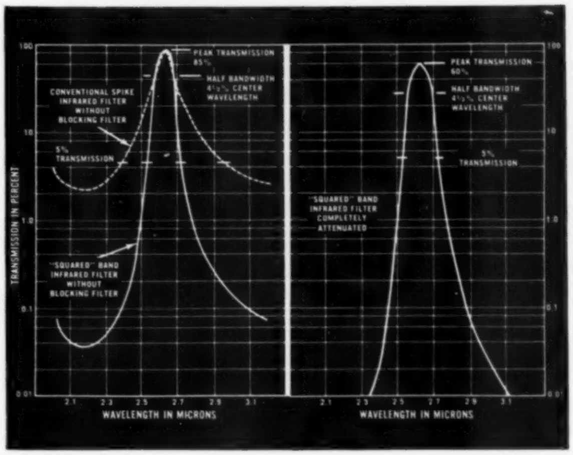

This new infrared filter by Optical Coating Laboratory, Inc. gives greatly increased ratios of transmission to rejection. Rejection is of extreme importance to the designer whose system is background noise limited. Typical obtainable ratio in the 2-3 micron region is 8000:1. Other advantages over conventional spike and line filter designs include:

- **High integrated transmission in the wavelength region of interest.**
- **Rapid transition slopes resulting in constant uniformity of bandwidth from low to high level transmission.**
- **Reduction of wavelength shift of the energy being received at angles other than normal to the filter surface.**
- **Sharper resolution of two closely spaced bands of energy due to the rapid transition of cuton and cutoff slopes.**

Plus greatly increased accuracy of wavelength location of the transmission band. For example, an accuracy of 0.01 micron in the 3 micron region can be obtained.

FOR FURTHER INFORMATION CONTACT:

OCLI

OPTICAL COATING LABORATORY, INC.
2789 GIFFEN AVENUE, SANTA ROSA, CALIFORNIA, U.S.A.
Teletype ZR 33 Telephone Liberty 5-6440

Farrand

FARRAND PULSAR The Farrand "Pulsar" Pulsed Light Ranging System applies infra-red radiation to provide armament fire control with high target selectivity. The system features light weight, low power requirements, and freedom from countermeasures.

FARRAND IRRAD T-13 This Farrand application of infra-red is designed for field survey applications and provides improved performance over existing transits. The unit operates over long distances with high accuracy and can be used equally well in the day or night.

FARRAND PLANT MONITORING SYSTEM This long path Infrared System is a highly sensitive industrial monitoring instrument that is used to detect contaminants in the atmosphere. The unit has sufficient sensitivity to detect concentrations of less than 2×10^{-9} grams per liter. The system operates on the selective absorption principle.

FARRAND FLASH LAMPS Farrand Flash Lamps are designed specifically as an efficient source of infrared radiation. They are widely used in many infrared ranging devices, infrared cameras, and many other devices.

Advanced Developments in Infra-Red

FARRAND AIRBORNE INFRARED GUNSIGHT Farrand has developed a Passive Infrared System for detection of infrared radiation for gunsight applications. The unit converts the signal into a television screen presentation with the brightness of each image point indicating the differential of radiation of the source with respect to its surrounding. A 10° square field of view, with a resolution of 15 minutes, is presented.

FARRAND SPECTRALARM The Farrand Spectralarm is a portable detection device operating on the Infrared absorption principle. It will passively detect contaminants in the atmosphere when it is pointed at the area to be monitored. The instrument is extremely light in weight, small in size, and easily operated by unskilled personnel.

INFRARED MONOCHROMATORS Grating Types.

Send for Farrand "SCOPE OF ACTIVITIES BROCHURE" for the complete story of many of Farrand's advanced devices. For specific information on the infrared devices outlined above, let us know of your intended use and we will provide all the information that you require.

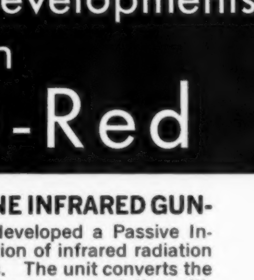

Farrand
Optical Co., Inc.
E. 238th ST. and BRONX BOULEVARD
NEW YORK 70, N. Y. (212) FA 4-2200

Nothing near it

See if you don't agree that, for value, this telescope stands alone. It is only $995 (mounting pier extra). Its 8" Cassegrain system has an f4 primary mirror—and all the optical surfaces are manufactured and coated by Tinsley with the same professional skill used for major university telescopes.

The cast aluminum mounting provides large bearing surfaces with unusually short axes lengths. These qualities combined with the short optical tube length permit an almost vibrationless mounting under windy observing conditions. Yet the mount weighs only 45 pounds.

The telescope has large engraved setting circles divided in 5 minutes of time in right ascension, and one degree of arc in declination. The sidereal drive is controlled directly by a variable speed motor. Adjustments of motor speed are achieved by means of a rheostat. The manual slow motion in declination uses a complete gear instead of conventional tangent screw arrangements. The right ascension slow motion is operated by a single hand control, to move the telescope east or west at twice the sidereal rate.

For viewing ease the zenith diagonal may be rotated in any direction about its axes permitting the observer to remain seated during long observation periods. The pier (an optional accessory) is supplied with an azimuth adjustment plate to permit fine adjustment when orienting the polar axis.

These are just a few of the convenient features of this fine instrument. Space doesn't permit us to describe them all, so write for comprehensive literature to: Tinsley Laboratories, Inc., Dept. D, 2448 Sixth Street, Berkeley 10, California.

Gentlemen: I am interested in applications of your new 8" telescope in
☐ Secondary School ☐ University or J.C. ☐ Astronomy Club
☐ Research in Industry ☐ Private Observatory
Hobby: ☐ Astronomy ☐ Photography

Name____________________

Street & No.____________________

City____________________ State__________

Company or Institution____________________ Title__________

FACTS FOR INFRAREDMEN ABOUT KODAK'S RUGGED POLYCRYSTALLINE OPTICS

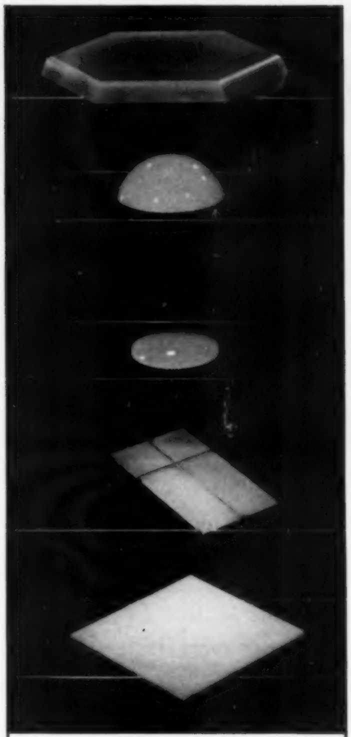

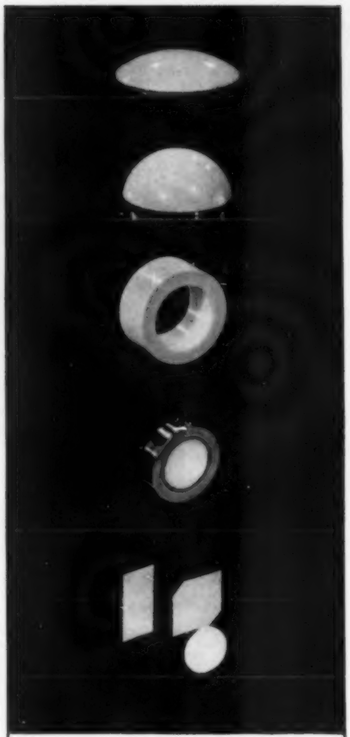

	IRTRAN-1	IRTRAN-2
RANGE:	2μ to 8μ.	1μ to 14μ.
REFRACTIVE INDEX:	1.37 to 1.31. Anti-reflection coating unnecessary and impossible. What would you use?	2.29 to 2.14. For lens power, deviation power, even a little dispersion power. Glad to coat.
MAXIMUM SIZE:	7-inch hemispheres. Other forms to 6½-inch diameter x 1 inch. Fusing extends possibilities.	6½-inch diameter x 1 inch. Stainless steel mounts can stand 600°C.
KNOOP HARDNESS:	576.	354.
ABRASION RESISTANCE:	Better than most conventional optical glasses.	Not quite as good as Irtran-1 but still better than many glasses.
THERMAL SHOCK RESISTANCE:	Survives quench from boiling water to 23°C. Good microwave characteristics.	Almost as good as Irtran-1. Resists more solvents than anything else we know for this transmittance band.

A big point of pride is the low emissivity. To achieve this relative immunity from blinding by high temperature, we have worked like galley slaves to get the absorption out. Lenses, domes, prisms, flats, filters. Some can even be shipped from stock. To get on the list of people we keep informed, write:

EASTMAN KODAK COMPANY
Apparatus and Optical Division
Rochester 4, N.Y.

Kodak
TRADEMARK

INFRARED STANDARD

ECI THERMAL RADIATION STANDARD MODEL 55A

Temperature adjustable within 1 °C from ambient to 1000 °C and controlled to ±1 °C. Biconical cavity with 1⅛ inch diameter aperture, total emissivity greater than .995. Radiation shield, aperture holder, 10 calibrated apertures, transistorized controller. This stable "black body" source has met wide acceptance. Purchasers include:

BELL TEL LABS
MARTIN COMPANY
UNIV. OF NEVADA
DOUGLAS AIRCRAFT
UNIV. OF MICHIGAN
U.S. WEATHER BUR
EASTMAN KODAK
NAT'L BUR STDS
OWENS-ILLINOIS
CONVAIR
AFCRL
NOTS

ELECTRONIC COMMUNICATIONS, INC.

Research Division 1830 York Road Timonium, Maryland
CLearbrook 2-1400 (Area Code 301)

SUPPLEMENT ON OPTICAL PUMPING AND MASERS

An *Applied Optics* **Supplement** on Optical Pumping and Masers will be published in December 1962. This special edition will gather together all the papers in that area of activity published in *Applied Optics* during the first year of publication and include articles not previously published such as a survey of gas lasers by W. R. Bennett, Jr. In addition, a 15,000 word review will be written by O. S. Heavens, *Royal Holloway*, which will not only survey the present state of the art and give fundamental theories but will integrate all the papers published in the **Supplement.** This **Supplement** will be sold at not more than $5.00 a copy.

ORDER FORM

Optical Society of America
1155 16th Street, N.W.
Washington 6, D.C.

Please enter my/our order for the **APPLIED OPTICS FIRST SUPPLEMENT—OPTICAL MASERS,** to be published in December 1962 at a cost of not more than $5.00 a copy

Name..
Address...
....
....

APPLIED OPTICS

Subscription Order

☐ 1 year, at OSA member rate of $6.00

☐ 1 year, at special rate, to other AIP Societies members, of $8.00

☐ 1 year, at non-member rate of $10.00

☐ Please send OSA membership information

Membership No..............

Name.................................

Address.............................

....

....

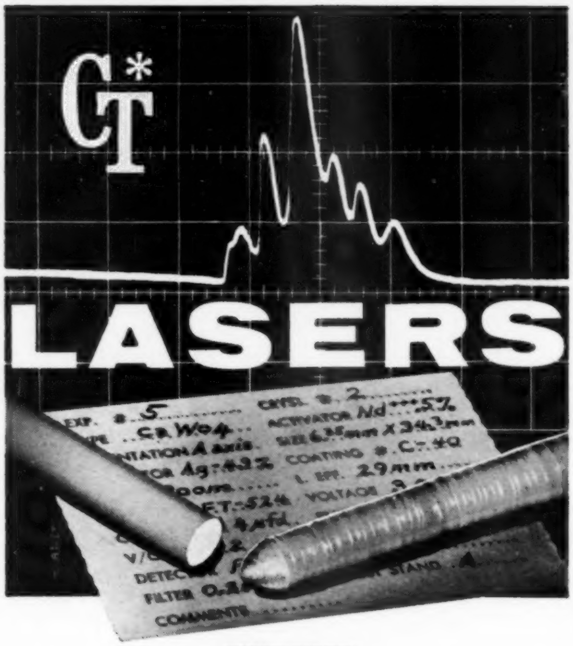

EXTEND YOUR LASER INVESTIGATION CAPABILITIES

Utilize the country's most extensive crystal growing—precision fabrication—crystal finishing facilities. ISOMET offers TOTAL CAPABILITY with FLEXIBILITY—Custom growth, fabrication, finishing, quantity production; one source for all. ISOMET lasers are of the highest quality and precision, assuring maximum performance.

TESTED LOW THRESHOLD LASER CRYSTALS

* *Certified Threshold* Each ISOMET laser rod is accompanied by an actual oscilloscope photograph of its output performance at threshold and complete data on the experimental conditions of the test.

BOULES OR FABRICATED RODS with ends polished optically flat and parallel. Also available with ends confocal, spherical or faceted to meet your special requirements.

Stocked for immediate delivery

$CaWO_4$, $SrMoO_4$, $PbMoO_4$ doped with Nd^{3+}
Chromium doped Ruby, 0° or 90° orientation
Nd^{3+} doped glass
CaF_2 and BaF_2 doped with Sm^{2+}, U^{3+}, Nd^{3+}

Grown to order

$CaWO_4$, $SrMoO_4$, $PbMoO_4$, CaF_2, CdF_2, BaF_2 or other hosts doped with any of the rare earths or transition elements.

REFLECTIVE SURFACES Evaporated metallic coatings or multiple dielectric layers

Write for new tech. bulletin M 1000

ISOMET
CORPORATION
PALISADES PARK, NEW JERSEY

For the latest developments in infrared research, read . . .

INFRARED PHYSICS

An International Research Journal

Editors: P. Goerlich, *VEB Carl Zeiss, Jena, Germany;* T. S. Moss, *Royal Aircraft Establishment, Surrey, England;* S. Passman, *Rand Corp., Santa Monica, Calif.;* W. K. Weihe, *U. S. Engineers, Ft. Belvoir, Va.;* G. A. Boutry, *Paris; and a distinguished Editorial Advisory Board*

INFRARED PHYSICS publishes original papers and articles on infrared physics and its applications. It is concerned with infrared theory, experiment and instrumentation as applied to infrared detection and transmission and to problems of atmospheric, meteorological, geophysical, astrophysical and space research.

Also included are specially-invited critical surveys, quickly-published research notes and book reviews.

An invaluable source of information on the latest findings and developments in the infrared field, this journal publishes authoritative papers written by eminent scientists throughout the world. INFRARED PHYSICS is "must" reading for every scientist and technician working in applied optics in relation to space and planetary research as well as in the physical sciences.

Articles published in the April/June issue

E. SCOTT BARR: The infrared pioneers—II., Macedonio Melloni; C. L. PATTERSON: Application of the lateral photoeffect to a tracking system; R. PENNDORF: Mie scattering in the forward area; M. LAURIENTE, R. F. HIGBY, J. BAGROWSKI and F. X. McNALLY: Sophisticated detector design for increased infrared sensitivity; H. MOENKE: Relationship between the lattice constant and an infrared active vibration of anhydrous carbonates in the spectral region 710–750 cm; S. NIELSEN: Note on the preparation and properties of glasses containing germanium disulphide.

Subscribe now to INFRARED PHYSICS—be sure of having the latest data in the field for your own reference.

Published quarterly in 1962—monthly in 1963.

Annual subscriptions: "A" rate, to libraries, industrial and other establishments, $20.00 (1963 rate increases to $30.00); "B" rate to individuals certifying it is for their own use, $10.00.

Sample copy sent on request.

PERGAMON PRESS, INC.
Dept. AO1
122 East 55th Street, New York 22, N.Y.

SCHOTT Narrow Band Interference Filters

Made by JENAer Glaswerk Schott & Gen.
WEST GERMANY

For the spectral region from 300 to 2,000 mμ.

Transmission up to 60%. Half-value width down to 5 mμ. Tolerance at peak wave length: ±1% for regular quality. ±0.5% for precision quality.

AVAILABLE AS

Line Filters • Line Double Filters • Band Filters
Band Double Filters • Wedge Filters • Broad Band Filters

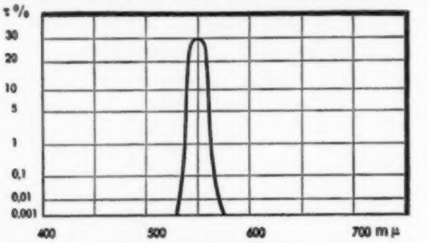

DOUBLE BAND FILTER

Tmax about 30%. Half width about 16 mμ.
Ratios: Tenth width to half width 1.5, Hundredth width to half width 2, Thousandth width to half width 3.5.

SCHOTT Colored Optical Filter Glass

Available in about 100 types for ultraviolet, visible and infrared spectral regions, including absorption filters containing neodymium for use in lasers and masers.

MULTI-LAYER INTERFERENCE FILMS

for dichroic and achromatic beam splitters and filters. High efficiency. Relatively wide band.

MULTI-LAYER HEAT DEFLECTORS

XUR-96. Reflects substantial portion of infrared spectrum while transmitting nearly all of the visible radiation.

#6143. Colorless, non-absorbing filter. Completely removes the ultra-violet and reflects the infrared. Transmits about 90% from 425 to 700 mμ reflecting longer wavelengths. Half transmission points at 412 mμ and 725 mμ.

Cold Mirror IRT-211. To reflect visible radiation from 400 to 700 mμ and transmit from 725 to 1200 mμ and longer.

COATINGS FOR LASERS and MASERS

For Ruby: #3132-N. 99% reflectivity from 694 to 760 mμ.

For Glass: #3117. 99% reflectivity from 1,000 to 1,200 mμ.

LOW REFLECTING COATING

Double and triple layer with minimum reflection of less than .1% on glass of low index.

Coatings also available to increase transmission to 9 micron on Germanium and Silicon.

FISH-SCHURMAN CORPORATION
90 Portman Road, New Rochelle, N. Y.

NOW!

OPTICALLY CORRECTED SINGLE CRYSTAL LASER RODS

Adolf Meller Co. offers optically corrected laser rods in Ruby or Sapphire-clad Ruby . . . also!

$CaWO_4$ with Nd^{3+}	.5% doping
$CaWO_4$ with Nd^{3+}	.025% doping
CaF_2 with U^{3+}	.1% doping
CaF_2 with Dy^{2+}	.1% doping
SrF_2 with Sa^{2+}	.1% doping
SrF_2 with Nd^{3+}	.5 % doping

Only Meller offers this optical correction service with its outstanding guarantees:

1. *Flat End Rods:* flat to 1/20*th* wave length or better . . ends optically parallel within 2 secs. of arc.
2. *Chisels:* right angle correct within 5 secs. of arc. All faces flat to 1/20*th* wave . . and apex of angle parallel to flat end within 4 secs. of arc so that maximum TIR (total internal reflection) will be attained.

All guarantees apply to ruby rods of any length from 1 1/2" to 9" . . . and up to 1 1/2" to 2" lengths (maximum available on other single crystals.

Meller offers round, square, triangular, and other special configurations to your specifications. Trumpet shape ruby/sapphire completely lapped and silvered available for less than $1,000.00! Also white sapphire tubes for any size ruby rod—piston fit.

Ask for new technical brochure and complete price schedule.
Adolf Meller Co., Box 6001, Providence, Rhode Island,
Phone (401) 331-3717

MELLER SAPPHIRE PRODUCTS

Synthetic Sapphires • Ruby Lasers & Masers
Alumina Powder

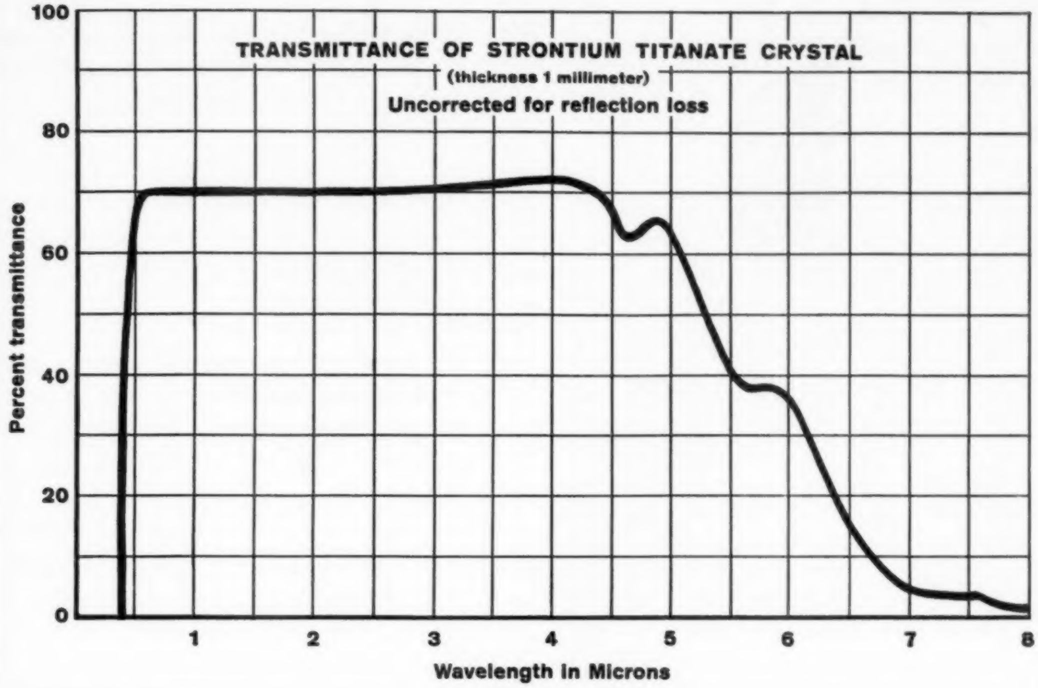

Strontium Titanate crystal for infrared optics

As may be noted from the above chart, strontium titanate crystal transmits well out into the infrared, its transmissivity still being high for infrared radiation of 6 micron wavelength. Although the high refractive index of this crystal accounts for reflection losses, it permits the design of lenses of suitable size and of great value for concentrating infrared energy.

Strontium titanate crystal is cubic, singly refracting, physically and chemically stable, and electrically insulating. No wonder it is being selected as the outstanding lens material for infrared optics in the range indicated in the above chart.

This crystal is a production product fully available to meet the requirements of infrared applications. In addition to strontium titanate crystal, we produce rutile (TiO_2) crystal also having interesting infrared properties but having double refraction.

Crystals that are Developmental Products— Single crystals of a number of compounds having interesting infrared transmitting characteristics in the range from 0.7 to 16 microns, have been produced in our continuing research and development program. We will welcome any opportunity to consider with you the relationship of these developmental products to your interests in infrared optics.

NATIONAL LEAD COMPANY
TITANIUM DIVISION
111 BROADWAY, NEW YORK 6, N. Y.

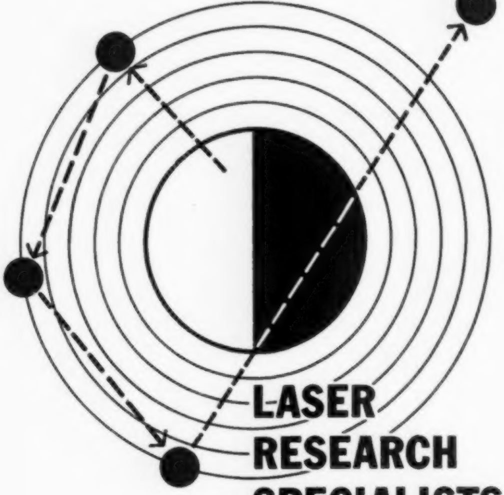

LASER RESEARCH SPECIALISTS

A major research program is now underway at the DOUGLAS Missile and Space Systems Division. You are invited to investigate the following outstanding staff and project scientist openings this program is providing:

Sr. Quantum Electronic Physicist—This senior physicist will direct the Laser research activities now in progress. Our research involves: Coherent Light Communications/Laser-Radar/Laser-Plasma Interaction/Basic Physics of Lasers vs. Matter. Ph.D. required, but consideration will be given to exceptionally well-qualified candidates with M.S. degree.

Staff Physicists—Ph.D. preferred but M.S. degree is a minimum requirement for these positions. Applicants must have related experience and/or a strong educational background and interest in Laser technology. For example, professionals with experience in radar cross-section measurements interested in applying these techniques to Laser-Radar would find these positions well worth investigating.

Propagation Physicists—Duties will include investigation of conventional RF and coherent light propagation both theoretically and experimentally. M.S. in Physics or Electrical Engineering with related experience preferred but not essential.

Write for complete information (including resume of background) to: F. V. Edmonds, Missile and Space Systems Division, Douglas Aircraft Company, Inc., 3000 Ocean Park Blvd., Santa Monica, California.

DOUGLAS

MISSILE & SPACE SYSTEMS DIVISION

An equal opportunity employer

PHYSICIST

MS or PhD in Physics. Equivalent degree in related fields is acceptable if strong formal training in Physics, particularly Optics, has been included.

Prefer formal training in theory of precision physical measurements including familiarity with interferometers and diffraction gratings as measurement scales.

Will involve investigation of physical phenomena which causes inaccuracy in precision measurements, such as temperature surface deformation due to contact pressure and/or pressure due to dynamic compressions of gauging heads. Will seriously consider inexperienced applicant with advanced degree in Physics.

This position is in our Livermore Laboratory, located in the sunny, smog-free Livermore Valley . . . country living just minutes from San Francisco.

Sandia Corporation offers liberal employee benefits including vacation, retirement and insurance plans, an educational assistance program, and paid relocation allowance.

Write to:
M. A. Pound
Professional Employment Section 545.

SANDIA CORPORATION
P. O. Box 969
Livermore, California

SANDIA
CORPORATION
LIVERMORE. CALIF.

An equal opportunity employer
U. S. citizenship required.

IF YOU USE GLASS BEAM SPLITTERS
MIRRORS • FILTERS • PRISMS

in apparatus you are designing, manufacturing or using

THIS FREE BOOKLET IS FOR YOU.

Thin film pellicles introduce neither refractive error nor ghost images, can be had flat to 1/20 wave, and offer full coating selection including dichroics. This booklet tells you how and when to specify thin film pellicles.

NATIONAL PHOTOCOLOR CORP.
225 EAST 44TH STREET NEW YORK 17, NEW YORK

Ask for "*Application and Specification of Pellicles*"

INFRARED OPTICS

DOMES — LENSES — WINDOWS — PRISMS

SILICON TO 16″ DIAMETER

GERMANIUM TO 24″ DIAMETER

are CAST TO SHAPE by an advanced low-cost, production technique!

Many sizes in stock, including single crystal materials.

INDIUM ARSENIDE, GALLIUM ARSENIDE & INDIUM ANTIMONIDE are available in sizes up to 1″ diameter.

Exotic Materials, Inc.
1534-E East Chestnut Ave. Santa Ana, California

Specialists in **LARGE** optical shapes

OCLI DEVELOPMENT REPORT
ANOTHER TOOL FOR INFRARED ENGINEERS
ALL-INTERFERENCE BANDPASS FILTERS FOR 8-20 MICRON REGION

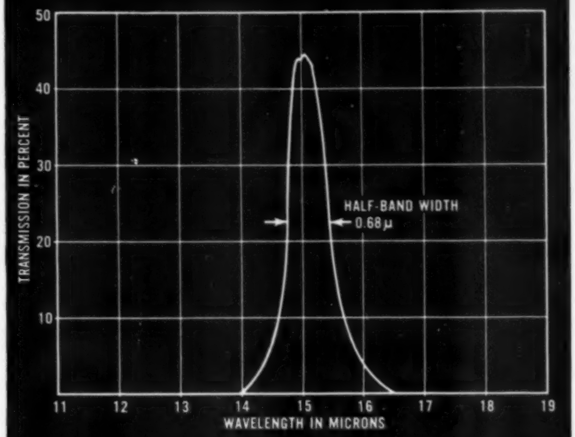

Curve plotted from actual performance data.
Note extremely steep slopes, cuton 3.5%, cutoff 5%.

One of the latest developments to come from Optical Coating Laboratory Research and Development is the new All-Interference Bandpass Filter for use in the 8-20 micron region. This development is a continuation of OCLI's research which provided industry with the first interference filter to isolate successfully the 8-13 micron window. These new filters isolate bands of energy with precision in location of center wavelength to within 2% . . . steep cuton, cutoff slopes (less than 5%). Transmission exceeds 40%, sideband rejection is also high (less than 0.5% transmission). Like all OCLI filters, the new All-Interference type is exceptionally durable and environmentally stable.

For further information on OCLI thin film products for space reconnaissance, military surveillance, infrared radiometry, infrared guidance, and various ultraviolet applications for both military and industrial purposes, contact:

OCLI

OPTICAL COATING LABORATORY, INC.
2789 GIFFEN AVENUE • SANTA ROSA, CALIFORNIA
Telephone 707 LI 5-6440 Teletype ZR 33

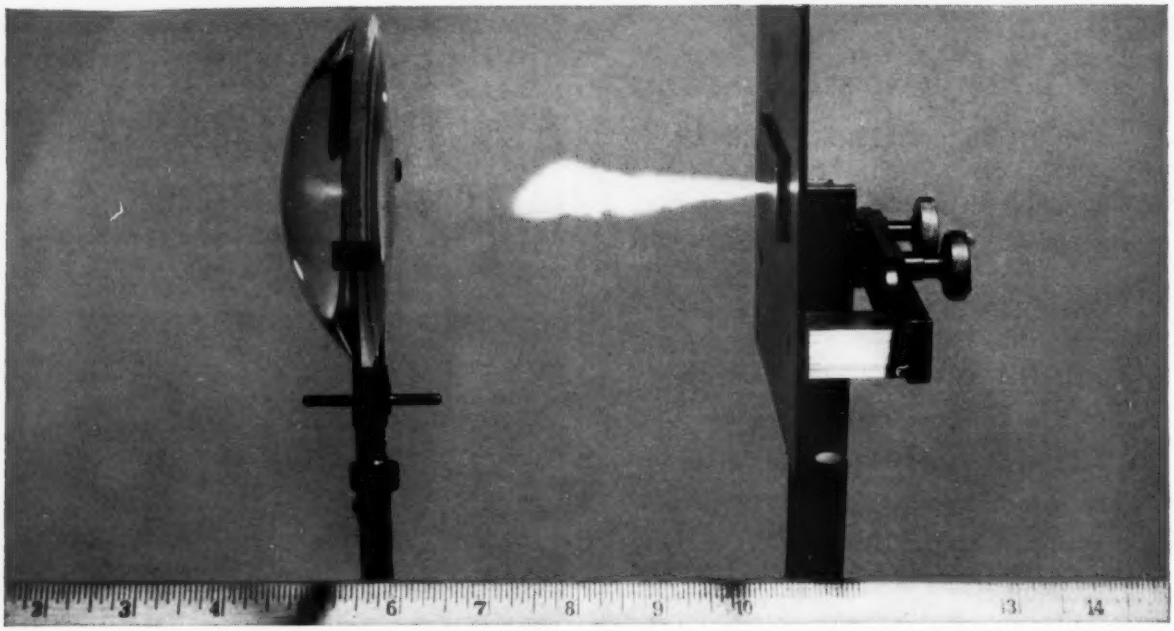

NEW AT AO: *A high energy laser beam produces a luminous plume when focused on a carbon steel plate. The 2-millisecond pulse delivered 73 joules of energy into a 0.010-inch diameter spot. A neodymium glass laser, developed at the AO Research Center, was used. This same laser produced an energy output of 113 joules, believed to be the highest output yet achieved in this new field.*

RESEARCH & DEVELOPMENT OPPORTUNITIES

Generation of coherent optical radiation and other optical maser phenomena are under intense investigation at the Research Center of American Optical Company. Advanced studies of wave propagation in small diameter optical fibers and IR and UV radiation phenomena also are being conducted. New opportunities for creative basic and applied research in these and other areas are available at both senior and junior levels.

- **SOLID STATE PHYSICISTS:**
  To investigate properties of materials for possible use in optical masers and other electro-optical devices.
- **OPTICAL PHYSICISTS:**
  To investigate the mechanics of stimulated emission and propagation of coherent radiation both within and outside the laser cavity.
- **MICROWAVE ENGINEERS:**
  To design and build equipment for investigation of modulation, propagation, and detection of coherent optical radiation.
- **OPTICAL ENGINEERS:**
  To design systems for efficient optical pumping and optimum utilization of optical maser output in both the visible and infrared.

Qualified personnel are invited to write to
Dr. S. M. MacNeille, Director of Research.

RESEARCH CENTER
American Optical
COMPANY
SOUTHBRIDGE, MASSACHUSETTS

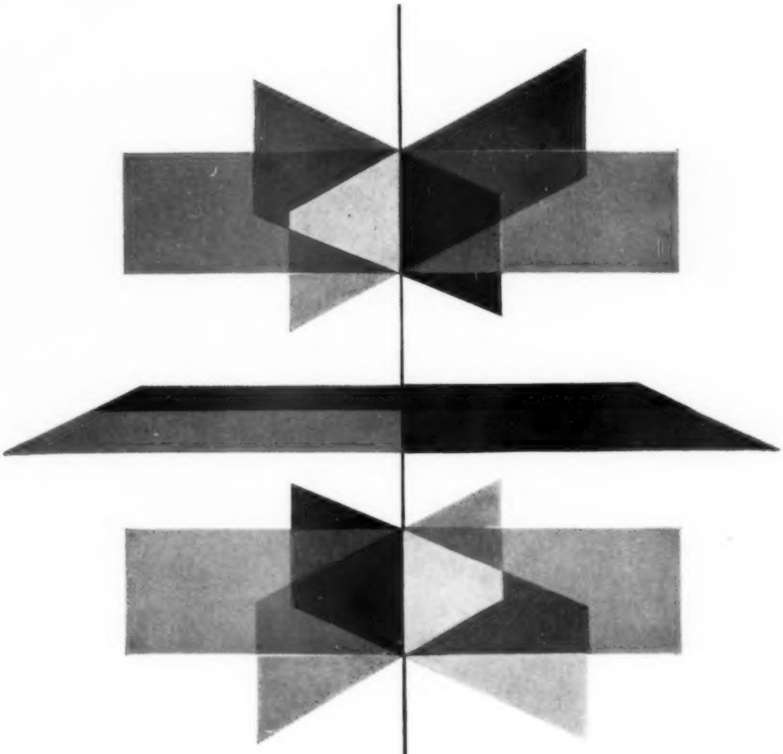

K&E ALIGNMENT TELESCOPE establishes precise reference lines of sight, reading to .001 inch in two dimensions, and to 1 second of arc about two axes. Focusing is zero to infinity. The unit will also auto-collimate.

IF IT'S OPTICAL ALIGNMENT, IT'S IN K&E'S SCOPE

To present and future problems in dimensional control—in tooling, assembly, inspection, or other areas—K&E brings a full line of precision equipment and over 90 years' experience in metrological techniques.

Whether the need is for simple measurement in a single plane, or alignment along 3 co-ordinate axes, K&E optical units meet the requirements. They are precise to .001 inch and 1 second of arc over distances up to 100 feet.

K&E designs and manufactures alignment telescopes, jig transits, collimators, metrological tooling bar systems, and complete accessory equipment. All are designed for use as individual units, or for operation together in a fully engineered system. This modular approach to equipment design and construction by K&E enhances flexibility of operation and holds down costs.

If you have problems in alignment or metrology, send in the coupon below.

K+E

OPTICS AND METROLOGY DIVISION

KEUFFEL & ESSER CO.
Hoboken, N. J.

KEUFFEL & ESSER CO., Optics & Metrology Division, Hoboken, N. J. 3464

☐ Please have a representative contact me.

Please send me the literature checked:

☐ K&E Optical Tooling & Industrial Alignment Equipment Catalog.

☐ The K&E Optical Tooling Bar System.

Name & Title________________

Company & Address________________

HIGH RESOLVING POWER APPARATUS

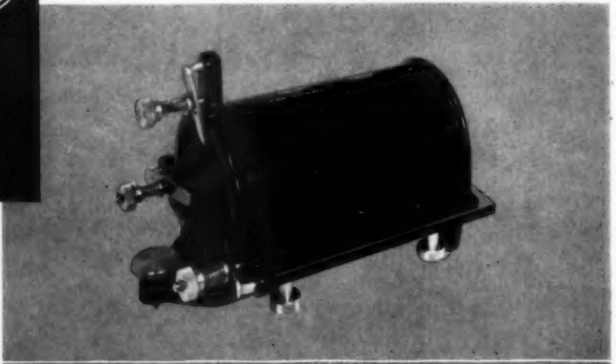

The development of the maser and laser has substantially broadened the use of high resolving power apparatus. Hilger & Watts now provide a comprehensive selection of equipment to meet the increased requirements.

Among the more important are etalon and interferometer plates — ranging from 20 mm. aperture to 100 mm. aperture; with flatnesses to 1/200 of a wavelength. Mounts for these plates, as well as wave length spectrometers designed to accommodate etalons within the instrument, are standard stock items.

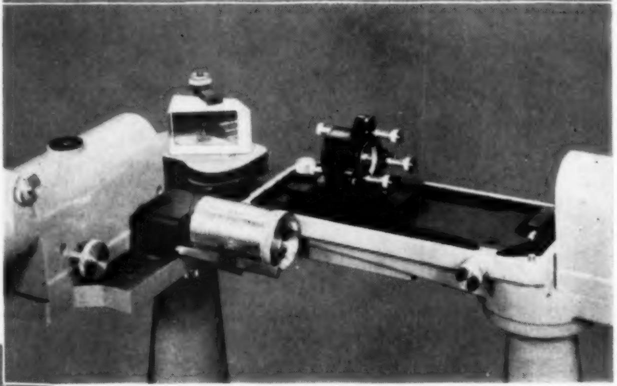

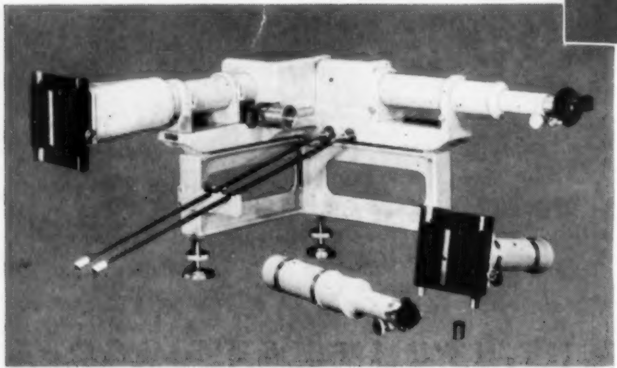

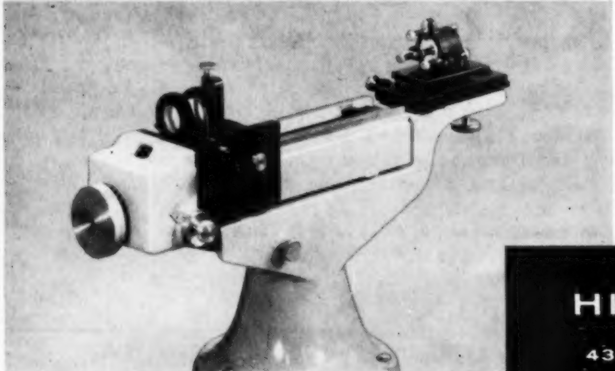

Other new developments include: motor driven Fabry-Perot and Michelson interferometers with fringe counting and amplitude measuring equipment; dielectric coatings for all plates. Lummer-Gehrcke plates and transmission echelon gratings are also available.

Illustrated Top Right—
B345 100 mm. Aperture Etalon

Illustrated Center Right—
D186 Spectrometer with Etalon mounted

Illustrated Center Left—
D260 Large Aperture Spectrometer with Etalon

Illustrated Bottom Left—
N34 Interferometer with Etalon

- *Ask for individual catalog sheets and for complete instrument listing.*

HILGER & WATTS, INC.

431 SOUTH DEARBORN ST. CHICAGO 5, ILL.

Sales, Service, Parts by

ENGIS EQUIPMENT COMPANY

CHICAGO 5, ILL.